DISSERTATION

STOCHASTIC ANALYSIS OF THE IMPACTS OF RAINFALL PATTERNS ON GROUNDWATER RECHARGE

Submitted by

Jarbou Abdullah Bahrawi

Department of Civil and Environmental Engineering

In partial fulfillment of the requirements

For the Degree of Doctor of Philosophy

Colorado State University

Fort Collins, Colorado

Fall 2009

COLORADO STATE UNIVERSITY

SEPTEMBER 23, 2009

WE HEREBY RECOMMEND THAT THE DISSERTATION PREPARED UNDER OUR SUPERVISION BY JARBOU A. BAHRAWI ENTITLED STOCHASTIC ANALYSIS OF THE IMPACTS OF RAINFALL PATTERNS ON GROUNDWATER RECHARGE BE ACCEPTED AS FULFILLING IN PART REQUIREMENTS FOR THE DEGREE OF DOCTOR OF PHILOSOPHY.

Committee on Graduate Work

William E. Sanford

Mohamed Dhbeel Aldhamari

Advisor: Darrell G. Fontane

Co-Advisor: Domenico Bau

Department Head: Luis Garcia

ABSTRACT OF DISSERTATION

STOCHASTIC ANALYSIS OF THE IMPACTS OF RAINFALL PATTERNS ON GROUNDWATER RECHARGE

Potential climate change can impact groundwater recharge. Climate change scenarios were constructed taking into account uncertainty concerning stochastic generation patterns of precipitation and change in the recharge. Because groundwater is directly connected to near-surface hydrologic processes, it intricately connected to the overall hydrologic cycle and could be directly affected by climatic change. Changes in groundwater recharge are likely to result from changes in the annual and seasonal distribution of precipitation. The relationship between the stochastic precipitation that infiltrates and recharges groundwater is the subject of active studies. This is an unprecedented and important research area. The goal of the present research is to attempt to characterize impacts on groundwater recharge by developing potential precipitation patterns and simulating the groundwater recharge in a groundwater simulation model. The stochastic generation of a precipitation model is estimated by adopting two processes for the rainfall. One model is a first order Markov chain. The second model used an exponential distribution model that was fitted to the historical time series of the amount of rain for rainy days. Based on the US Global Change Research Program report's of general predictions for the climate in northeastern North America over the next 100 years, six scenarios for a synthetic time series of precipitation ware developed.

Precipitation is assumed to increase or decrease, with an average change ranging between 5 and 45 percent with 10 percent increments. The generated synthetic time series of precipitation were used in the GSFLOW model. Characteristic statistics and the frequency analysis of the recharge scenarios were estimated. The investigation shows that for the different scenarios, the recharge can be affected and changed to a much greater degree than the percentage change in precipitation. For example a scenario of 25% increase in precipitation showed an increase in recharge of approximately 60% while a 25% decrease in precipitation showed a 70% decrease in recharge.

Jarbou A. Bahrawi
Department of Civil and Environmental Engineering
Colorado State University
Fort Collins, Colorado 80523
Fall 2009

ACKNOWLEDGMENTS

The author wishes to express his sincere gratitude to his advisor Dr. Darrell G Fontane, Professor of Civil and Environmental Engineering at Colorado State University for all his assistance in getting this dissertation together, supporting me through the process and believing in me to the end; for his help, guidance, and for the great efforts he put into this research. Special thanks are extended to my co-Adviser, Dr. Domenico Bau, Assistant Professor in the Civil and Environmental Engineering Department. I would like to also thank my committee members, Dr. William E. Sanford and Dr. Mohamed Dhbeel Aldhamari. Each provided unique perspectives and invaluable guidance and comments that enrich this work.

The author would like to thank his sponsor, King Abdullaziz University – Saudi Arabia, for financial support during his graduate studies, and would like also to extend thanks to Colorado State University for enabling him to carry out the research. Finally, the author wishes to express his sincere appreciation to his family, especially to his parents and wife, Amna, for their sincere encouragement and moral support. He also thanks his daughters Areej, Abeer, and Jorie and his son, Muhammad, for their patience during the time spent working on this degree.

Table of Contents

CHAPTER FOUR: METHODOLOGY

CHAPTER FIVE: RESULTS AND DISCUSSION

CHAPTER SIX: SUMMARY, CONCLUSIONS AND RECOMENDATIONS

LIST OF TABLES

LIST OF FIGURES

Chapter 1

INTRODUCTION

1.0 Introduction

Water is constantly moving within and above the earth in what is called the hydrologic cycle (Figure 1.1). The cycle ends when the water returns back to the ocean. In a simplistic view of the hydrologic cycle, water is evaporated from the oceans by the sun's energy and travels as atmospheric water flux over land areas and falls as precipitation. Part of the precipitation returns to the atmosphere again as evapotranspiration (ET) and the remaining water may partly infiltrate and recharge the subsurface while another part flows as surface runoff. In addition, there are numerous flow paths water can take completing the hydrologic cycle. In Figure 1.1, the major water flow pathways in the hydrologic cycle are shown in blue, while the minor flow pathways are shown with a red dashed line. The major water flow path in the hydrologic cycle will be discussed next.

When discussing the hydrologic cycle, one also must study the flow path. Part of the precipitation falls over the oceans and part over the land. In completing the hydrologic cycle, all of the water must pass through the atmospheric stage, which is estimated to be nine days in length. The water precipitated on the earth's land surface will follow one of three pathways (Broadbridge & White, 1988):

- Evaporated/transpired (ET) directly back to the atmosphere as water vapor;
- Infiltrated into the subsurface;
- Runoff as overland flow or surface runoff.

Since fresh water is one of the earth's most important and limited resources, understanding the hydrologic cycle is essential to maintaining the supply of clean, potable water. Groundwater is the major source of water in many regions, supplying a large proportion of water globally. In the United States, more than half of the drinking water comes from the subsurface; in arid regions, it is generally the only source of water. Therefore, the availability of clean groundwater is of fundamental importance to the sustainability of most humans (Pinder & Celia, 2006).

Water supplied to the soil surface by precipitation or irrigation typically undergoes one of the following processes: infiltration into the soil surface, ponding on the surface, surface runoff, or evaporation (Broadbridge & White, 1988). The water infiltrating into the subsurface is either used by plants, emerges as stream flow, or recharges the groundwater reservoir. In the conceptual model of the hydrologic cycle, infiltration of precipitation is the major source of groundwater and ultimately discharges to a nearby lake, river, or ocean, representing surface water base flow. Unsaturated flow involves flow through the porous media in the saturated flow, which can be described by Darcy's Law (Hillel, 1980).

Of major significance in this study is the infiltration of precipitation into the subsurface versus surface runoff or overland flow. Surface runoff to the river represents direct runoff or flood flow response to the precipitation event. Evaporation of precipitation may start even before precipitation strikes the earth's surface. Surface water

as overland flow or stream flow is subject to evaporation by the sun's radiation. This water continues in the hydrologic cycle and is available for precipitation elsewhere.

When precipitation first reaches a land surface, the infiltration capacity of the soil exceeds the rate of rainfall and little or no surface runoff occurs (Figure 1.2). Infiltration is a counter-current flow situation in which water flows downward and air flows upward. Water is the wetting fluid and air is the non-wetting fluid. Water tends to wet soil particles in preference to air.

Once the water enters the soil, the surface tension force between the air and water causes a pressure difference between the subsurface air and the water. At the start of the infiltration process, the subsurface air is in a continuum phase with the outside atmospheric air and therefore is at an atmospheric pressure of zero. The difference between air pressure (P_a) and water pressure (P_w) is defined as the capillary pressure P_c, where $P_c = (P_a - P_w)$. This capillary pressure causes the subsurface water to be at negative pressure i.e, $P_w < P_a$ in the unsaturated zone. This capillary pressure causes precipitation lying on the ground surface to be sucked or infiltrated into the subsurface. In the unsaturated zone, the subsurface water at negative pressures will not discharge into an adjacent surface water body or enter the saturated groundwater system until the water pressure becomes positive.

At the start of a precipitation event, the combined forces of capillary action and gravity initially result in 100 percent of the precipitation infiltrating the soil. In the early stage of precipitation, capillary forces dominate gravity and the infiltration capacity of the soil is very large.

Therefore, water in the unsaturated zone is at negative pressures $P_w < P_a$ (less than atmospheric). As long as the infiltration capacity of the soil exceeds the rainfall rate, no runoff occurs and all of the precipitation either infiltrates the subsurface or undergoes evapotranspitration back to the atmosphere. As time progresses, the infiltration capacity of the soil declines and surface runoff or overland flow occurs. This happens when the precipitation rate exceeds the soil infiltration capacity. In the conceptual model (ignoring anthropologic influences), this overland flow is collected into streams, rivers, and lakes that take the water back to the ocean. Typically, once the water molecule is in a surface water body (river or lake), the time required to complete the hydrologic cycle and return to the ocean varies from a few weeks to a few months. The root zone is typically considered to extend to approximately six feet below ground surface (Sutton & Tinus, 1983; Phillips, 1963) (Figure 1.4). Within the root zone, infiltration of precipitation is subject to evaporation/transpiration by the sun's radiation or uptake by the roots of plants. Below the root zone, the infiltrated precipitation eventually migrates downward to the groundwater table.

This study focuses on that part of precipitation that percolates below the land surface. Groundwater recharge is the deep percolation that becomes groundwater storage or stays in the root's plant, or laterally returns to the surface through evaporation/transpiration. In the root zone (Figure 1.3), there is a struggle for water between the capillary action in the soil and the osmotic forces in plant roots. The capillary force is responsible for driving groundwater from the soil, which has higher water content than the dry areas in the root zone. This force causes the water to rise in the soil during hot weather or insufficient periods of precipitation; this water goes back

up into the atmosphere through evaporation/transpiration (ET). The osmotic force in the plant roots is a suction force, creating a wilting point where the plant roots start to take in less moisture and, consequently, wilt. The ET in the root zone is variably dependent on plant root suction and water quality, where ET rates can fluctuate depending on the length of the plant roots.

On a global scale, the amount of precipitation that infiltrates the subsurface versus surface runoff is approximately 50 percent (The Trust for Public Land, 2008). Locally, this percentage may vary, ranging from near zero to 100, and it is typically subject to large measurement and/or estimation errors. In order to predict how these systems may respond to future rainfall change and other disturbances, we must have quantitative understanding of how variability of rainfall interacts to control infiltration water fluxes.

Infiltration of precipitation is the process of water penetration from the ground surface into the soil and is an important process in groundwater recharge because it represents that part of precipitation that percolates below the land surface, whereas percolation is the process of water flow from one point to another within the soil. Precipitation is a very important factor in semi-arid and arid regions where groundwater occurs in shallow weathered zones and where the rise in groundwater level is a direct consequence of infiltration of precipitation. The rise in the water level at a particular place is a characteristic of an unsaturated zone. Therefore, there is a definite relationship between the uncertain stochastic nature of precipitation and the infiltration and recharge of groundwater for a particular region. Water can infiltrate the soil as quickly as it is applied. The amount of precipitation that is infiltrated is affected and characterized by

some uncertain parameters (Dunne, Zhang, & Aubry, 1991) and correlates to the amount of recharge in the subsurface or groundwater. The parameters are:

- Characteristics and physical properties of the soil (type, porosity, hydraulic conductivity, texture, salinity, and roughness of the soil surface). Soils such as clays absorb less water at a slower rate than sandy soils. Soils absorbing less water result in more overland runoff into streams. Like a wet sponge, soil already saturated from previous rainfall cannot absorb much more.
- Characteristics of the intermittent nature of precipitation both in time and space (intensity, duration, space, timing).
- Evaporation/transpiration (ET). Some water stays near the land surface, where plants put down their roots. Plants need this shallow ground water to grow, and, by the process of evapotranspiration, water is moved back into the atmosphere.
- Climate (temperature, wind speed, humidity).
- Topography (elevation, slope).
- Land cover and vegetation type (can slow the movement of runoff, allowing more time for it to seep into the ground (Youngs, 1995; Tarboton, 2003a)).

Estimating the infiltration of precipitation is very important and requires knowledge of the type and physical properties of the soil and rainfall data.

This study will focus on the variability, or stochastic nature, of the precipitation to examine its impact on groundwater recharge by developing potential precipitation patterns and simulating the groundwater recharge in a groundwater simulation model.

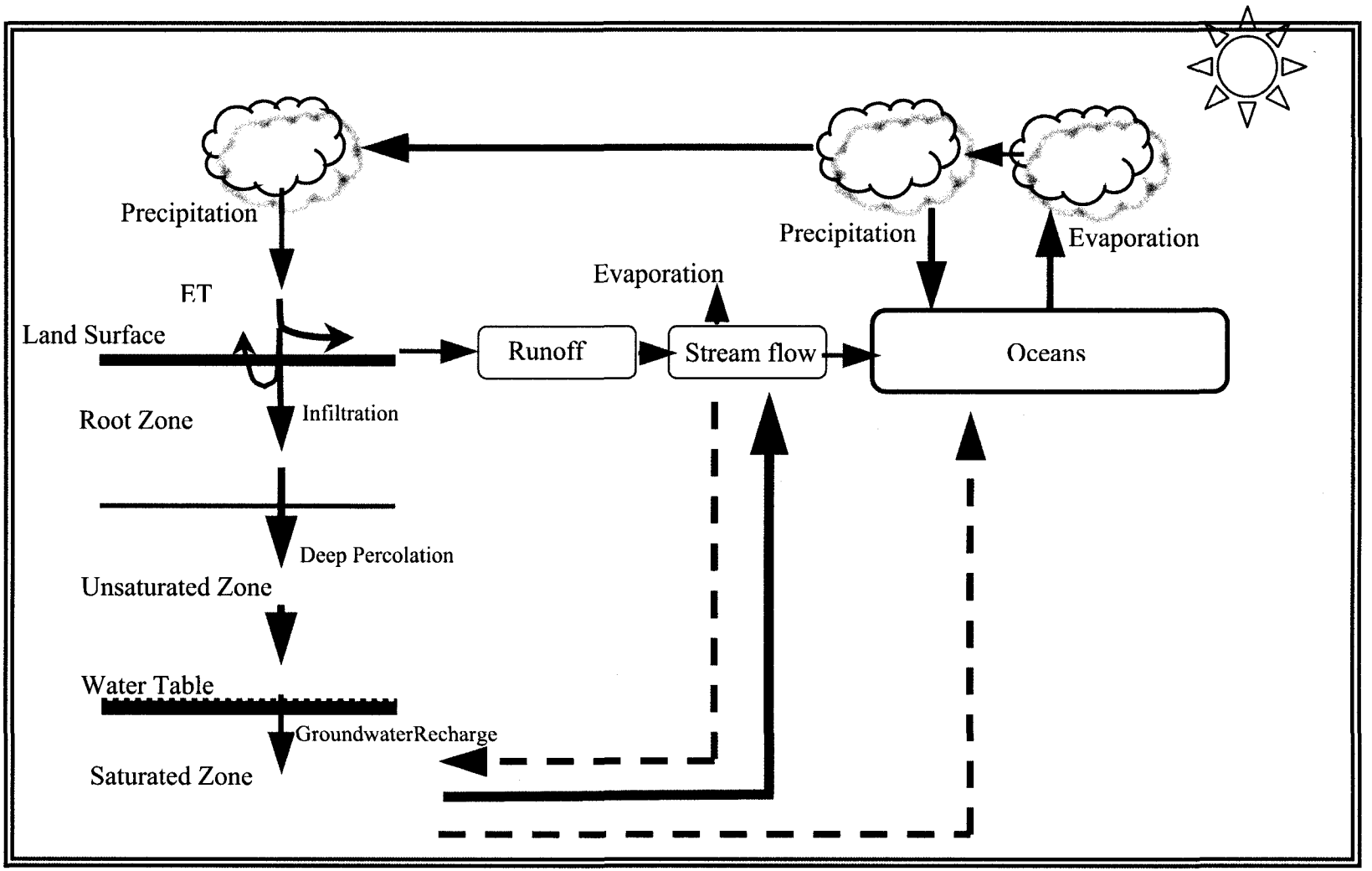

Figure 1.1: Hydrologic cycle

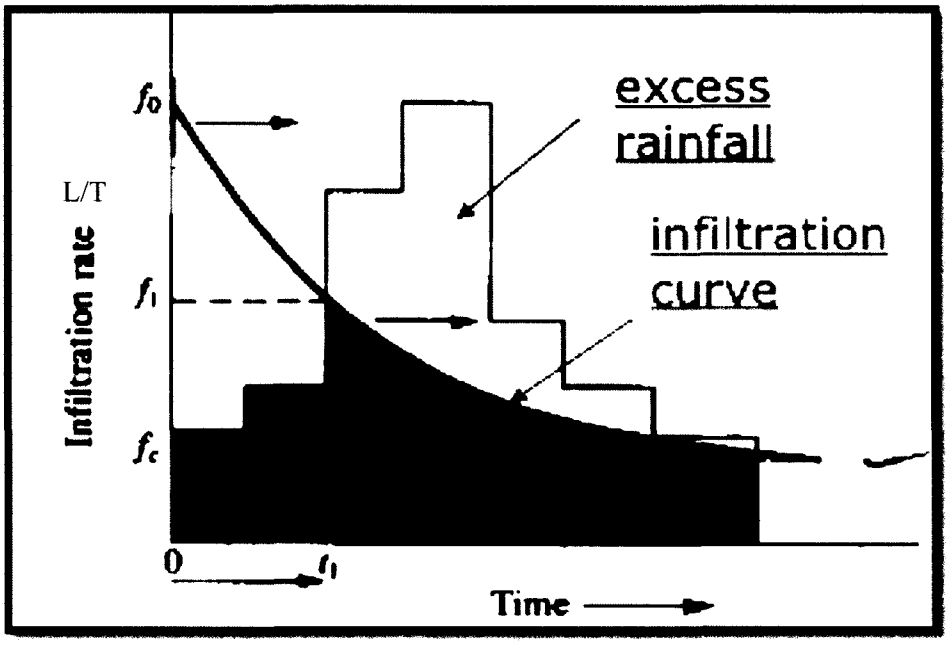

Figure 1.2: Infiltration rate will generally be high in the first stages of rainfall but will decrease with time. f_o is the initial infiltration capacity and f_c is the final infiltration capacity(Todd, 2005).

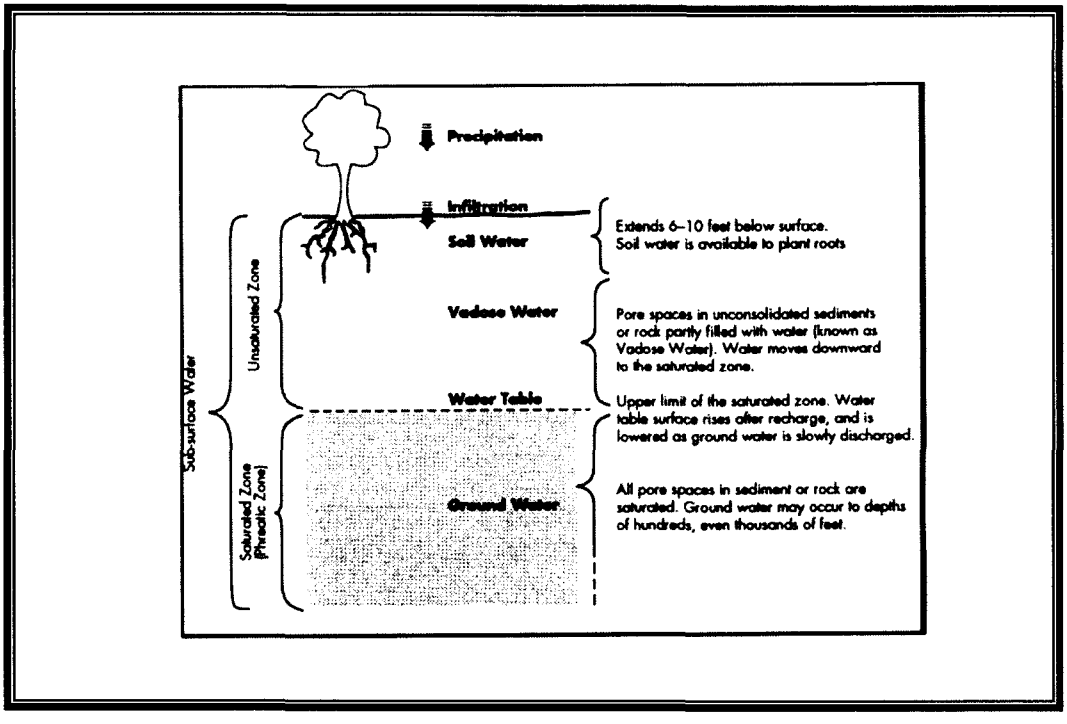

Figure 1.3: Groundwater Process©, American Ground Water Trust (www.agwt.com).

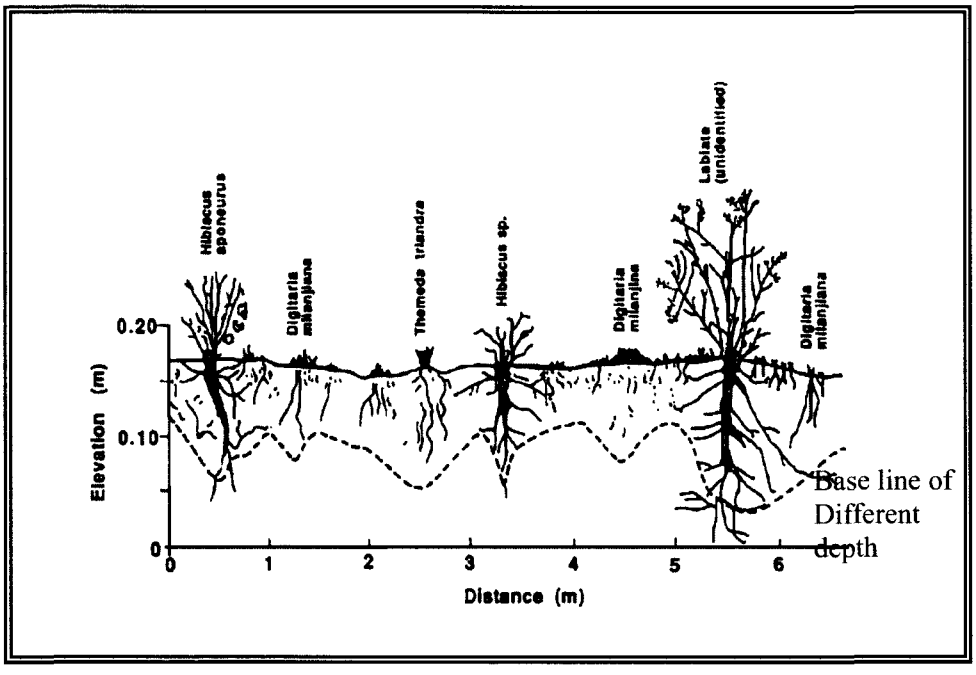

Figure 1.4: Watering depth for different type of plants (Glover et al., 1962).

1.1 Research Motivation

The division of precipitation between infiltration and ET is controlled by a variety of climatic factors (frequency, rate, duration and type of precipitation) and physical properties (hydraulic conductivity, soil type, slope, soil texture, moisture conditions, vegetation, land use, and surface roughness). Scholars in the hydrologic literature describe change as the nature of the process responsible for the transfer of infiltrating rain to the water table (Smith, 1976). Corradini, Melone, and Smith (1994) mention specifically that most realistic problems in soil physics and hydrology imply infiltration and redistribution.

On a global scale (Oki & Kanae, 2006), total precipitation over land areas is approximately 111 billon cubic meters (bcm) per year. This precipitation has two major components: net atmospheric flux from the oceans, equal to about 45.5 bcm per year, and terrestrial ET from land areas equal to 65.5 bcm per year, which represents approximately 59 percent of the total precipitation rate. Direct surface runoff to rivers and lakes is 15.3 bcm per year, which represents 13.78 percent of the total precipitation of 111 bcm. On a global average, infiltration for groundwater recharge amounts to 30.2 bcm per year, which is 27.2 percent of the total precipitation. The global hydrologic cycle is shown in Figure 1.5. (Oki & Kanae, 2006). Figure 1.6 shows the distribution of mean annual runoff, mean annual discharge, and the water scarcity index (Oki & Kanae, 2006)

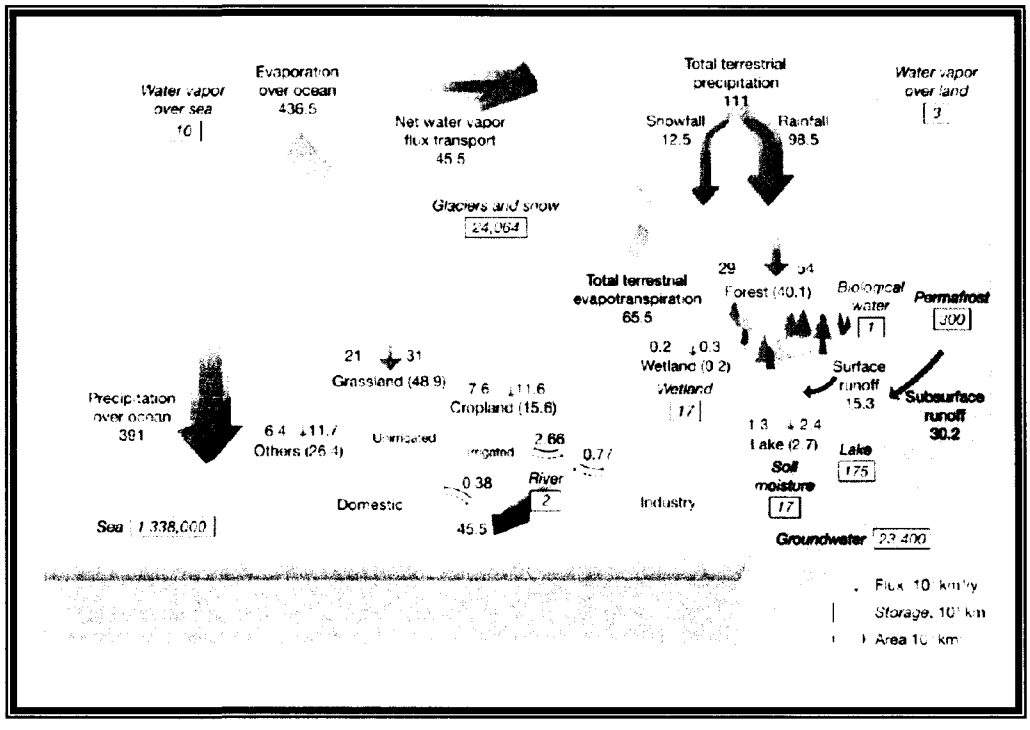

Figure 1.5: The global hydrologic cycle (Oki and Kanae, 2006).

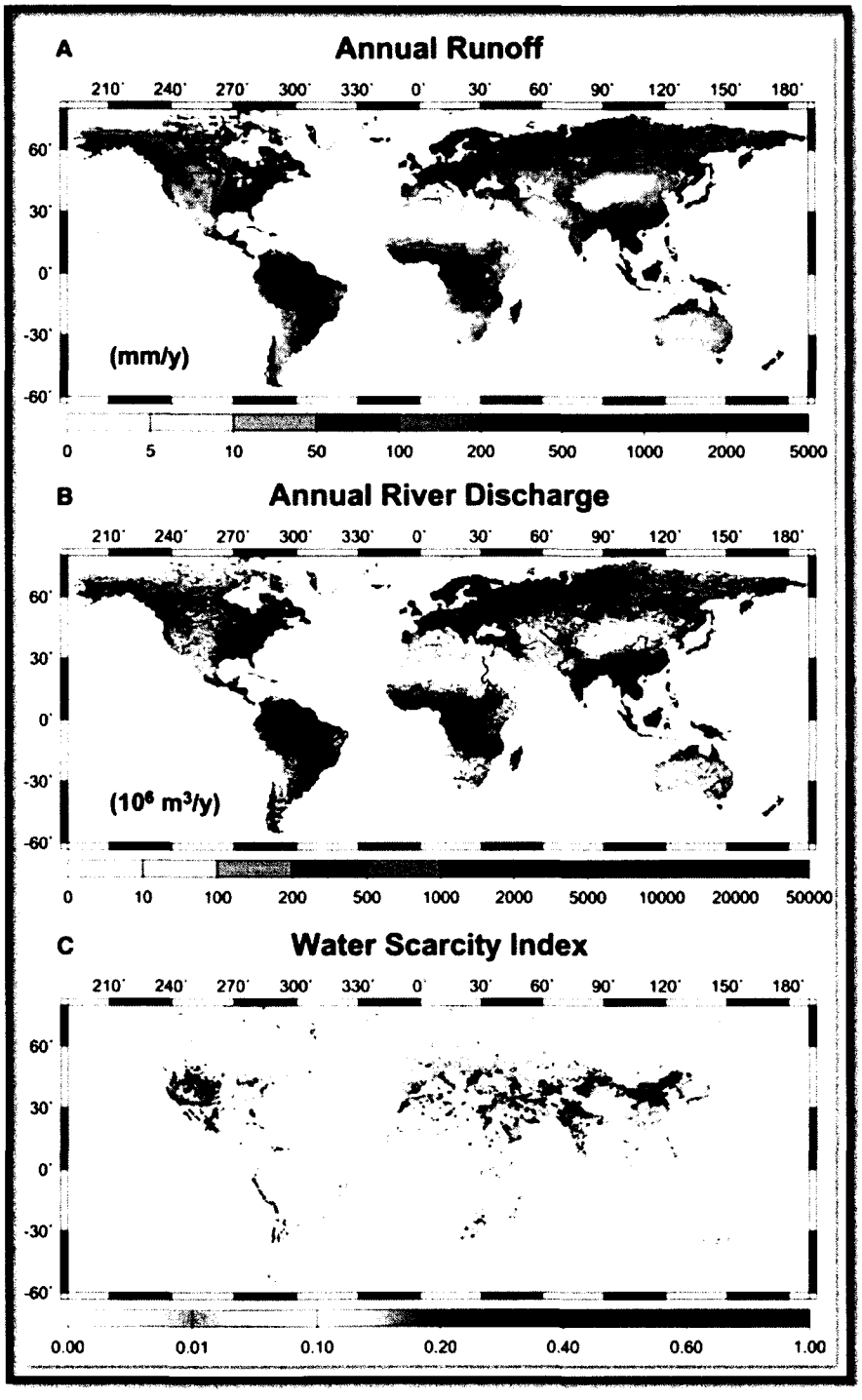

Figure 1.6: Global distribution of (A) mean annual runoff (mm/year), (B) mean annual discharge (million m3/year), and (C) water scarcity index Rws (3,11). Water stress is higher for regions with larger Rws. (Oki and Kanae, 2006)

Global warming is a phenomenon that affects the local hydrologic cycle in terms of the amount of precipitation that infiltrates.

Increasing global surface temperatures (Figure 1.7) are likely to lead to changes in precipitation and atmospheric moisture because of changes in atmospheric circulation, a more active hydrological cycle, and increases in the water holding capacity throughout the atmosphere (Folland & Karl et al., 2001). On a global average, the Second Assessment Report (SAR) from the Intergovernmental Panel on Climate Change (IPCC) concluded that land surface, air, and sea surface temperature increased between 0.3°C and 0.6°C between the late nineteenth century and 1994. Figure 1.7 shows the IPCC's conclusions regarding long-term (1880 to 1998) global land-surface air temperature variations and trends. Jones et al. (2001) and Hansen et al. (1999) reviewed the database from the Global Historical Climatology Network (GHCN) (1880 to 1998) and found that rural trends were 0.70°C/century. Peterson et al. (1999) observed a slight divergence in the rural (0.80°C/century) and full set of station trends (0.92°C/century). According to Peterson et al., the 1951-1989 trend for urban stations alone was 0.10°C/decade. Jones and Hulme (1996) and Hulme et al. (1998) concluded that global land precipitation has increased by approximately 2% since the early twentieth century.

In other studies, Karl and Knight (1998) and Doherty et al. (1999) found this increase to be statistically significant. They collected data from more than 20,000 stations that contributed to changes of precipitation since 1900 shown in Figures (1.8 and 1.9). From 1910 to 1995 over many regions of Australia , there was a 10 to 45 percent increase in heavy rainfall, as defined by the 99th percentile of daily totals (Hennessy et al., 1999).

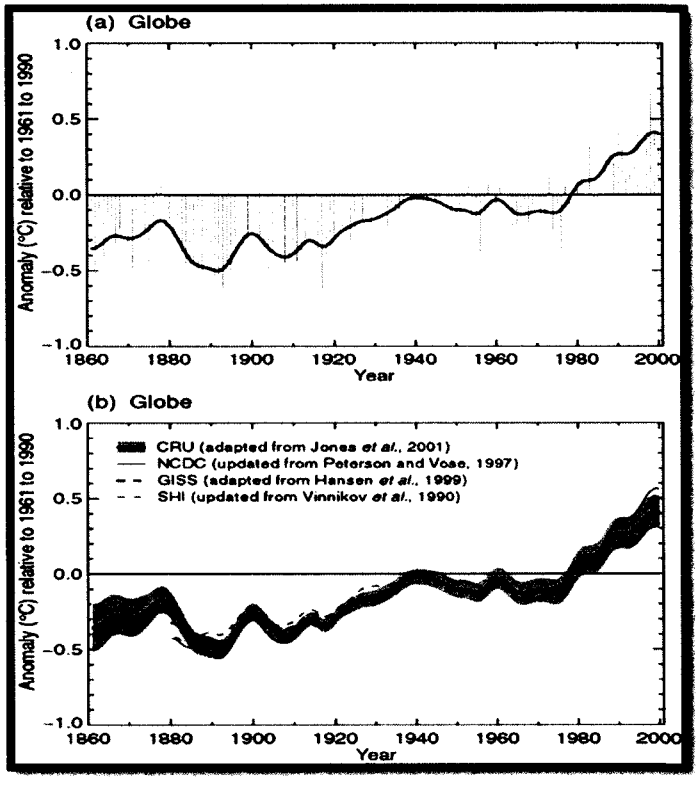

Figure 1.7: a) Annual anomalies of global average land-surface air temperature (°C), 1861 to 2000, relative to 1961 to 1990 values. Bars and the solid curve are from Climatic Research Unite (CRU) (Jones et al., 2001). b) Same as (a) but smoothed curves only from National Climatic Data Center (NCDC) (updated from Peterson and Vose, 1997) – thin solid curve: Goddard Institute for Space Studies(GISS) (adapted from Hansen et al., 1999) – thick dashed curve: (SHI) (updated from Vinnikov et al., 1990) – thin dashed curve to 1999 only: Peterson and Vose (1997) – thin solid curve. Thick solid curve – as in (a): Folland, and Karl et al., (2001) observed climate variability and change.

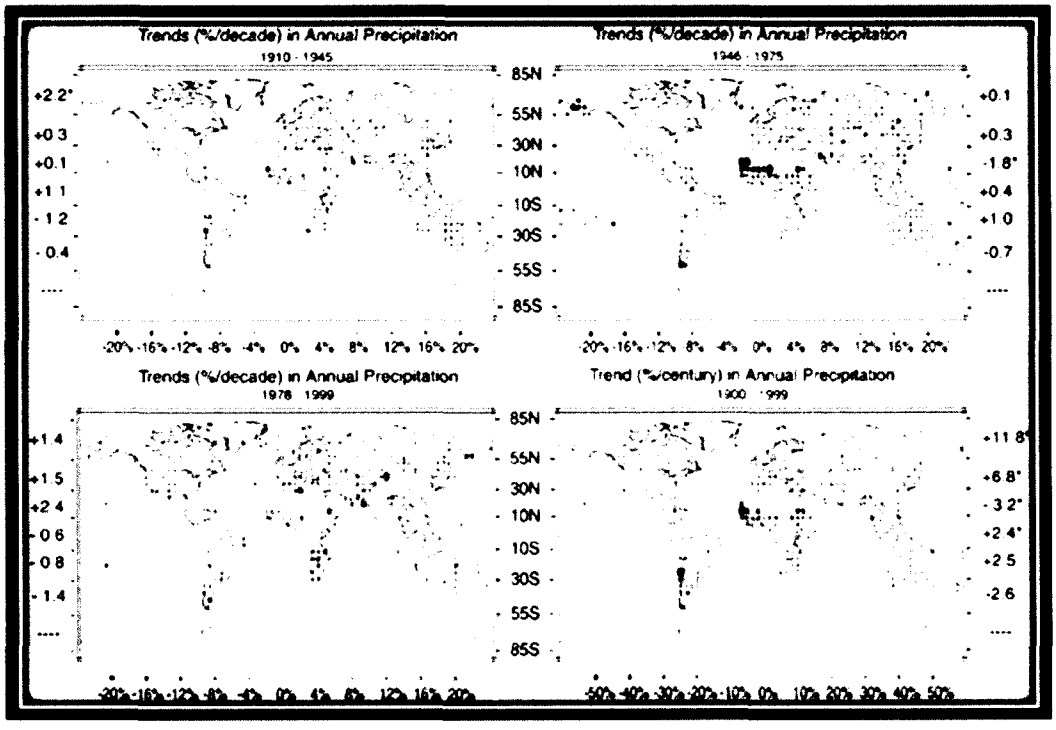

Figure (1.8): Increases in precipitation since 1900 along the South American eastern coastal areas, with less extensive increases since 1976. Trends for 1900 to 1999 for the four seasons. Precipitation trends are represented by the area of the circle, with green representing increases and brown representing decreases (Climate Change 2001: The Scientific Basis).

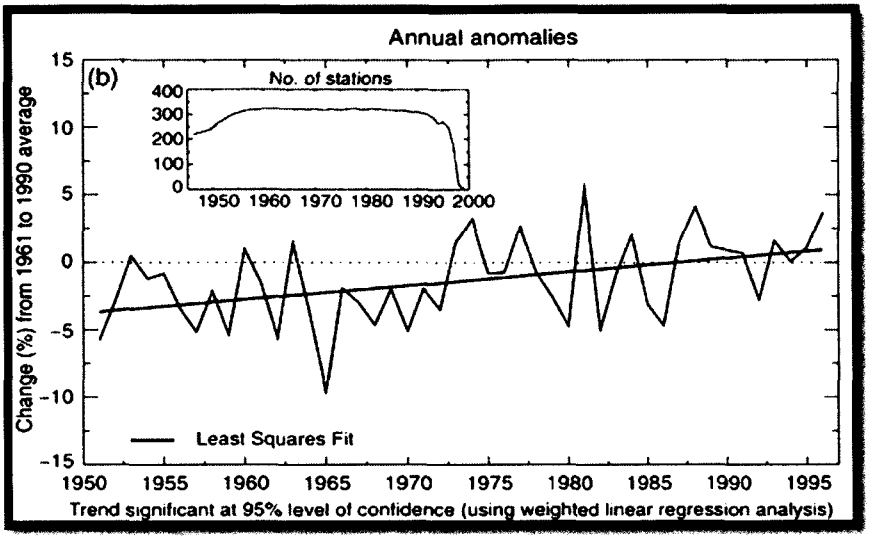

Figure 1.9: Changes in the maximum annual five-day precipitation total. Figure shows the average annual values of the quantities expressed as percentage differences from their 1961 to 1990 average values. The trend is statistically significant at the 5 % level (Climate Change 2001: The Scientific Basis).

Karl and Knight (1998) and Groisman et al. (1999) showed increasing precipitation on the local hydrologic cycle in the Northern Hemisphere at mid- and high latitudes, especially during autumn and winter. They also found this increase varies spatially and temporally. For example, precipitation over the United States has increased between 5 to 10 percent since 1900 (Figures 1.8; 1.9; 1.10). In Canada, the precipitation has increased by an average of greater than 10 percent during the twentieth century (Mekis & Hogg, 1999). Moreover, Zhang et al. (2000) showed that the heavy snowfall amounts north of 55°N have increased, and Akinremi et al. (1999) found that rainfall increased in the Canadian prairies from 1956 to 1995. However, on the other side of the world, annual precipitation decreased in China (Zhai et al., 1999a). In Northern Europe there were marked increases in precipitation in the latter

part of the twentieth century; however, there was a decrease southward to the Mediterranean (Schönwiese & Rapp, 1997).

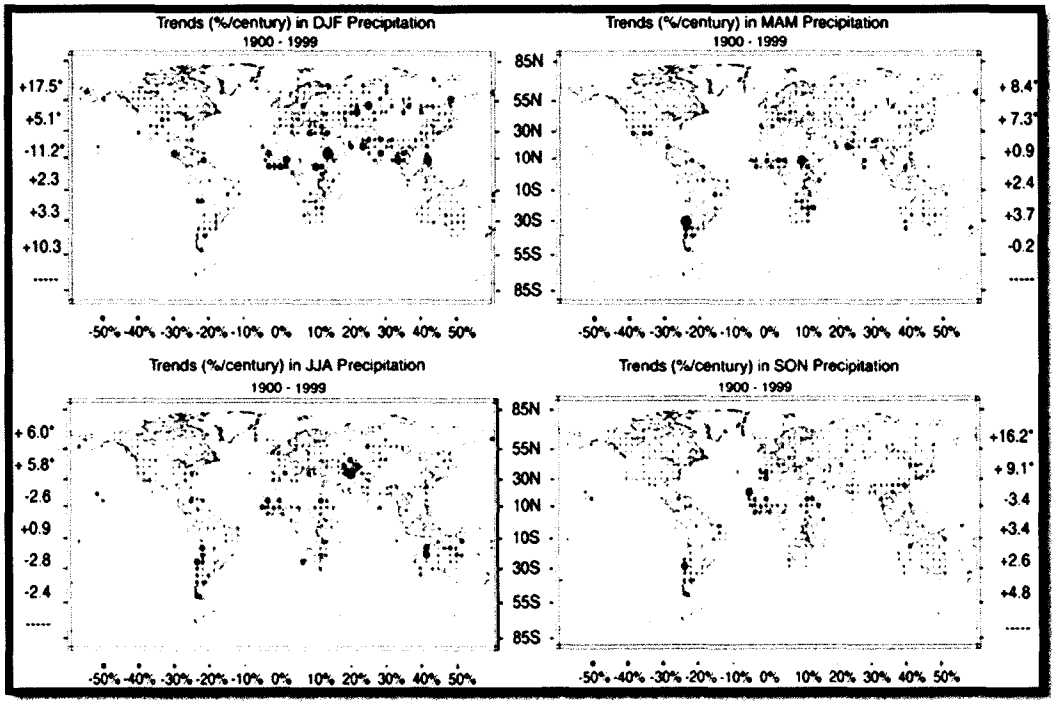

Figure (1.10): Trends for 1900 to 1999 for the four seasons. Precipitation trends are represented by the circles, with green representing increases and brown representing decreases. (Climate Change 2001: The Scientific Basis).

The distribution of precipitation (water resources) varies considerably. Continents and regions of continents are different. It is fairly simple to measure total precipitation but difficult to measure transpiration, surface runoff, and subsurface infiltration, especially in arid and semi-arid areas (Wu & Zhang, 1994). Most often, previous and current studies estimate the portion of precipitation that infiltrates based on the long-term average over several years of water cycle.

This research focuses on the potential changing precipitation patterns have to affect groundwater recharge. Infiltration of precipitation and groundwater recharge is still an active area of research, and understanding the connection between surface processes (rainfall/runoff) and infiltration and groundwater recharge will improve the

ability to sufficiently assess the effects of changing precipitation patterns on groundwater resources.

The main purpose of this research is to attempt to characterize the impact of climate change on groundwater recharge by developing potential precipitation patterns and simulating the groundwater recharge in a groundwater simulation model. The simulation model is a new model released by the U.S. Geological Survey (USGS). It is called the Ground-water and Surface-water Flow (GSFLOW) model, and it is based on the USGS Precipitation-Runoff Modeling System (PRMS) and the USGS Modular Ground-Water Flow Model (MODFLOW-2005).

Understanding the link between surface processes (rainfall/runoff) and infiltration and groundwater recharge will improve the ability to adequately assess the effects of changing precipitation patterns on groundwater resources.

1.2 Research objectives

In this study, the objectives are:

1. Analyze the time series of precipitation and investigate if more precipitation scenarios may be lead to more recharge.
2. Apply the stochastic precipitation model to data to generate different stochastic precipitation scenarios.
3. Use stochastic precipitation as a drive in the USGS GSFLOW model.
4. Study the stochastic precipitation events versus groundwater recharge.
5. Study how the relative amounts of recharge vary as a function of the stochastic nature of long-term precipitation.

1.3 Outline of the dissertation

This dissertation presents, in its first chapter, a general description of the research topic and the purpose and specific objectives of the intended research. Chapter 2 reviews the literature related to the stochastic rainfall model. Chapter 3 presents a detailed description of the USGS GSFLOW model. Chapter 4 also will focus on the stochastic rainfall amounts and occurrences by using two common methods of empirical frequency analysis based on plotting position and probability models for the amount of rainfall. Rainfall occurrence will be modeled using a Markov chain model. The simulation results and the discussion are presented in Chapter 5. Finally, summary and conclusions are given in Chapter 6.

Chapter 2

LITERATURE REVIEW

2.0 Introduction

Most hydrological processes have some level of randomness and uncertainty. Hydrological systems have both stochastic and deterministic components. Deterministic components can be expressed mathematically by a set of equations, a graphical relation, or a set of rules, whereas the stochastic components and parameters can be defined by means of probability distributions. A model of a system determines the value of outputs resulting from inputs. If any of the inputs are stochastic, then the output is also stochastic.

Two independent processes control the runoff discharges of a drainage basin. One process determines the rate of input to the system and the other process establishes the response of the system. This concept in hydrology is known as the system concept. In this research, the first process related to the system input is precipitation. The second process concerns the system response (recharge) to this input. Determination of the system input is a quite important and complex process because system input should be considered as the excess precipitation that represents minor retentions, and infiltration must be subtracted from the total precipitation. Thus, it is important to define the elements of input to the system.

Lack of pertinent data has been the major obstacle to the development of a comprehensive climatology of extreme rainfall intensities. McClaran and Van Devender

(1995) explained that arid and semi-arid ecosystems are particularly vulnerable to climate variability, of which precipitation is the most important component, while Reynolds et al. (1999a) and Schlesinger et al. (1990) indicated that water is a major determinant of many processes in arid ecosystems, and that a slight shift in seasonal precipitation and/or the frequency of extreme rain events may lead to major ecological and biogeochemical impacts. Thus, in order for us to predict how these systems may respond to future rainfall change and other disturbances, we must have a quantitative understanding of how atmospheric variability in rainfall contributes to control of water fluxes. Because of the complexity of the many cause and effect relationships that exist within and between infiltration, storage, and the atmosphere (e.g radiation balance, variability in rainfall, etc.), it is extremely difficult for experimental studies to quantify the magnitude and importance of many of these interactions, particularly for longer time periods. Field studies are usually based on different locations and over conducted relatively short time periods. As a result, collected field data provide an incomplete representation of the variability of infiltration, especially as a function of annual variability in rainfall.

Rainfall is one of the hydrological processes that are typically described by probability functions. Modelling precipitation is important to various disciplines in science and engineering. Synthetic precipitation sequences are used in applications as diverse as agricultural planning, reservoir and watershed management, groundwater recharge, erosion prediction, design of landfills, and design of facilities for storage and disposal of hazardous wastes. Simulation models typically consider rainfall as a random process, attempting to simulate daily rainfall sequences that are ``representative" of the observed records. However, most precipitation simulation models reproduce only a few of the features that characterize daily rainfalls. In this chapter, the frequency analysis for

rainfall amount is presented by using two common methods of empirical frequency analysis based on plotting position and probability models. The probability models (mathematical models) include a wide range of distributions that have been used to fit historical sequences. Examples of frequency analyses are the Weibul distribution, the exponential distribution, the gamma distribution, a skewed normal distribution and the kappa distribution. In this study rainfall occurrence will be modeled by using Markov chain, and the exponential distribution model. This chapter will explain the probability functions model that is used in this research.

2.1 Stochastic Rainfall Model

Numerous studies have described stochastic models of rainfall. Researchers from a number of disciplines have proposed both physical and stochastic approaches for synthesizing daily rainfall and some of these studies are reviewed here.

Ramesh (1998) illustrated the application of Cox process models in the modeling of temporal rainfall at a single rain gauge where two stochastic point process models are considered. The models are developed using a class of Cox processes to describe the probabilistic structure of the rainfall intensity process. Ramesh (1998) found that the rectangular pulse model is much more satisfactory than the Markov-modulated Poisson process. One key characteristic of this model is that it appears to be capable of representing effects on timescales. Ramesh (1998) presented the analysis for 5 years of summer rainfall data and mentioned that, for a longer period, extensive analysis of rainfall observation could provide more accurate inferences, but difficulties such as increased parameter uncertainty across years might arise. Finally, he recommended further research on fitting Pareto or gamma distributions for the pulse depth, which would possibly improve the fitting procedure.

Rao and Biazi (1983) examined the fitting of two stochastic models to daily rainfall data for an interior station in Brazil. Both of these models used a truncated negative probability model in comparison with a Markov chain probability model. The results show a better fit to describe the data. By using the Kolmogorov-Smirnov test at the 5 percent significance level, it is observed that dry day and wet day spells for both models are coherent. Comparing the models for dry and wet spells, the truncated negative binomial model shows a good fit to describe the data.

Markov chain models have been used in many studies to describe rainfall occurrence. Gamma distributions are usually used for modeling rainfall amounts. All the models declared are examples of generalized linear models (GLMs). Considering them as such has advantages because the methods used for the analysis of GLMs have close analogies with ordinary regression methods used for normally distributed data. The familiar terminology involved in fitting curves to the data thus replaces the relatively daunting prospect of analyzing non-stationary Markov chains. Many studies have used Markov chains to model the daily occurrence of rainfall.

Coe and Stern (1982) applied first and second order Markov chains in which the transition probabilities vary with time of year to data from sites in Jordan, Niger, Botswana, and Sri Lanka. Gamma distributions with parameters varying with time are also fitted.

Gabriel and Neumann (1962) analyzed the occurrence of rain at Tel Aviv, Israel, by fitting a two-state, first-order Markov chain. The two states corresponded to "rain" and "no rain". Later, some studies looked at chains with more than two states; for example, Haan et al. (1976) analyzed a seven-state chain, the seven states representing different amounts of rain. The models have also been extended to include Markov chains

of higher than first order. Katz (1977) fitted zero-, first- and second-order chains to daily data.

Lund and Grantham (1977) fitted up to 12^{th} order chains to hourly rainfall data. The observed proportion of rainy days usually changes through the year. Heermann et al. (1968) fitted separate Markov chains to each month, but gave no indication of whether the differences between months were important. The transition probabilities are likely to change smoothly through the year and can thus be modeled by continuous functions of time.

Mimikdu (1983) studied the seasonality of the Markov chain order for proper modeling by applying it to stations in Greece through modeling daily rainfall occurrences for these stations. The conclusions of the study are that "(a) The appropriate selection, on a seasonal basis, of the order of a Markov chain considerably enhances its efficiency for modeling daily rainfall occurrences. (b) The average seasonal storm duration, being the average seasonal percentage of the number of wet days to the number of storm events and impacted by the rainfall station's meteorology and geography, is recommended as a standard for determining the proper seasonal Markov order of a chain for modeling daily rainfall occurrences. (c) For seven rainfall stations in Greece the error of modeling daily rainfall occurrences with a Markov chain are minimized with chains of seasonally varying order. The proper monthly Markov order is the closest positive integer to the average monthly storm duration in days reduced by one. Further research work is required for examining the sensitivity of the average seasonal storm duration to the order of the chain and for studying the extension to different climatic controls, geographical locations, Markov chain applications, etc., of the seasonal relationship between the suggested standard and the proper Markov order of conditional dependence of daily

rainfall occurrences. (d) Present is prevalence of Markov orders higher than 1 in wet periods and of orders 1 or 0 in dry periods. The appearance at each station of the period with orders higher than 1, relative to the beginning of the hydrological year, is delayed and its duration decreases going eastwards and with decreasing elevation. (e) The monthly quantities of wet days are better modeled by a second order autoregressive model than by accumulating daily rainfall occurrences generated from a Markov chain" (Mimikdu, 1983).

Tsakeris (1988) analyzed data on a continuous time scale from the Mikra Station in Greece to rainfall occurrence in continuous time. He simplified the solution by assuming that the individual wet and dry intervals are random variables following an Erlang distribution, in particular an exponential distribution. In conclusion, Tsakeris (1988) found that "recorder rainfall data are not always available. Using the model, important information regarding expected irrigation water requirements may be derived. Also due to the detailed information obtained, the model can be used in a variety of hydrological problems, dependent on the duration of the rainy period".

Hershfield (1984) computed statistics of the total time, in minutes, that extreme rainfall rates are exceeded from weighing rain-gage records at stations in several rainfall regimes. Measures of areal variability were calculated from data at seven stations within an 8 km^2 area. The total-time-intensity data have only an imprecise relationship to clock-hour frequencies, the shortest duration rainfall data published regularly.

Rajagopalan et. al. (1997a) presented a nonparametric multivariate resampling scheme for generating daily weather variables at a site. The model samples the original data with replacement while smoothing the empirical conditional distribution function. Rainfall is generated from the non-parametric wet/dry spell model (Lall et. al., 1996). A

vector of solar radiation, maximum temperature, minimum temperature, dew point temperature, and wind speed is then simulated by conditioning the vector of these variables on the preceding day and the rainfall amount on the day of interest. The model was applied to 30 years of daily weather data for Salt Lake City, UT. The results showed that the means and the quantiles are well reproduced

Sharma and Lall (1999) found that the modelling and assessment of rainfall events could be achieved through parametric and non-parametric techniques. They use nearest neighbour methods to conditionally simulate rainfall amounts, and a ``local" subset of the observed record to formulate the conditional densities needed for simulation. The model was applied to 123 years of daily rainfall for Sydney, Australia, using models in a two-stage process. First, dry and wet spell lengths were conditionally simulated. Next, rainfall amounts for each day of the wet spell were simulated assuming an order one Markov dependence structure. Higher order dependence was modelled by considering the number of days from start of the spell as an additional variable. Rainfall distributional characteristics were observed to have distinctly different characteristics depending on the length of the wet spell.

Srikanthan and McMahon (2001) reviewed the state of research and practice in the stochastic generation of annual, monthly, and daily climate data. They found that one of the most important gaps in the design and operation of hydrological systems is the quantification of uncertainty as a result of climatic variability. This applies whether the systems are complex water resources systems or simple planning models of catchment behavior.

Ochola and Kerkides (2003) mentioned that the occurrence of wet and dry spells is a phenomenon most often used to identify the arid and semi-arid lands (ASAL) in Kenya.

They used first-order Markov processes to determine the critical climate extremes. Their model uses the concepts of conditional probability, Poisson probability distribution function, and chi-square testing to predict the critical spells. The daily rainfall data (1981– 2000) for two weather stations in the Kano Plains (Kenya) were used to illustrate model application. For example, based upon the bimodal rainfall pattern in the study area, the model revealed the length of the critical dry spell to be 14 days in the long rainy season and 12 days in the short rainy season, while the critical wet spell was found to be 12 and eight days for the long and short rains, respectively, for the Ahero Irrigation Scheme.

Harrold et al. (2003) used kernel density estimation techniques for daily rainfall from Sydney, Australia, to reduce the assumptions that are made about the underlying probability density. Representation of seasonal variations was achieved through the use of a moving window approach. Four different classes of rainfall amount considered and categorized according to the number of adjacent wet days, and the model conditioned on the rainfall amount on the previous day.

2.2 The Recharge Modeling

Groundwater is the main source of water for both irrigation and municipal and industrial demands in most communities, and because groundwater is often directly connected to near surface hydrologic process, it is thus intricately tied to the overall hydrologic cycle and could be directly affected by climatic change. Changes in groundwater recharge (both increases and decreases) are likely to result from changes in the annual and seasonal distribution of precipitation. Alley (2001) noted that the aquifer of groundwater response to climate variability can lead to changes in groundwater quality

and can affect contaminant transport. For example, water recharged during a dry period may have a higher concentration of salts in water, which is called total dissolved solids (TDS), while during a wet period the opposite may occur (Sukhija et al., 1998). Moreover, changes in precipitation timing, location, intensity, and magnitude may lead to increased potential for flooding with potential for contamination of water supply wells and property damage. Richard et al. (2003) examined the effects of daily precipitation and evapotranspiration patterns on flow and volatile organic compound (VOC) transport to groundwater along a watershed flow path. They mentioned that the methyl tert-butyl ether (MTBE) and other VOCs are widely observed in shallow groundwater in the United States. They found that that daily precipitation and evapotranspiration patterns may have a significant effect on recharge to groundwater. Pankow et al. (1997) simulated one-dimensional unsaturated/saturated vertical transport of VOCs in the subsurface. They concluded the precipitation and ET patterns could be responsible for the widespread low-level contamination of groundwater from an atmospheric source. Baehr et al. (2001) concluded that while a number of VOCs were detected in groundwater, only the concentration of MTBEs in the observed groundwater was greater than the concentration measured in the atmosphere.

Recharge is generally defined as the process of water penetration from the ground surface into the soil and percolated to groundwater. Lerner et al. (1990) defined the various sources of recharge to a groundwater system. They mainly divided the recharge into (1) direct recharge; excess water of soil moisture content and evapotranspiration and vertical percolation to the groundwater reservoir through the soil zone; (2) indirect recharge: percolation to the water table through the beds of surface-water paths and (3) localized recharge: horizontal percolation near surface water.

Recharge is an important process in the hydrological cycle by which surface runoff and groundwater recharge can be linked. Soil water movement or percolation is the process of water flow from one point to another within the soil. Infiltration and percolation cannot be treated independently, because the rate of infiltration is controlled by the rate of percolation below the surface.

Buckingham (1907) modified Darcy's law, originally defined for only saturated conditions, to describe unsaturated flow by generalizing the relationship between soil water pressure head c and hydraulic conductivity K. He reasoned that K becomes a function of the volumetric soil water content u, and called it capillary conductivity. Buckingham (1907) also mentioned that the soil water potential c in an unsaturated soil would be negative because of the presence of capillary suction forces.

A general solution to the problem of hydrological modelling in arid and semi-arid zones requires explanation and developments in physically based to use numerical equation modelling techniques. Representation of the hydrological components of rainfall, infiltration, runoff, and (particularly important in these regions) transmission losses need to be combined in such models. The relationship between the changing climate variables and groundwater is very complex and weakly understood. Groundwater resources are related to climate change through direct interaction with surface water resources, such as lakes and rivers, and indirectly through the recharge process. Therefore, quantifying the impact of climate change on groundwater resources requires not only reliable forecasting of changes in the major climatic variables, but also accurate estimation of groundwater recharge (Delleur, 2007).

The phenomenon of recharge in natural soils represents a fundamental in the hydrologic cycle and in hydrologic modeling applications. A physically based model of

flow through the unsaturated zone is constituted by the Richards' equation (Fitts, 2002) and (Delleur, 2007).

$$\frac{\partial \theta}{\partial t} = \frac{\partial}{\partial z}\left[K(\theta)\left(\frac{\partial \psi}{\partial z} + 1 \right) \right]$$

where K is the hydraulic conductivity, ψ is the pressure head, z is the elevation above a vertical datum, θ is the water content, and t is time. Exact solutions of this equation are difficult due to a variety of reasons that include the strong nonlinear dependency of the parameters on the dependent variable and the difficulty of establishing the governing soil-water physical relationships, such as the water content versus pressure-head relationship and the hydraulic conductivity versus pressure head relationship. These curves are strongly nonlinear and are affected by the phenomenon of hysteresis in the presence of cyclic wetting and drying conditions occurring in natural watersheds. In addition, the pressure head at the ground surface (i.e., the top soil boundary condition) is controlled by mass balance and ultimately rainfall rate, which exhibits unusual time variability, difficult to characterize deterministically. Other complications involve the characterization of soil heterogeneity in the hydraulic conductivity. For these reasons, only a limited set of solutions to the Richards' equation has been developed under ideal laboratory assumptions. Even under such circumstances, the application of these solutions is difficult, and hydrologic engineers have traditionally opted for simple empirical equations of infiltration (Serrano, 1997).

In the past, special solutions of the horizontal and vertical infiltration, which represent the recharge equations under constant boundary conditions, were reported by soil physicists (e.g., Philip, 1955, 1972; Parlange, 1971; Philip and Knight, 1974). Exact solutions for constant flux infiltration using Lie Backlund transformations were reported

in Broadbridge and White (1988). Attempts to apply infiltration models to watershed conditions have adopted a domain discretization and a numerical approximation with special treatment (i.e., Freeze, 1971) or a linearization and an analytical solution. Dagan (1983), Yeh et al. (1985) and Serrano (1990 a, b).

Stochastic analyses have been helpful in characterizing soil parameter variability of infiltration. Serrano (1998) presented a procedure to approximate the water content version of the Richards' equation under constant boundary conditions with extensions to the stochastic characterization of hysteresis and temporal rainfall variability. Because of the data requirements, the application of these models is usually beyond the realm of practical field applications. Recent studies have focused on implicit numerical and semi-analytical algorithms of the nonlinear Richards' equation (e.g., El-Hames and Richards, 1995; Short and Dawesian White, 1995; Tabuada et al., 1995; Moldrup et al., 1996; Corradini et al., 1997, 2000; Romano et al., 1998; Stekauerovââ et al., 1999; Van Dam and Faddes, 2000; Zhang et al., 2002; Pachepsky et al. ,2003; Tartakovsky et al. ,2003).

Loaiciga (2003) conducted a review of climate change predictions and associated hydrologic consequences and presented the results of a case study of an aquifer in south-central Texas. The study considered a confined karst aquifer that receives recharge only in sections of streams that are hydraulically connected to the underlying water table. The impact of climate change on the indirect recharge was estimated using runoff scaling factors based on the ratio of historical and future streamflows predicted from linked general and regional climate models. The study also considered the impact of changes in pumping rates (i.e., predicted changes in groundwater use) on groundwater resources of the aquifer. The study concluded that the rise in groundwater use associated with predicted growth would pose a higher threat to the aquifer than climate change. Goddard

et al. (2001) stated that the variations in climate arise through a variety of temporal and spatial scales, making their observation very uncertain.

Vaccaro (1992) applied a depth percolate model (DPM) to estimate the consequence of climate change on recharge variability in a basin in the northwestern United States. He found that the variability in annual recharge was less in the GCM using historical data.

Delleur (2007) mentioned that Rosenberg et al. (1999) used the hydrologic model Soil & Water Assessment Tool (SWAT) and the GIS-based program Hydrologic Unit Model of the United States (HUMUS) (Arnold et al., 1998) to study the impact of climate change on the water yield and groundwater recharge of the Ogallala aquifer in the central United States. Three different General Circulation Models (GCMs) were used to predict changes in the future climate due to anticipated changes in temperature and CO_2 concentrations. The study found that recharge was reduced under all scenarios, ranging up to 77%, depending on the simulation conditions.

Eckhardt and Ulbrich (2003) investigated the impact of climate change on groundwater recharge and streamflow by using a revised version of the SWAT model. They simulated and adjusted stomatal conductance and leaf area in the SWAT model as a response to increased CO_2 levels, and they applied that simulation to a small catchment in Germany. Four different climate scenarios were considered based on simulations from five different GCMs. The results of the study indicated that more precipitation will fall as rain in winter due to increased temperatures, resulting in higher recharge and streamflow in January and February. They also found that the snowmelt will increase the recharge but will disappear in March disappears, while recharge and streamflow were shown to be potentially reduced in the summer months.

VanderKwaak (1999) developed a fully integrated surface water and groundwater model that rigorously considers the flow and transport processes on the land surface and in the variably saturated, dual-continua subsurface. The two-dimensional diffusion wave equation is used to describe the shallow surface water flow, while groundwater flow is described using the three-dimensional form of the Richards' equation. The linkage between the surface and subsurface systems is through first order, physically based flux relationships or through continuity assumptions. The entire system of equations is also solved simultaneously, resulting in a truly integrated model. The weakness of the model, however, is that it ignores important hydrologic processes such as interception and evapotranspiration, which can account for significant losses in long term flow simulations. Snowmelt processes are also ignored, limiting the application of the model to warmer climates or short-term simulations. Parameterization and the scaling problem between the surface and subsurface processes furthermore restrict the application of the model to smaller areas with small variations in properties or characteristics (VanderKwaak and Sudicky, 2000) (Delleur, 2007).

Croley and Luukkonen (2003) and Kirshen (2002) used MODFLOW to study the impact of climate change on groundwater. The results of the study indicated that the simulated groundwater levels were generally predicted to increase or decrease due to climate change, depending on the GCM. The results of the Kirshen (2002) study were mixed, showing higher, no different, and significantly lower recharge rates and groundwater elevations, depending on the climate scenario used.

Chapter 3

GSFLOW (Ground water and Surface water FLOW)

3.0 Introduction

GSFLOW (Ground water and Surface water FLOW) is the latest model developed by the US Geological Survey to simulate ground and surface water interaction. GSFLOW couples two existing models: the Precipitation-Run-off Modelling System (PRMS) and Modular Three-Dimensional Groundwater Flow Model. This combination of modeling surface runoff and groundwater recharge is a key characteristic that makes GSFLOW applicable for this research. (MODFLOW) is the name that has been given by U.S. Geological Survey (USGS) . By combining there two models, GSFLOW addresses the shortcomings of the each model when used independently. GSFLOW integrates three parts, namely:

1) partitioning of precipitation, snow melt, and soil moisture into overland flow, infiltration, evapotranspiration, interflow, and recharge;
2) routing of surface flow in channels; and
3) computing unsaturated flow and ground-water discharge. (Niswonger et al.,2006).

GSFLOW simulates infiltration, where compute infiltration during storm events using a modified Green and Ampt infiltration approach (Green and Ampt, 1911), runoff generation, and lateral flow in temporarily saturated material (i.e., interflow beneath storm-generated perched water tables) with physically based equations. Unsaturated-

zone flow beneath the soil zone is based on a 1-d kinematic-wave approximation to the Richards' equation.

The GSFLOW simulates the flow of water between the three regions. First region is bounded on top by the plant canopy and the bottom by the lower limit of the soil zone. Second region deals with all streams and lakes. Finally, is the subsurface zone beneath the soil zone. The PRMS module is used to simulate flow in the first region while MODFLOW-2005 simulates hydrologic activities in regions 2 and 3 (Niswonger et al., 2008). The following design principles were used in the creation of GSFLOW:

1) Use existing PRMS modules and MODFLOW-2005 packages where possible;
2) Use a flexible and adaptive modular design that incorporates both PRMS and MODFLOW-2005 programming frameworks so that existing and new PRMS and MODFLOW-2005 simulation techniques can be added to GSFLOW in the future;
3) Use general design procedures that can be used to integrate other simulation models into GSFLOW;
4) Allow simulations using only PRMS or MODFLOW-2005 within the integrated model for the purpose of initial calibration of model parameters prior to a comprehensive calibration using the integrated model;
5) Solve equations governing interdependent surface- water and ground-water flow using iterative solution techniques;
6) Compute model-wide and detailed (for example, soil- zone flow and storage) water balances in both time and space;
7) Allow flexibility in the spatial discretization of the hydrologic response units used for PRMS and the finite-difference grid used for MODFLOW-2005; and

8) Allow model boundaries to be defined using standard specified-head, specified-flow, and head-dependent boundary conditions to account for inflows to and outflows from the modeled region (Niswonger et al., 2008).

To make the combined models to work, some modifications in each individual model had to be made to make GSFLOW work. The modifications to PRMS and MODFLOW include:

1) development of algorithms relating the spatial discretization of MODFLOW relative to PRMS.
2) development of a new algorithm for routing overland- and inter-flow to the streams.
3) development of a feedback scheme where ground-water and surface-water interact in the soil zone.
4) combining the PRMS soil-moisture and subsurface-reservoirs into a single soil-zone reservoir; and
5) distributing runoff and interflow to associated stream reaches.

3.1 Organization of the GSFLOW

GSFLOW integrates five components.

1. The first "spatially distributes precipitation, temperature, and solar radiation and computes potential evapotranspiration, interception, snowmelt, and surface evaporation (PRMS)."
2. The second component divides precipitation into "surface infiltration, overland flow, evapotranspiration, interflow, and shallow seepage (PRMS Soil Zone)."

3. The third indicates the flow routes of channels and streambeds (SFR2).

An updated package of MODFLOW (Modular Ground-Water Flow Model; Harbaugh, 2005) contained a new family of packages for simulating processes in stream and the unsaturated zone. These packages include the SFR2 Package (Niswonger and Prudic, 2005) that routes flow in channels and streambeds and the UZF Package (Niswonger, et. al., 2006) that routes water through unsaturated zones.

The Streamflow-Routing Package (SFR2) is used in GSFLOW to route water in channels, to calculate streambed leakage, and to receive surface runoff and interflow from PRMS model. Simulating vertical seepage through a homogeneous unsaturated zone is by simplifying Richards' equation. "The approach assumes that unsaturated flow occurs in response to gravity potential gradients only and ignores negative potential gradients; the approach further assumes uniform hydraulic properties in the unsaturated zone for each vertical column of model cells. The Brooks-Corey function is used to define the relation between unsaturated hydraulic conductivity and water content. Variables used by the SFR2 Package include initial and saturated water contents, saturated vertical hydraulic conductivity, and an exponent in the Brooks-Corey function files as templates for new problems and to verify proper code installation"(Niswonger et al., 2006). It can be written in the vertical dimension as (Smith and Hebert 1983):

$$\frac{\partial\theta}{\partial t}=\frac{\partial q}{\partial z}=\frac{\partial}{\partial z}\left[D(\theta)\frac{\partial\theta}{\partial z}-K(\theta)\right], \tag{3.1}$$

where

θ is the water content (volume of water per volume of soil);

q is the water flux (volume of water per time per unit area);

K(θ) is the unsaturated hydraulic conductivity as function of water content(length per time);

D(θ) is the hydraulic diffusivity (length squared per time);

z is the elevation in the vertical direction (m);

t is time.

By assuming the vertical flux is driven by gravitational forces the diffusive term D(θ) is removed. And the equation (3.1) become the following:

$$q = -K(\theta), \tag{3.2}$$

where

q is the water flux as positive upward (volume of water per time per unit area)

Substituting equation (3.2) into equation (3.1), neglecting diffusive term yields:

$$\frac{\partial \theta}{\partial t} + \frac{\partial K(\theta)}{\partial z} = 0, \tag{3.3}$$

by obtaining the method of characteristics solution to equation (3.3) by dividing both sides by $\frac{\partial \theta}{\partial z}$ gives the following equation:

$$\frac{\partial z}{\partial t} = \frac{\partial K(\theta)}{\partial \theta} = v(\theta), \quad d\theta = 0 \ , \tag{3.4}$$

where $v(\theta)$ is the characteristic velocity, and q is a constant along a characteristic path. The characteristic velocity, which has positive and negative characteristics in the case of open channel flow. A decrease in the surface infiltration rate will cause internal drainage to occur, which is represented by a trailing wave.

The derivative $\frac{\partial K(\theta)}{\partial \theta}$ is discontinuous over a sharp wetting front fromneglecting diffusive term. The hydraulic diffusion for a wetting front in equation (3.1) one should integrating over a control volume containing a single wetting front (Charbeneau, 1984):

$$\frac{\partial}{\partial t}\int_{z_1}^{z_2}\theta\, dz + \left(K(\theta) - D(\theta)\frac{\partial \theta}{\partial z}\right)\Big|_{z_1}^{z_2} = 0\ , \tag{3.5}$$

z_1 and z_2 are points above and below the wetting front and $D(\theta)$ is neglected because $\frac{\partial \theta}{\partial z} \approx 0$ *at* z_1 *and* z_2 so eq.(3.5) becomes;

$$\frac{\partial}{\partial t}\int_{z_1}^{z_2}\theta\, dz + K(\theta_2) - K(\theta_1) = 0\ , \tag{3.6}$$

where $K(\theta_1)$ *and* $K(\theta_2)$ are the $K(\theta)$ at depth z_1 and z_2.

$$\int_{z_1}^{z_2}\theta\, dz = \theta_1(z_f - z_1) + \theta_2(z_2 - z_f)\ , \tag{3.7}$$

where; z_f is the depth of the sharp front. Equations (3.6) and (3.7) becomes the following equation after combining.

$$\frac{dz_f}{dt} = v_s(\theta_1, \theta_2) = \frac{K(\theta_1) - K(\theta_2)}{\theta_1 - \theta_2}, \tag{3.8}$$

where

v_s is the velocity of a sharp wetting front (length per time); θ_1 is the volumetric water content above a depth z_f; and θ_2 is the volumetric water content below a depth z_f.

The Brooks-Corey unsaturated hydraulic conductivity function can be used to evaluate $\frac{\partial K(\theta)}{\partial \theta}$, so

$$K(\theta) = K_s \left[\frac{\theta - \theta_r}{\theta_s - \theta_r} \right]^{\varepsilon}, \tag{3.9}$$

where

K_s is the saturated hydraulic conductivity; θ_s is the residual water content; θ_s is the saturated water content; and ε is the Brooks-Corey exponent. By taking the derivative of eq. (3.9) with respect to θ to find the velocity of the deepest point along a trailing wave. Also by approximating S_r with θ_r, and S_y with $\theta_s - \theta_r$

$$v(\theta) = \frac{\varepsilon K_s}{S_y} \left[\frac{\theta - \theta_r}{S_y} \right]^{\varepsilon - 1}, \tag{3.10}$$

To find a relation between the deepest point along a trailing wave and all other points, substituting eq.(3.10) into eq.(3.8) and results in:

$$z(\theta) = z_0 \left[\frac{\theta - \theta_r}{\theta_0 - \theta_r} \right]^{\varepsilon - 1}, \tag{3.11}$$

where

$z(\theta)$ is the depth of a point on a trailing wave; θ is the water content of a point; θ_0 *and* z_0 are water content and depth of the deepest point, respectively. A relation between water content and infiltration using equations (3.2) and (3.9) is:

$$\theta = \left(\frac{q_{in}}{K_S}\right)^{1/\varepsilon} (S_y) + \theta_r \qquad 0 \prec q_{in} \leq K_S \,, \qquad (3.12)$$
$$\theta = \theta_s \qquad\qquad K_S \prec q_{in} \,,$$

where θ is the water content of a wave generated from infiltration, and q_{in} is the vertical flux or infiltration rate (length per time). The water content is set to the saturated water content when the infiltration rate exceeds the saturated vertical hydraulic conductivity. The seepage out of the stream is computed using:

$$q = \frac{K}{m}(h_s - h_b) \,, \qquad (3.13)$$

where q is the infiltration rate; K is the saturated hydraulic conductivity of streambed sediments; hs is the hydraulic head in stream determined from top of streambed sediments; h_b is the hydraulic head at the bottom of the streambed; and m is the thickness of streambed sediment as defined by the user.

4. The fourth calculates the "vertical unsaturated flow below the soil zone (UZF)." The Unsaturated Zone Flow Package (Niswonger and others, 2006a) was developed for GSFLOW to simulate ground-water recharge and discharge to land surface by accounting for vertical flow through an unsaturated zone. One of approach solving the vertical flow through a homogeneous unsaturated zone is by simplifying Richards' equation. "The approach assumes that unsaturated flow occurs in response to gravity potential gradients only and ignores negative potential gradients; the approach further assumes uniform hydraulic properties in the unsaturated zone for each vertical column of model cells. The Brooks-Corey function is used to define the relation between unsaturated hydraulic conductivity and water content. Variables used by the UZF1 Package include initial and saturated water contents, saturated vertical hydraulic conductivity, and an exponent in the

Brooks-Corey function files as templates for new problems and to verify proper code installation"(Niswonger et al., 2006). It can be written in the vertical dimension as (Smith and Hebert 1983):

$$\frac{\partial \theta}{\partial t} = \frac{\partial q}{\partial z} - i = \frac{\partial}{\partial z}\left[D(\theta)\frac{\partial \theta}{\partial z} - K(\theta) \right] - i, \tag{3.14}$$

where

θ is the water content (volume of water per volume of soil);

q is the water flux (volume of water per time per unit area);

K(θ) is the unsaturated hydraulic conductivity as function of water content(length per time);

D(θ) is the hydraulic diffusivity (length squared per time);

i is the ET rate per unit depth (length per time per length);

z is the elevation above a vertical datum;

t is time.

By assuming the vertical flux is driven by gravitational forces the diffusive term D(θ) is removed. The equation (3.14) become the following:

$$q = -K(\theta), \tag{3.15}$$

where

q is the water flux as negative downward (volume of water per time per unit area)

Substituting equation (3.15) into equation (3.14), neglecting $\left[D(\theta)\frac{\partial \theta}{\partial z} \right]$, and evaporation is removed from the soil profile and all flow is downward vertical yields:

$$\frac{\partial \theta}{\partial t} + \frac{\partial K(\theta)}{\partial z} + i = 0, \tag{3.16}$$

by obtaining the method of characteristics solution to equation (3.16) by taking θ partially in terms of t and z:

$$\frac{\partial \theta}{\partial t} + \frac{\partial K(\theta)}{\partial \theta}\frac{\partial \theta}{\partial z} = -i, \tag{3.17}$$

and by using the equation of variation (Abbott,1966) (Niswonger et al., 2006):

$$\frac{\partial \theta}{\partial t} dt + \frac{\partial \theta}{\partial z} dz = d\theta, \tag{3.18}$$

so equation (3.17) and (3.18) can be written in matrix form

$$\begin{bmatrix} 1 & \dfrac{\partial K(\theta)}{\partial \theta} \\ dt & dz \end{bmatrix} \begin{bmatrix} \dfrac{\partial \theta}{\partial t} \\ \dfrac{\partial \theta}{\partial z} \end{bmatrix} = \begin{bmatrix} -i \\ d\theta \end{bmatrix}, \tag{3.19}$$

The determinant of the coefficient matrix in equation (3.19) and the determinants of the matrices obtained by substituting the right hand side vector for each column in the coefficient matrix are all zero; (Niswonger et al., 2006).

$$\begin{bmatrix} 1 & \dfrac{\partial K(\theta)}{\partial \theta} \\ dt & dz \end{bmatrix} = 0 \,, \tag{3.20a}$$

$$\begin{bmatrix} 1 & -i \\ dt & d\theta \end{bmatrix} = 0, \tag{3.20b}$$

$$\begin{bmatrix} -i & \dfrac{\partial K(\theta)}{\partial \theta} \\ d\theta & dz \end{bmatrix} = 0 \,, \tag{3.20c}$$

by expanding equations (2.20)(a,b,c) produce:

$$\frac{dz}{dt} = \frac{\partial K(\theta)}{\partial \theta} = v(\theta), \tag{3.21a}$$

The characteristic of this equation defines the velocity of a wave.

$$\frac{d\theta}{dt} = -i, \tag{3.21b}$$

The characteristic of this equation defines the change in water content of the wave with time of a wave.

$$\frac{d\theta}{dt} = \frac{-i}{v(\theta)}, \tag{3.21c}$$

The characteristic of this equation defines the change in water content of the wave with depth behind the wave.

where

$v(\theta)$ is the characteristic velocity restricted to the downward (positive z) direction (length per time) and θ decreases according to the ET rate along a characteristic path.

Neglecting the diffusive term in equation (3.14) causes the derivative $\frac{\partial K(\theta)}{\partial \theta}$ to be discontinuous over a sharp wetting front in the soil profile, so to consider the hydraulic diffusion for a wetting front in equation (3.14) one should integrating over a control volume containing a single wetting front (Charbeneau, 1984):

$$\frac{d}{dt}\int_{z_1}^{z_2}\theta\, dz+\left(K(\theta)-D(\theta)\frac{\partial\theta}{\partial z}\right)\Big|_{z_1}^{z_2}=0, \tag{3.22}$$

where

z_1 and z_2 are points above and below the wetting front and $D(\theta)$ is neglected because so $\frac{\partial\theta}{\partial z}\approx 0$ *at* z_1 *and* z_2 so equation (3.22) becomes;

$$\frac{d}{dt}\int_{z_1}^{z_2}\theta\, dz+K(\theta_2)-K(\theta_1)=0, \tag{3.23}$$

where $K(\theta_1)$ *and* $K(\theta_2)$ *are* the $K(\theta)$ at depth z_1 and z_2.

$$\int_{z_1}^{z_2}\theta\, dz=\theta_1(z_f-z_1)+\theta_2(z_2-z_f), \tag{3.24}$$

where; z_f is the depth of the sharp front. Equations (3.23) and (3.24) becomes the following equation after combining.

$$\frac{dz_f}{dt} = v_s(\theta_1, \theta_2) = \frac{K(\theta_1) - K(\theta_2)}{\theta_1 - \theta_2}, \tag{3.25}$$

where

v_s is the velocity of a sharp wetting front (length per time);

θ_1 is the volumetric water content above a depth z_f; and
θ_2 is the volumetric water content below a depth z_f .

The Brooks-Corey unsaturated hydraulic conductivity function can be used to evaluate $\frac{\partial K(\theta)}{\partial \theta}$, so

$$K(\theta) = K_s \left[\frac{\theta - \theta_r}{\theta_s - \theta_r} \right]^{\varepsilon}, \tag{3.26}$$

where

K_s is the saturated hydraulic conductivity; θ_r is the residual water content; θ_s is the saturated water content; and ε is the Brooks-Corey exponent. By taking the derivative of eq. (3.26) with respect to θ to find the velocity of the deepest point along a trailing wave. Also by approximating S_r with θ_r, and S_y with $\theta_s - \theta_r$

$$v(\theta) = \frac{\varepsilon K_s}{S_y} \left[\frac{\theta - \theta_r}{S_y} \right]^{\varepsilon - 1}, \tag{3.27}$$

To find a relation between the deepest point along a trailing wave and all other points, substituting eq.(3.27) into eq.(3.25) and results in:

$$z(\theta) = z_0 \left[\frac{\theta - \theta_r}{\theta_0 - \theta_r} \right]^{\varepsilon - 1}, \tag{3.28}$$

where

$z(\theta)$ is the depth of a point on a trailing wave; θ is the water content of a point;

θ_0 *and* z_0 are water content and depth of the deepest point, respectively.

5. Finally, the fifth calculates the ground-water flow (MODFLOW-2005). MODFLOW is the U.S. Geological Survey modular finite-difference flow model, which is a computer code that solves the groundwater flow equation. The USGS MODFLOW model (McDonald and Harbaugh, 1988), have been used to assess ground-water resource problems and to manage and develop ground-water supplies.

The governing partial differential equation or the three-dimensional movement of ground water of constant density through porous media used in MODFLOW is:

$$\frac{\partial}{\partial x}\left(K_{xx} \frac{\partial h}{\partial x} \right) + \frac{\partial}{\partial y}\left(K_{yy} \frac{\partial h}{\partial y} \right) + \frac{\partial}{\partial z}\left(K_{zz} \frac{\partial h}{\partial z} \right) + W = S_S \frac{\partial h}{\partial t} \tag{3.29}$$

where

- K_{xx}, K_{yy} and K_{zz} are the values of hydraulic conductivity along the x, y, and z coordinate axes (L/T)
- h is the potentiometric head (L)
- W is a volumetric flux per unit volume representing sources and/or sinks of water, where negative values are extractions, and positive values are injections (T^{-1})
- S_S is the specific storage of the porous material (L^{-1}); and
- t is time (T)

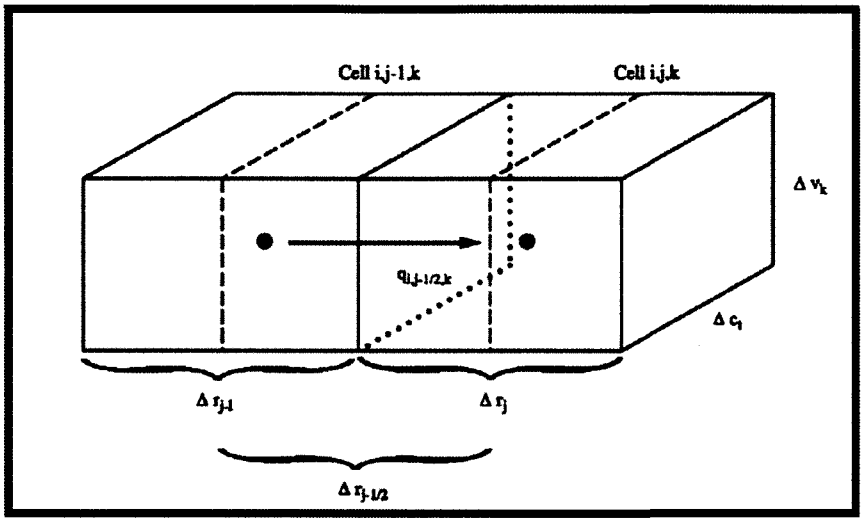

Figure (3. 1):Flow into cell i,j,k from cell i,j-1,k. (McDonald and Harbaugh, 2005)

Development of the ground-water flow equation in finite-difference form follows from the application of the continuity equation. The continuity equation expressing the balance of flow for a cell is:

$$\sum Q_i = SS\frac{\Delta h}{\Delta t}\Delta V \ , \tag{3.30}$$

where

Q_i is a flow rate into the cell (L3T-1);

SS has been introduced as the notation for specific storage in the finite-difference formulation; SS is the volume of water that can be injected per unit volume of aquifer material per unit change in head (L1); ΔV is the volume of the cell (L3); and

Δh is the change in head over a time interval of length Δt.

The finite difference form of the partial differential in a discretized aquifer domain (represented using rows, columns and layers) (figure 3.1) is:

$$q_{i,j-1/2,k} = KR_{i,j-1/2,k}\Delta c_i \Delta v_k \frac{(h_{i,j-1,k} - h_{i,j,k})}{\Delta r_{j-1/2}} \tag{3.31}$$

where

$h_{i,j,k}$ is the head at node i,j,k, and hi,j-1,k is the head at node i,j-1,k;

$q_{i,j-1/2,k}$ is the volumetric flow rate through the face between cells i,j,k and i,j-1,k ($L3T^{-1}$);

$KR_{i,j-1/2,k}$ is the hydraulic conductivity along the row between nodes i,j,k and i,j-1,k (LT^{-1});

$\Delta c_i \Delta v_k$ is the area of the cell faces normal to the row direction; and

$\Delta r_{j-1/2}$ is the distance between nodes i,j,k and i,j-1,k (L).

The previous equation gives the exact flow for a one-dimensional steady-state case through a block of aquifer.

Figure 3.2 shows how each component is organized and associated with the other.

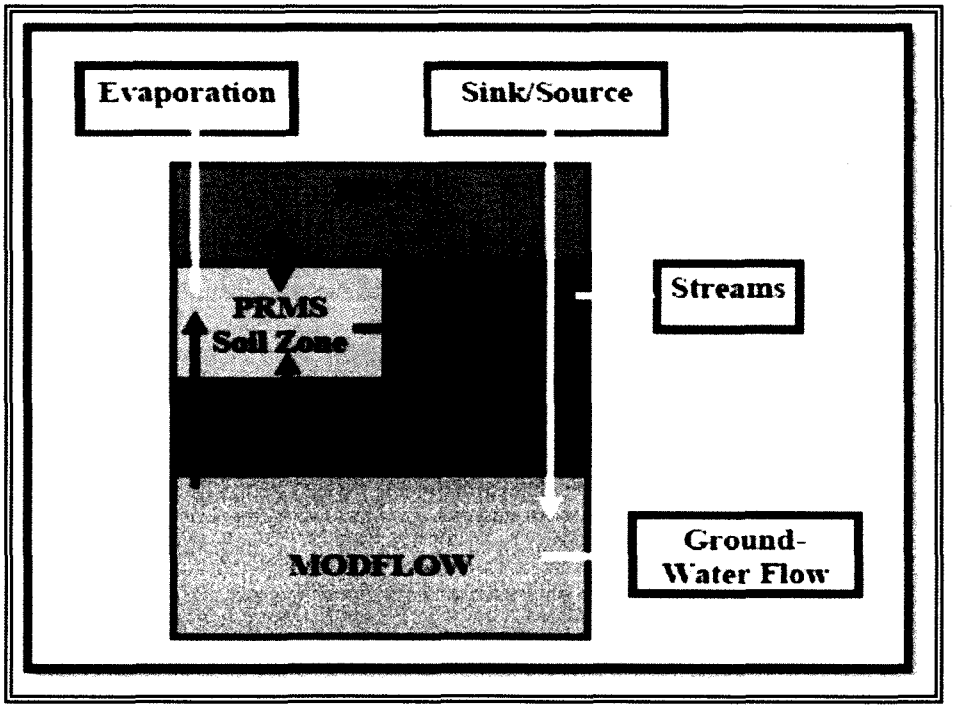

Figure (3.2): Diagram showing the five components of GSFLOW(Niswonger et al.,2006).

Using the MODFLOW-2005 and the Modular Modeling System (MMS), the five components are integrated. The modular programming frameworks allow users to attach their software to configure the system to fit their needs. Each component within GSFLOW represents a process in the hydrologic system. The program is flexible because it allows the addition of more components to "provide new or alternative numerical solutions for hydrologic processes." (Niswonger et al.,2008). Compatibility of the new components to spatial and temporal resolution is essential. Moreover, the principles involved in the development of GSFLOW are:

1) Modular design to allow new and existing simulation techniques to be added;
2) Standard PRMS and MODFLOW source code and data files are used without modification;
3) Spatial discretization is according to the requirements of each component;
4) Isolate integration algorithms from components; and
5) Use geographical information system (GIS) tools to relate spatial features between components.

The PRMS is implemented as a set of Modular Modeling System (MMS) models. The modules are written in Fortran or C Programming languages. The MMS was primarily developed to:

1) support developing, testing, and evaluation of physical-process models as compatible sets of computer code;
2) facilitate integration of user-selected codes into operational physical-process models;

3) facilitate the coupling of models for application to complex, multidisciplinary problems; and

4) provide utility software for optimization, sensitivity, forecasting, visualization, and statistical analyses (Niswonger et al.,2008).

With the integration of the PRMS and the MODFLOW-2005, the flow is exchanged among the three regions of GSFLOW namely, Region 1 - Plant canopy, snowpack, surface-depression storage, and soil zone (PRMS), Region 2 - Streams and lakes (MODFLOW-2005), and Region 3 - Subsurface (unsaturated and saturated zones) beneath soil zone(MODFLOW-2005). A total of 25 PRMS modules and 16 MODFLOW-2005 packages are implemented in GSFLOW. The modules are reformatted and use Fortran language for upgrade ability. There are three simulation modes allowable in GSFLOW, integrated, PRMS only and MODFLOW-2005 only. To meet the requirements of the integrated program, some changes in the PRMS include:

1) a new Hydrological Response Unit (HRU)-based distribution method for solar radiation that may improve the calculations of evapotranspiration and the energy budget of the snowpack;

2) a new Cascade Module designed to simulate more complex flow paths in watersheds;

3) a new Soil-Zone Module designed to link with MODFLOW-2005; and

4) a new type of Hydrological Response Unit (HRU) designed to link precipitation and evaporation with the Lake Package in MODFLOW-2005.

As to the MODFLOW-2005 program, a few refinements were introduced to allow integration. Revisions to the Streamflow-Routing Package were made "so that streams

can receive surface runoff and interflow from HRUs and for kinematic-wave routing of streamflow down channels." (USGS, 2008). The Lake Package was also modified "to link a MODFLOW designated lake with a lake HRU, to refill intermittent lakes from surface–water inflow, and to simulate unsaturated flow beneath lakes."

The two modules integrated remain independent programs within GSFLOW. GSFLOW is organized using two computation control modules - one for PRMS (gsflow_prms) and another for MODFLOW-2005 (gsflow_modflow)." For time-step incrementing, GSFLOW follows the standards applied to PRMS. Five new modules were incorporated in GSFLOW written in Fortran 90. The following describes the function of each new additional module.

1) Module gsflow_setconv computes unit conversions between PRMS and MODFLOW-2005.
2) Modules gsflow_prms2mf and gsflow_mf2prms integrate the spatial units and transfer dependent variables and volumetric flow rates between PRMS and MODFLOW-2005.
3) Module gsflow_budget is used to compute and write an overall water budget for the simulated system; and
4) Module gsflow_sum is used to produce detailed water budgets for all flow components.

3.2 Concepts and Design

In order to make predictions about hydrological behavior and features, it is essential that "the conditions of flow and storage of water both above and below land

surface affect water resources, these conditions often need to be simulated together (coupled) to make predictions." (Niswonger, et al., 2006) Several concepts provide GSFLOW the framework to make calculations. GSFLOW uses "physically based equations to describe critical processes in the soil zone (the uppermost part of the unsaturated zone), including infiltration, runoff generation, and lateral flow in temporarily saturated material." For example, in determining the flow through the unsaturated zone beneath the soil zone, the program borrows from the "kinematic-wave approximation" of Richard's equation. Determining the flow in streams is "routed while considering interaction with ground water." Precipitation is divided between "evapotranspiration, runoff, infiltration, and storage by balancing daily energy and mass budgets of the snowpack, soil zone, and unsaturated zone."

3.3 Conversion of Units

The PRMS module measures volume in acre-inches and volumetric flow rates are expressed in acre-inch per day while MODFLOW-2005 use cubic length to measure volume and volumetric flow rates are expressed in units of cubic length per time (Markstrom, et al., 2008). Volume flow rates are converted from PRMS to MODFLOW-2005 and vice versa depending on how the rates were transferred (PRMS to MODFLOW-2005 or MODFLOW-2005 to PRMS).

3.4 Computations of Flow

3.4.1 Temperature

Option 1 – Calculation for data if one or more measurement stations are available (module temp_1sta_prms) (Markstrom, et al., 2008)

$$T_{HRU}^{m} = T_{sta}^{m} - b_{month}\left(\frac{Z_{HRU} - Z_{tsta}}{1000}\right) - taf_{HTU} \tag{3.32}$$

Where,

T $^{m}_{HRU}$ = min/max of daily temperature at each HRU for time step m in Fahrenheit or Celsius. T $^{m}_{STA}$ = min/max of daily temperature at each station for time step m in Fahrenheit or Celsius. b_{month} = the monthly maximum (or minimum) daily temperature lapse rate representing the change in maximum (or minimum) air temperature per 1,000 feet or meters of altittude change for each month, January to December parameter (or), in degrees Fahrenheit or Celsius per 1,000 length units. Z_{HRU} = mean land-surface altitude of the HRU. Z_{tsta} = altitude of air temperature measurement station. taf_{HRU} = min/max daily HRU temperature adjustment factor in Fahrenheit or Celsius.

Option 2 – Calculation for data if data are from at least two stations at different altitudes are used to estimate air temperature of each HRU. (module temp_laps_prms) (Markstrom, et al., 2008)

$$T_{HRU}^{m} = T_{base}^{m} + \left(T_{lapse}^{m} - T_{base}^{m}\right)\left(\frac{Z_{HRU} - Z_{base}}{Z_{lapse} - Z_{base}}\right) - taf_{HRU} \tag{3.33}$$

Where,

T^{m}_{base}= the monthly maximum (or minimum) daily temperature at base station assigned to an HRU in degrees Fahrenheit or Celsius. T^{m}_{lapse} = the monthly maximum (or minimum) daily temperature lapse at the lapse station assigned to an HRU in degrees Fahrenheit or Celsius. Z_{lapse}= altitude at lapse station in length

Z_{base} = altitude at base station in length

Option 3 - uses a three-dimensional multiple-linear regression based on longitude (x), latitude (y), and altitude (z) to distribute temperature from two or more stations (module xyz_dist).

$$T^{m}_{HRU} = c_{T1} + c_{T2} - taf_{HRU}$$

(3.33a)

$$c_{T1} = bt_{X,month}\bar{X}_{HRU} + bt_{Y,month}\bar{Y}_{HRU} + bt_{Z,month}\bar{Z}_{HRU}$$

$$c_{T2} = \bar{T}^{m}_{stas} - \left(bt_{X,month}\bar{X}_{sta} + bt_{Y,month}\bar{Y}_{sta} + bt_{Z,month}\bar{Z}_{sta}\right)$$

(3.33b)

Where $bt_{x,month}, bt_{y,month}$, *and* $bt_{z,month}$ are the maximum(or minimum) air temperature regression coefficient for longitude, latitude, and altitude, respectively by month (in degrees Fahrenheit or Celsius,

$\bar{X}_{HRU}$, $\bar{Y}_{HRU}$, $\bar{Z}_{HRU}$ are the normalized, longitude, latitude, and altitude, respectively of HRU dimensionless.

$\bar{X}_{sta}$, $\bar{Y}_{sta}$, $\bar{Z}_{sta}$ are the mean normalized, longitude, latitude, and altitude of all stations , respectively, dimensionless.

Option 4 - weights measured daily air temperatures from two or more stations by the inverse of the square of the distance between the centroid of an HRU and each station location (module temp_dist2_prms) (Markstrom, et al., 2008)

$$b_{lapse}^{m} = \sum_{i=1}^{ntstas} X_i^2 \left(\left(T_i^m - T_{i+1}^m \right) / \left(Z_{tsta,i} - Z_{tsta,i+1} \right) \right) / ntstas \tag{3.34}$$

$$T_{HRU}^{m} = \frac{\sum_{i=1}^{ntstas} \left[\left(T_i^m - \left(b_{lapse}^m \frac{Z_{HRU} - Z_i}{1{,}000} \right) \right) \left(Ldist_{HRU,i} \right)^2 \right]}{\sum_{i=1}^{ntstas} \left(Ldist_{HRU,i} \right)^2} - taf_{HRU} \tag{3.35a}$$

$$Ldist_{HRU,i} = 1 / \left(\sqrt{\left(Y_{HRU} - Ytemp_i \right)^2 + \left(X_{HRU} - Xtemp_i \right)^2} \right) \tag{3.35b}$$

where

b_{lapse}^{m} is the daily basin average maximum or minimum temperature lapse rate for time step m, in degrees Fahrenheit or Celsius per length. T_i^m *and* T_{i+1}^m are the measured maximum or minimum temperature at measurement station i and i+1 for time step m,in degrees Fahrenheit or Celsius. $Z_{tsta,i}$ *and* $Z_{tsta,i+1}$ are the latitudes of measurement station i and i+1 in length; and nstas is number of air temperature dimensionless.

3.4.2 Precipitation

Precipitation is measured in one or more stations. Each is extrapolated at each HRU with the altitudes measured in feet or meters.

Equation 3.36 – Measuring precipitation as rain.

$$Frain_{HRU}^{m} = \left(\frac{T_{mx_{HRU}^{m}} - T_{mxsnow_{HRU}}}{T_{mx_{HRU}^{m}} - T_{mn_{HRU}^{m}}} \right) pmixaf_{month} \tag{3.36}$$

where

$Frain^{m}_{HRU}$ is the decimal fraction of total precipitation occurring as rain on an HRU for time step m, dimensionless; $T_{mx}{}^{m}{}_{HRU}$ and $T_{mn}{}^{m}{}_{HRU}$ are the maximum and minimum air temperture assigned to HRU for time step m; $pmixaf_{month}$ is the monthly rain adjustment factor for a mixed precipitaion event.

Equation 3.37 – Equation used to calculate daily precipitation at HRU

$$P_{HRU}^{m} = P_{sta}^{m} \; CF_{HRU} \tag{3.37}$$

Where,

$P^{m}{}_{HRU}$= precipitation at the HRU during time step m, in inches

$P^{m}{}_{sta}$ = precipitation at the station during time step m, in inches

CF_{HRU}= monthly correction factor as a decimal fraction used to adjust rain or snow at HRU, no units.

Equation 3.38 – Three-dimensional multiple regression to calculate distribution of precipitation from two or more stations (Markstrom, et al., 2008).

$$
\begin{aligned}
P_{HRU}^{m} &= c_{P1} + c_{P2} - CF_{xyz}, \\
c_{P1} &= bp_{X,month}\bar{X}_{HRU} + bp_{Y,month}\bar{Y}_{HRU} + bp_{Z,month}\bar{Z}_{HRU}, \\
c_{P2} &= \bar{P}_{stas}^{m} - \left(bp_{X,month}\bar{X}_{HRU} + bp_{Y,month}\bar{Y}_{HRU} + bp_{Z,month}\bar{Z}_{HRU}\right),
\end{aligned}
\tag{3.38}
$$

Equation 339 - weights measured precipitation from two or more stations by the inverse of the square of the distance between the centroid of an HRU and each station location.

$$
P_{HRU}^{m} = \frac{\sum_{i=1}^{npstas}\left[\left(CF_{HRU,\,rain}P_{i}^{m} + CF_{HRU,\,snow}P_{i}^{m}\right)\left(Ldist_{HRU,\,i}\right)^{2}\right]}{\sum_{i=1}^{npstas}\left(Ldist_{HRU,\,i}\right)^{2}}
\tag{3.39a}
$$

$$
CF_{HRU,rain} = \frac{\bar{R}ain_{HRU,\,month}}{\bar{P}_{sta,\,month}},
$$

for monthly fraction of precipitation that is rain, and

$$
CF_{HRU,\,snow} = \frac{\bar{S}now_{HRU,\,month}}{\bar{P}_{sta,\,month}},
\tag{3.9)(b,c,d}
$$

for monthly fraction of precipitation that is snow

3.4.3 Solar Radiation

Solar radiation for each HRU is computed based on the hours between sunrise and sunset for each day of the year.

Equation 3.40- Daily estimates of obliquity (Markstrom, et al., 2008)

$$E^m = 1 - [EC * \cos(jd - 3) * rad], \tag{3.40}$$

where: E_m is the obliquity of the sun's eclipitic for time step m, in angular degree; EC is the eccentricity of the earth's orbit(~0.01671), in radians; jd is the julian day number(3 is subtracted as the solar year begins on December 29), in days, and rad is the revolution speed of the earth (~0.0172), in radians per day.

Equation 3.41 – Daily estimates of declination.

$$\begin{aligned} DM^m = {} & 0.006918 - 0.399912 * \cos(E_{rt}) + 0.070257 \\ & * \sin(E_{rt}) - 0.006758 * \cos(E_{rt}) \\ & + 0.000907 * \sin(2 * E_{rt}) - 0.002697 \\ & * \cos(3 * E_{rt}) + 0.00148 * \sin(3 * E_{rt}), \end{aligned} \tag{3.41}$$

where: DM_m is the solar declination for time step m in angular degree; and E_{rt} = rad*(jd-1)

Equation 3.42 – Computing for the angle between the local meridian and the sunset (sunrise) meridian.

$$ss^m = \cos^{-1}[-\tan(lat)\tan(DM^m)]\ , \qquad (3.42)(a,b,c)$$

$$sr^m = -ss^m, \text{ and}$$

$$sh^m_{HRU} = \frac{\left(ss^m_{HRU} - sr^m_{HRU}\right)24}{2\pi}\ ,$$

where:

ss^m is the hour angle of sunset, measured from the local meridian of a horizontal surface (HRU or equivalent-slope surface) for time step m, in radians. Sr^m is the hour angle of sunrise, measured from the local meridian of a horizontal surface (HRU or equivalent-slope surface) for time step m, in radians. ss^m_{HRU} is the hour angle of sunset on the sloped surface of HRU for time step m , in radians. sr^m_{HRU} is the hour angle of sunrise on the sloped surface of HRU for time step m , in radians. *lat* is the latitude of the horizontal surface (basin centroid) positive values are in the northern hemisphere and negative values are in the southern hemisphere, in radians.

Equation 3.43– Calculating daily potential solar radiation at each HRU (Markstrom, et al., 2008).

$$Rsp^m_{HRU} = sc^m\left(c1_{PSR} + c2_{PSR}\right),$$

$$c1_{PSR}\sin(DM^m)\sin(lat'_{HRU})sh^m_{HRU}, \quad and$$

$$c2_{PSR} = \frac{\cos(DM^m)\cos(lat'_{HRU})\left[\sin(ss^m_{HRU} + long'_{HRU}) - \sin(sr^m_{HRU} + long'_{HRU}\right]24}{2\pi}$$

(3.43)(a,b,c)

3.4.4 Potential Evaporation

Option 1 - (module potet_hamon_hru_prms) PET is computed as a function of daily mean air temperature and possible hours of sunshine.

$$PET^m_{HRU} = HC_{HRU}\left(\frac{sh^m_{HRU}}{12}\right)^2 \rho_{HRU}\ , \quad and$$

$$\rho_{HRU} = 216.7\frac{6.108e^{17.26939\frac{\bar{T}_{HRU}}{\bar{T}_{HRU}+273.3}}}{\bar{T}_{HRU}+273.3}, \tag{3.44}$$

Option 2 - (module potet_jh_prms) Modified Jensen-Haise formulation (Jensen and others, 1969), in which potential evapotranspiration is computed as a function of air temperature, solar radiation, and two coefficients that can be estimated using regional air temperature, altitude, vapor pressure, and plant cover (Markstrom, et al., 2008).

$$PET^m_{HRU} = JH_{month}\left(\bar{T}_{HRU} - JH_{HRU}\right)\frac{Rasw^m_{HRU}}{2.54\lambda_{HRU}}, \quad and$$

$$\lambda_{HRU} = 597.3 - \left(0.5653\bar{T}_{HRU}\right), \tag{3.45}$$

Option 3 - (module potet_pan_prms) Used if pan evaporation data from one or more measurement stations are available (Markstrom, et al., 2008)

$$PET_{HRU}^{m} = Pancoef_{month} Panecap_{sta}^{m}, \tag{3.46}$$

Chapter 4

METHODOLOGY

4.0 Overview

Most hydrological processes have some level of randomness and uncertainty. Rainfall is one of the hydrological processes that are generally described by probability functions. Modeling precipitation is of importance to several disciplines in science and engineering. The use of generation of synthetic precipitation data for hydrologic systems allows one to get the answer for the system for many of the possible hydrologic scenarios and the result thus obtained can be considered representative of the future behavior of the system.

Systems such as agricultural planning, e.g. the optimum planting and cropping time, reservoir and watershed management, erosion prediction, design of landfills, and design of facilities for storage and disposal of hazardous wastes require. Simulation models very detailed (spatially and temporally) rainfall forecast consider rainfall as a random process, attempting to simulate daily rainfall sequences that are ``representative" of the observed record. Most precipitation simulation models reproduce only a few of the features that characterize daily rainfalls. In this chapter, the frequency analysis for rainfall amount is presented by using two common methods of empirical frequency analysis based on plotting position and probability models.

This chapter will focus on the most common plotting formula used in empirical frequency analyses. However the probability models present a wide range of distributions that have been used to fit historical sequences. Examples of frequency analyses are the

Weibul distribution, the exponential distribution, the gamma distribution, a skewed normal distribution and the kappa distribution. On other hand rainfall occurrence has be modeled by using Markov chain, the truncated negative binomial distribution, and the Poisson distribution. This chapter will explain the stochastic rainfall occurrence model and the stochastic rainfall amount model that used. Moreover this chapter also will spot on the proposed model, simulation process and scenarios of precipitation that proceed in this research.

4.1 Stochastic Rainfall occurrence Model

Rainfall forecast models are key inputs to many important water resource projects. The actual magnitude of future rainfall is important in most water resources applications but certain physical systems depend on the occurrence of rainfall rather than its magnitude e.g. short-term municipal water demand process. Many researchers have employed the occurrence of rainfall as a significant input variable rather than the magnitude of rainfall in water demand modeling and management. One can find numerous articles in the literature focusing on the modeling of rainfall magnitude based on the affecting climatic variables; however, it is difficult to find articles about modeling the occurrence of rainfall. Therefore, it is important to develop mathematical models that can predict the occurrence of rainfall.

4.1.1 Markov chain

The Markov chain is a stochastic process with a finite number of states in which the probability of occurrence of a future state is conditional only upon the current state; past states are inconsequential. In hydrology, Markov chains have been used for modeling processes such as rainfall and stream flow. Gabriel and Neumann (1962) developed a Markov chain model for daily rainfall, and also modeled the occurrence of dry and wet days in daily rainfall.

To define the Markov chain lets presume X*(t)* to be a discrete-value process which started at time *0* and developed through time *t*. The values that the *X(t)* process takes on are denoted by x_t, $t = 0,1,\ldots\ldots\ldots\ldots$ Then

$$P\left[X(t)=x_t \mid X(0)=x_0, X(1)=x_1, \ldots\ldots, X(t-1)=x_{t-1}\right] \tag{4.1}$$

This represents the probability of the processes begin equal to x_t at time t, given its entire history. If the foregoing probability simplifies to

$$P\left[X(t)=x_t \mid X(t-1)=x_{t-1}\right] \tag{4.2}$$

This means that the outcome of the process at time t can be defined by using only the outcome at time $t-1$. This process is a first-order Markov chain.

The notation $X(t)=j, j=1,\ldots\ldots,r$ will be used instead of x_t

Where: $j=1$ for dry day (no rain) $j=2$ for a wet day

Figure 4.1 shows schematically the definition of states. A simple Markov chain is defined by its transition probability matrix *P(t)* which is a square matrix with elements $p_{ij}(t)$ given by

$$p_{ij}(t)=P[X(t)=j|X(t-1)=i]$$

or all *i,j* pairs

$$\sum_{j=1}^{r} p_{ij}(t)=1 \qquad i=1,.....,r \tag{4.3}$$

(4.4)

Assume that the chain is in state i and after n time steps it is in state j, so the transition probability from *i* to *j* in n time steps is given by Parzen (1962)

$$p_{ij}^{(n)}=\sum_{k=1}^{r} p_{ik}^{(n-1)}\ p_{kj} \qquad n \succ 1 \tag{4.5}$$

The probability distribution of the chain being at any state j at time t is denoted by

$$q_j(t)=P[X(t)=j] \quad , \quad j=1,.....,r \tag{4.6}$$

The marginal distribution of the process given by.

$$q_j(t)=\sum_{i=1}^{r} q_j^{(0)}\ p_{ij}^{(t)} \tag{4.7}$$

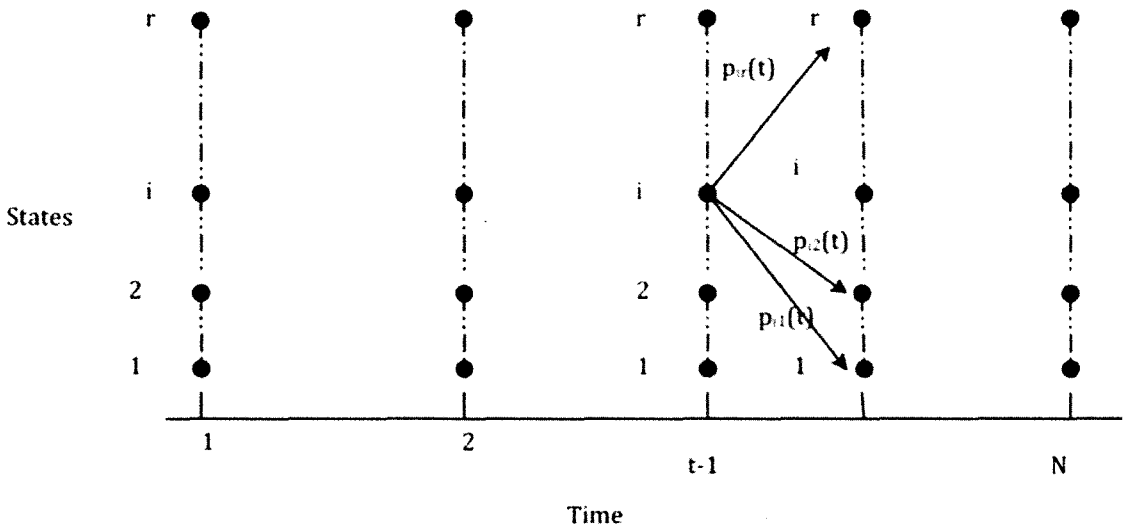

Figure (4.1): Definition of states for Markov chain X(t) and the corresponding transition probability $p_{ij}(t)$, j=1,.....,r.

4.2 Stochastic Rainfall amount Model

The modeling of daily rainfall amounts has been the point of much discussion in past research. There are many difficulties that are encountered when modeling rainfall amounts and many suggestions as to how they can be overcome. One of the more prominent difficulties involves the continuity of the data. If particular day is dry, then a rainfall amount of exactly zero is observed. If it rains, then an observed amount greater than zero is recorded. For this reason we have considered the rainfall process as two separate circumstances. One circumstance includes a model for whether a particular period of time will be dry or wet. The second circumstance examines the amount of rain when the day is wet. A probabilistic distribution function, also known as a mathematical model, is a method developed for describing the distribution of a random variable and

making probability statements. Empirical frequency techniques depend on the order of the sample. Values are arranged in increasing order of magnitude and probability assigned by empirical formula. Exponential probability distribution model have been used for fitting the distribution of hydrologic data. In this section, empirical and exponential probability distribution models are described.

4.2.1 Empirical a non-parametric distribution

An empirical frequency distribution (EFD) is a non-parametric or distribution free methods which do not rely on assumptions that the data are drawn from a given probability distribution method for building probability estimates of the cumulative distribution function (CDF) of a random variable (X). Empirical frequency distributions are typically used to estimate the probability distribution function (mathematical model) that might best fit the given data (Salas et. al., 2002). A plotting-position equation is used to estimate the CDF. The median plotting position estimates the non-exceedance probability as:

$$F(i) = P(X \leq x_i) = \frac{(i-\alpha)}{(N+\beta-2\alpha)}, \quad i = 1, \ldots\ldots\ldots, N \tag{4.8}$$

where:

$F(i)$ is non-exceedance probability estimate for the i the smallest event;

i is the order number of the event from smallest to largest;

N is the number of events or size;

ß is a coefficient;

α is a coefficient that depends on the parent distribution of the random variable x (in this case rainfall, r). The steps for determining the CDF are:

1. Arrange the data in increasing order of magnitude.
2. Denote the arranged series by $x_1, x_2, \ldots, x_i, \ldots x_n$.
3. Assign a probability $F(i) = P(X \leq x_i)$ for each value x_i by using the plotting position equation. To account for data record repetition, repeat values were given the same rank number (Viessman and Lewis, 1996).

Haan (1977) notes five criteria for plotting position relationships: "First, the plotting position must be such that all observations can be plotted. Secondly it should lie between m-1/n and m/n. Third, the return period equal or larger than the largest observation and the return period equal or smaller than the smallest observation. Fourth the observations should be equally spaced on the frequency scale. Finally the plotting position should have an intuitive meaning, be analytically simple, and easy to use". This research used the plotting position of the Weibull formula (1939). Where $\alpha = 0$ and $\beta = 1$, the Weibull formula meets all five of the above criteria.

4.2.2 Exponential distribution

The exponential distribution is a commonly used distribution in reliability engineering. Mathematically, it is a fairly simple distribution, which many times leads to its use in inappropriate situations. The exponential distribution is used to model hydrologic processes. For instance, rainfall intensity at a point and duration of storm rainfall has been assumed to be exponential distribution by Eagleson 1978, and Rodriguez-Itrube and other (1984). Parzen (1962) also applied an exponential distribution for the time between storms if a Poisson process generates the storms. The exponential

distribution is a special case of a gamma distribution. The density function of the exponential distribution with two parameters is given by Johnson and Kotz, (1970).

$$f(x)=\frac{1}{\alpha}\exp\left[-\frac{(x-x_0)}{\alpha}\right] \tag{4.9}$$

where $x_0 \leq x \prec \infty$, $\alpha \succ 0$, *and* x_0 *and* α are the location and the scale parameters, respectively. The cumulative distribution function of the exponential distribution with two parameters is

$$F(x)=1-\exp\left[-\frac{(x-x_0)}{\alpha}\right] \tag{4.10}$$

The population moments are given by the following relations:

$$\mu = x_0 + \alpha \tag{4.11}$$

$$\sigma^2 = \alpha^2 \tag{4.12}$$

The coefficients of skewness and kurtosis are:

$$\gamma = 2 \tag{4.13}$$

$$\kappa = 9 \tag{4.14}$$

4.3 Generation stochastic model of synthetic data.

Precipitation occurrence and intensity are two processes within a simulated precipitation event (Richardson, 1981; Richardson et al., 1984; Wilks, 1999). First, whether the simulated day is a wet day or dry day must be known. There are several methods to simulate precipitation, including two-state (precipitation either occurs or it does not) first order Markov Chains. . Since the first order Markov Chain is relatively simple and widely applicable, it was used in most of this type of research. Models of this kind are adopted for simulating daily rainfall records of any length, based on simulating occurrences and rainfall amounts separately. The amount of rain can be generated using an exponential distribution model that was fitted to the historical time series of the amount of rain for the rainy days. The estimation of parameter is needed for transitional probabilities for occurrences and fitting parameters through a frequency distribution for rainfall amounts. This research presented used a first order Markov Chain for generation of a wet on dry day and exponential distribution for the amount of rain.

4.4 The Proposed Model

Climate change can impact both the patterns and magnitude a precipitation events. Most climate studies have discussed the potential changes in the magnitude of precipitation as opposed to the potential changes in the patterns of rainfall. For example, one possible impact of climate change is that precipitation may be distributed in similar pattern; however, there may be an increase in heavy precipitation events. The model this kind of scenario one approach is to hold the pattern of precipitation constant and then change the magnitude of the precipitation events on the wet days. This can be

accomplished by using the historical pattern of dry and wet days and then on the wet days stochastically generating a precipitation event that is either increased or decreased on average from the historical record.

Modeling potential changes in the pattern of precipitation is more difficult due to the presence of seasonality. If seasonality is to be preserved then the seasonality must be characterize and the number of dry days and wet days within a season must be stochastically generated. If seasonality is not to be preserved then the question becomes how to alter the seasonality. One possibility is that the seasonality might be accentuated were more the rainfall occurs over a shorter portion of the year. Another possibility is that the seasonality might be lessened and the precipitation might become uniform throughout the year. To create such a scenario where the impact of seasonality is lessened, the number of dry days and wet days within a year might be stochastically generated without regard to seasonality. This will have the impact of basically removing seasonality and creating a more equal distribution precipitation throughout the year.

The focus of this study was to characterize the response of recharge to potential changes in precipitation where the basic seasonality of precipitation does not change; however, the magnitude of the precipitation might increase or decrease. Most of the precipitation scenarios generated in this study were of this type. For comparison purposes, two precipitation scenarios were created where the seasonality of rainfall was removed and only the magnitude of precipitation were varied.

4.5 Simulation Process

The daily precipitation scenarios are generated from a stochastic model that

captures the statistical properties of the historical observations. The generated scenarios are then used to drive various process models, - the GSFLOW Model hydrologic models (for recharge)- and consequently, to provide probabilistic scenarios of the variables of interest. Traditional generators, also known as "parametric" weather generators, typically use precipitation as the driving variable (Jones et al., 1972; Nicks and Harp, 1980; Richardson, 1981). In this study, the precipitation occurrence (i.e., wet or dry) is generated by a first state Markov Chain model and the rainfall amount on a wet day from an exponential density function (PDF) fitted to the observed data.

4.5.1 First part - generation of the occurrence of rainfall

1. A uniform random number between [0,1] is generated, say, U_1. It was developed for each day at every year.
2. The precipitation state of day 1 (S_1) is dry if $U_1 \leq (P_0)$ or wet if $U_1 > (P_0)$ (see table (5.4) for both stations).
3. To decide the rain stage for the rest of the days, the transition probability matrix (the average matrix) was used.

1. If "Rain stage $_{(i-1)}$" and $U_i \leq (P_{00})$, then "Rain stage $_{(i)}$" =0. Otherwise, "Rain stage $_{(i)}$" =1.
2. If "Rain stage $_{(i-1)}$" and $U_i \leq (P_{10})$, then "Rain stage $_{(i)}$" =0. Otherwise, "Rain stage $_{(i)}$" =1.
3. Using the above-mentioned Markov process, the occurrence of rainfall for the entire generated record was determined.

Assuming that the occurrence of precipitation for each day is an independent random

process. This assumes the occurrence of rainfall is uncorrelated and seasonality is not preserved.

1. The probabilities P_0 and P_1 were obtained from the historical record (see table (5.1)).
2. The transition probabilities consider the temporal dependence in the occurrence of rainfall. This is the advantage of this Markov Chain model, which is parameterized by the transition probability matrix, and it is defined:

P_{00} = Transition probability to have a dry day, given a dry day in the previous day

P_{01} = Transition probability of having a rainy day, given a dry day in the previous day

P_{10} = Transition probability of having a dry day, given a rainy day in the previous day

P_{11} = Transition probability of having a rainy day, given a rainy day in the previous day

The transition probability matrix (TPM) is calculated by the following equations for every year of the historical record for both stations.

$$TP_{00} = \frac{\sum_{i=1}^{N} P_{00}}{\sum_{i=1}^{N} P_{00} + \sum_{i=1}^{N} P_{01}} \quad and \quad TP_{01} = \frac{\sum_{i=1}^{N} P_{01}}{\sum_{i=1}^{N} P_{00} + \sum_{i=1}^{N} P_{01}}$$

$$TP_{10} = \frac{\sum_{i=1}^{N} P_{10}}{\sum_{i=1}^{N} P_{10} + \sum_{i=1}^{N} P_{11}} \quad and \quad TP_{11} = \frac{\sum_{i=1}^{N} P_{11}}{\sum_{i=1}^{N} P_{10} + \sum_{i=1}^{N} P_{11}}$$

4.5.2 Second part - generation of the amount of rainfall

Once the occurrence of rainfall has been generated, a fitted exponential distribution model was used to estimate the amount of rain in every day with rain. The cumulative

distribution function CDF, in equation (4.10). The generation of the amount of rain is determined by using:

$$X = -\alpha \ln(1 - F(x)) \tag{4.15}$$

where F(x) is the probability obtained from a generated uniform random number(0-1). Again, the generated random numbers represent the values of the probabilities F(x), used in equation (4.15).

4.6 Scenarios of Precipitation

In addition to global changes, the US Global Change Research Program. reported the following general predictions that the entire US is projected to have increases and decreases in precipitation. In which the average US precipitation has increased by 5-10% over the last century and the decreased exceeding 20%. The largest percentage increases in precipitation are projected to be in the Southwest and Southern California, where in the Sierra Nevada much of the increased precipitation is likely to fall as rain rather than snow.

To evaluate the response of groundwater recharge to potential changes in precipitation the following scenarios were evaluated:

- **First Scenario:** Precipitation is projected to increase, with an average change ranging between 5 and 45 percent, using 10 percent increments with the same pattern of occurrence as the historical data. In order to cover the range of the extremes changes (decrease or increase) in precipitation and evaluate the response of groundwater

recharge to extremes potentially variations in precipitation, a 45 percent as maximum changes limited in precipitation was used. For historical wet days the historical precipitation amount was increased by the designed percentage.

- **Second Scenario:** Precipitation is projected to decrease, with an average change ranging between 5 and 45 percent, using a 10 percent increment with the same pattern of occurrence as the historical data.
- **Third Scenario:** Generate a synthetic precipitation pattern without regard to seasonality by a stochastic model with an average change with increasing range between 5 and 45 percent, using a 10 percent increment.
- **Fourth Scenario:** Generate a synthetic precipitation pattern without regard to seasonality by a stochastic model with an average change with decreasing range between 5 and 45 percent, using a 10 percent increment.
- **Fifth Scenario:** Generate a synthetic precipitation pattern with regard to seasonality by a stochastic model with an average change increasing only 45 percent.
- **Six Scenario:** Generate a synthetic precipitation pattern with regard to seasonality by a stochastic model with an average change decreasing only 45 percent.

Chapter 5

RESULT AND DISCUSSIONS

5.0 Overview of the Study Area

The Sagehen Creek watershed was used in this research for modeling daily rainfall and recharge with GSFLOW model. The Sagehen Creek watershed is used as a test watershed in the documentation of the GSFLOW model, and the GSFLOW model has been calibrated by the USGS for this watershed. The Sagehen Creek watershed Located in the east of the northern Sierra Nevada near Truckee, California, the Sagehen Creek watershed is one of the USGS Hydrologic Benchmark Network Basins. The drainage area of the watershed is 27 km2 and ranges in elevation from 1,935 to 2,653 m (Fig 5.1). According to Burnett and Jennings, 1965, and Rademacher et al., 2005, the geology of this watershed is granodiorite bedrock overlain by andesitic, Tertiary volcanics. On the northwestern side there are Quaternary gravels. The vacancies are considered the main components of this watershed so the aquifer and the volcanics are assumed to range between 50 and 300 m in thickness. Soils the in basin are classified as rocks that contain up to 90 percent rock fragments. A typical profile has a surface layer of dark grayish brown, gravelly, sandy loam that is 60 cm thick overlying a subsoil of yellowish-brown, cobbly, sandy, loam that extends to a depth of 115 cm. The principal human activity in the basin is hydrologic and biological research conducted by the USGS and the

University of California (Markstrom & Niswonger, 2008). The annual temperature near Sagehen Creek from 1980 to 2002 was 4°C (Western Region Climate Center, 2006b).

Daily mean streamflow values were obtained for Sagehen Creek at the streamflow gage near the outlet of the watershed. The gage is a U.S. Geological Survey hydrologic benchmark station near Truckee, California (Mast and Clow, 2000; station identification number–10343500). Mean daily streamflow was approximately 1 m3/s during snowmelt in May and June for 1953–2003. The maximum daily mean discharge on record was approximately 23.0 m3/s on January 1, 1997.

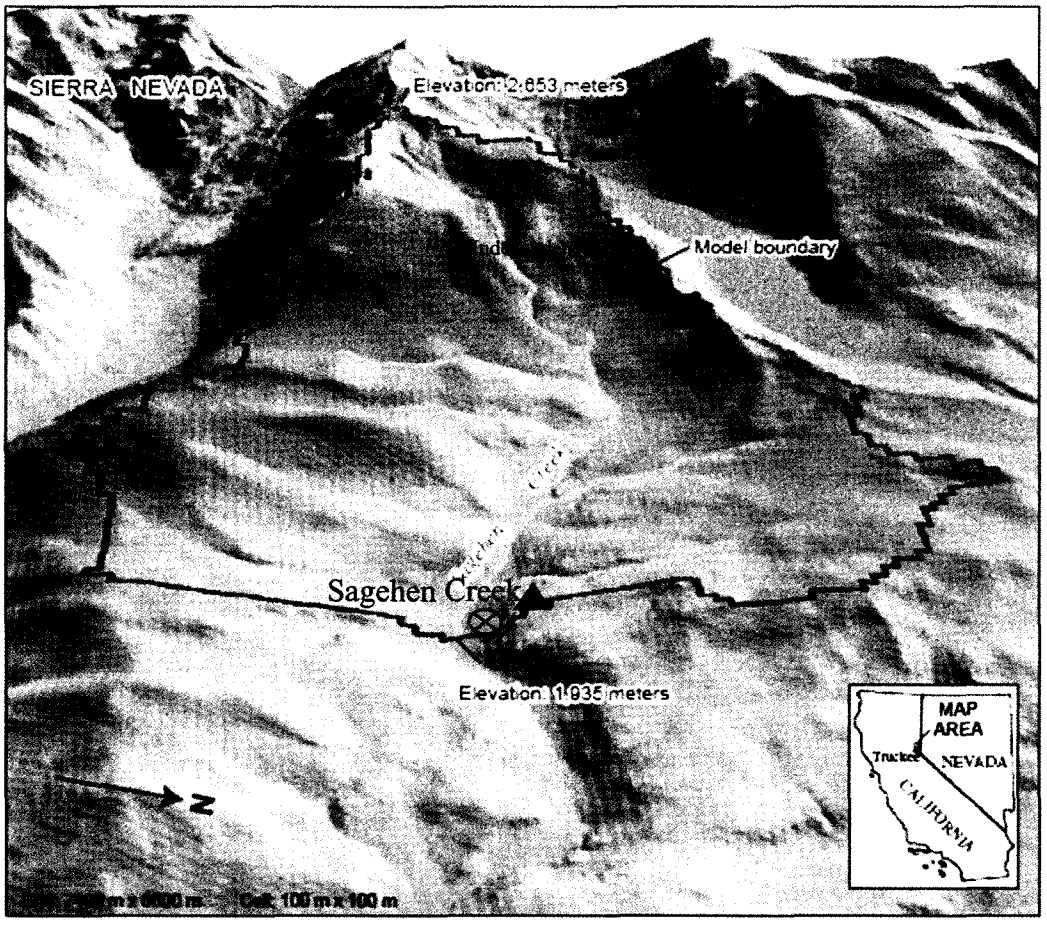

Shaded relief base from USGS 10-meter National Elevation Data, illumination from the northwest at 45°. Universal Transverse Mercator projection, Zone 11. North American Datum of 1983. Perspective Information: Attitude is 6,300 meters above land surface, viewing angle is 24 degrees, vertical exaggeration = 2x.

Legend

⊗ Sagehen Creek near Truckee (10343500) Streamgage

▲ Independence Lake (station 1)

▲ Sagehen Creek National Weather Service Cooperative station (station 2)

Figure (5.1): Location of Sagehen Creek watershed (Markstrom, & Niswonger, 2008).

5.1 Data Analysis

Daily precipitation (rainfall) data wear acquired from the U.S. Department of Agriculture. Independence Lake (station 1) (Western Region Climate Center, 2006b), and Sagehen Creek co-operative station (station 2) data were provided by the University of California, Berkeley (2005) (Markstrom et al., 2008).

Independence Lake is located at latitude 39°27'07" N, longitude 120°17'23" W. The elevation of Independence Lake is 8450 ft (2,575.57 m). The data period used was from 1980 to 2001. The mean daily precipitation for years 1980-2001 is 0.459 inches with a variance of 0.351 inches (Table 5.1). The maximum precipitation of 7.9 inches occurred on 3/10/1997. The Sagehen Creek co-operative station (station 2) is located at latitude 39 26' N, longitude 120 14'W. The elevation of the Sagehen Creek co-operative station is 6337 ft (1,931.52 m), and the data period used was from 1980 to 2001. The mean daily precipitation for years 1980-2001 is 0.40 inches with a variance of 0.359 inches (Table 5.1). The maximum precipitation of 5.43 inches occurred on 2/17/1986. The region has a humid continental climate with four distinct seasons. June to mid-August spans the summer months, with abundant rainfall and thunderstorm activity. A long winter period lasts from mid-November to mid-March. Precipitation in the watershed is highly variable in form and intensity and generally increases with altitude

Several sample statistics were computed, such as the sample mean (μ), standard deviation (σ) and variance (σ^2), coefficient of variation (CV), and coefficient of skewness (γ). Table (5.1) shows the characteristics of the daily mean rainfall amount for both precipitation stations and plots are shown in figure 5.2. Analyzing the plot of the daily,

weekly, and monthly time series in both locations, the series show a periodic or seasonality behavior with similar cycles each year. The daily average plots for annual cycles (water years 1980-2000 in figure (5.3)) permit observation of a high variability along every specific year, with the highest rainfall values between 1980 and 1981, and the lowest ones between 1986 and 1987. see figures (5.4) and (5.5) for weekly and monthly performance plots and table (5.2) for cumulative monthly plots and table (5.3) for weekly plots.

On the other hand, if we analyze the cycles in the weekly and monthly periodic time series plots (see figures (5.6) and (5.7)) consecutively in both locations, a low variability is observed. The peak values are observed in weeks 4, 5, 15, 16, 28, 29, 39 and 40 and January and February for both sites. The low peaks of rainfall are in weeks 10, 11, 21, 22, 33, 34, 45, July, and August, respectively. Analyzing the coefficient of variation (CV) for the annual series for both sites, CV values are high (1.29 and 1.15, respectively), table (5.1). The effects of the seasonality in both stations are seen in every year, with high rainfall values between February and May and low values between June and September. Since the coefficient of skewness (γ) gives an indication of the symmetry of data distribution for each time series, daily data sets present a significant asymmetry considering the computed values of (γ) 3.44 and 3.23 in both locations as daily values table (5.1) and average monthly values (1.1 and 1.73) (table (5.2)). This result indicates that the daily and monthly series do not distribute as a Gaussian shape. In other words, it is expected that the distribution functions of monthly data do not fit a normal distribution. Instead, the asymmetry presented in the monthly series in both locations is not as strong

as the daily series, and for them, a normal distribution could be a more appropriate model.

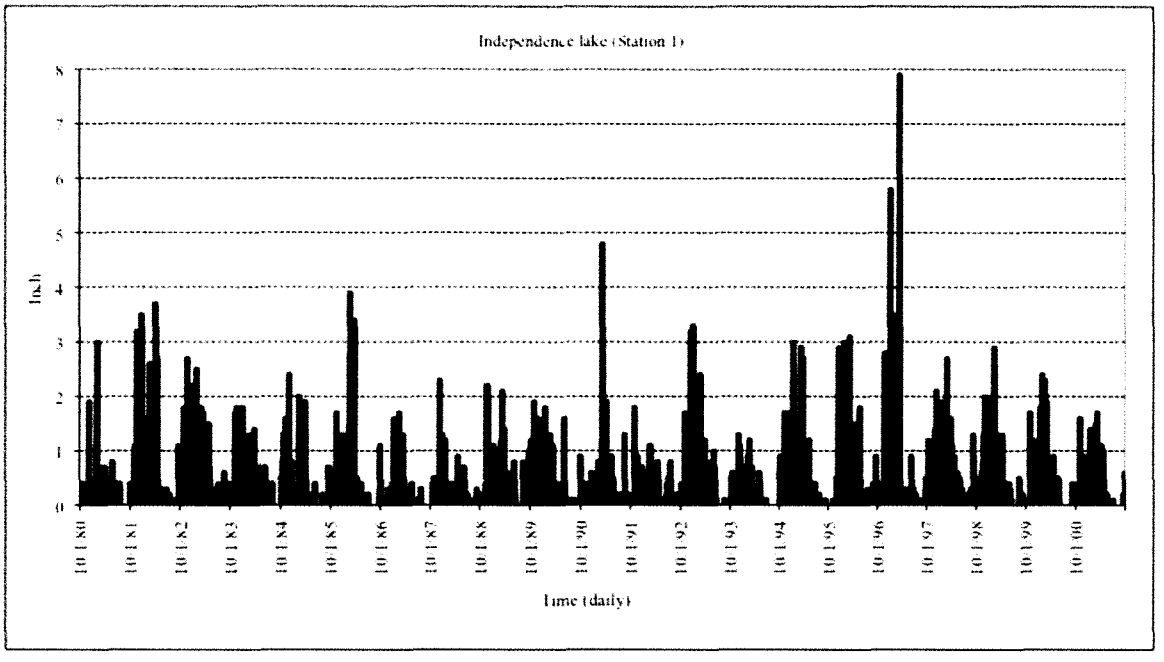

(a)

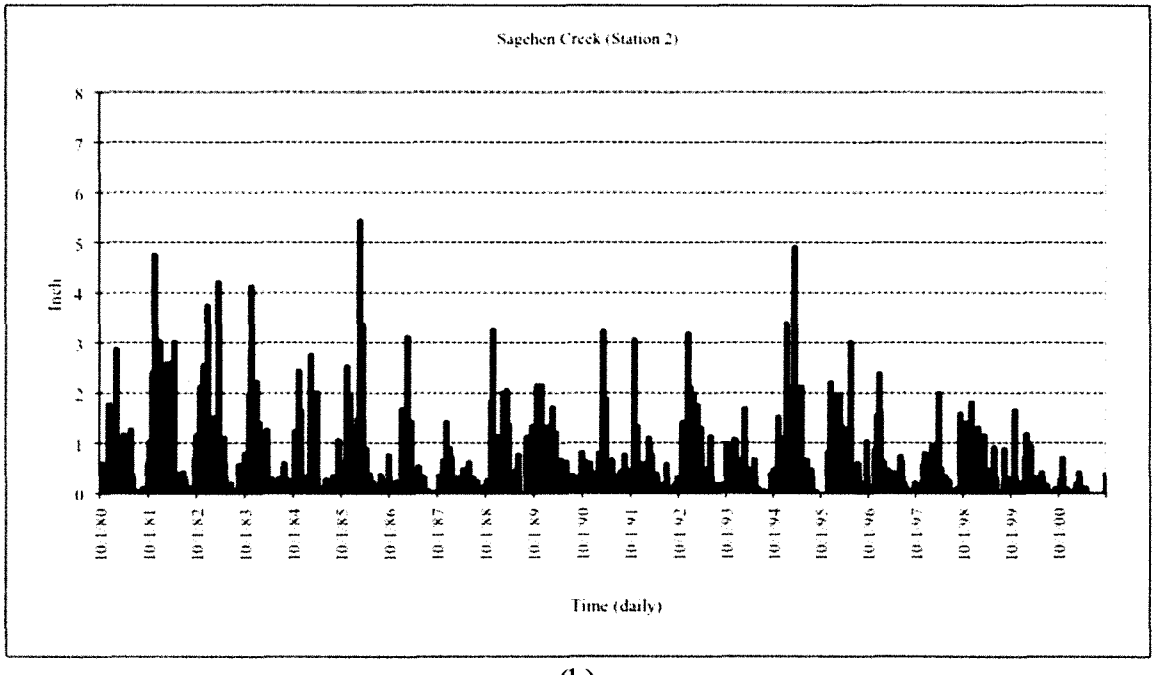

(b)

Figure (5.2): Time series of rainfall for (a) Independence Lake (station 1) and (b) Sagehen Creek (station 2) for period 1980-2000.

Table (5.1) : Statistic properties of daily rainfall for both stations on wet days.

Site index	Mean	St.Dev.	Variance	Covariance	Skewness
Station 1 (Independence Lake)	0.516	0.517	0.30	1.169	2.340
Station 2 (Sagehen Creek)	0.447	0.540	0.327	1.191	2.433

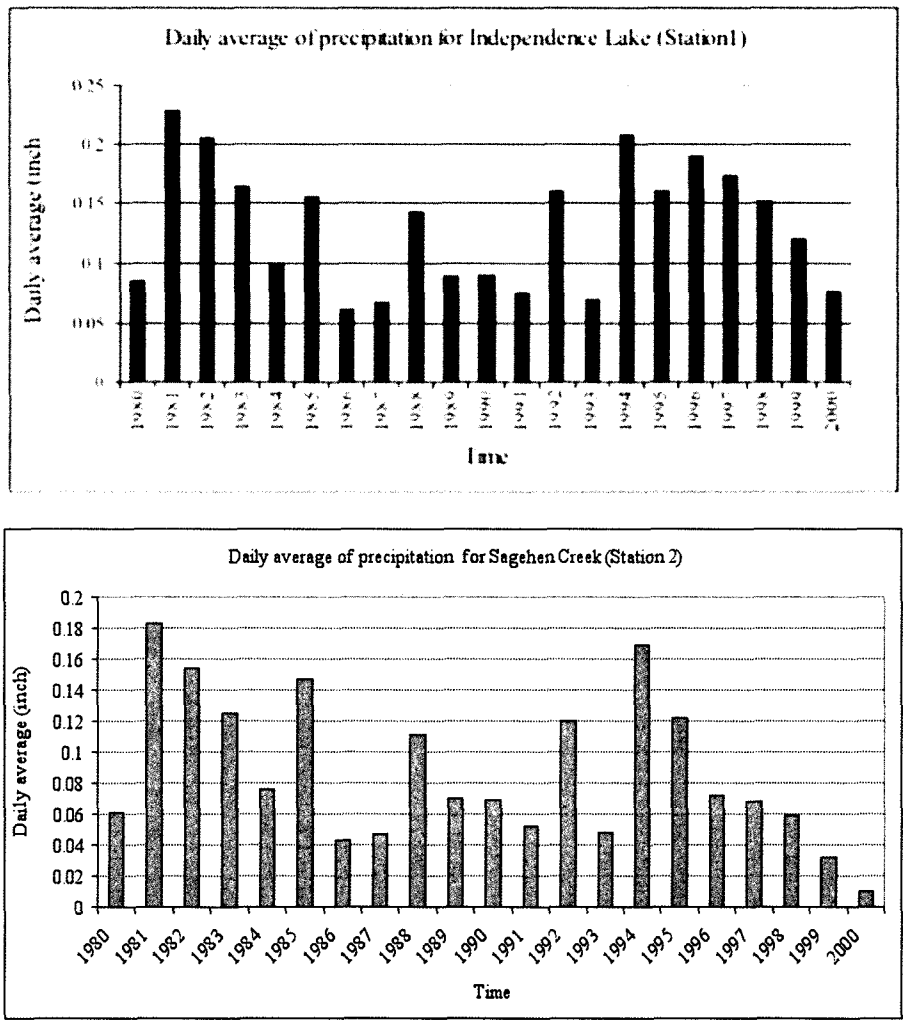

Figure (5.3): Daily average of rainfall for period 1980-2000 at both stations.

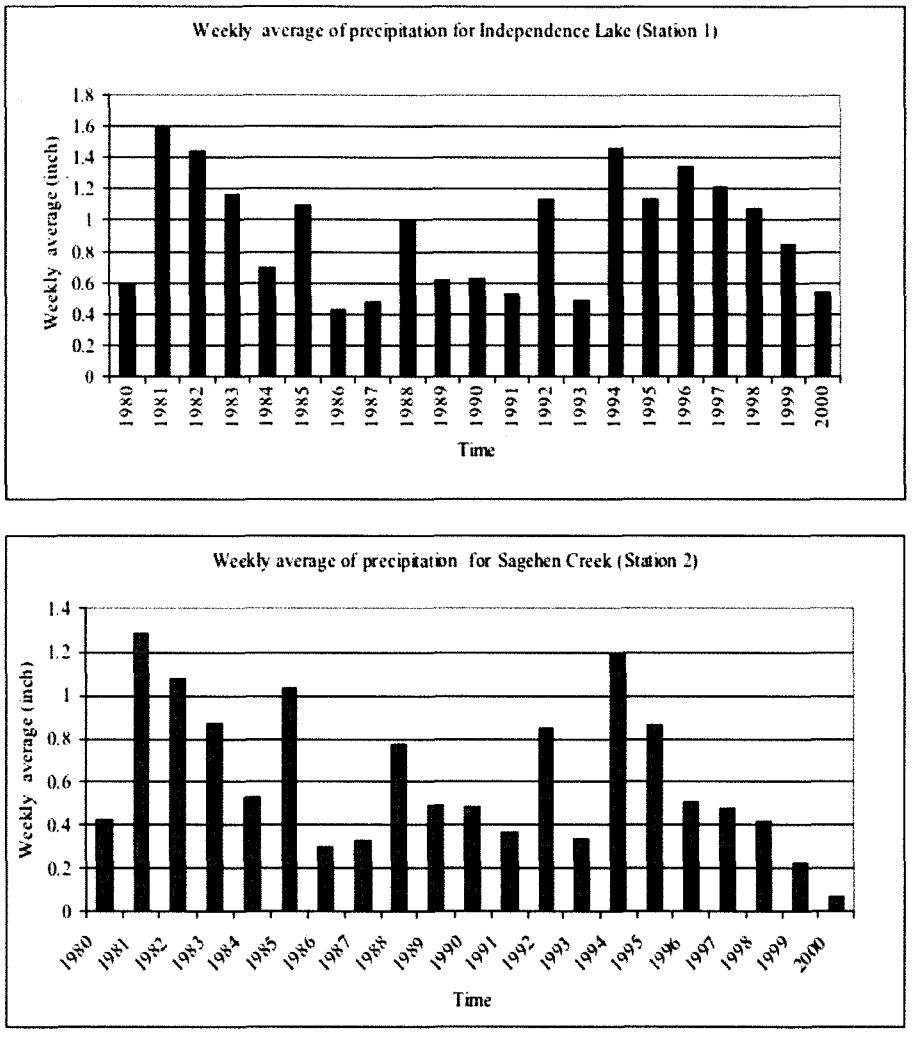

Figure (5.4): Weekly average of rainfall for period 1980-2000 at both stations.

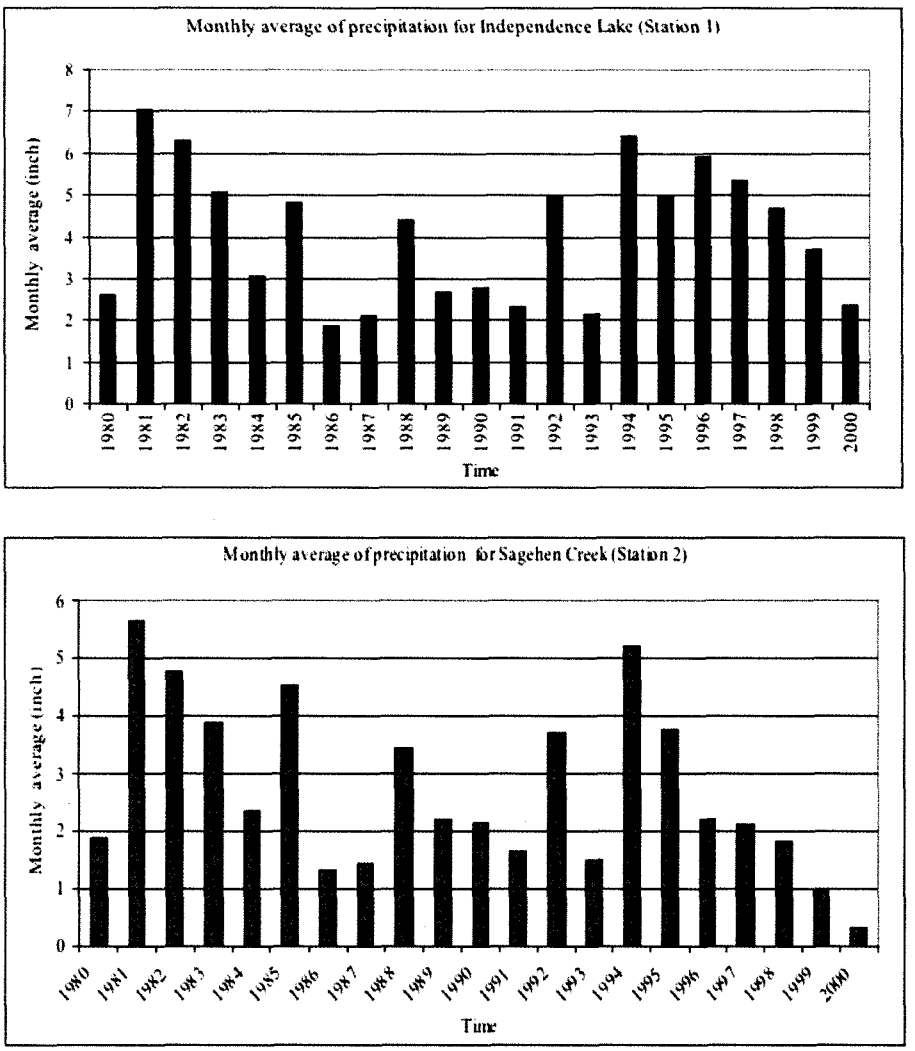

Figure (5.5): Monthly average of rainfall for period 1980-2000 at both stations.

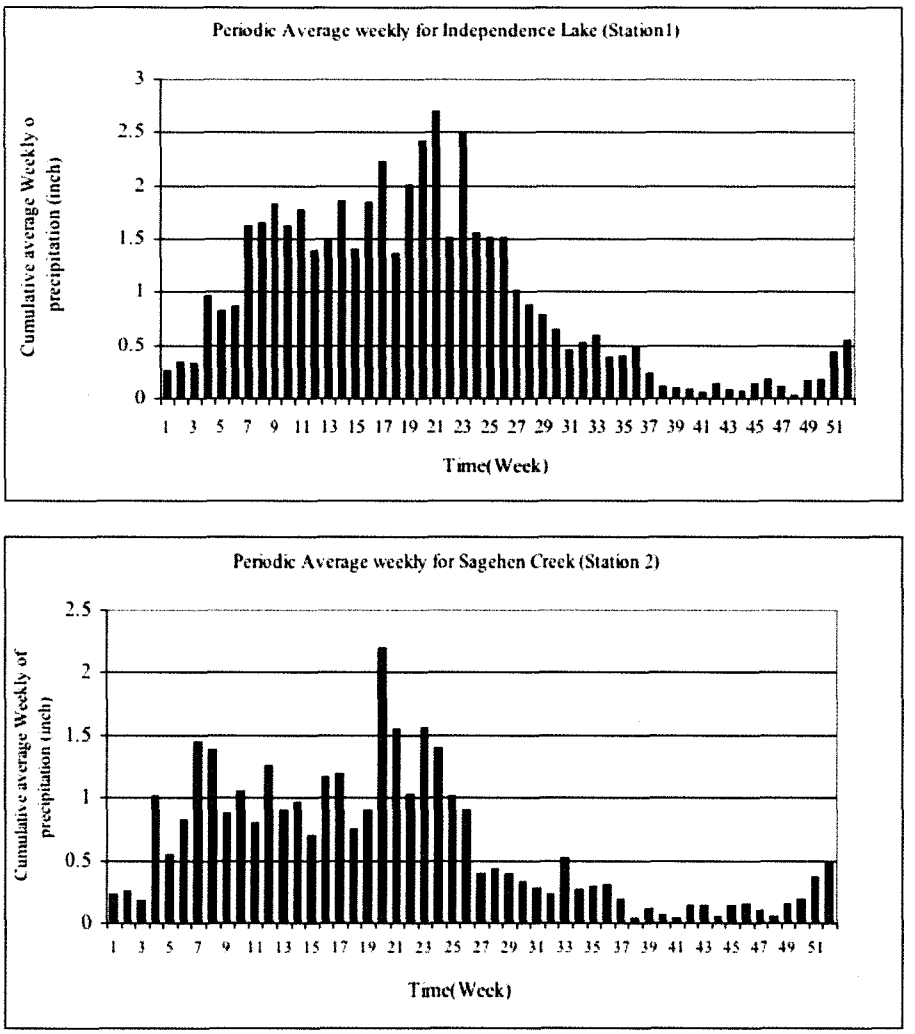

Figure (5.6): Periodic weekly average of rainfall for period 1980-2000 at both stations.

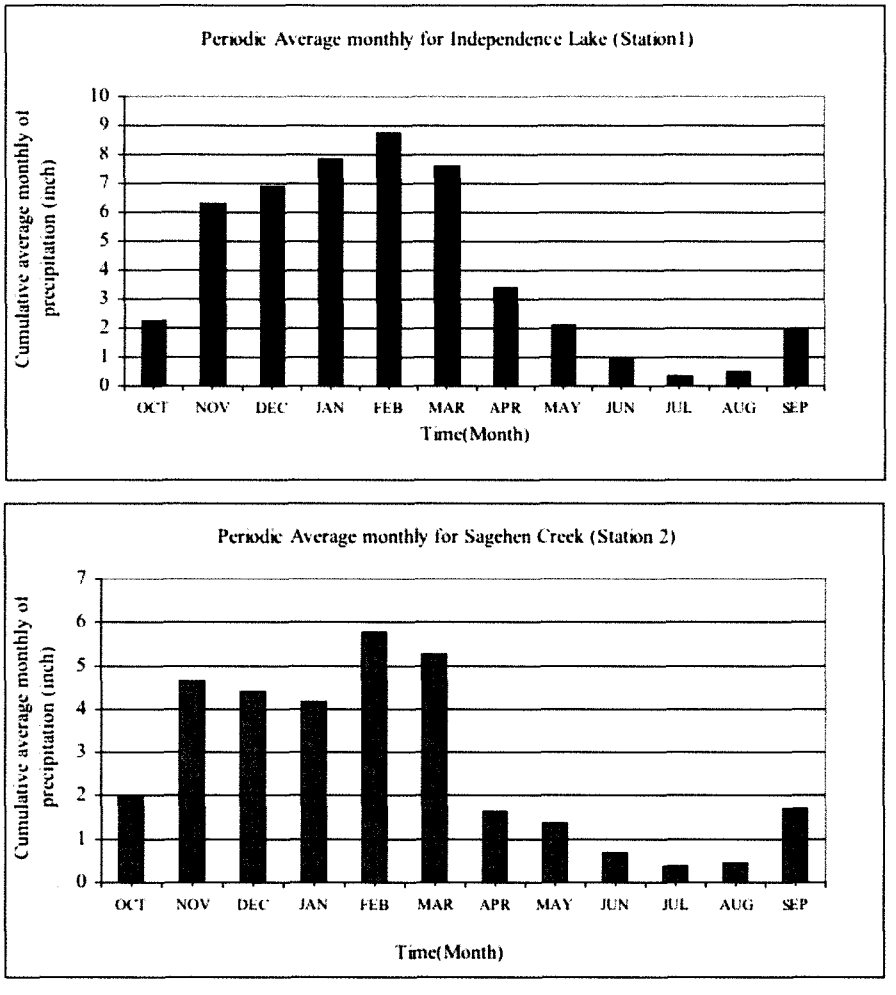

Figure (5.7): Periodic monthly average of rainfall for period 1980-2000 at both stations.

Table (5.2) Cumulative monthly rainfall statistics.

Month		***Independence Lake***				***Sagehen Creek***			
		μ	σ	*Var*	Skewness	μ	σ	*Var*	Skewness
OCT	10	2.238	1.967	3.867	1.490	1.990	1.979	3.917	1.410
NOV	11	6.319	5.456	29.772	1.154	4.627	5.185	26.885	1.597
DEC	12	6.900	6.283	39.479	1.463	4.409	4.447	19.774	1.222
JAN	1	7.867	5.931	35.180	0.822	4.155	3.497	12.232	1.121
FEB	2	8.743	5.731	32.850	0.579	5.781	5.117	26.181	2.255
MAR	3	7.619	5.210	27.148	0.845	5.270	5.564	30.962	2.092
APR	4	3.386	2.485	6.177	1.389	1.641	1.735	3.009	2.094
MAY	5	2.110	1.642	2.697	1.296	1.372	1.373	1.884	2.596
JUN	6	0.933	0.768	0.589	0.353	0.668	0.648	0.421	1.403
JUL	7	0.343	0.337	0.114	0.542	0.361	0.484	0.234	1.758
AUG	8	0.514	0.718	0.515	1.485	0.447	0.628	0.394	1.902
SEP	9	1.949	1.753	3.072	1.620	1.703	1.495	2.235	1.285

Table (5.3) Weekly characteristics of rainfall for both station sites.

	Independence Lake				***Sagehen Creek***			
Weeks	μ	σ	*Var*	Skew	μ	σ	*Var*	Skewness
1	2.238	1.967	3.867	1.490	0.230	0.359	0.129	1.736
2	6.319	5.456	29.772	1.154	0.250	0.325	0.105	1.654
3	6.900	6.283	39.479	1.463	0.177	0.263	0.069	1.390
4	7.867	5.931	35.180	0.822	1.016	1.618	2.619	1.989
5	8.743	5.731	32.850	0.579	0.547	1.026	1.053	2.583
6	7.619	5.210	27.148	0.845	0.829	1.461	2.134	1.816
7	3.386	2.485	6.177	1.389	1.444	2.420	5.858	2.401
8	2.110	1.642	2.697	1.296	1.386	1.913	3.660	1.966
9	0.933	0.768	0.589	0.353	0.874	1.111	1.234	1.675
10	0.343	0.337	0.114	0.542	1.054	1.289	1.663	1.442
11	0.514	0.718	0.515	1.485	0.800	1.105	1.222	1.657
12	2.238	1.967	3.867	1.490	1.258	2.271	5.158	2.136
13	6.319	5.456	29.772	1.154	0.907	1.482	2.196	1.940
14	6.900	6.283	39.479	1.463	0.961	1.291	1.666	1.624
15	7.867	5.931	35.180	0.822	0.702	1.678	2.814	3.473
16	8.743	5.731	32.850	0.579	1.165	1.161	1.347	0.428
17	7.619	5.210	27.148	0.845	1.187	1.481	2.192	1.574
18	3.386	2.485	6.177	1.389	0.743	0.940	0.884	1.435
19	2.110	1.642	2.697	1.296	0.895	1.050	1.103	0.937
20	0.933	0.768	0.589	0.353	2.200	2.954	8.726	3.000
21	0.343	0.337	0.114	0.542	1.550	2.367	5.601	1.991
22	0.514	0.718	0.515	1.485	1.032	1.438	2.069	1.834
23	1.949	1.753	3.072	1.620	1.557	2.166	4.690	1.798
24	2.238	1.967	3.867	1.490	1.401	2.020	4.082	2.496
25	6.319	5.456	29.772	1.154	1.018	1.584	2.511	2.559
26	6.900	6.283	39.479	1.463	0.902	1.489	2.217	2.234
27	7.867	5.931	35.180	0.822	0.392	0.612	0.375	2.707
28	8.743	5.731	32.850	0.579	0.432	0.886	0.785	3.421
29	7.619	5.210	27.148	0.845	0.388	0.557	0.311	2.613
30	3.386	2.485	6.177	1.389	0.324	0.627	0.393	3.366
31	2.110	1.642	2.697	1.296	0.279	0.699	0.488	4.163
32	0.933	0.768	0.589	0.353	0.233	0.301	0.090	1.384
33	0.343	0.337	0.114	0.542	0.521	1.361	1.853	3.927
34	0.514	0.718	0.515	1.485	0.261	0.310	0.096	1.229
35	1.949	1.753	3.072	1.620	0.298	0.479	0.229	2.033
36	2.238	1.967	3.867	1.490	0.307	0.500	0.250	1.965
37	6.319	5.456	29.772	1.154	0.185	0.343	0.118	2.328
38	6.900	6.283	39.479	1.463	0.044	0.105	0.011	3.139
39	7.867	5.931	35.180	0.822	0.108	0.184	0.034	1.513
40	8.743	5.731	32.850	0.579	0.061	0.132	0.017	3.184
41	7.619	5.210	27.148	0.845	0.034	0.130	0.017	4.354
42	3.386	2.485	6.177	1.389	0.139	0.254	0.065	2.121
43	2.110	1.642	2.697	1.296	0.135	0.219	0.048	1.449
44	0.933	0.768	0.589	0.353	0.048	0.098	0.010	2.466
45	0.343	0.337	0.114	0.542	0.141	0.382	0.146	3.025
46	0.514	0.718	0.515	1.485	0.146	0.315	0.099	2.882
47	1.949	1.753	3.072	1.620	0.097	0.202	0.041	2.391
48	1.949	1.753	3.072	1.620	0.045	0.103	0.011	2.347
49	1.949	1.753	3.072	1.620	0.152	0.426	0.182	3.166
50	1.949	1.753	3.072	1.620	0.186	0.281	0.079	1.466
51	1.949	1.753	3.072	1.620	0.366	0.587	0.344	2.209
52	1.949	1.753	3.072	1.620	0.499	0.795	0.632	1.905

5.1.1 First part - generation of the occurrence of rainfall

1. A uniform random number between [0,1] is generated, say, U_1. It was developed for each day at every year.
2. The precipitation state of day 1 (S_1) is dry if $U_1 \leq (P_0)$ or wet if $U_1 > (P_0)$ (see table (5.4) for both stations).
3. To decide the rain stage for the rest of the days, the transition probability matrix (the average matrix) was used.

1. If "Rain stage $_{(i-1)}$" and $U_i \leq (P_{00})$, then "Rain stage $_{(i)}$" =0. Otherwise, "Rain stage $_{(i)}$" =1.
2. If "Rain stage $_{(i-1)}$" and $U_i \leq (P_{10})$, then "Rain stage $_{(i)}$" =0. Otherwise, "Rain stage $_{(i)}$" =1.

Using the above-mentioned Markov process, the occurrence of rainfall for the entire generated record was determined.

Table (5.4): The probabilities P_1 and P_0 for the historical record for Stations 1 and 2.

Site index	Station 1	Station 2
Total days	7670	7670
Rainy days	2206	1679
Dry days	5464	5991
P_1	0.29	0.22
P_0	0.71	0.78

Table (5.5): The transition probability matrix (TPM) for the historical record for Stations 1 and 2.

Site index	Station 1	Station 2
P_{00}	0.83	0.87
P_{01}	0.17	0.13
P_{10}	0.43	0.47
P_{11}	0.57	0.53

5.1.2 Second part - generation of the amount of rainfall

Once the occurrence of rainfall has been generated, a fitted exponential distribution model was used to estimate the amount of rain in every day with rain.

The generation of the amount of rain is determined by using:

$$X = -\alpha \ln\left(1 - F(x)\right) \tag{5.2}$$

where F(x) is the probability obtained from a generated uniform random number(0-1). Again, the generated random numbers represent the values of the probabilities F(x), used in equation (5.2). Table (5.5) shows a comparison of simulated and historical rainfall data for both sites which shows how simulation (generation) related to the historical data.

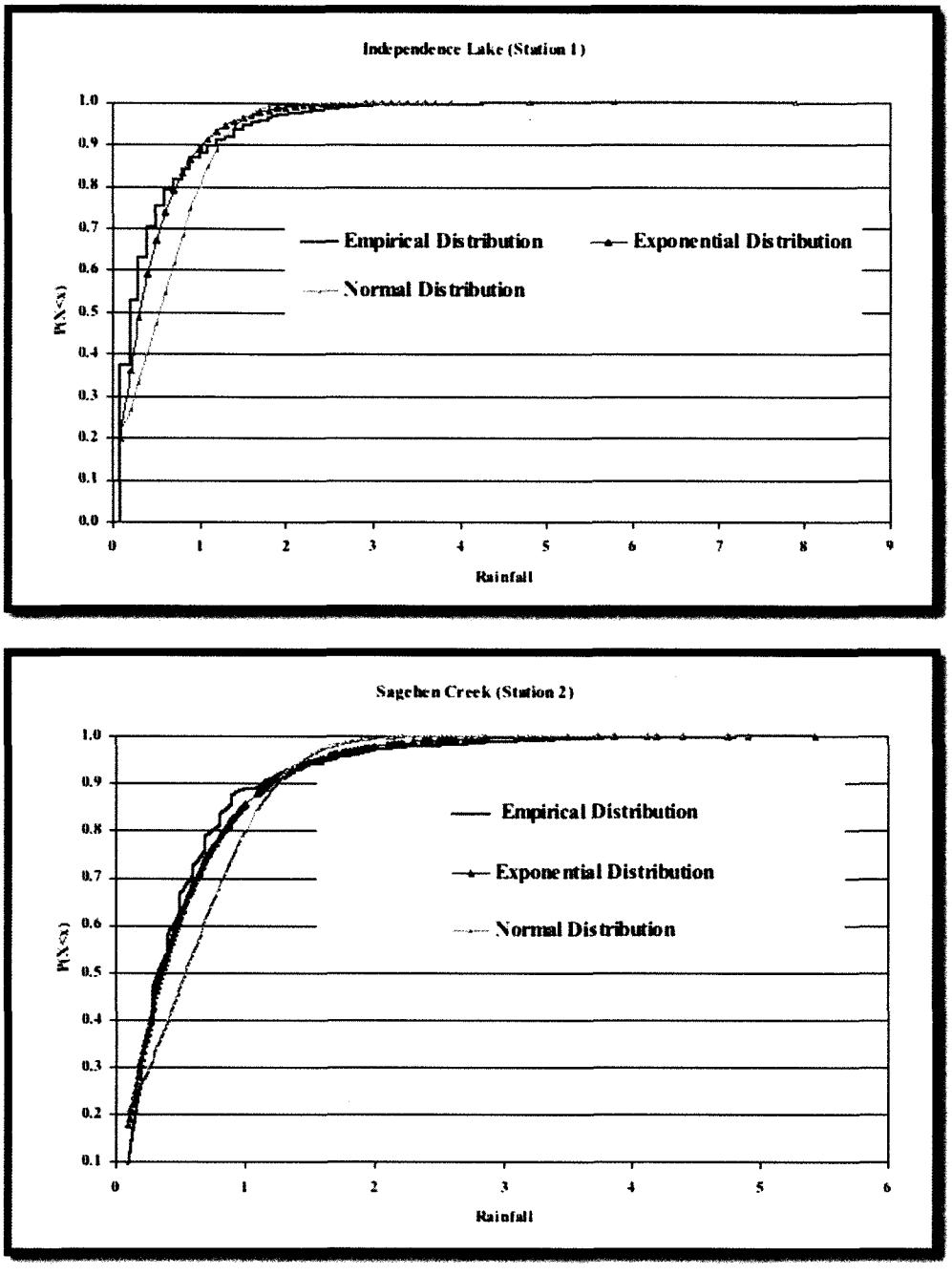

Figure (5.8): The fitted cumulative distribution function (CDF) of an exponential distribution model for rainfall at both stations.

Table (5.6): Statistical properties of daily historical rainfall compared to 1000 synthetic daily time series produced by the generation model.

Site index		Mean	St.Dev.	Variance	Covariance	Skewness
Station 1	Historical	0.516	0.517	0.3	1.169	2.34
	Generation	0.518	0.630	0.397	1.2149	3.192
Station 2	Historical	0.447	0.540	0.327	1.191	2.433
	Generation	0.504	0.509	0.265	0.800	1.733

5.2 Parameters Used in GSFLOW Model

As stated previously, GSFLOW is a new U.S. Geological Survey model for simulating groundwater/surface -water interactions. At the Sagehen Creek site, in California, Niswonger et al. (2008) concluded that the preliminary results indicated that the model performs well as shown by a comparison between the measured and simulated streamflow at the basin outlet. Niswonger et al., (2008) found that there is a good correspondence between the measured and simulated streamflow components. The hydrograph indicated that the surface and soil-zone components of the model were sufficiently calibrated. GSFLOW is being used in Chamokane Creek Basin, Stevens County, in northeastern Washington State to investigate aquifer creek interactions their and simulate the effects of potential groundwater withdrawals and climate scenarios on Chamokane Creek (Matthew et al., 2009). GSFLOW can be used to address many questions. One question that we consider is what are the effects of different climate

scenarios (e.g., floods and droughts) on a surface water and groundwater system?

To reach our main objective, the GSFLOW model for simulation of the Sagehen Creek watershed was used because all files, including parameters for watershed that are required for the PRMS model and the MODFLOW-2005 model to run the GSFLOW model, are available. Moreover, the dataset of precipitation used in this study has a reasonably long and complete record. The precipitation is highly variable in intensity and generally increases with altitude. As mentioned above, the region has a humid continental climate with four distinct seasons. In this study the required files and parameters exist to run the GSFLOW model for the Sagehen Creek watershed. The following tables show the parameters used in the GSFLOW model tables (5.7) and (5.8). For more information about parameter the reader should refer to the GSFLOW manual ((Markstrom, et.al, 2008)

A data file was collected for the Sagehen Creek basin model for the time period from October 1, 1980, to September 30, 2000. This data file included both streamflow and climate data. The climate data included in this file were from Independence Lake (station 1) and Sagehen creek (station 2). The Saghen Creek basin was divided into 128 HRUs, 5913 grid cells, and 201 streams reaches. Parameters were estimated using valid spatial data sets, standard model default values, regional values determined by earlier studies in the area and optimum hydrologic principles. In addition to, some parameters were fitted and adjusted by the Rosenbrock automated calibration method (Rosenbrock, 1960), Markstrom et al., (2006). According to Markstrom et al., (2008) recharge to the saturated zone is calculated at the end of a time step based on the volumetric flow in the unsaturated zone across the water table in addition to any water that may be in depot in

the unsaturated zone when the water table rises. Therefore, great variations in the water table can occur throughout a time step, but the volumetric flow and storage of the unsaturated zone are kept in balance with recharge to the saturated zone even in these large variations in the water table. A complete description of the coupling between the unsaturated and saturated zones is presented by Niswonger (2006a, p. 8-10). Unsaturated-zone flow is simulated in GSFLOW using a kinematic-wave approximation to Richards' equation that assumes diffusive gradients (capillary pressure gradients) are negligible (Colbeck, 1972; Smith, 1983). This enables Richards' equation to be solved using the method of characteristics, which was originally done by Smith (1983) and Charbeneau (1984). The approximation of simulating unsaturated flow in GSFLOW varies from previous approaches that coupled a one-dimensional finite-difference form of Richards' equation to two or three dimensional groundwater flow equations (Refsgaard & Storm, 1995) because it does not have a fixed-grid structure. The approach adds flexibility for simulating an unsaturated zone that can change in thickness through space and time. The package simulates groundwater discharge directly to the soil zone or land surface as well as evapotranspiration from the unsaturated and saturated zones, Markstrom et al., (2008).

Table (5.7) : Hydraulic properties and variables used in the Layer-Property Flow, Unsaturated-Zone Flow, and Streamflow Routing Packages.

Variable	Units	Minimum value	Maximum value
Variables assigned to the Layer-Property Flow Package			
Horizontal hydraulic conductivity for upper layer	meters per day	0.026	0.39
Vertical hydraulic conductivity for upper layer	meters per day	.026	.39
Horizontal hydraulic conductivity for lower layer	meters per day	.00045	.027
Vertical hydraulic conductivity for lower layer	meters per day	.00045	.027
Specific storage for both layers	per meter of aquifer	2×10^{-6}	2×10^{-6}
Specific yield	cubic meter of water per cubic meter of aquifer	.08	.15
Variables assigned to the Unsaturated-Zone Flow Package			
Vertical hydraulic conductivity of the unsaturated zone below land surface	meters per day	0.018	0.27
Brooks-Corey exponent for unsaturated zone below land surface	dimensionless	4	4
Saturated water content of unsaturated zone below land surface	cubic meter of water per cubic meter of unsaturated zone	.15	.25
Initial water content of unsaturated zone below land surface	cubic meter of water per cubic meter of unsaturated zone	Not required for steady-state stress period [see note]	Not required for steady-state stress period [see note]
Steady-state infiltration rate	meters per day	.0007	.0019
Variables assigned to the Streamflow-Routing Package			
Hydraulic conductivity of streambed	meters per day	5.0	5.0
Streambed thickness	meters	1.0	1.0
Vertical hydraulic conductivity of unsaturated zone beneath streams	meters per day	.3	.3
Brooks-Corey exponent for unsaturated zone beneath streams	dimensionless	3.5	3.5
Saturated water content of unsaturated zone beneath streams	cubic meter of water per cubic meter of unsaturated zone	.3	.3
Initial water content of unsaturated zone beneath streams (see note)	cubic meter of water per cubic meter of unsaturated zone	.2	.2

Source: Markstrom, et al., 2008.

Table (5.8). Values and source of non-default PRMS parameters.

Parameter	Minimum value	Maximum value	Source
adjmix_rain	0.0055	2.32	L
covden_sum	.683	1.0	CG
covden_win	.683	1.0	CG
dday_intcp	-36.0	-10.0	L
dday_slope	.31	.65	L
fastcoef_lin	.4	.4	C
gwflow_coef	.00365	.00365	C
jh_coef	.0163	.0267	C
jh_coef_hru	13.6	15.7	CG
potet_sublim	.75	.75	C
pref_flow_den	.1	.1	C
rad_trncf	.233	.558	CG
sat_threshold	3.34	5.16	C
smidx_coef	.00037	.00037	C
snarea_curve	.05	1.0	L
snarea_thresh	.0	106.3	CG
snowinfil_max	2.75	2.75	C
soil_moist_max	2.39	3.68	CG
soil_rechr_max	1.48	2.09	CG
srain_intcp	.05	.05	L
ssr2gw_exp	.75	.75	C
ssr2gw_rate	.0378	.0557	C
tmax_allrain	60.0	70.0	L
tmax_allsnow	38.2	38.2	L
transp_beg	3	3	C
transp_end	11	11	C
tstorm_mo	0	1	C
wrain_intcp	.05	.05	L

Abbreviations: C, parameters that are adjusted during calibration; CG, parameters that are initiallycomputed in GIS and are adjusted, during calibration; L, parameters obtained from the literature.
Source: Markstrom, et al., 2008.

5.3.1 Probabilistic analysis of time series of recharge

5.3.1.1 Overview

Most hydrological processes have some level of randomness and uncertainty. Time series of recharge are one of the hydrological processes that are generally described by probability functions. Sometimes the hydrologic systems are impacted by external events, such as storms, floods and drought. According to Chow et al. (1988) "The magnitude of an extreme event is inversely related to its frequency of occurrence". The technique involves using observed annual flow recharge data to calculate statistical information such as mean values, standard deviations, skewness, and recurrence intervals. These statistical data are then used to construct frequency distributions, which are graphs and tables that tell the likelihood of various levels of recharge as a function of recurrence interval or exceedence probability. Thus the main objective of this part of the research is to estimate a frequency analysis for the recharge time series so that it gives us a clear picture of the magnitude of extreme events of recharge that are impacted by precipitation. Different scenarios allow forecasting groundwater recharge magnitude, and relates to their frequency of occurrence. This illustrates the differences between scenarios, differences that are used for further purposes such as groundwater modeling, management and well design. The frequency analysis curve is estimated by using a common method of empirical frequency analysis based on plotting position.

5.4.1 First scenario

In this first scenario the rainfall amount was increased relative to the observed data assuming the precipitation is projected to increase with an average change ranging between 5 and 45 percent (using 10 percent increments) with the same pattern of occurrence as the historical data. Variations of this scenario increased the rainfall amount by 5%, 15%, 25%, 35%, and 45% of the average of the historical data following the same pattern and seasonality of the historical data. The pattern was preserved by only considering changes on the wet days.

5.4.1.1 Changes to daily, monthly and annual recharge flow

Recharge in the unsaturated zone is simulated in GSFLOW by the Unsaturated-Zone Flow Package of MODFLOW 2005 that solves a vertical, one-dimensional form of Richards' equation and neglects the capillary pressure gradient (section 3.5). This assumes that the unsaturated zone is homogeneous in the vertical direction. Figures (5.9) (a, b, c, and d) show the time series of the recharge flow for all scenarios 5%, 15%, 25%, 35%, and 45%. All figures show the change in the recharge. In particular, the time series of resulting recharge for the whole period (1980-2000) is plotted figure (5.9) (a). The plot is divided into the first seven-year period (figure (5.9) (b)), the second seven-year period (c), and the rest of the period (figure (5.9) (d)). The results show the recharge increases for all scenarios by approximately the same relative increase that was applied to the rainfall.

The descriptive statistics of the gained recharge from the different scenarios have been analyzed and the mean annual recharge and multi-mean annual recharge have been

calculated to all scenarios, as illustrated in table (5.9). To further illustrate the changes, the data in the table are plotted, as shown in figure (5.10) (a, b).

The percentages of the changes are shown in table (5.10). The table shows the daily average of the percentage change to the historical recharge. Table (5.11) shows the yearly average percentage changes of the recharge, which is illustrated in figure (5.11). The descriptive statistics of the increased recharge from different increases in precipitation (the standard deviation, skewness coefficient and kurtosis) were calculated for the annual increased recharge. The standard deviations for annual recharge and multi-annual standard deviation have been calculated to all increases as illustrated in table (5.12), where the standard deviation is a measure of the variability of the recharge around the mean. The data in the table have been plotted and are shown in figures (5.12) (a, b). The percentages of the changes are shown in Table (5.13) and plotted in Figure (5.13).

The skewness coefficient and kurtosis are plotted in Figure (5.14) (a, b). The skewness coefficient is a measure of symmetry of the data and kurtosis is a measure of whether the data are peaked or flat relative to a normal distribution. These figures show how the standard deviation, skewness coefficients, and kurtosis for the annual increased recharge are changed corresponding to the change in precipitation. The results presented are consistent with the previous results that showed increased precipitation yielded higher and increasing daily and annual recharges. Furthermore, the mean monthly recharge for the water years (1980-2000) was calculated to all months. Additionally plots for specific months of June, July, August, December, January, and February are provided to help demonstrate behavior of the change. Figures (5.15) (c, d, e) and (5.16) (a, b, c) show the mean monthly recharge for June, July, and August and December, January, and February.

Figure (5.15) (a) shows the mean monthly recharge for all scenarios for the period 1980-2000. We notice the recharge gradually increasing starting from February and reaching a peak point in the month of June (see figure (5.15, and 5.16). in some months increasing precipitation yields less recharge than historical but in other months yields more recharge than the historical recharge. Finally, a flow duration curve frequency analysis for all increases 5%, 15%, 25%, 35%, and 45% was conducted and plotted for daily and monthly results. Figures (5.17) (a, b, c, d, e) show the flow duration curves based on daily and monthly analyses for specific months of June, July, and August. In this study these flow duration curves are a plot of recharge vs. percent of time that a particular recharge was equaled or exceeded by a specified value of interest. The area under the flow duration curve gives the average daily recharge, and the median daily recharge is the 50 percent value. A flow duration curve characterizes the ability of the basin to provide flows of various magnitudes. Moreover, it illustrates the relationship between the frequency and magnitude of the recharge. This information is extremely useful for the design of structures on a stream or in a basin. For example, a structure can be designed to perform well within some range of flows, such as flows that occur between 20 and 80 percent of the time (water.oregonstate.edu/streamflow/analysis/flow/index.htm) or for water resources management (groundwater). A flat curve indicates that moderate flows are sustained throughout the year due to natural or artificial streamflow regulation, or due to a large groundwater capacity that sustains the base flow to the stream. Flow duration curves have a long history in the field of water resource engineering and have been used to solve problems in water quality management, hydropower, in streamflow methodologies, water-use planning, flood control, and river and reservoir sedimentation,

and for scientific comparisons of streamflow characteristics across watersheds (Richard & Fennessey, 1996).

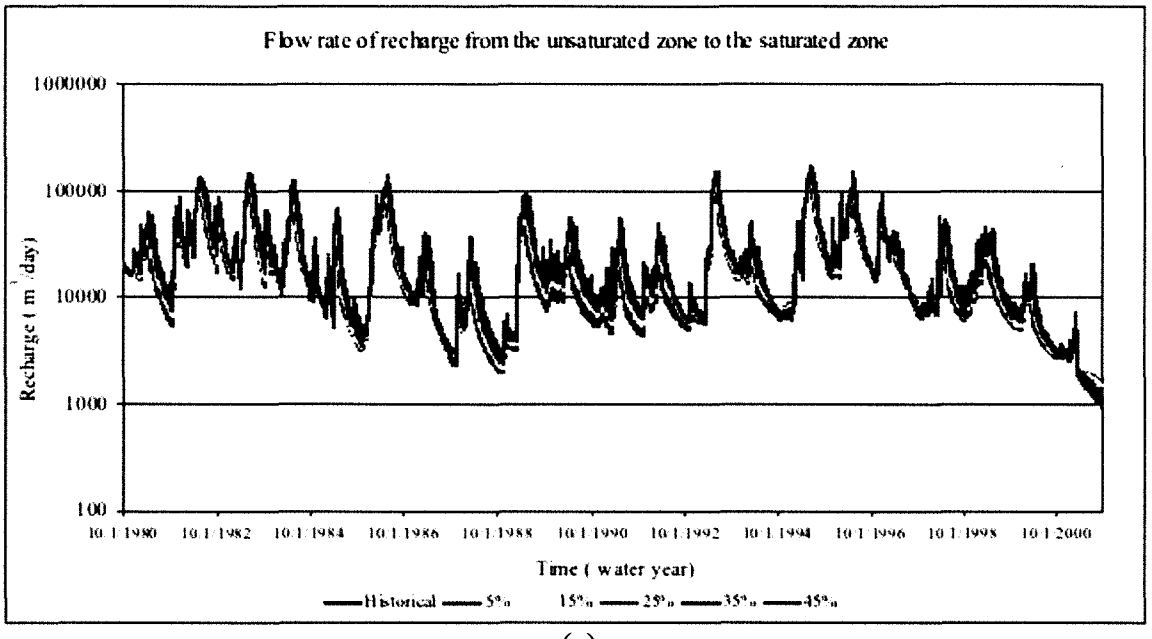

(a)

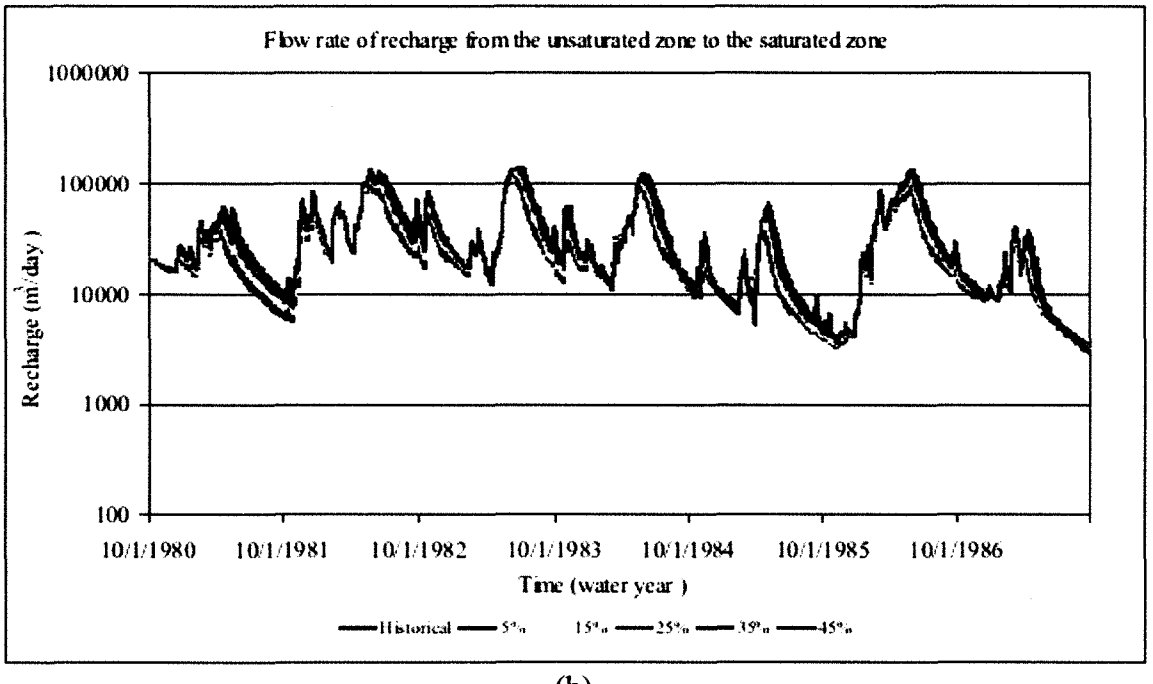

(b)

Figure (5.9): The time series of flow rate of the recharge at whole period (a), first seven years (b), second seven years, (c) and rest of the time period (d) (first scenario).

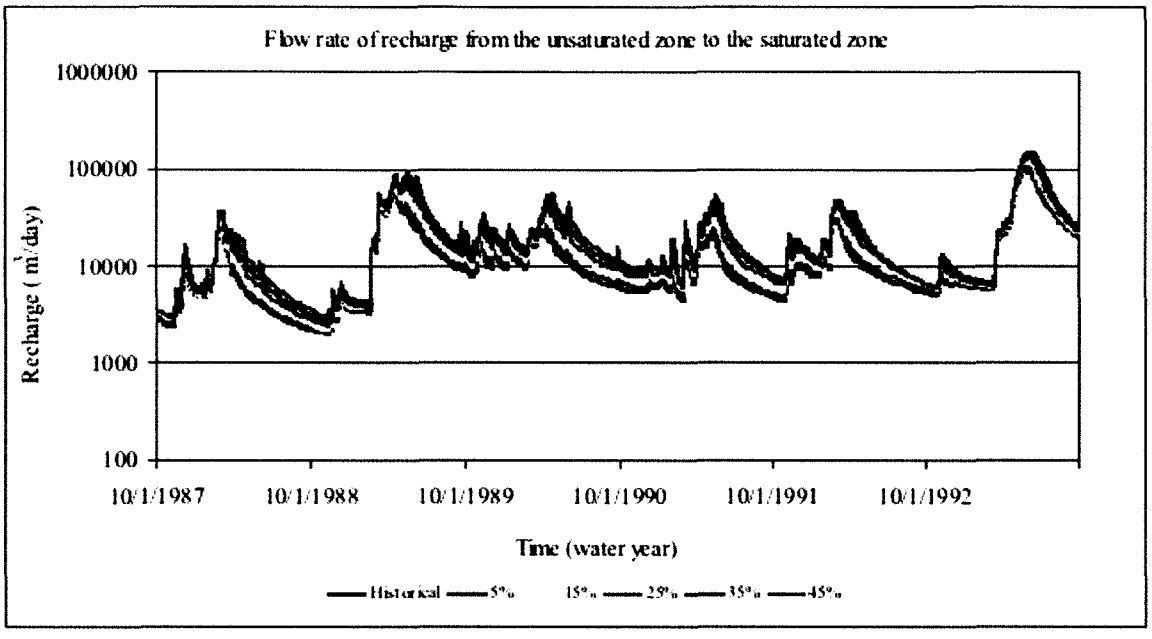

(c)

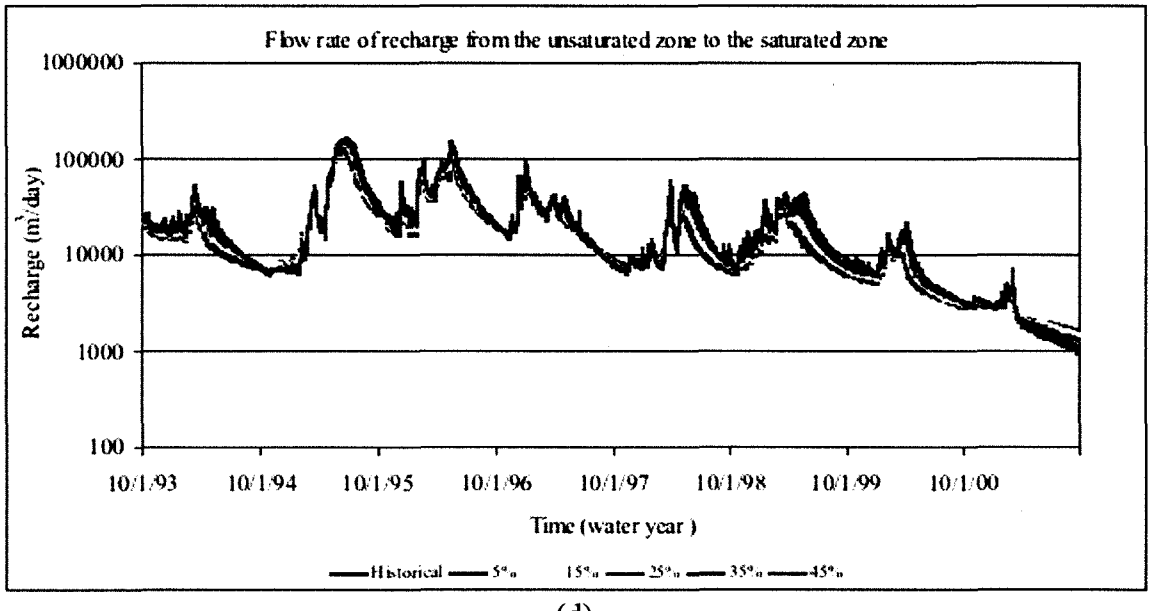

(d)

Figure (5.9): The time series of flow rate of the recharge at whole period (a), first seven years, (b), second of seven years, (c) and rest of the time period (d) (first scenario) (continued).

Table(5.9) The mean annual recharge for the first scenario (m^3/day).

Time	Historical	5%	15%	25%	35%	45%
1980-2000	18926.7884	19940.479	21904.68	23806.402	25617.714	27334.845
1980	17708.1627	18565.314	20375.077	22443.743	24545.279	26617.796
1981	41879.8538	43701.884	47425.575	50864.301	54127.909	57336.279
1982	37911.3434	39754.44	43597.948	47047.333	49867.821	52146.231
1983	28973.9942	30424.239	32823.771	35295.042	37887.393	40722.744
1984	12057.1829	12667.455	13783.287	14960.514	16198.966	17312.576
1985	30296.3478	31888.367	34887.386	37742.86	40259.058	42432.795
1986	9821.54262	10229.011	10924.567	11453.371	11979.132	12646.053
1987	5758.73895	6001.9471	6651.5666	7419.2546	8372.0326	9427.3523
1988	15813.6588	17154.504	20134.979	23183.614	26089.426	28841.866
1989	11420.0475	12728.796	15316.344	17857.702	20476.687	23212.863
1990	8317.21959	9284.7365	11083.643	12961.237	14904.115	16508.524
1991	9557.23394	10541.251	12530.299	14357.759	15841.415	17069.107
1992	26949.5853	28796.608	32130.911	35081.805	37763.722	40329.227
1993	13498.1349	14106.859	15407.958	16799.336	18044.01	19335.863
1994	37135.3337	38783.647	41508.87	43888.884	46189.122	48401.104
1995	36033.3971	37909.105	41099.938	43971.905	46589.981	48668.425
1996	22612.0557	23009.808	23647.546	24312.641	24863.873	25404.421
1997	11818.4302	12225.448	13361.716	14570.24	15768.945	16883.106
1998	12097.975	12914.893	14708.133	16570.053	18551.727	20620.171
1999	5498.99704	5706.0283	6204.6421	6806.2519	7391.2386	7935.6627
2000	2327.46214	2380.6951	2422.1026	2377.2277	2293.0456	2214.797
Mean	18927.94	19941.67	21906.01	23807.86	25619.28	27336.52
MAX	41879.85	43701.88	47425.58	50864.30	54127.91	57336.28
MIN	2327.46	2380.70	2422.10	2377.23	2293.05	2214.80
SD	12193.14	12717.25	13667.77	14516.76	15277.03	15967.58

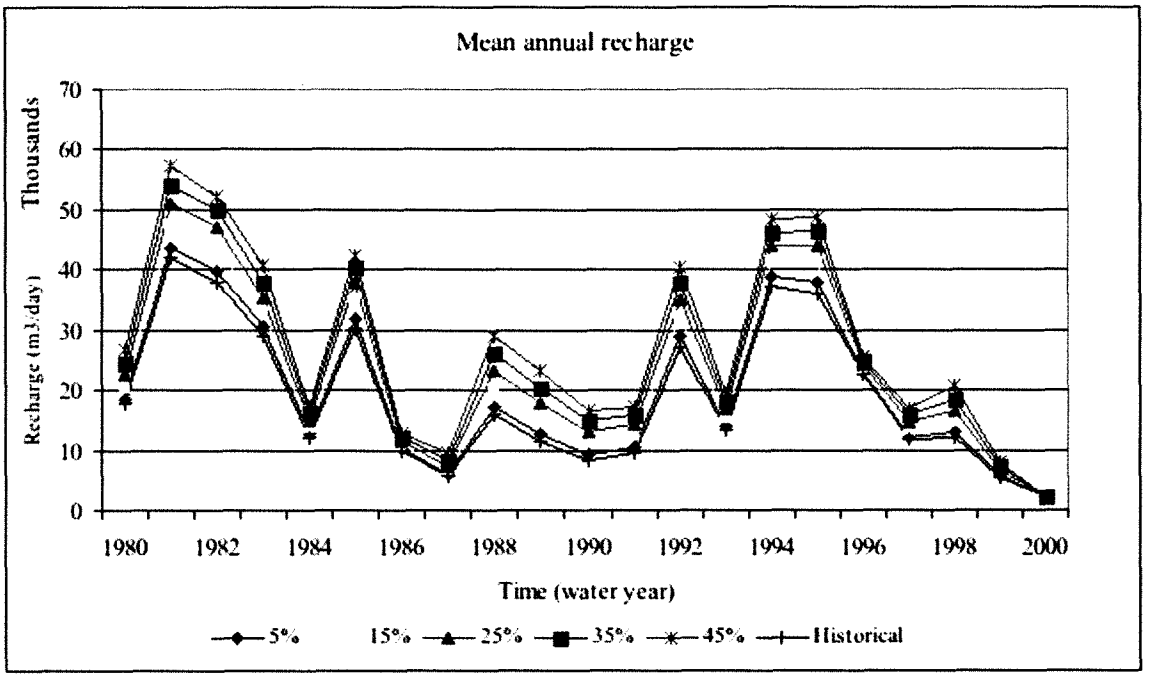

(a)

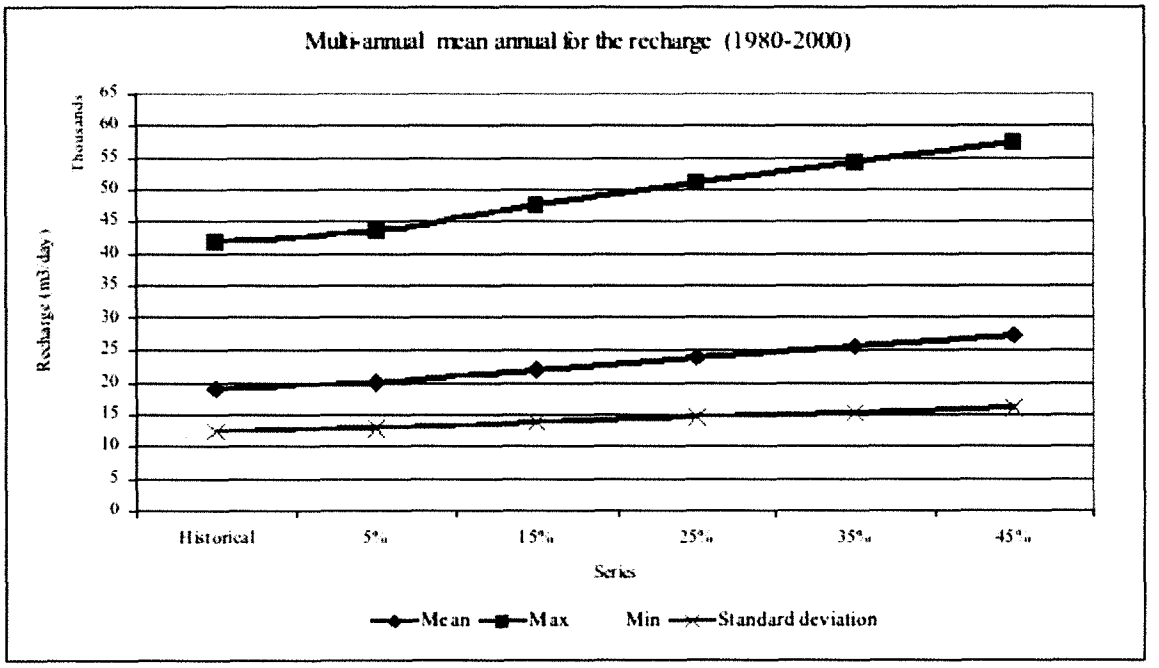

(b)

Figure (5.10): (a) Time series of mean annual and (b) Multi-mean annual of the recharge for first scenario (m^3/day).

Table (5.10): The daily average relative percentage change for the first scenario.

Scenarios	5%	15%	25%	35%	45%
Average	5.07%	15.21%	25.49%	35.85%	46.19%

Table (5.11): The annual average relative percentage change for the first scenario.

Time	5%	15%	25%	35%	45%
1980-2000	5.36%	15.73%	25.78%	35.35%	44.42%
1980	4.84	15.06	26.74	38.61	50.31
1981	4.35	13.24	21.45	29.25	36.91
1982	4.86	15.00	24.10	31.54	37.55
1983	5.01	13.29	21.82	30.76	40.55
1984	5.06	14.32	24.08	34.35	43.59
1985	5.25	15.15	24.58	32.88	40.06
1986	4.15	11.23	16.61	21.97	28.76
1987	4.22	15.50	28.83	45.38	63.71
1988	8.48	27.33	46.60	64.98	82.39
1989	11.46	34.12	56.37	79.30	103.26
1990	11.63	33.26	55.84	79.20	98.49
1991	10.30	31.11	50.23	65.75	78.60
1992	6.85	19.23	30.18	40.13	49.65
1993	4.51	14.15	24.46	33.68	43.25
1994	4.44	11.78	18.19	24.38	30.34
1995	5.21	14.06	22.03	29.30	35.06
1996	1.76	4.58	7.52	9.96	12.35
1997	3.44	13.06	23.28	33.43	42.85
1998	6.75	21.58	36.97	53.35	70.44
1999	3.76	12.83	23.77	34.41	44.31
2000	2.29	4.07	2.14	-1.48	-4.84
Mean	**5.65**	**16.85**	**27.89**	**38.62**	**48.93**
MAX	**11.63**	**34.12**	**56.37**	**79.30**	**103.26**
MIN	**1.76**	**4.07**	**2.14**	**-1.48**	**-4.84**
SD	**2.72**	**8.27**	**14.20**	**20.39**	**26.27**

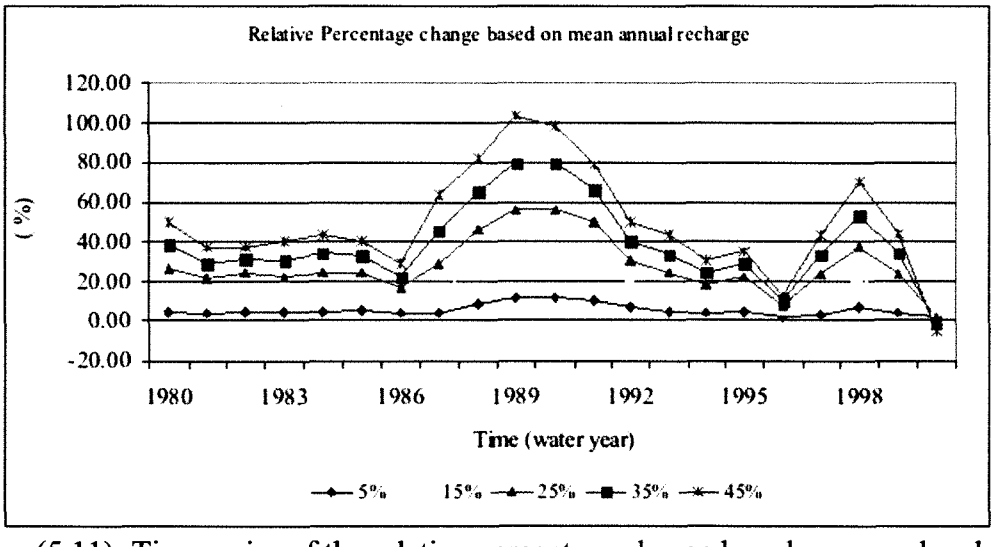

Figure (5.11): Time series of the relative percentage change based on annual recharge (first scenario).

Table(5.12) The standard deviation of annual recharge for the first scenario (m^3/day).

Time	Historical	5%	15%	25%	35%	45%
1980-2000	20161.22	21306.39	23453.77	25412.12	27187.00	28796.51
1980	7731.89	8114.66	8931.39	9992.64	11324.86	12930.83
1981	23603.27	24706.53	26960.92	29061.56	31043.98	33071.68
1982	29059.45	30159.81	32520.55	34230.06	35656.53	37197.76
1983	20038.97	21443.37	23779.89	26223.47	28610.51	30619.84
1984	7447.23	8120.03	9446.22	11013.11	12679.11	14421.28
1985	25600.68	27290.14	30315.51	33092.55	35493.58	37490.89
1986	5641.41	6087.31	6961.44	7625.03	8167.88	8774.24
1987	4685.37	5006.31	5614.25	6278.45	6977.78	7645.19
1988	14846.74	16069.28	18750.57	21751.84	24874.61	27800.48
1989	4473.41	4980.14	5983.39	7281.77	8647.73	10240.93
1990	4574.19	5195.55	6462.04	7872.54	9432.55	11025.58
1991	5491.31	6028.90	7153.39	8344.06	9499.25	10654.02
1992	27090.32	29533.14	33931.49	37596.68	40966.26	43971.89
1993	5454.27	5697.27	6205.42	6955.48	7724.28	8558.95
1994	35890.30	37916.34	41705.36	45147.11	48228.69	50644.95
1995	19295.44	21028.93	24084.09	26303.51	27454.19	27974.66
1996	12193.18	12908.21	13907.76	14825.38	15232.52	15464.03
1997	6504.91	7086.09	8451.69	10048.17	11777.83	13424.25
1998	6107.53	6530.30	7482.05	8540.90	9564.42	10662.59
1999	2426.48	2537.99	2785.77	3146.43	3485.08	4011.27
2000	621.51	657.96	780.90	900.54	998.77	1056.36
Mean	12798.95	13671.35	15343.53	16963.39	18468.59	19887.70
MAX	35890.30	37916.34	41705.36	45147.11	48228.69	50644.95
MIN	621.51	657.96	780.90	900.54	998.77	1056.36
SD	10338.30	10933.27	12026.69	12901.70	13639.59	14217.19

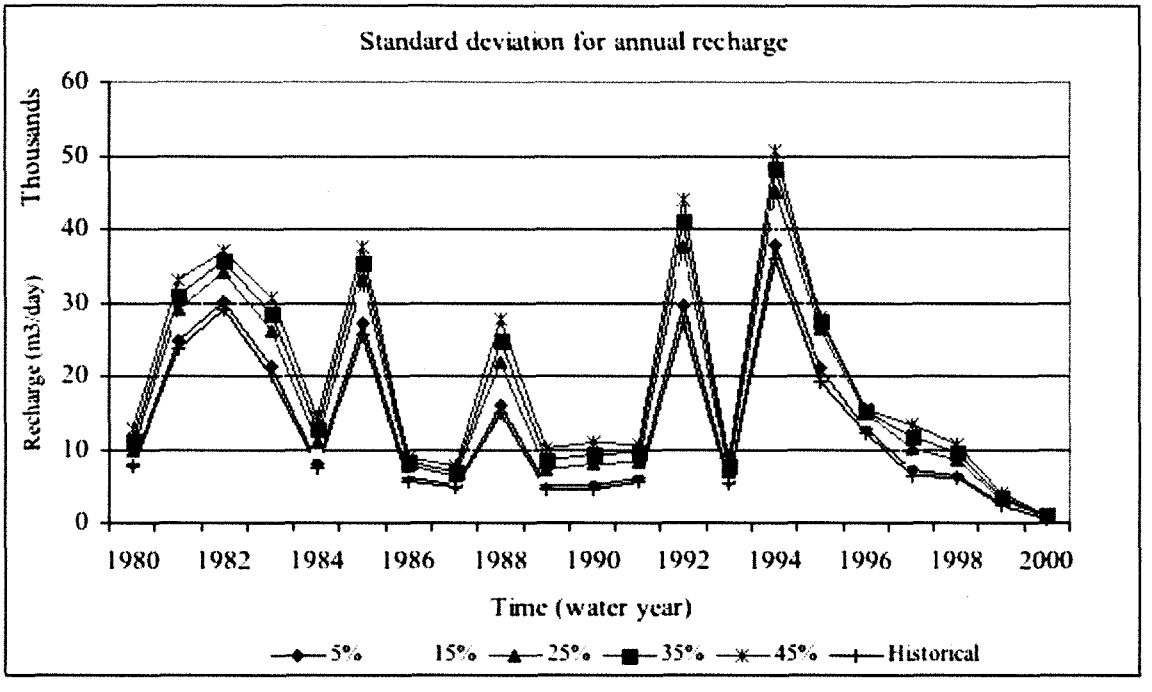

Figure (5.12) : Time series of standard deviation of annual recharge for the first scenario (m^3/day).

Table (5.13): The annual standard deviation relative percentage change for the first scenario (m^3/day).

Time	5%	15%	25%	35%	45%
1980-2000	5.68%	16.33%	26.04%	34.85%	42.83%
1980	4.950	15.514	29.239	46.469	67.240
1981	4.674	14.225	23.125	31.524	40.115
1982	3.787	11.910	17.793	22.702	28.006
1983	7.008	18.668	30.862	42.774	52.801
1984	9.034	26.842	47.882	70.253	93.646
1985	6.599	18.417	29.264	38.643	46.445
1986	7.904	23.399	35.162	44.784	55.533
1987	6.850	19.825	34.001	48.927	63.171
1988	8.234	26.294	46.509	67.542	87.250
1989	11.328	33.754	62.779	93.314	128.929
1990	13.584	41.272	72.108	106.212	141.039
1991	9.790	30.267	51.950	72.987	94.016
1992	9.017	25.253	38.783	51.221	62.316
1993	4.455	13.772	27.524	41.619	56.922
1994	5.645	16.202	25.792	34.378	41.110
1995	8.984	24.818	36.320	42.283	44.981
1996	5.864	14.062	21.587	24.927	26.825
1997	8.935	29.928	54.471	81.061	106.371
1998	6.922	22.505	39.842	56.600	74.581
1999	4.596	14.807	29.671	43.627	65.312
2000	5.865	25.645	44.894	60.699	69.965
Mean	7.335	22.256	38.074	53.455	68.885
MAX	13.584	41.272	72.108	106.212	141.039
MIN	3.787	11.910	17.793	22.702	26.825
SD	2.475	7.630	14.005	21.803	30.511

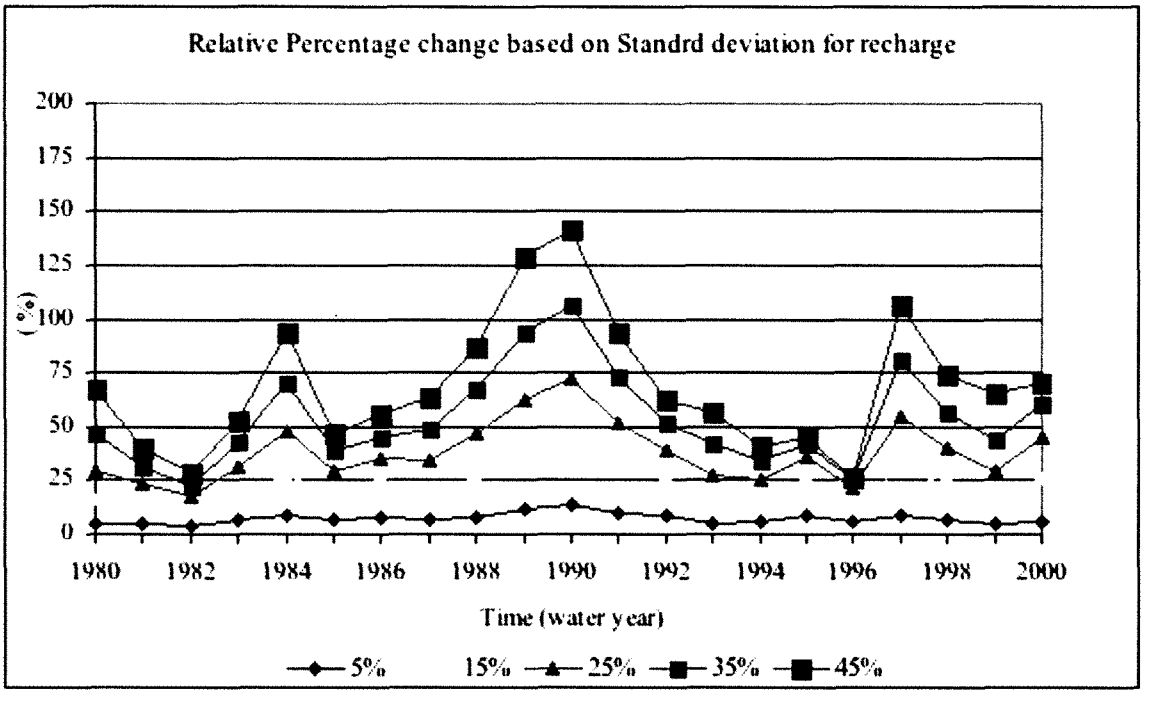

Figure (5.13): Time series of the relative percentage change based on standard deviation for the first scenario (m^3/day).

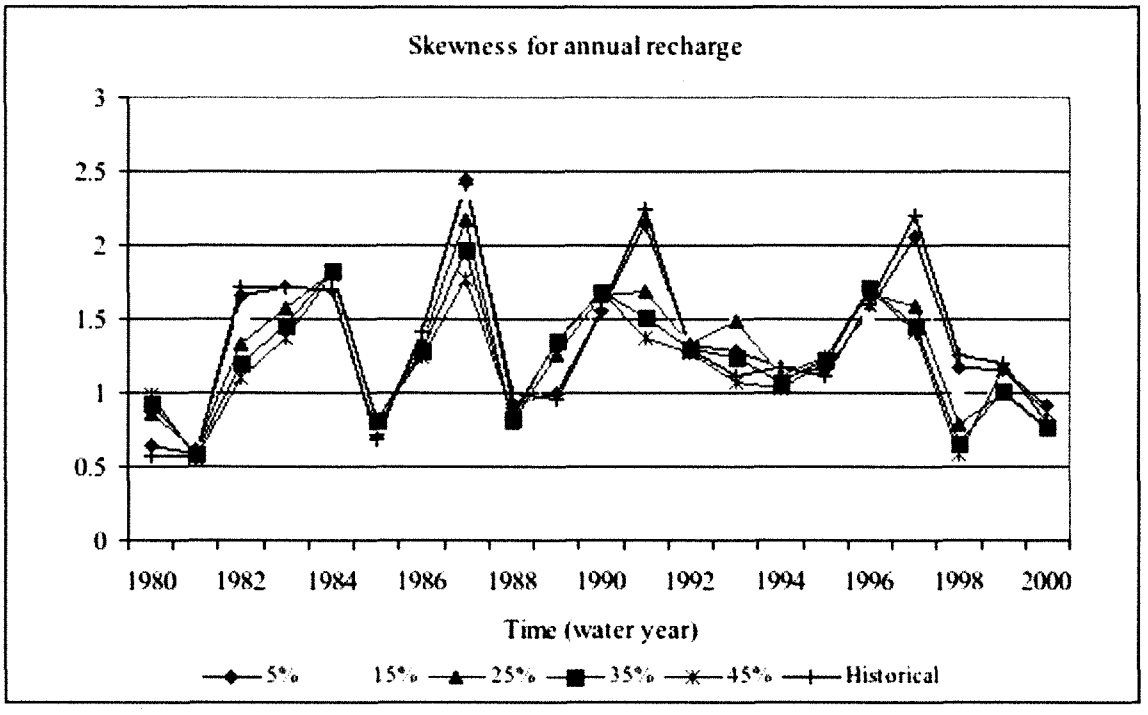

(a)

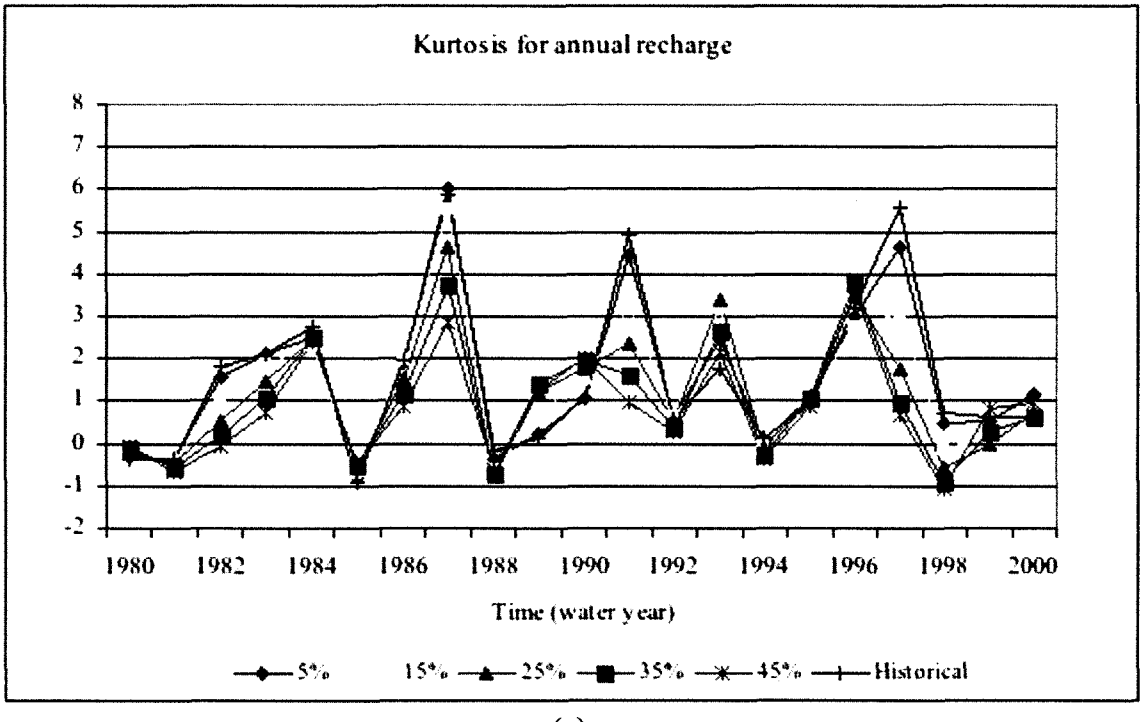

(a)

Figure (5.14): (a) Skewness coefficient and (b) kurtosis for annual recharge (the first scenario (m^3/day)).

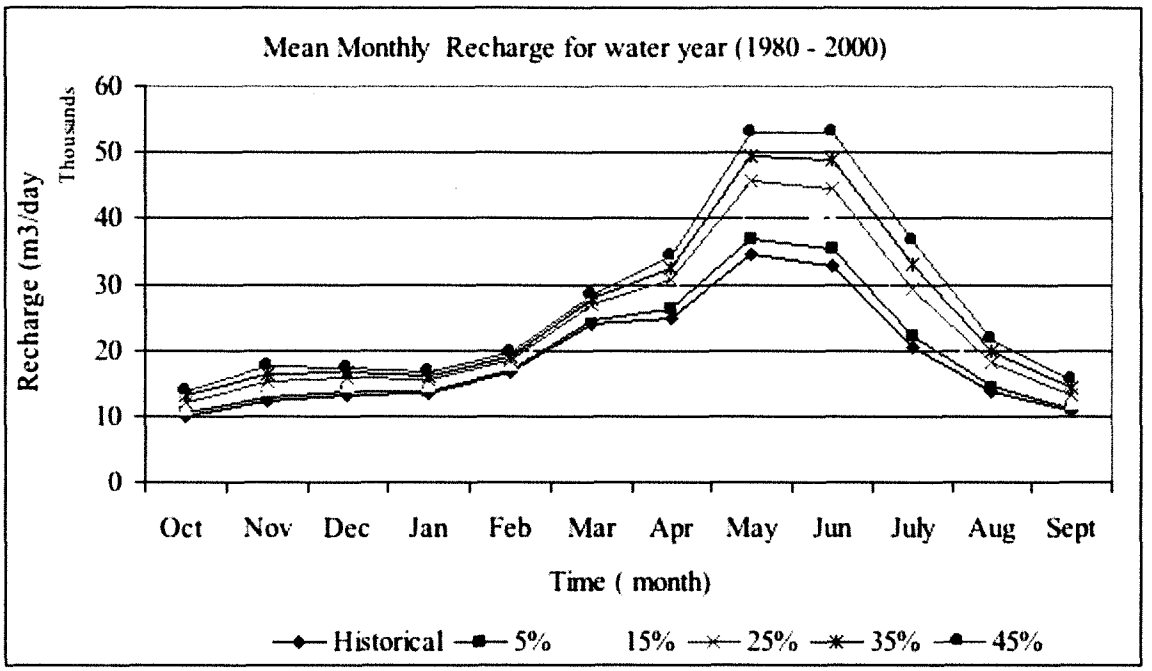

(a)

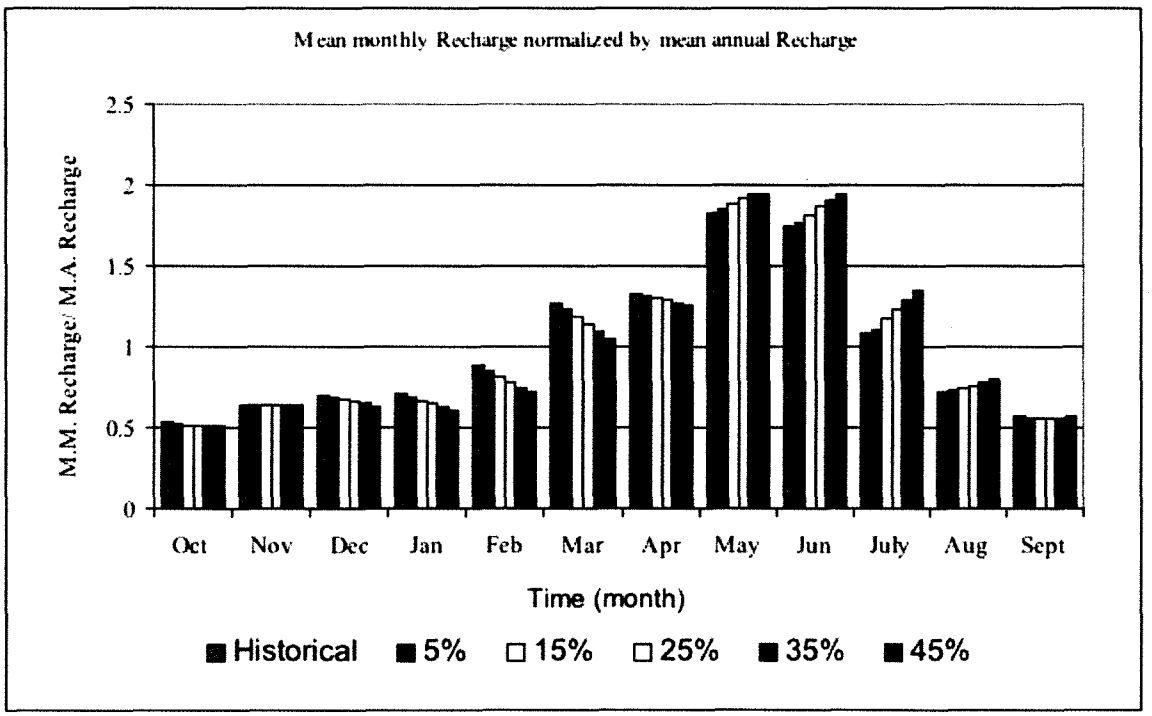

(b)

Figure (5.15): (a) Time series of the mean monthly recharge, (b) time series of the mean monthly recharge normalized by mean annual recharge (c) time series of the mean monthly of June, (d) time series of the mean monthly recharge of July, (e) time series of the mean monthly recharge of August for the first scenario (m^3/day)).

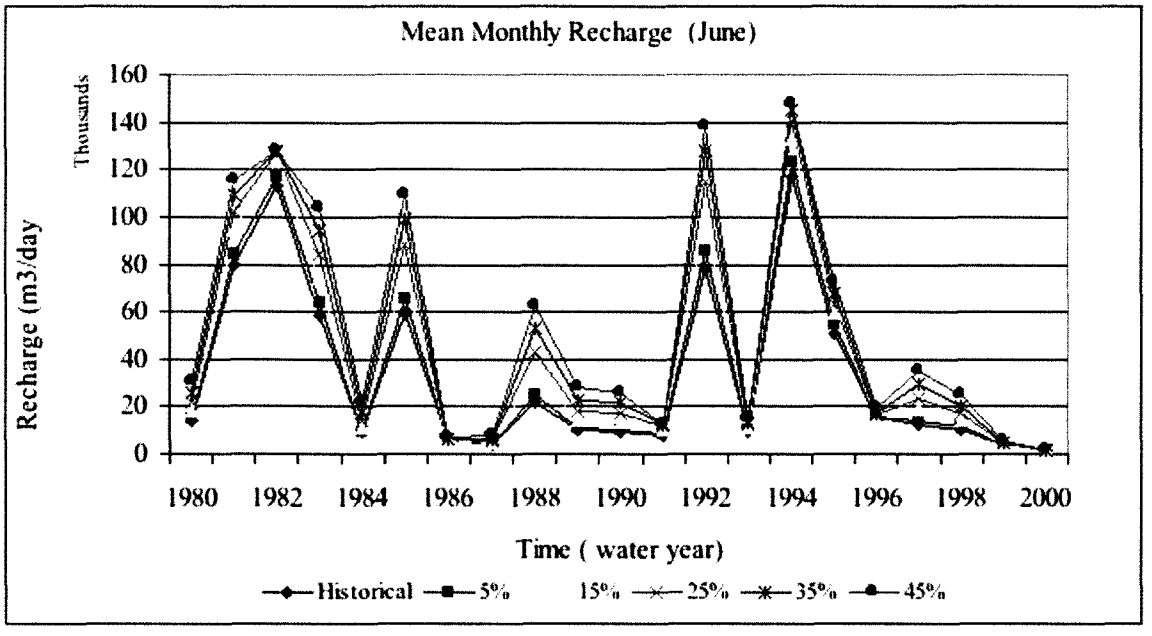

(c)

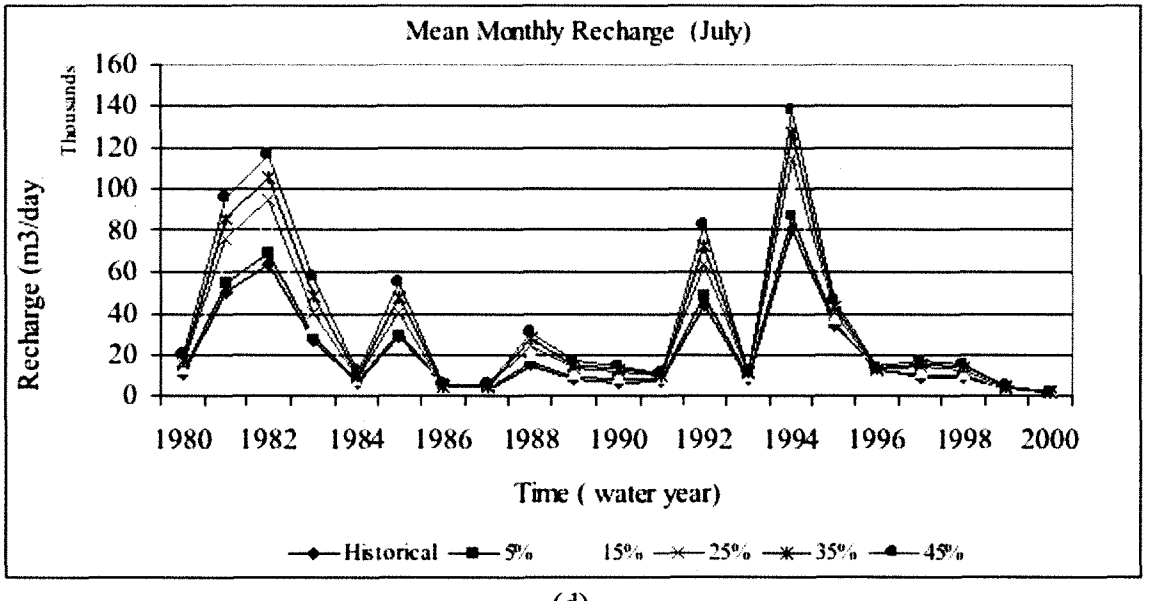

(d)

Figure (5.15): (a) Time series of the mean monthly recharge, (b) time series of the mean monthly recharge normalized by mean annual recharge (c) time series of the mean monthly of June, (d) time series of the mean monthly recharge of July, (e) time series of the mean monthly recharge of August for the first scenario (m^3/day)).
(continued).

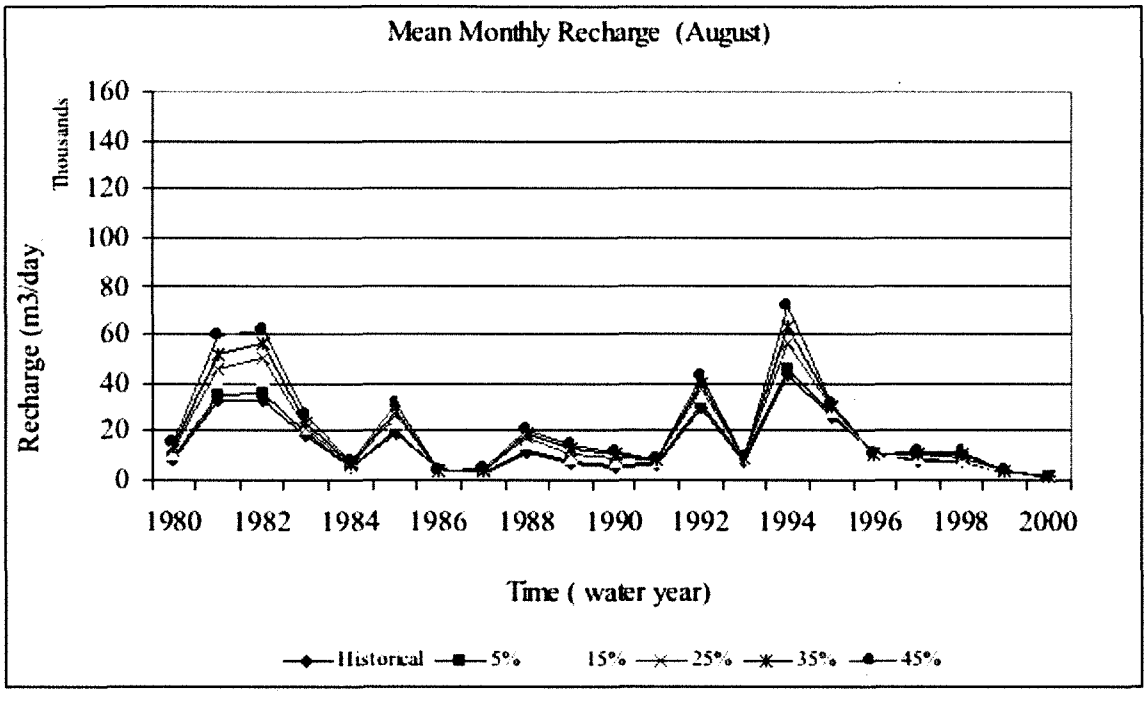

(e)

Figure (5.15): (a) Time series of the mean monthly recharge, (b) time series of the mean monthly recharge normalized by mean annual recharge (c) time series of the mean monthly of June, (d) time series of the mean monthly recharge of July, (e) time series of the mean monthly recharge of August for the first scenario (m^3/day)).
(continued).

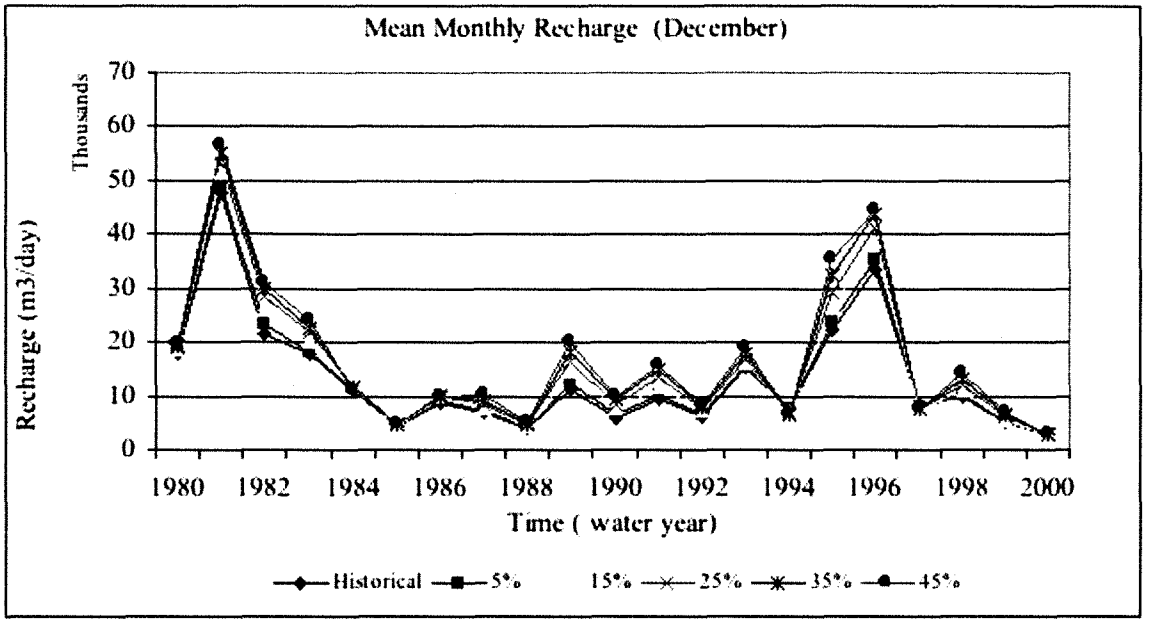

(a)

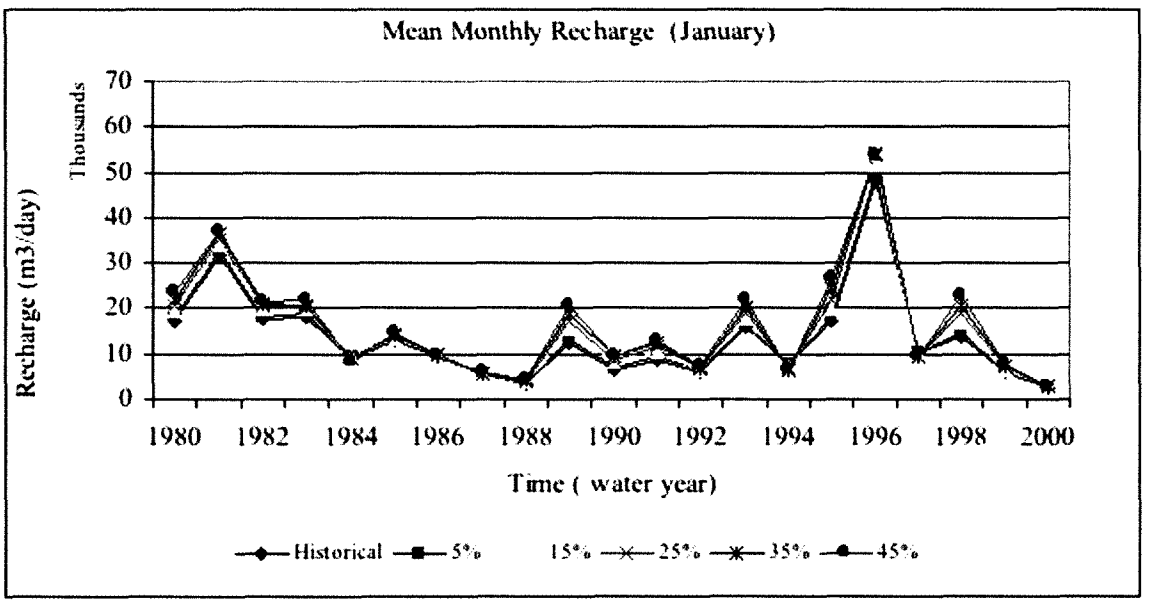

(b)

Figure (5.16): (a) Time series of the mean monthly recharge of December, (b) time series of the mean monthly recharge of January, (c) time series of the mean monthly recharge of February for the first scenario (m^3/day).

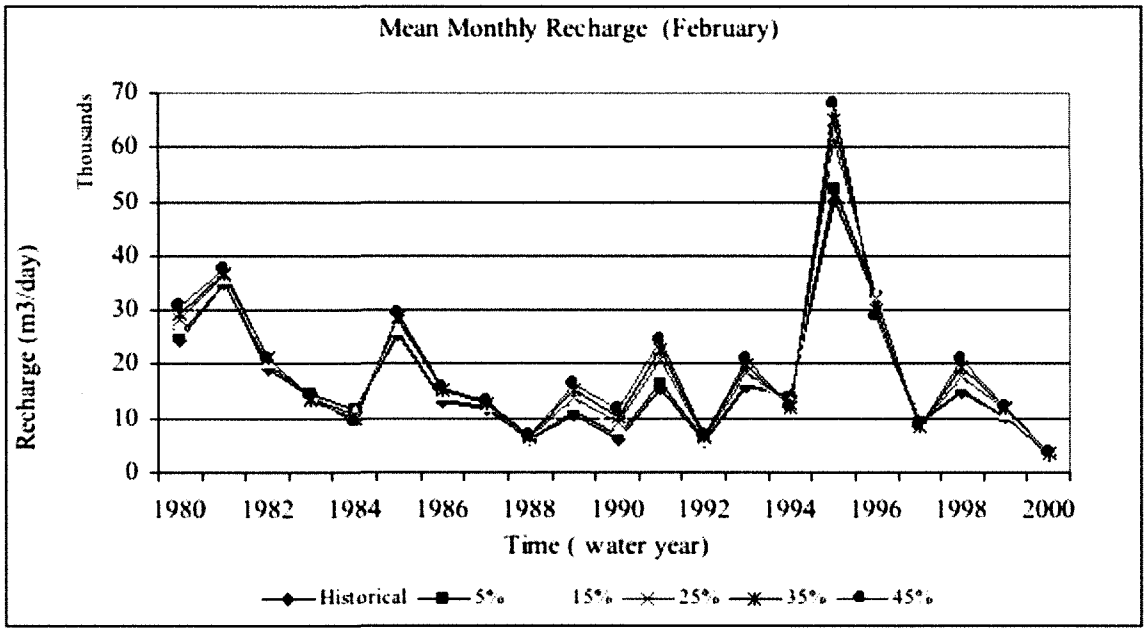

(c)

Figure (5.16): (a) Time series of the mean monthly recharge of December, (b) time series of the mean monthly recharge of January, (c) time series of the mean monthly recharge of February for the first scenario (m^3/day) (continued).

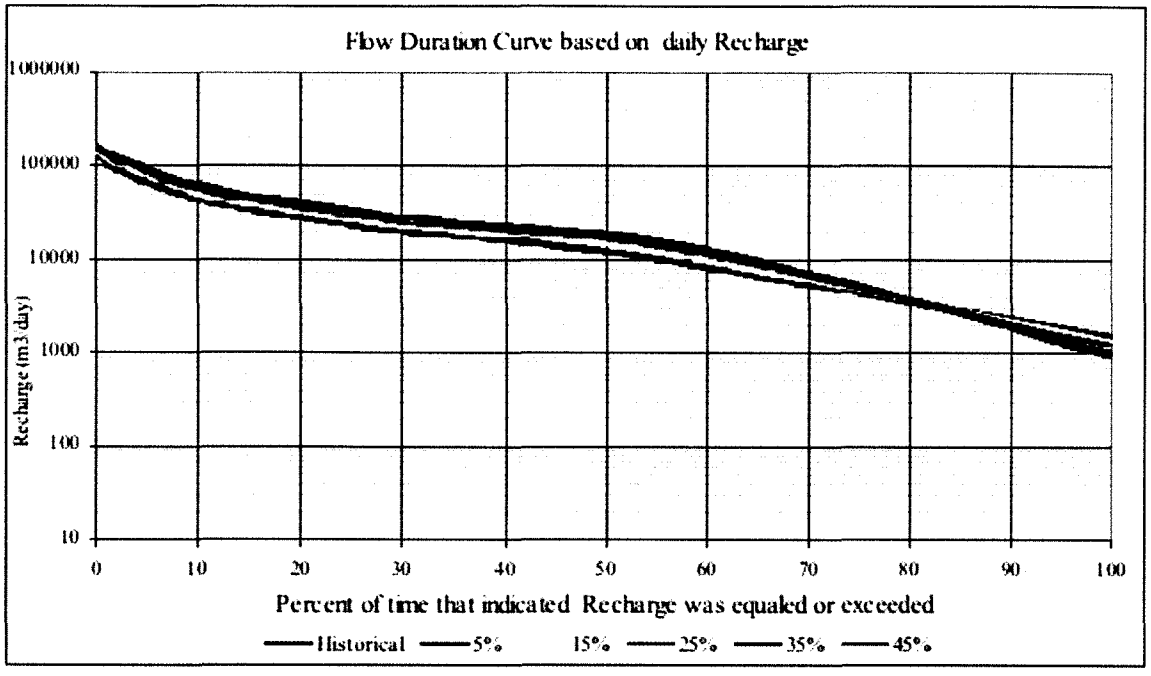

(a)

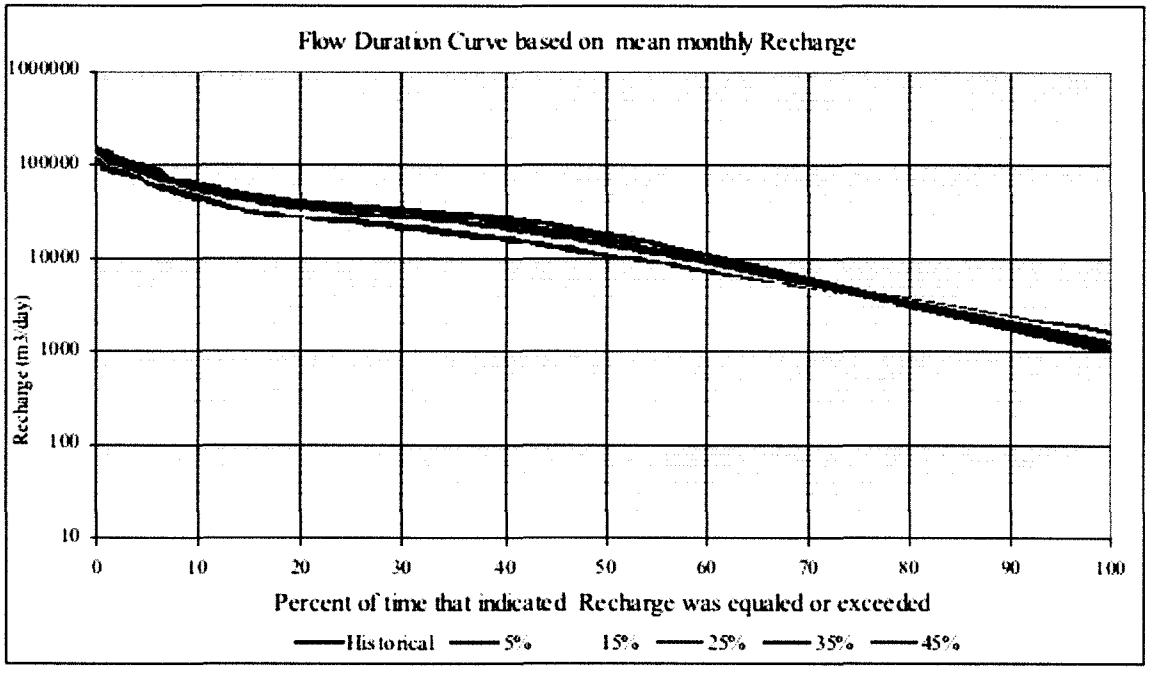

(b)

Figure (5.17): (a) Flow duration curve (daily), (b) Flow duration curve (monthly), (c) Flow duration curve of June, (d) Flow duration curve of July, (e) Flow duration curve of August for the first scenario (m^3/day).

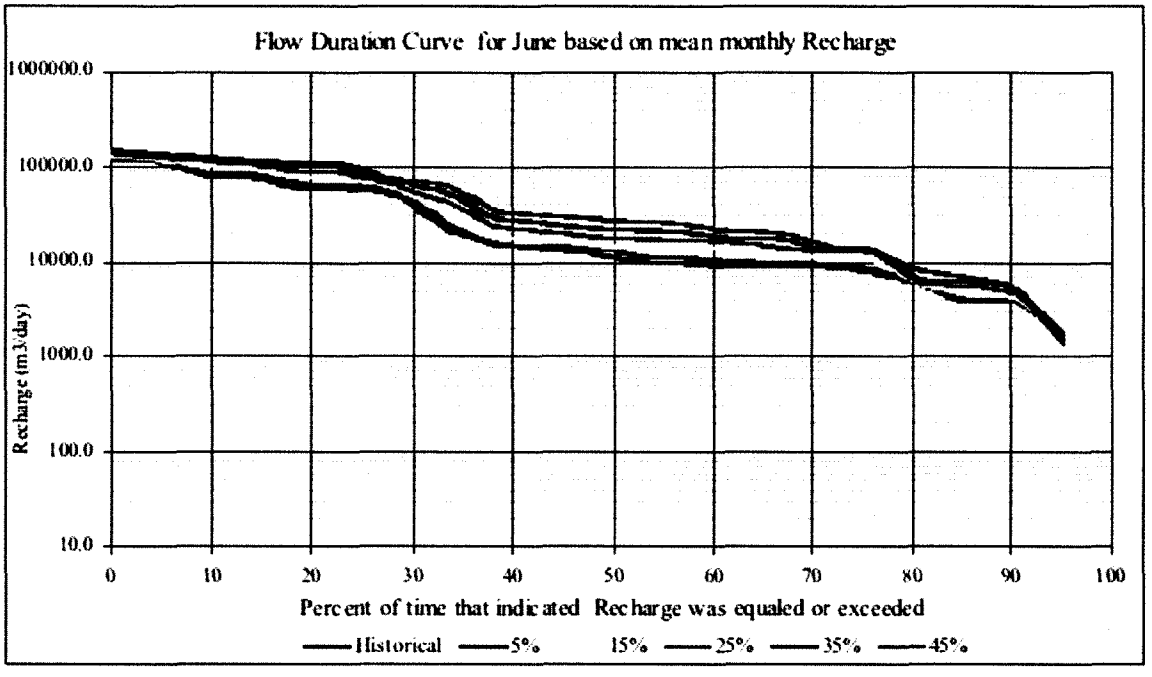

(c)

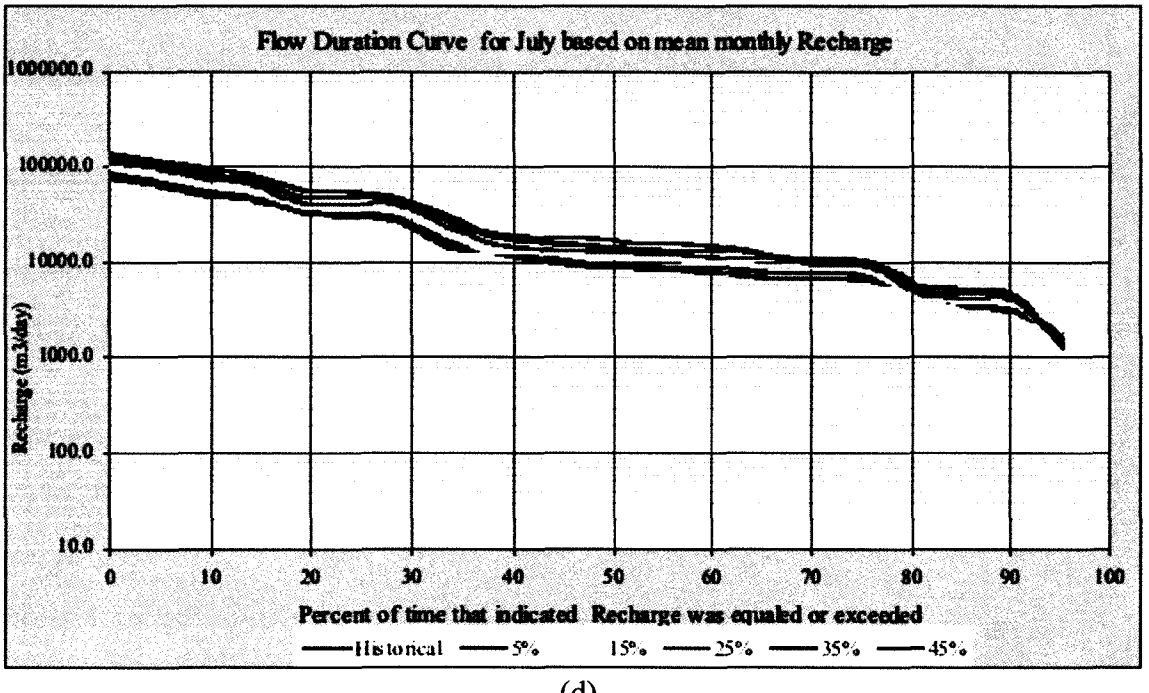

(d)

Figure (5.17): (a) Flow duration curve (daily), (b) Flow duration curve (monthly), (c) Flow duration curve of June, (d) Flow duration curve of July, (e) Flow duration curve of August for the first scenario (m^3/day) (continued).

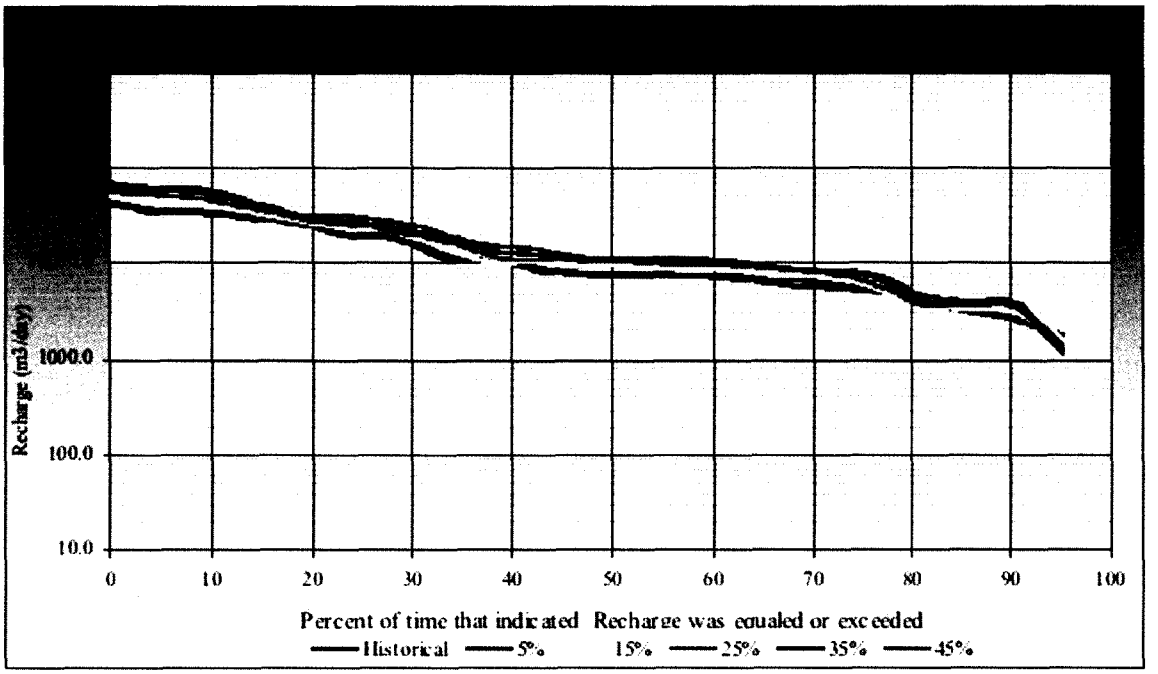

(e)

Figure (5.17): (a) Flow duration curve (daily), (b) Flow duration curve (monthly), (c) Flow duration curve of June, (d) Flow duration curve of July, (e) Flow duration curve of August for the first scenario (m^3/day) (continued).

5.4.2 Second scenario

In this second scenario the rainfall amount was decreased relative to the observed data assuming the precipitation is projected to decrease with an average change ranging between 5 and 45 percent (using 10 percent increments) with the same pattern of occurrence as the historical data. Variations of this scenario decreased the rainfall amount by 5%, 15%, 25%, 35%, and 45% of the average of the historical data following the same pattern and seasonality of the historical data. The pattern was preserved by only considering changes on the wet days.

5.4.2.1 Changes to daily, monthly and annual recharge flow

Figures (5.18) (a, b, c, and d) show the time series of the recharge flow for all decreases (5%, 15%, 25%, 35%, and 45%). All figures show the change in the recharge, and for a more clear presentation the time series of result recharge for the whole period (1980-2000) is shown in figure (5.18) (a). Plots are provided of the first seven-year period (figure (5.18) (b)), the second seven-year period (c), and the rest of the period in figure ((5.18) (d)). Notice the recharge for all scenarios decreases on the same relative magnitude as the decrease applied to the rainfall.

The descriptive statistics of the decreased recharge from this second scenario were analyzed. The mean annual recharge and multi-mean annual were calculated for all decreases, as illustrated in table (5.14) and in figure (5.19).

The percentages of the changes are shown in table (5.15). The table shows the daily average of the percentage change to the historical recharge. Table (5.16) shows the yearly average percentage changes to the recharge, which is shown graphically in figure (5.20). The descriptive statistics of the decreased recharge from the second scenario, include the standard deviation, skewness coefficient and kurtosis, which were calculated for annual recharge, where the standard deviation for annual recharge and multi-annual standard deviations have been calculated for all scenarios, as illustrated in table (5.17). The table has data were plotted and shown in figure (5.21) (a, b). The percentages of the changes are show in table (5.18) and in figure (5.22).

The skewness coefficient and kurtosis are shown in figure (5.23) (a, b). These figures show how the standard deviation, skewness coefficients and kurtosis for annual decreased recharge are changed corresponding to the change in the amount of

precipitation. The results presented are consistent with the results shown above in terms of changes in the precipitation amounts and have lower and decreasing daily and annual recharges. Furthermore, the mean monthly recharges for the water years (1980-2000) were obtained from the GSFLOW model to all months. The specific months of June, July, August, December, January, and February are shown for illustration purpose. Figure (5.24) (a) shows the mean monthly recharge for all decreases for the period (1980-2000).

The shifting in the time series of recharge in the figures shows it decreasing 5%, 15%, 25%, 35%, and 45% according to the decrease in precipitation. Figures (5.24) (c, d, e) and (5.25) (a, b, c) show the mean monthly recharge for June, July, August, December, January, and February. The flow duration curve frequency analysis for all scenarios 5%, 15%, 25%, 35%, and 45% have been calculated and plotted for daily and monthly recharge. Figures (5.26) (a, b, c, d, e) show the flow duration curve based on daily and monthly and specific month (June, July, and August) analysis.

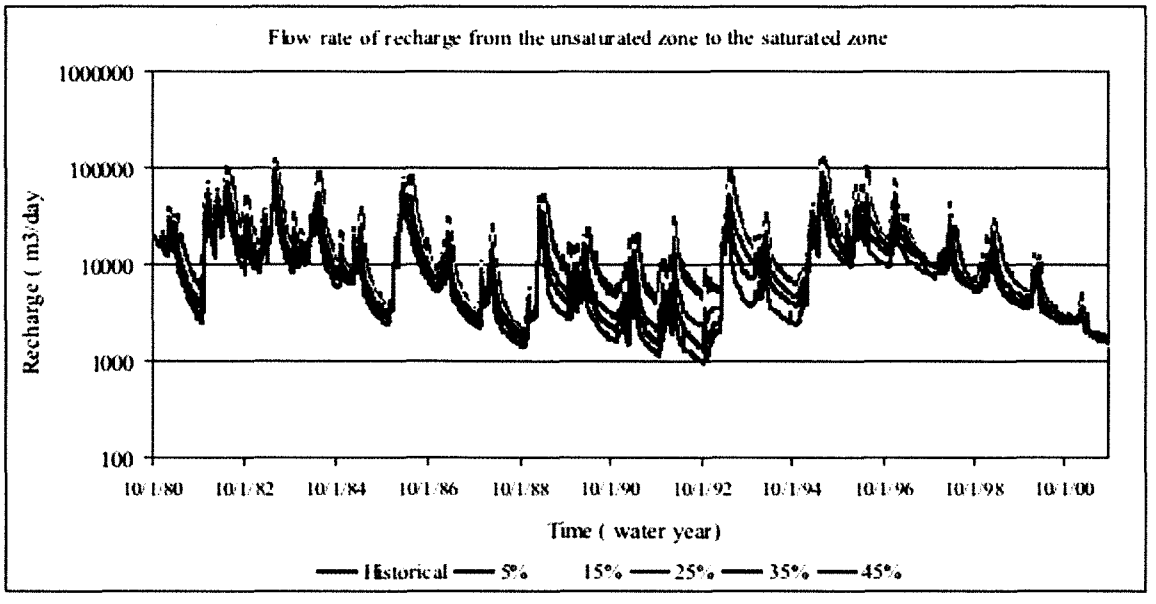

(a)

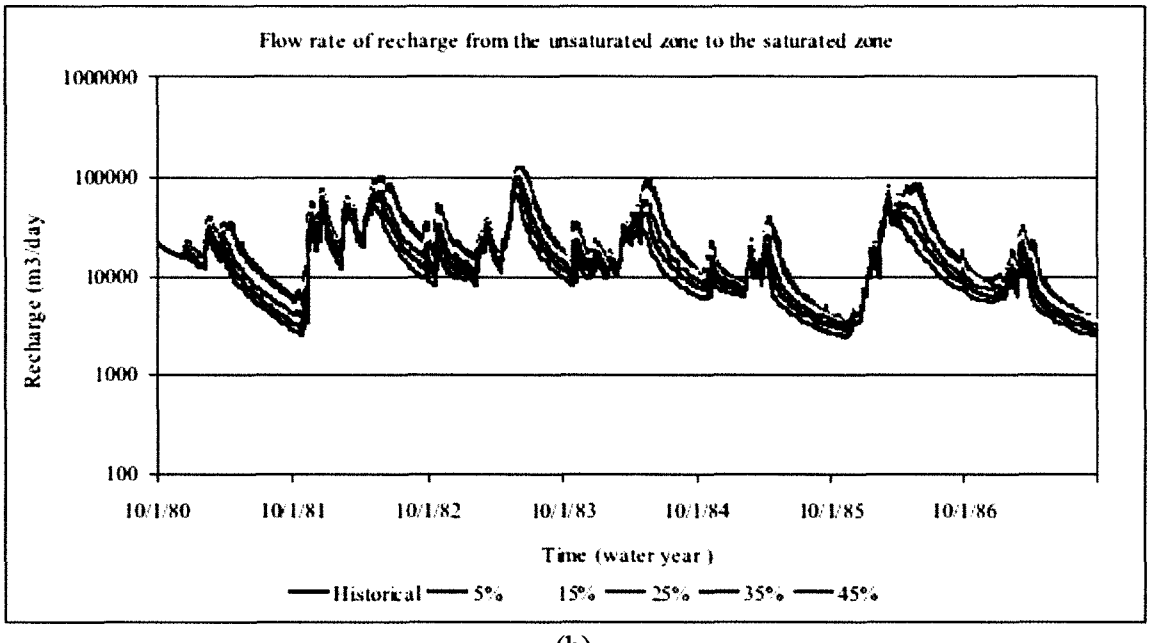

(b)

Figure (5.18): The time series of flow rate of the recharge at whole period (a), first seven years (b), second seven years(c) and rest of the time period (d) for the second scenario (m^3/day).

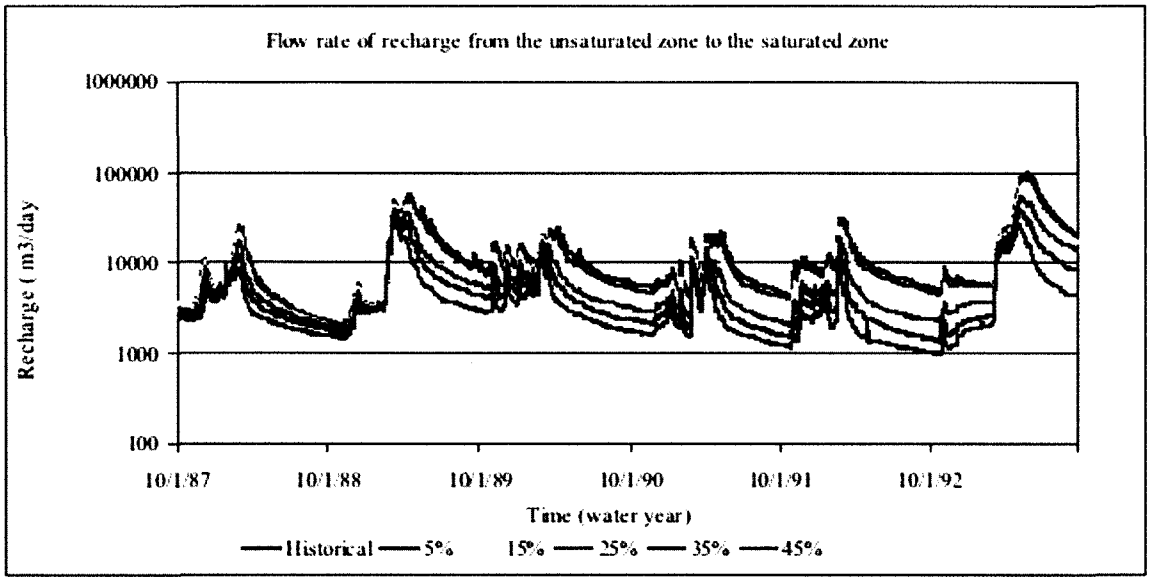

(c)

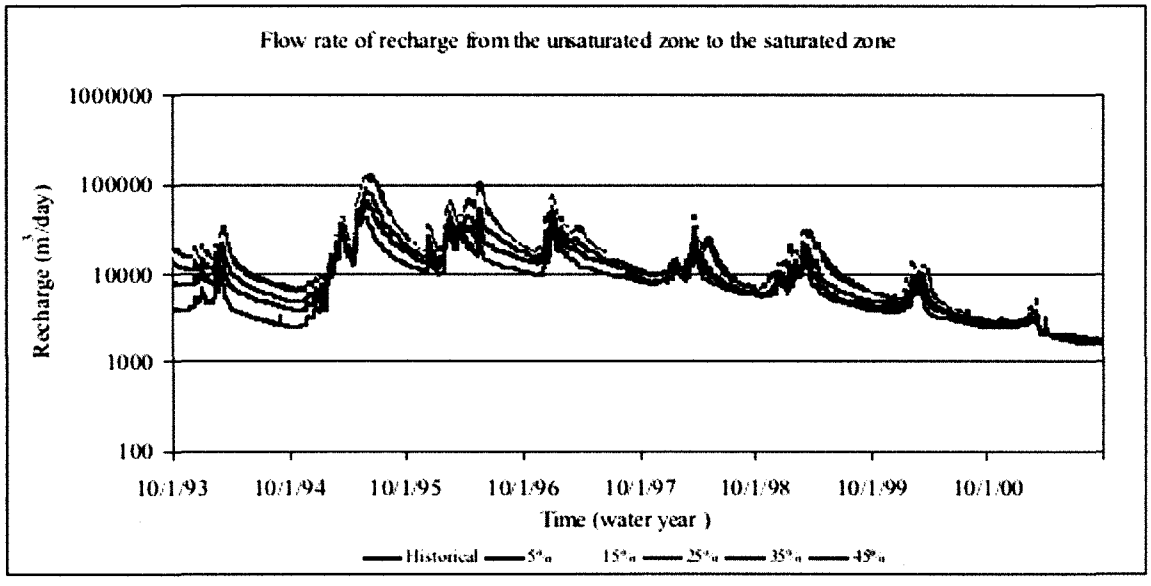

(d)

Figure (5.18): The time series of flow rate of the recharge at whole period (a), first seven years (b), second seven years(c) and rest of the time period (d) for the second scenario (m^3/day) (continued).

Table (5.14): The mean annual recharge for the second scenario (m^3/day).

Time	Historical	-5%	-15%	-25%	-35%	-45%
1980-2000	18926.788	17884.131	15740.67	13476.789	11077.871	8618.4849
1980	17708.163	16888.018	15303.127	13769.072	12360.721	11290.642
1981	41879.854	39935.635	35935.217	31660.034	27034.022	21939.863
1982	37911.343	35831.803	31920.565	27875.17	23435.792	18751.202
1983	28973.994	27535.12	24334.696	20889.001	17206.529	13337.259
1984	12057.183	11454.371	10241.344	9000.2471	7757.2171	6286.7102
1985	30296.348	28649.659	25354.128	21941.429	18305.931	14393.11
1986	9821.5426	9399.9126	8416.8657	7341.7142	6281.4962	5248.2218
1987	5758.739	5533.9366	5058.0292	4449.372	3729.2426	3020.6524
1988	15813.659	14533.995	12040.676	9890.7712	7904.1248	5879.8562
1989	11420.047	10201.564	8127.9442	6361.2927	4893.1677	3542.6636
1990	8317.2196	7312.7634	5559.8546	4160.91	3084.8891	2308.9819
1991	9557.2339	8533.6587	6361.359	4366.0418	2917.2239	1962.6558
1992	26949.585	24861.406	20333.867	15374.522	10366.844	6651.6731
1993	13498.135	12858.661	11442.998	9548.5696	6911.801	4068.1395
1994	37135.334	35344.812	31172.848	26289.636	20778.707	15102.325
1995	36033.397	34283.092	30371.242	25539.875	19990.752	14701.738
1996	22612.056	22131.513	20873.786	18956.017	15993.305	12093.629
1997	11818.43	11418.482	10800.898	10400.885	9985.7447	8324.5649
1998	12097.975	11285.44	9778.4904	8318.5992	7183.7198	6284.155
1999	5498.997	5315.6076	4975.8317	4694.1803	4237.6424	3583.0891
2000	2327.4621	2279.8149	2171.1365	2205.635	2296.4413	2234.8245
Mean	18927.938	17885.203	15741.662	13477.761	11078.824	8619.3312
MAX	41879.854	39935.635	35935.217	31660.034	27034.022	21939.863
MIN	2327.4621	2279.8149	2171.1365	2205.635	2296.4413	1962.6558
SD	12193.138	11632.473	10429.345	9044.492	7488.1161	5898.0026

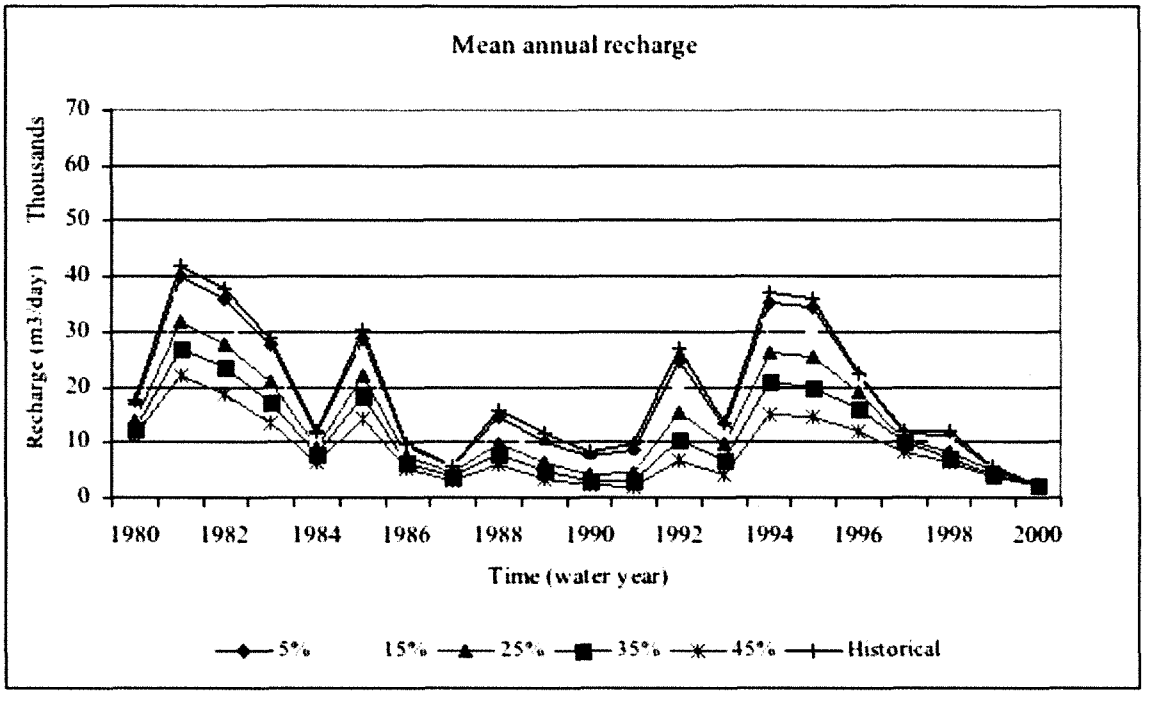

Figure (5.19): Time series of mean annual recharge (m^3/day).

Table (5.15): The daily average relative percentage change for the second scenario.

	-5%	-15%	-25%	-35%	-45%
Average	-5.05%	-15.18%	-25.24%	-35.69%	-47.33%

Table (5.16): The annual average relative percentage change for the second scenario.

Time	-5%	-15%	-25%	-35%	-45%
1980-2000	-4.631	-13.582	-22.244	-30.198	-36.240
1980	-4.642	-14.195	-24.403	-35.449	-47.612
1981	-5.485	-15.802	-26.473	-38.183	-50.539
1982	-4.966	-16.012	-27.904	-40.614	-53.968
1983	-5.000	-15.060	-25.354	-35.663	-47.859
1984	-5.435	-16.313	-27.577	-39.577	-52.492
1985	-4.293	-14.302	-25.249	-36.044	-46.564
1986	-3.904	-12.168	-22.737	-35.242	-47.547
1987	-8.092	-23.859	-37.454	-50.017	-62.818
1988	-10.670	-28.827	-44.297	-57.153	-68.979
1989	-12.077	-33.152	-49.972	-62.910	-72.239
1990	-10.710	-33.439	-54.317	-69.476	-79.464
1991	-7.748	-24.548	-42.951	-61.532	-75.318
1992	-4.737	-15.225	-29.260	-48.794	-69.861
1993	-4.822	-16.056	-29.206	-44.046	-59.332
1994	-4.857	-15.714	-29.122	-44.522	-59.200
1995	-2.125	-7.687	-16.169	-29.271	-46.517
1996	-3.384	-8.610	-11.994	-15.507	-29.563
1997	-6.716	-19.173	-31.240	-40.620	-48.056
1998	-3.335	-9.514	-14.636	-22.938	-34.841
1999	-2.047	-6.717	-5.234	-1.333	-3.980
2000	-5.699	-17.141	-28.466	-39.957	-52.047
Mean	**-5.75**	**-17.31**	**-28.76**	**-40.42**	**-52.80**
MAX	**-12.077**	**-33.439**	**-54.317**	**-69.476**	**-79.464**
MIN	**2.734**	**7.618**	**12.141**	**15.883**	**17.360**
SD	**-4.631**	**-13.582**	**-22.244**	**-30.198**	**-36.240**

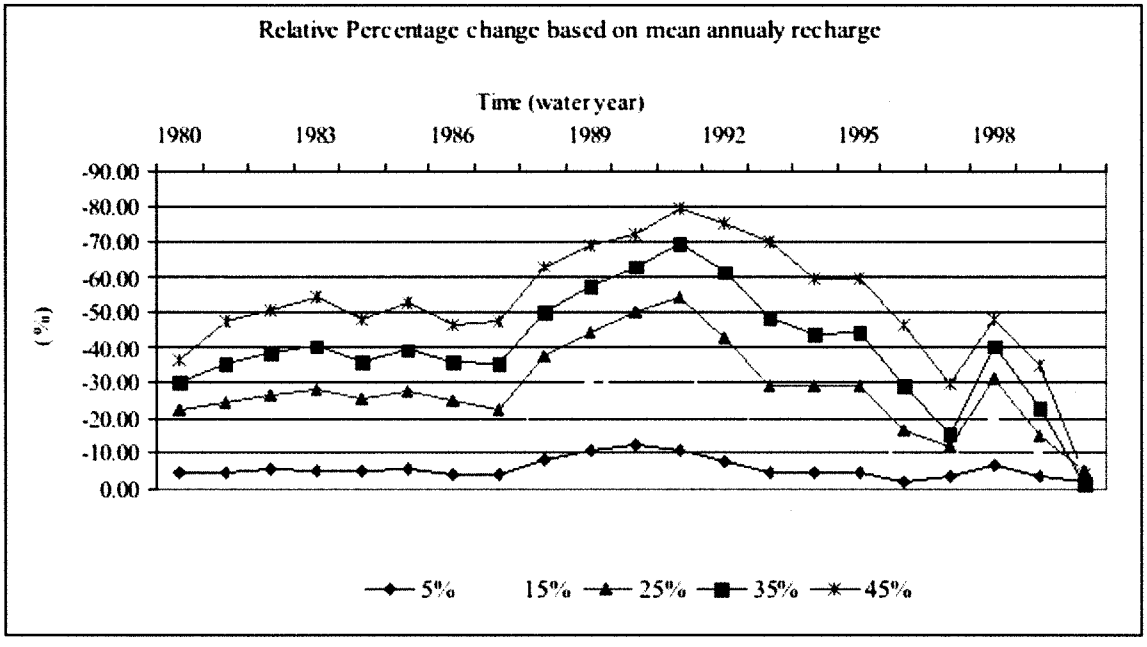

Figure (5.20): Time series of the relative percentage change based on annual recharge (m^3/day).

Table(5.17) The standard deviation of annual recharge for the second scenario (m^3/day).

Time	Historical	-5%	-15%	-25%	-35%	-45%
1980-2000	20161.22	18961.08	16462.40	13803.67	11136.59	8637.73
1980	7731.89	7413.73	6856.08	6502.11	6279.23	6067.86
1981	23603.27	22434.39	20130.03	17812.00	15604.10	13057.61
1982	29059.45	27769.84	25087.09	21541.55	17749.24	13329.34
1983	20038.97	18448.20	15177.56	11884.03	8865.33	6250.70
1984	7447.23	6800.17	5594.80	4636.78	3787.72	2908.11
1985	25600.68	23845.72	20638.19	17567.11	14718.42	12015.07
1986	5641.41	5241.29	4493.59	3835.87	3132.68	2437.31
1987	4685.37	4347.59	3703.07	2960.29	2239.96	1686.30
1988	14846.74	13666.05	11474.93	9561.70	7745.79	6139.70
1989	4473.41	4030.91	3511.19	3022.97	2492.93	1920.02
1990	4574.19	4002.36	3122.01	2436.13	1930.40	1517.30
1991	5491.31	4957.04	3995.24	2945.84	2073.91	1433.44
1992	27090.32	24560.48	19309.38	14308.16	9827.12	6505.79
1993	5454.27	5150.24	4477.95	3644.10	2481.88	1595.75
1994	35890.30	33758.11	28750.73	22996.42	16757.75	11493.01
1995	19295.44	17586.94	13635.48	9744.93	6771.47	5289.67
1996	12193.18	11384.87	9776.37	7828.59	6115.64	4947.81
1997	6504.91	5996.43	5018.73	4225.40	3520.63	2475.21
1998	6107.53	5686.41	4689.30	3738.85	3079.79	2359.94
1999	2426.48	2331.56	2068.83	1797.65	1352.28	1004.18
2000	621.51	587.09	520.04	507.36	477.94	359.37
Mean	12798.95	11904.73	10096.69	8261.80	6524.01	4990.17
MAX	35890.30	33758.11	28750.73	22996.42	17749.24	13329.34
MIN	621.51	587.09	520.04	507.36	477.94	359.37
SD	10338.30	9697.33	8320.85	6850.46	5447.58	4187.63

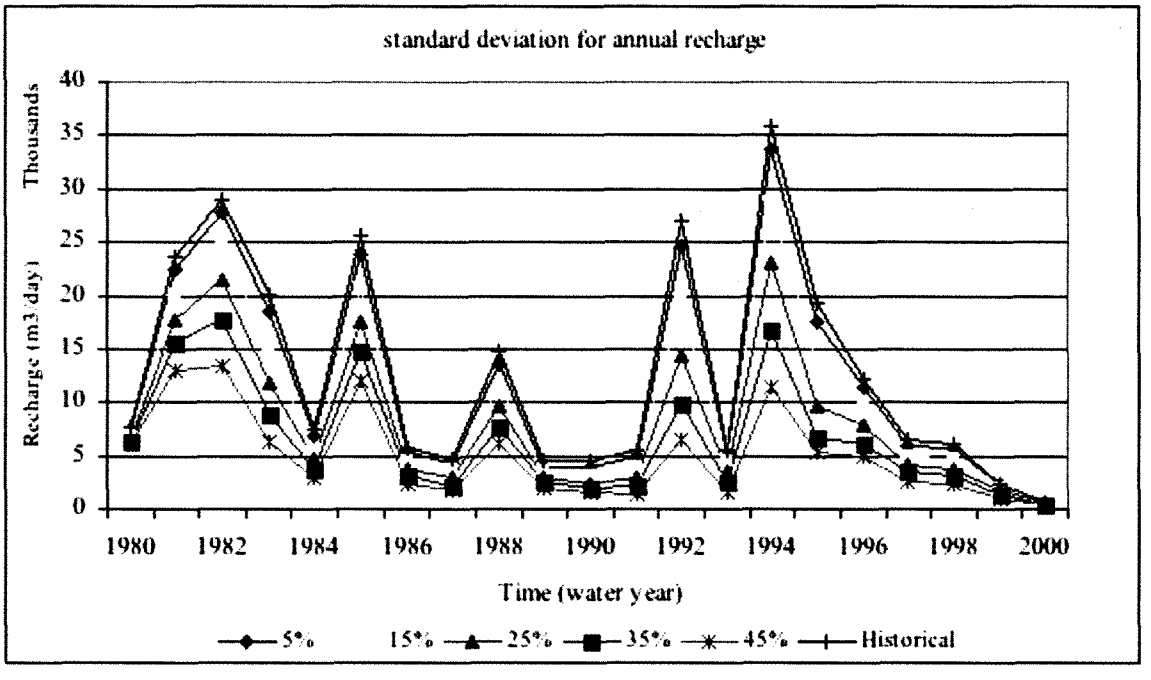

Figure (5.21): Time series of standard deviation of annual recharge for second scenario (m^3/day).

Table (5.18): The annual standard deviation relative percentage change for the second scenario.

Time	-5%	-15%	-25%	-35%	-45%
1980-2000	-5.95%	-18.35%	-31.53%	-44.76%	-57.16%
1980	-4.115	-11.327	-15.905	-18.788	-21.522
1981	-4.952	-14.715	-24.536	-33.890	-44.679
1982	-4.438	-13.670	-25.871	-38.921	-54.131
1983	-7.938	-24.260	-40.695	-55.760	-68.807
1984	-8.689	-24.874	-37.738	-49.139	-60.950
1985	-6.855	-19.384	-31.380	-42.508	-53.067
1986	-7.092	-20.346	-32.005	-44.470	-56.796
1987	-7.209	-20.965	-36.818	-52.192	-64.009
1988	-7.953	-22.711	-35.597	-47.828	-58.646
1989	-9.892	-21.510	-32.424	-44.272	-57.079
1990	-12.501	-31.747	-46.742	-57.798	-66.829
1991	-9.729	-27.244	-46.354	-62.233	-73.896
1992	-9.339	-28.722	-47.183	-63.725	-75.985
1993	-5.574	-17.900	-33.188	-54.496	-70.743
1994	-5.941	-19.893	-35.926	-53.308	-67.977
1995	-8.854	-29.333	-49.496	-64.906	-72.586
1996	-6.629	-19.821	-35.795	-49.844	-59.422
1997	-7.817	-22.847	-35.043	-45.877	-61.949
1998	-6.895	-23.221	-38.783	-49.574	-61.360
1999	-3.912	-14.739	-25.915	-44.270	-58.616
2000	-5.540	-16.327	-18.367	-23.100	-42.178
Mean	-7.232	-21.217	-34.560	-47.471	-59.582
MAX	-3.912	-11.327	-15.905	-18.788	-21.522
MIN	-12.501	-31.747	-49.496	-64.906	-75.985
SD	2.160	5.398	9.026	11.855	12.385

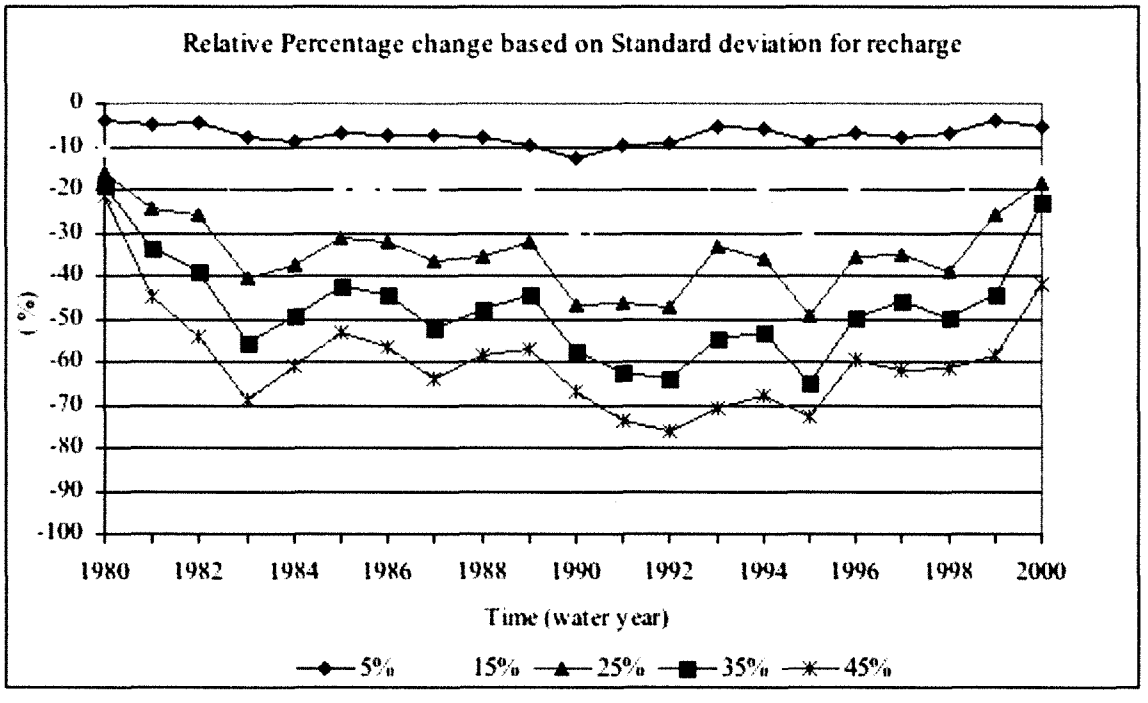

Figure (5.22): Time series of the relative percentage change based on standard deviation for the second scenario

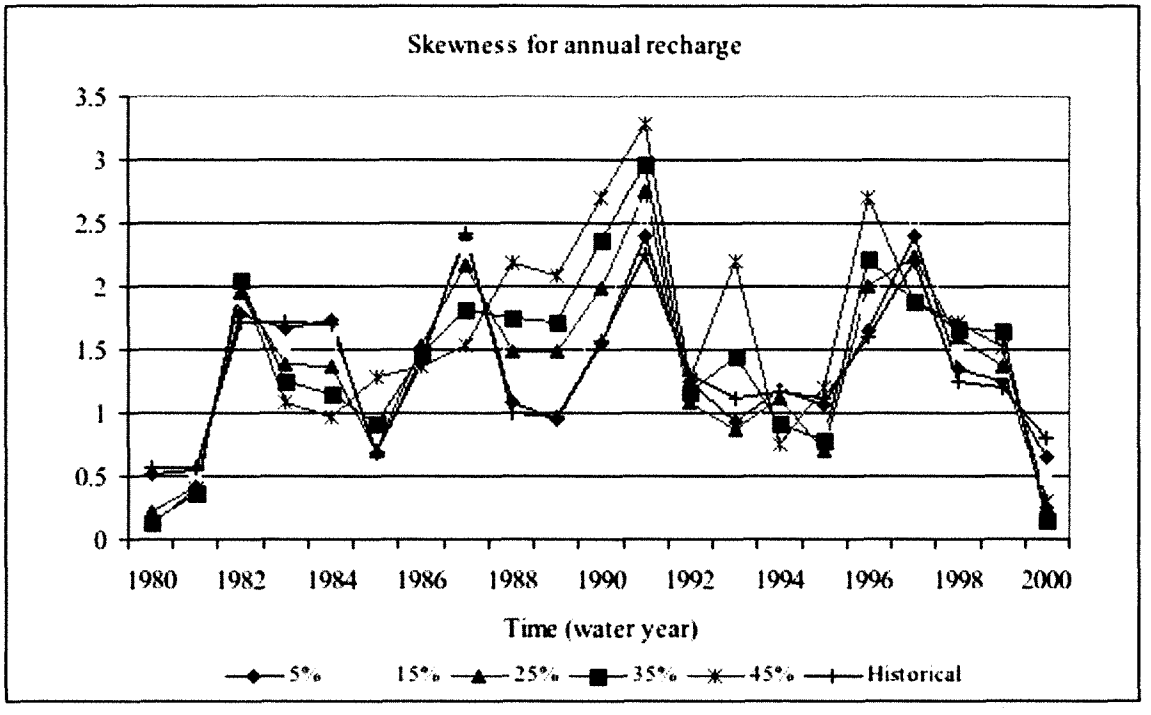

(a)

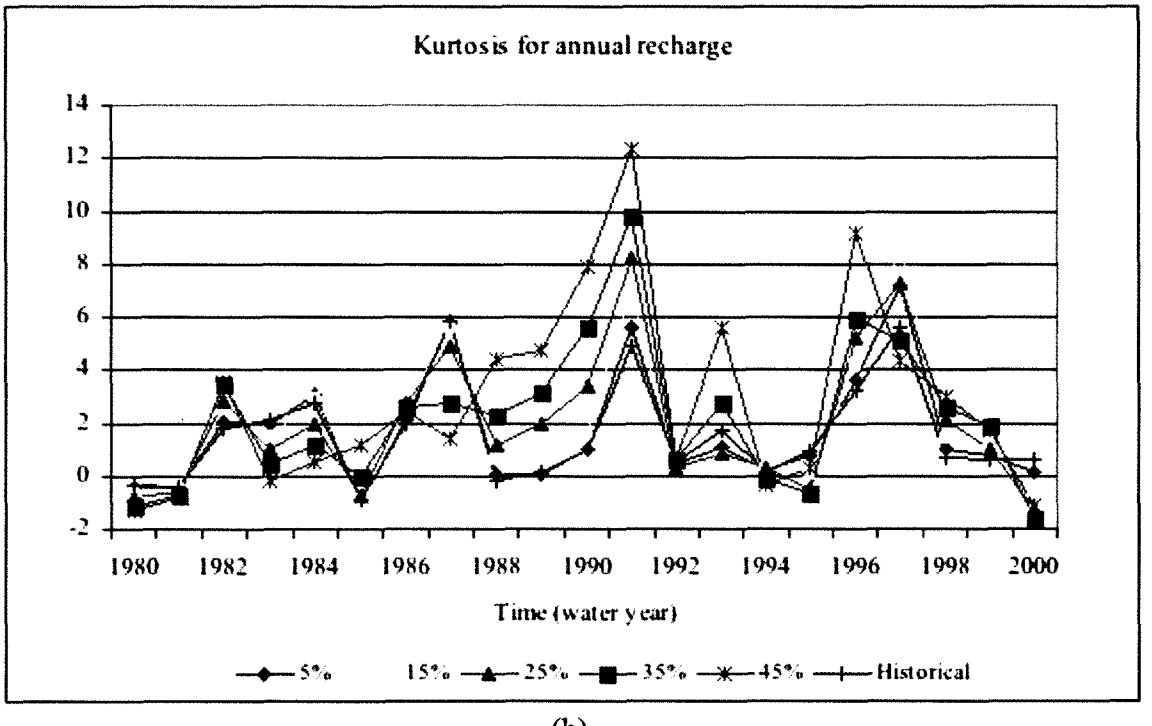

(b)

Figure (5.23): Time series of (a) skewness coefficient and (b) kurtosis annual recharge (m^3/day) for second scenario.

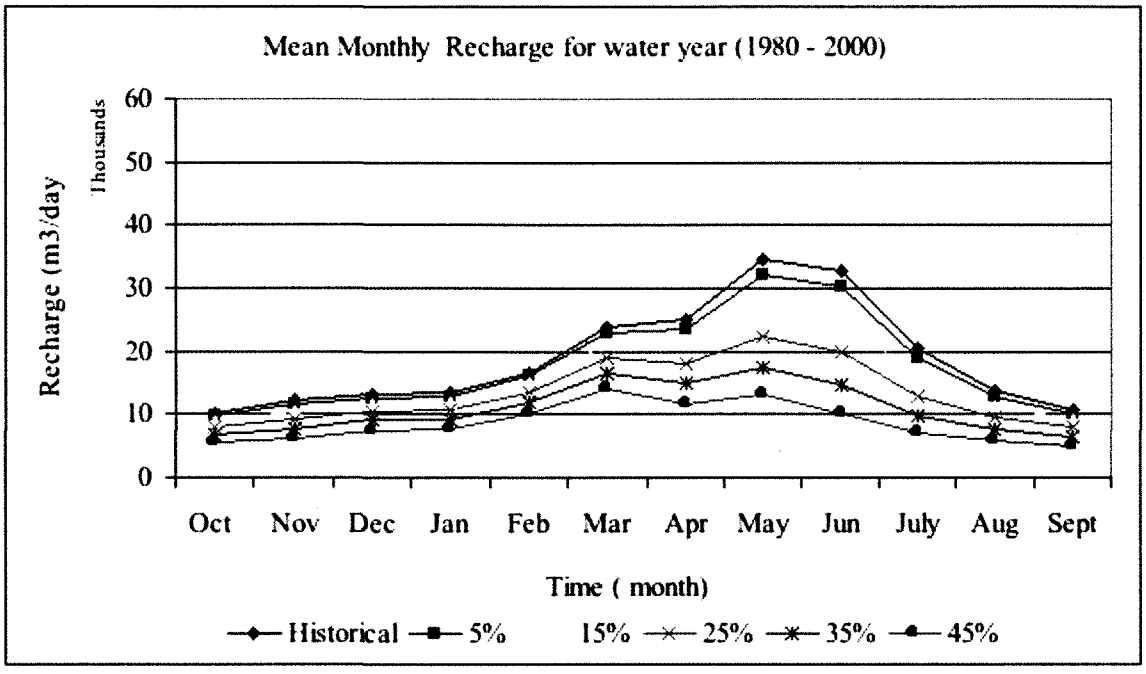

(a)

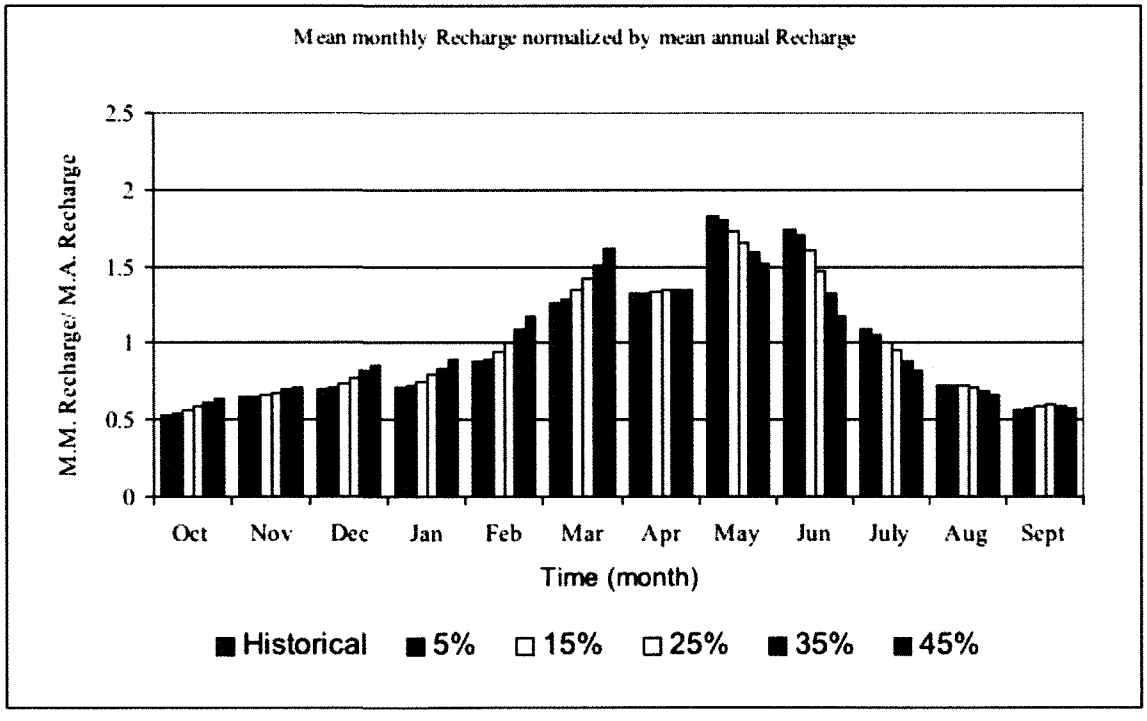

(b)

Figure (5.24): (a) Time series of the mean monthly recharge (b) time series of the mean monthly recharge normalized by mean annual recharge (c) time series of the mean monthly of June, (d) time series of the mean monthly recharge of July, (e) time series of the mean monthly recharge of August for second scenario (m3/day).

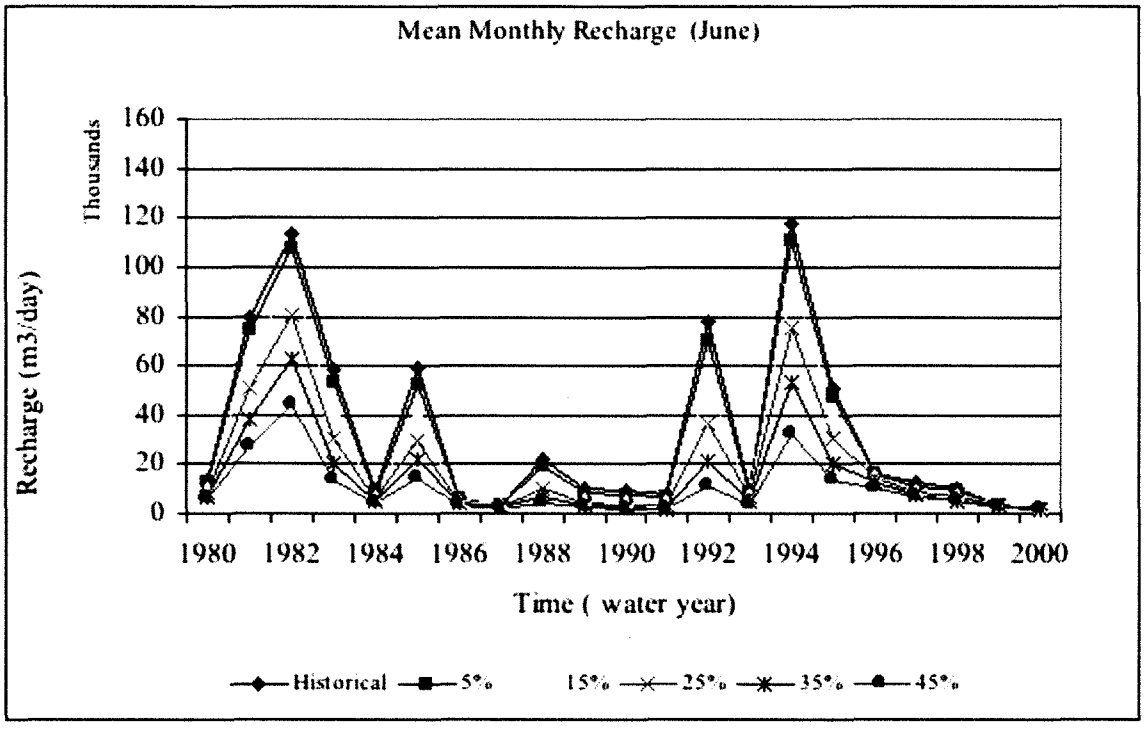

(c)

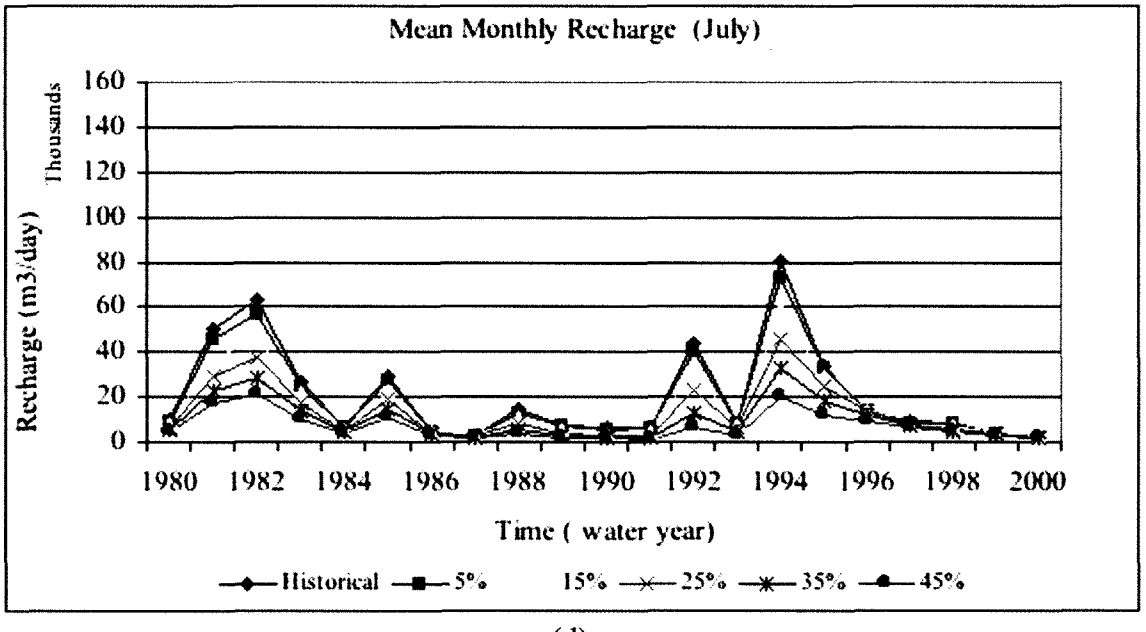

(d)

Figure (5.24): (a) Time series of the mean monthly recharge (b) time series of the mean monthly recharge normalized by mean annual recharge (c) time series of the mean monthly of June, (d) time series of the mean monthly recharge of July, (e) time series of the mean monthly recharge of August for second scenario (m3/day) (continued).

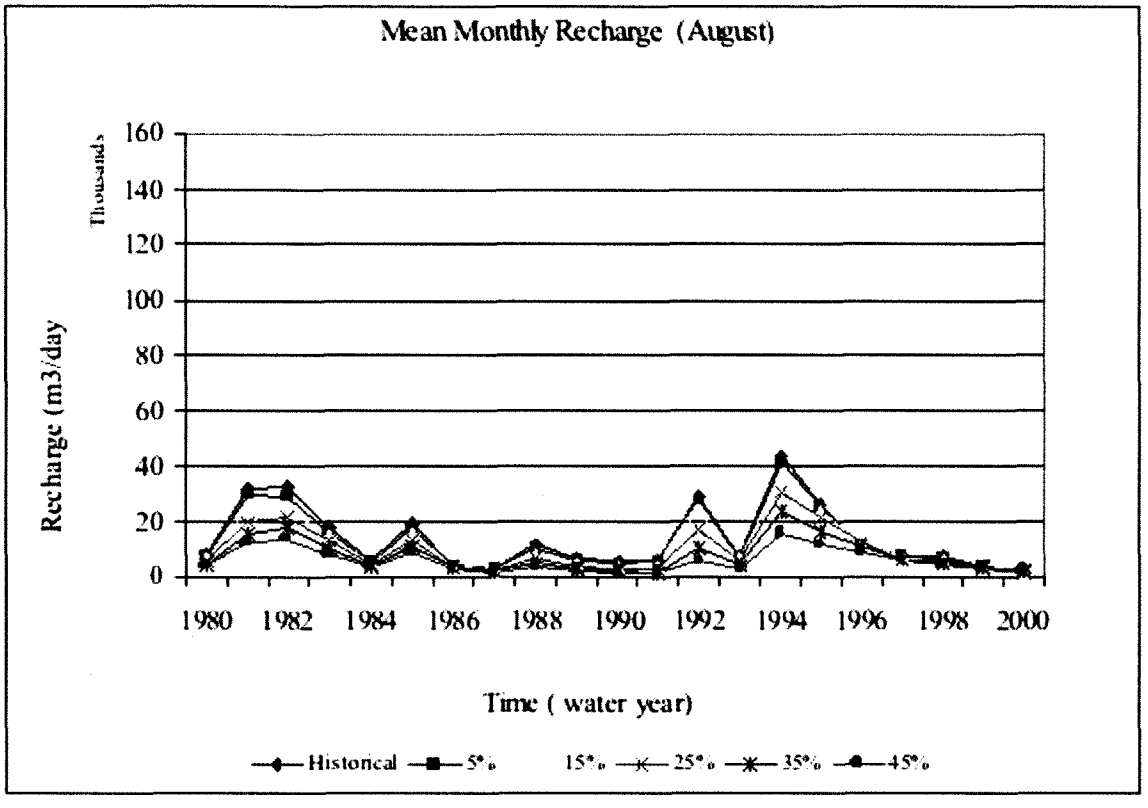

(e)

Figure (5.24): (a) Time series of the mean monthly recharge (b) time series of the mean monthly recharge normalized by mean annual recharge (c) time series of the mean monthly of June, (d) time series of the mean monthly recharge of July, (e) time series of the mean monthly recharge of August for second scenario (m3/day) (continued).

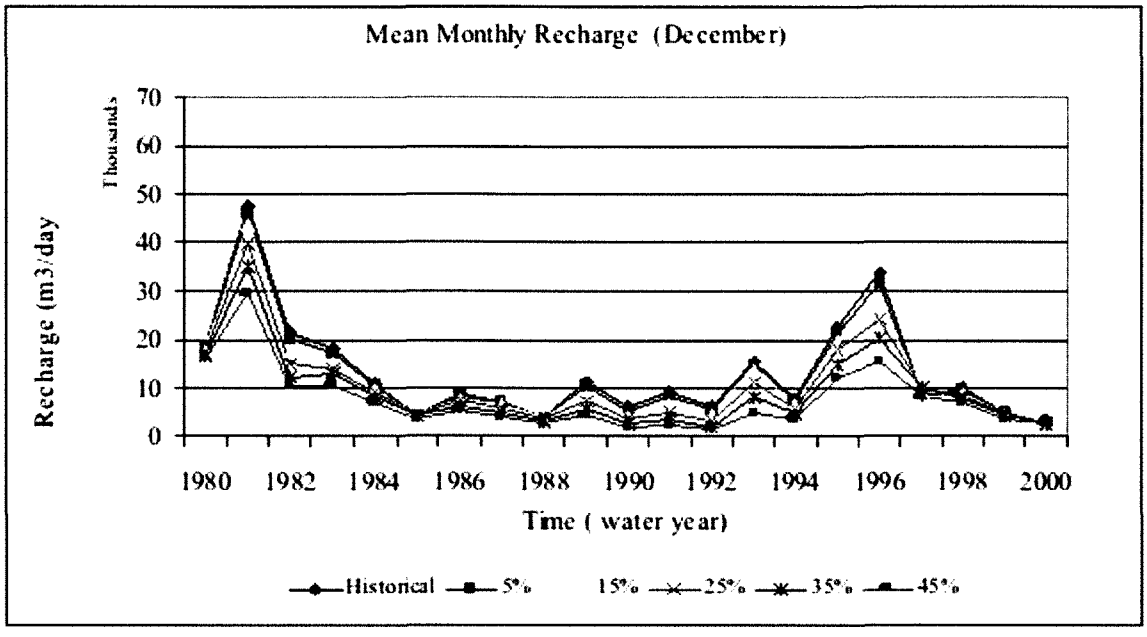

(a)

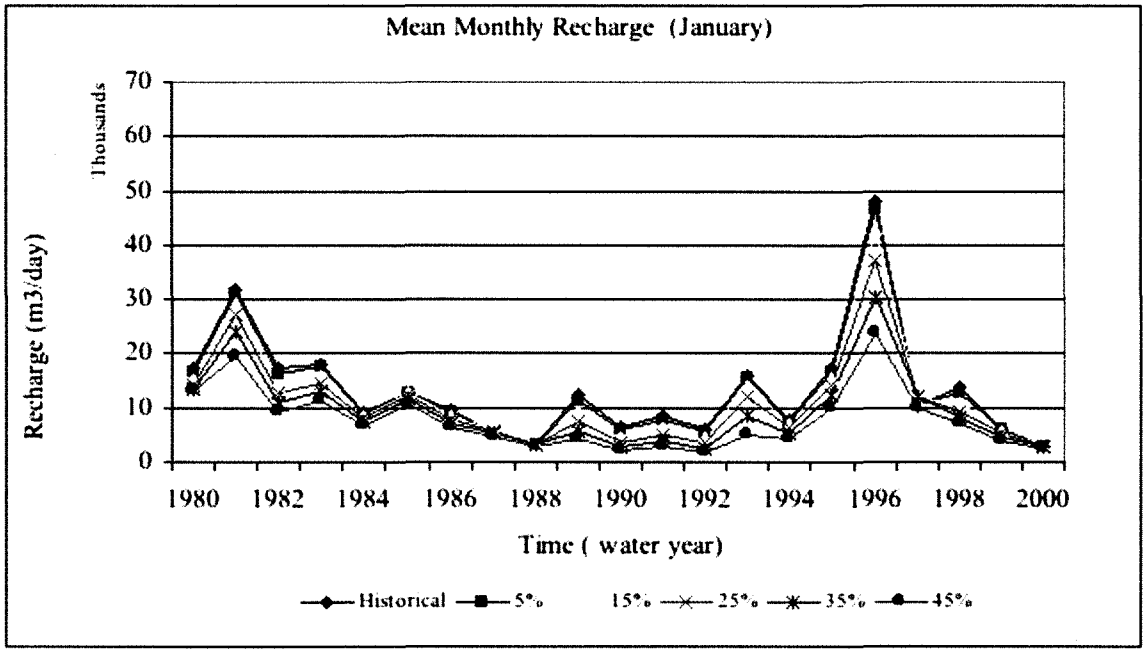

(b)

Figure (5.25): (a) Time series of the mean monthly recharge of December, (b) time series of the mean monthly recharge of January, (c) time series of the mean monthly recharge of February for second scenario (m3/day).

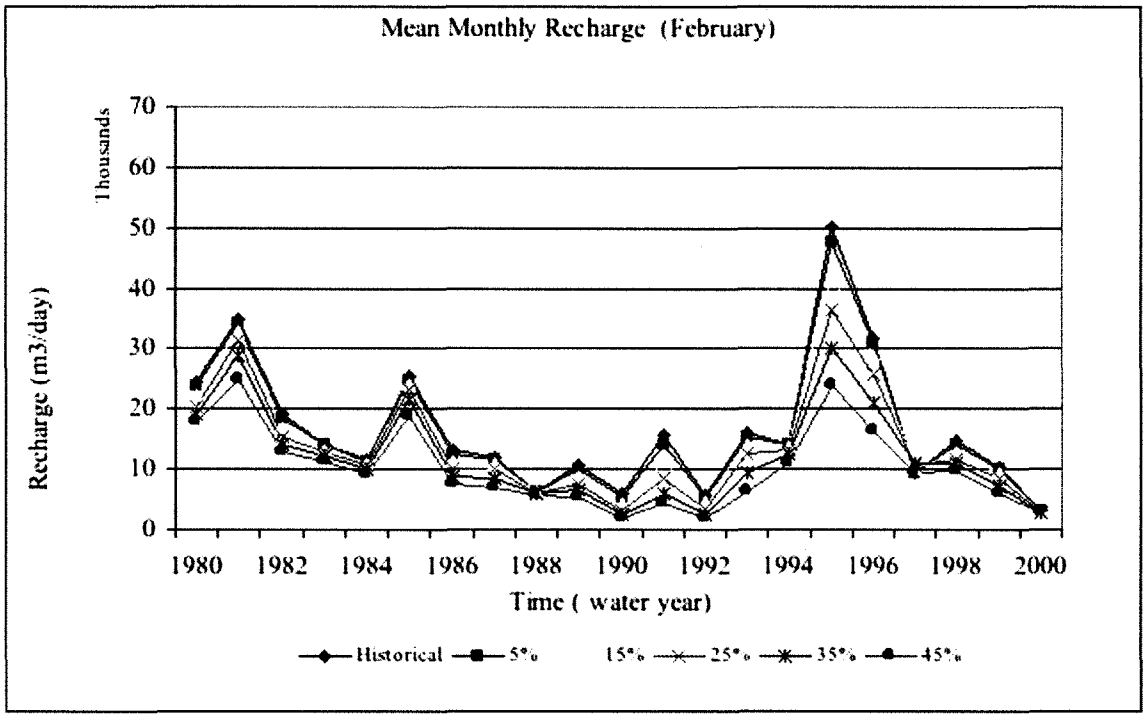

(c)

Figure (5.25): (a) Time series of the mean monthly recharge of December, (b) time series of the mean monthly recharge of January, (c) time series of the mean monthly recharge of February for second scenario (m3/day) (continued).

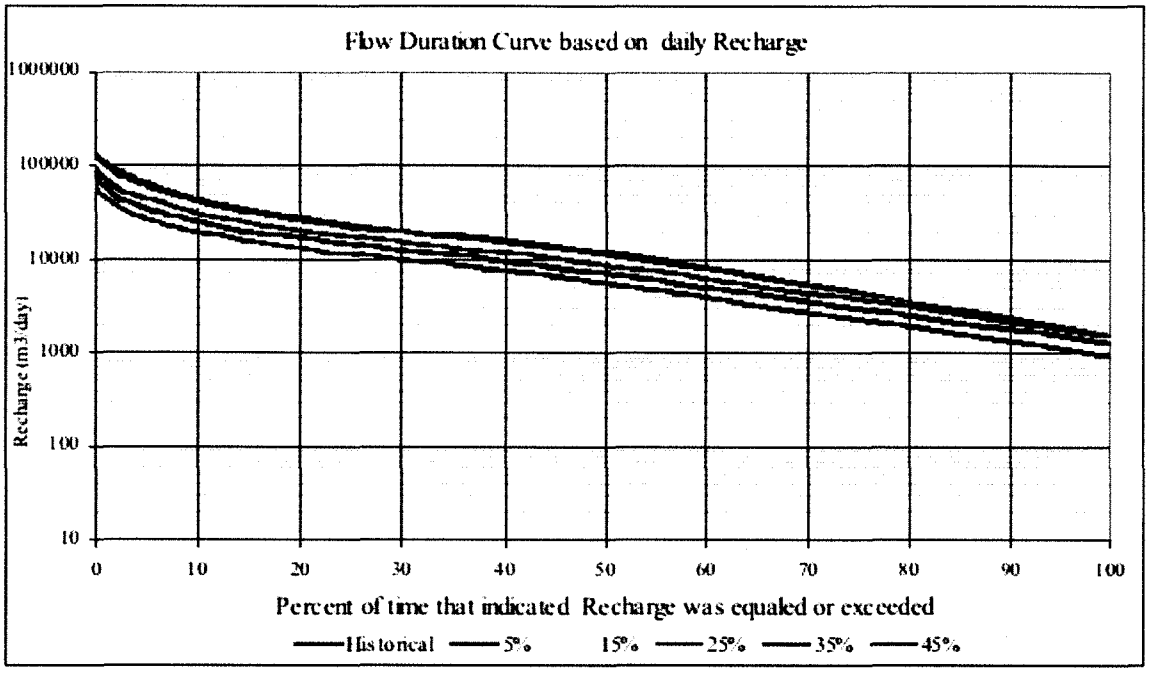

(a)

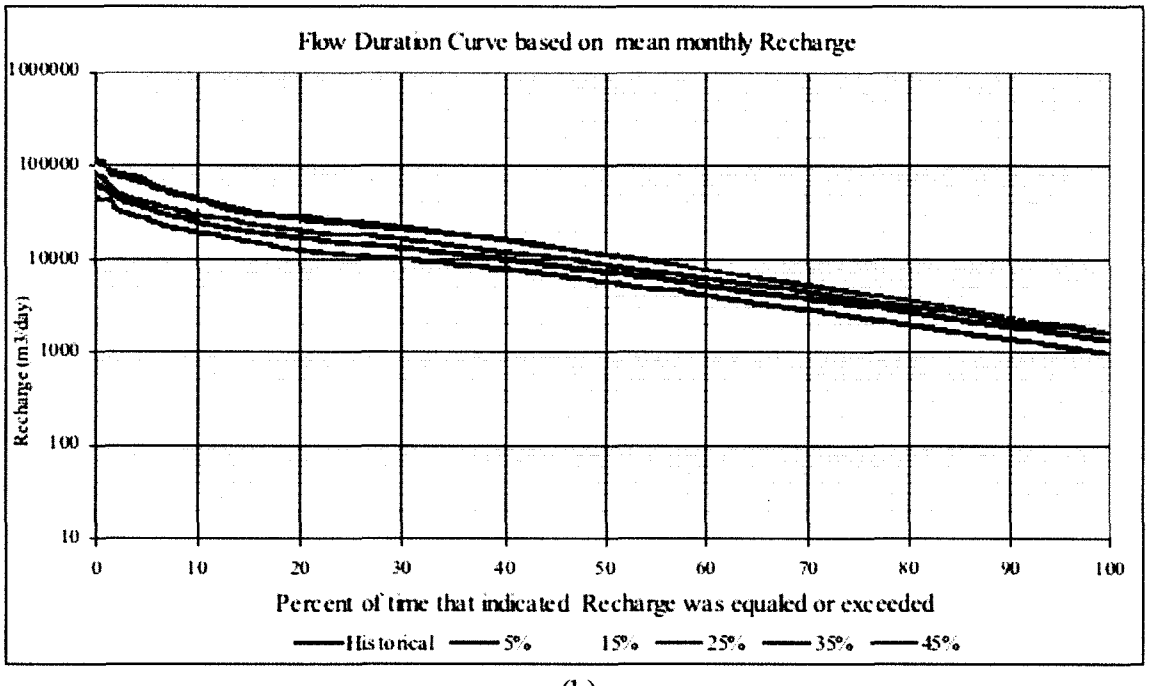

(b)

Figure (5.26): (a) Flow duration curve for daily recharge (b) Flow duration curve for monthly recharge (c) Flow duration curve for June, (d) Flow duration curve for July, (e) Flow duration curve for August for second scenario (m3/day).

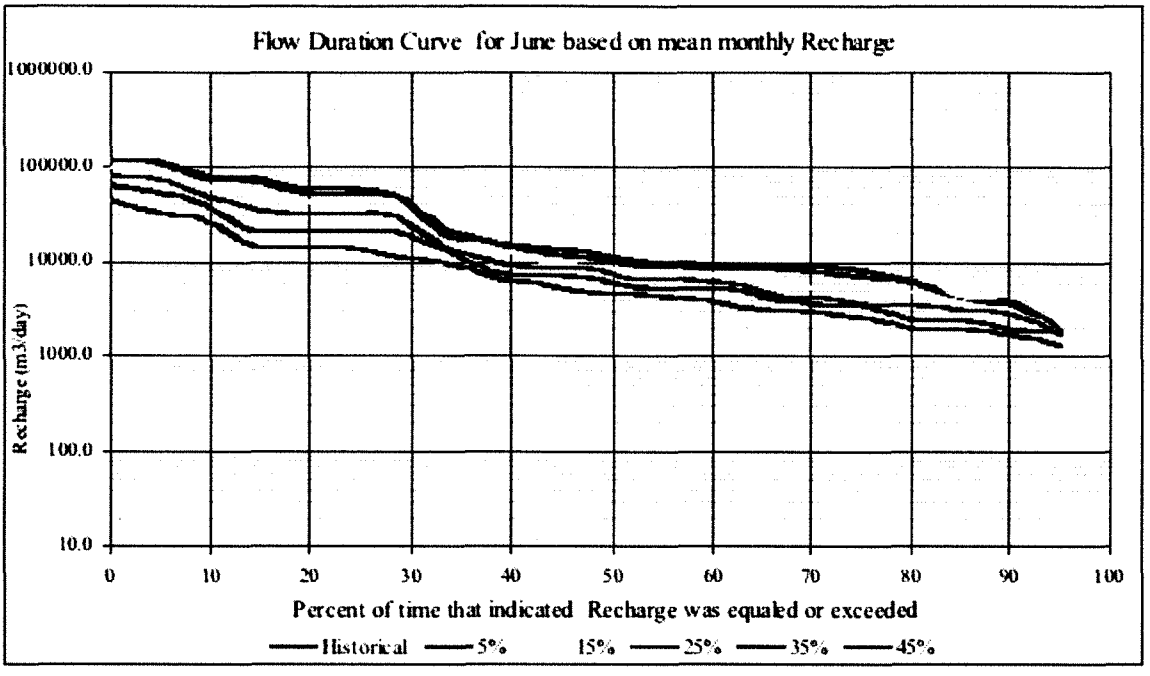

(c)

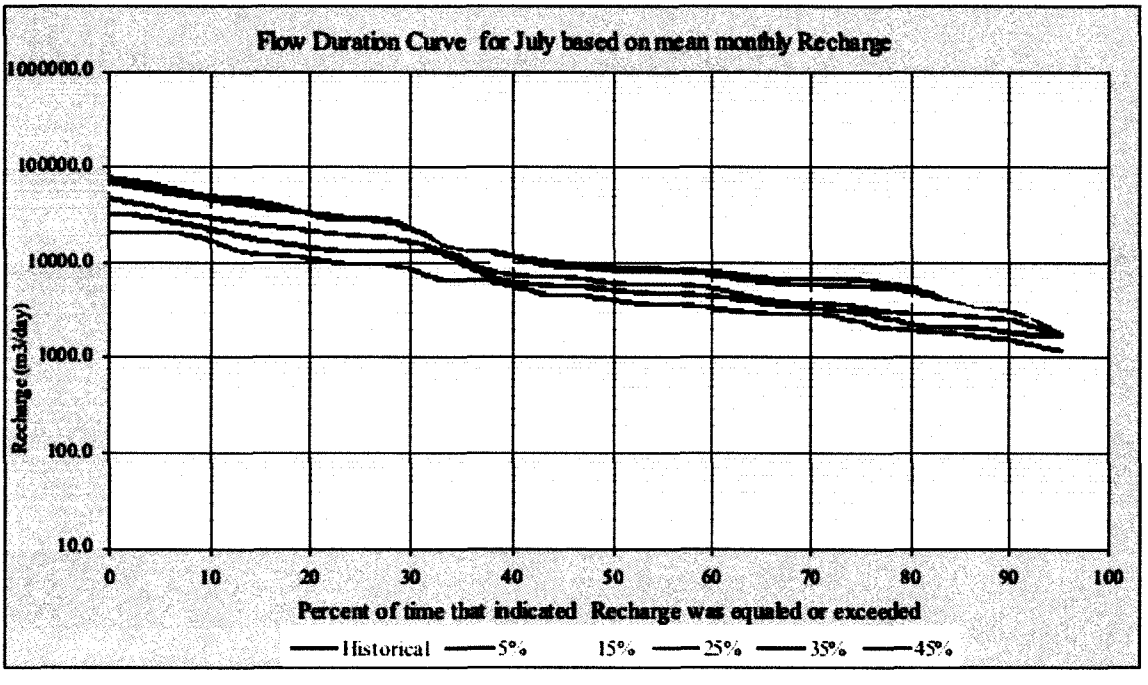

(d)

Figure (5.26): (a) Flow duration curve for daily recharge (b) Flow duration curve for monthly recharge (c) Flow duration curve for June, (d) Flow duration curve for July, (e) Flow duration curve for August for second scenario (m3/day) (continued).

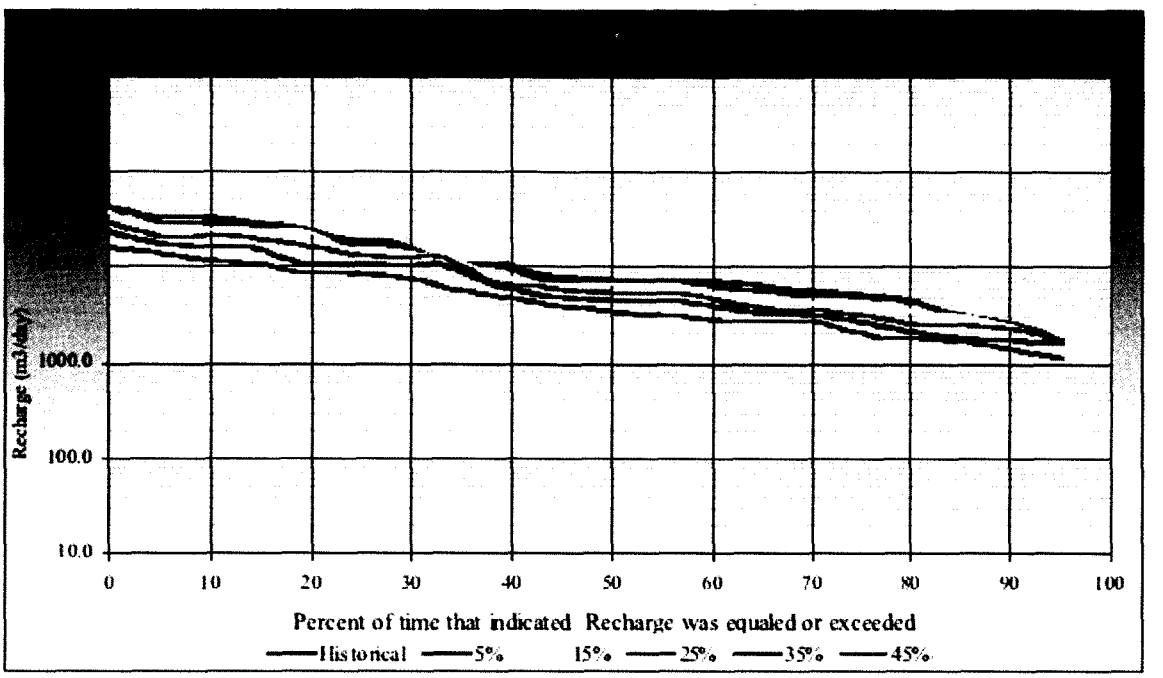

(e)

Figure (5.26): (a) Flow duration curve for daily recharge (b) Flow duration curve for monthly recharge (c) Flow duration curve for June, (d) Flow duration curve for July, (e) Flow duration curve for August for second scenario (m3/day) (continued).

5.4.3 Third scenario

In this scenario a synthetic data set was generated that maintained the number of wet days per year but removed the seasonality. This simulates a potential climate change without seasonality but with an increase in annual precipitation. The occurrence of wet days was generated by a first order a Markov Chain and an exponential distribution model was used to increases the rainfall amount of the observed data with an average change ranging between 5 and 45 percent with 10 percent increments. In this section only an increases of 25 percent is presented as an illustration of the results.

5.4.3.1 Changes to annual recharge flow

The descriptive statistics of the increased recharge from 25 percent scenario have been analyzed where the mean annual recharge and multi-mean annual were calculated to the 25 percent scenario, as illustrated in table (5.19). To give greater clarification, the table has been plotted as shown in figure (5.27) (a, b). Notice from this table and the figures how the recharges change according to the change in the stochastically generated precipitation time series.

Table (5.20) shows the yearly average percentage changes to the annual recharge, which is shown graphically in figure (5.28). The descriptive statistics of the increased recharge from third scenario include the standard deviation, skewness coefficient and kurtosis, which were calculated for annual recharge, where the standard deviation for annual recharge was calculated for the 25 percent scenario, as illustrated in table (5.21) and shown in figure (5.29).

Table (5.22) shows the yearly average percentage changes to the standard deviation of the recharge. The skewness coefficient and kurtosis have been calculated and plotted in figure (5.30) (a, b). These figures show how the standard deviation, skewness coefficients, and kurtosis for the annual increased recharge are changed corresponding to the change in precipitation. The results presented are consistent with the previous results that showed increased precipitation yielded higher and increasing annual recharges

Table (5.19) The mean annual recharge for the third scenario (m^3/day).

Time	Historical	S+25%
1980-2000	18926.788	17494.8216
1980	17708.163	21946.4798
1981	41879.854	17448.563
1982	37911.343	17052.6916
1983	28973.994	12026.539
1984	12057.183	16065.1474
1985	30296.348	19146.3122
1986	9821.543	18739.3546
1987	5758.739	21103.8076
1988	15813.659	15852.0256
1989	11420.047	13721.3366
1990	8317.220	18543.932
1991	9557.234	18570.9214
1992	26949.585	19360.4932
1993	13498.135	17282.652
1994	37135.334	16197.6506
1995	36033.397	15924.3758
1996	22612.056	17174.8778
1997	11818.430	18186.308
1998	12097.975	18450.1588
1999	5498.997	16589.0852
2000	2327.462	18017.4736
Mean	18927.938	17495.247
MAX	41879.854	21946.480
MIN	2327.462	12026.539
SD	12193.138	2221.711

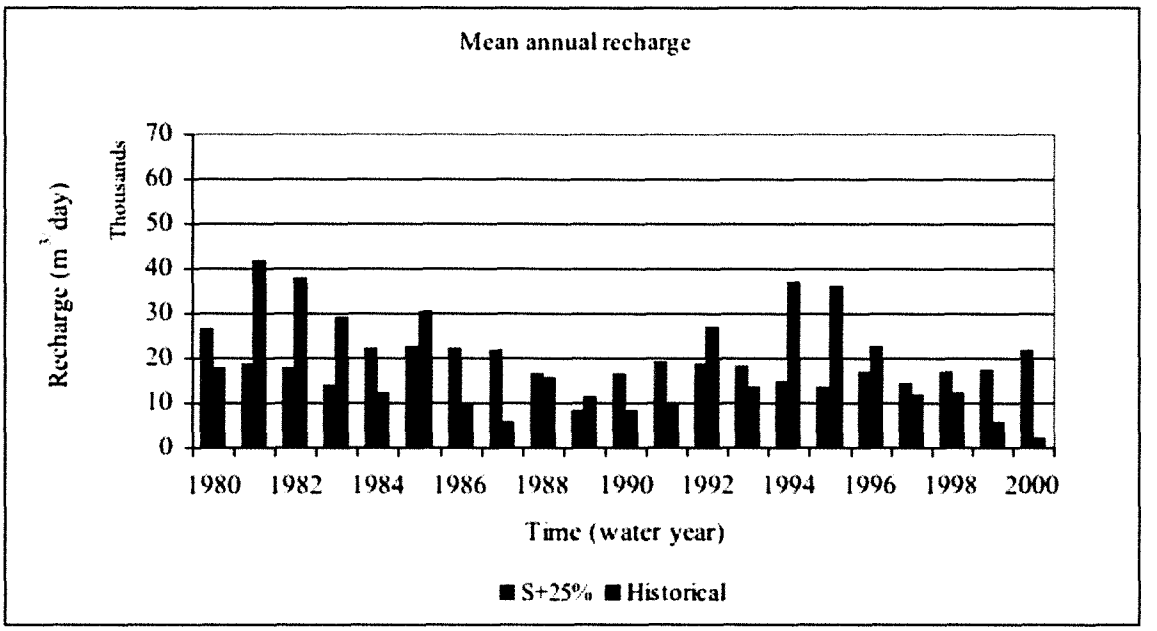

(a)

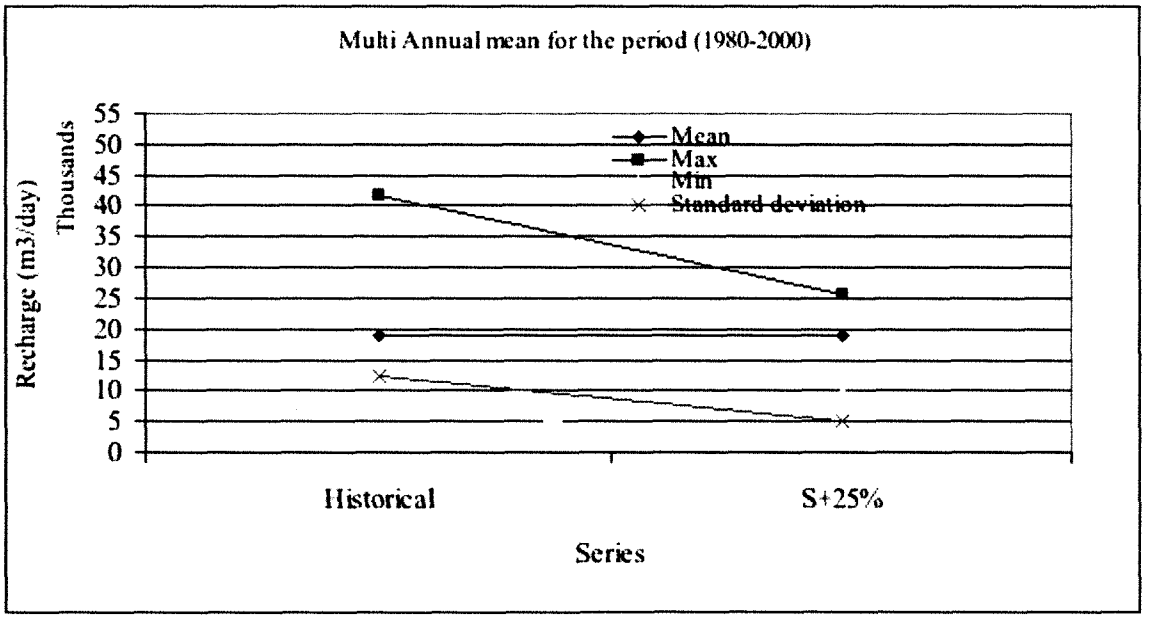

(b)

Figure (5.27): (a) Time series of mean annual and (b) multi-mean annual of recharge for the third scenario (m^3/day).

Table (5.20): The annual average relative percentage change for the third scenario (m^3/day).

Time	S+25%
1980-2000	-0.08
1980	23.93
1981	-58.34
1982	-55.02
1983	-58.49
1984	33.24
1985	-36.80
1986	90.80
1987	266.47
1988	0.24
1989	20.15
1990	122.96
1991	94.31
1992	-28.16
1993	28.04
1994	-56.38
1995	-55.81
1996	-24.05
1997	53.88
1998	52.51
1999	201.67
2000	674.13
Mean	61.39
MAX	674.13
MIN	-58.49
SD	165.32

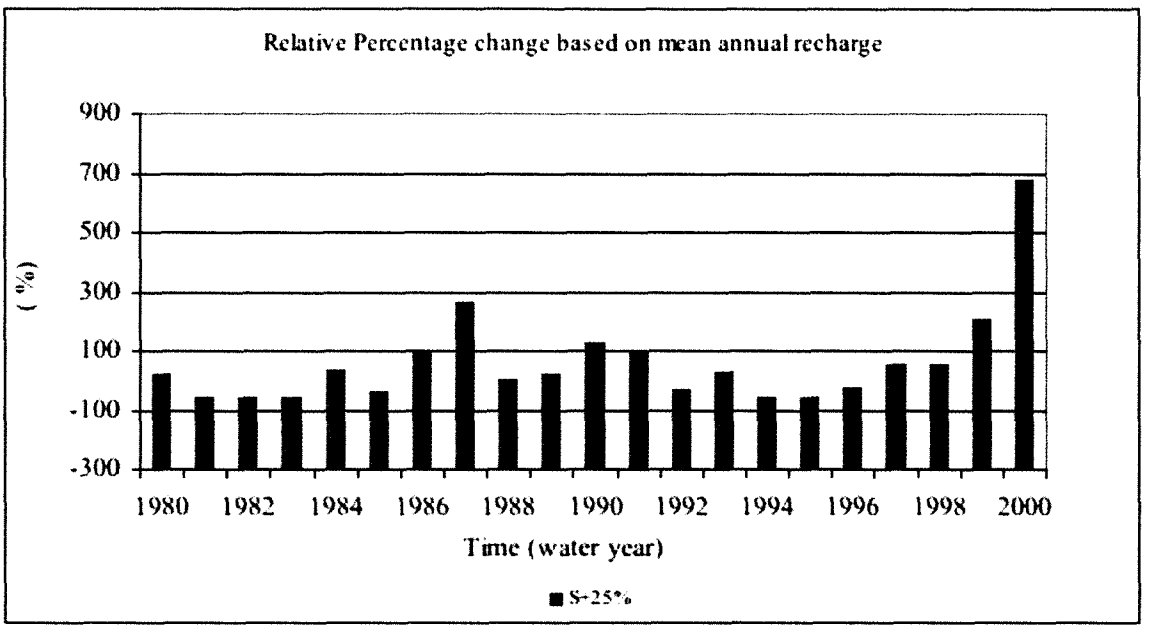

Figure (5.28): Time series of the relative percentage change based on annual recharge for the third scenario (m^3/day).

Table (5.21): The standard deviation of annual recharge for the third scenario (m^3/day).

Time	Historical	S+25%
1980-2000	20161.22	10140.144
1980	7731.89	10479.64
1981	23603.27	9612.894
1982	29059.45	10601.078
1983	20038.97	5826.336
1984	7447.23	12906.854
1985	25600.68	10775.16
1986	5641.41	8778.76
1987	4685.37	12342.824
1988	14846.74	7691.35
1989	4473.41	6336.354
1990	4574.19	8976.676
1991	5491.31	9776.522
1992	27090.32	10667.496
1993	5454.27	6560.698
1994	35890.30	7009.022
1995	19295.44	6949.576
1996	12193.18	7022.17
1997	6504.91	10209.886
1998	6107.53	6738.42
1999	2426.48	6554.27
2000	621.51	7188.054
Mean	12798.95	8714.478095
MAX	35890.30	12906.854
MIN	621.51	5826.336
SD	10338.30	2111.775413

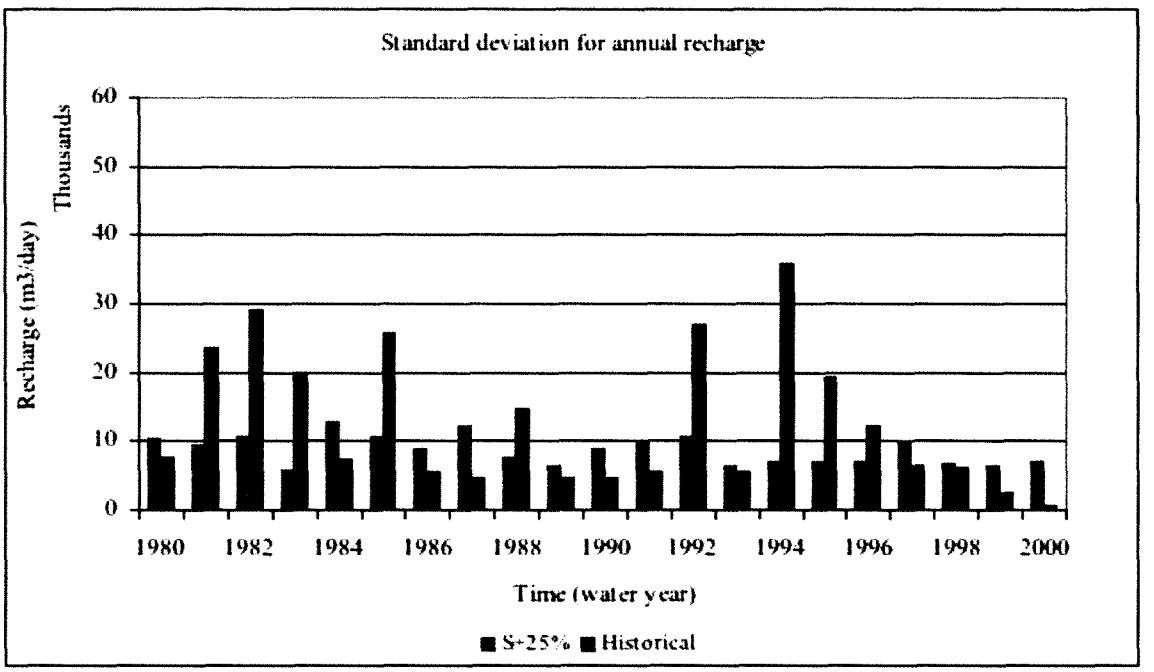

Figure (5.29): Time series of standard deviation of annual recharge for the third scenario (m^3/day).

Table (5.22): Relative percentage change of the annual standard deviation for the third scenario (m^3/day).

Time	S+25%
1980-2000	-49.70%
1980	35.54
1981	-59.27
1982	-63.52
1983	-70.93
1984	73.31
1985	-57.91
1986	55.61
1987	163.43
1988	-48.20
1989	41.64
1990	96.25
1991	78.04
1992	-60.62
1993	20.29
1994	-80.47
1995	-63.98
1996	-42.41
1997	56.96
1998	10.33
1999	170.11
2000	1056.54
Mean	62.416
MAX	1056.539
MIN	-80.471
SD	240.311

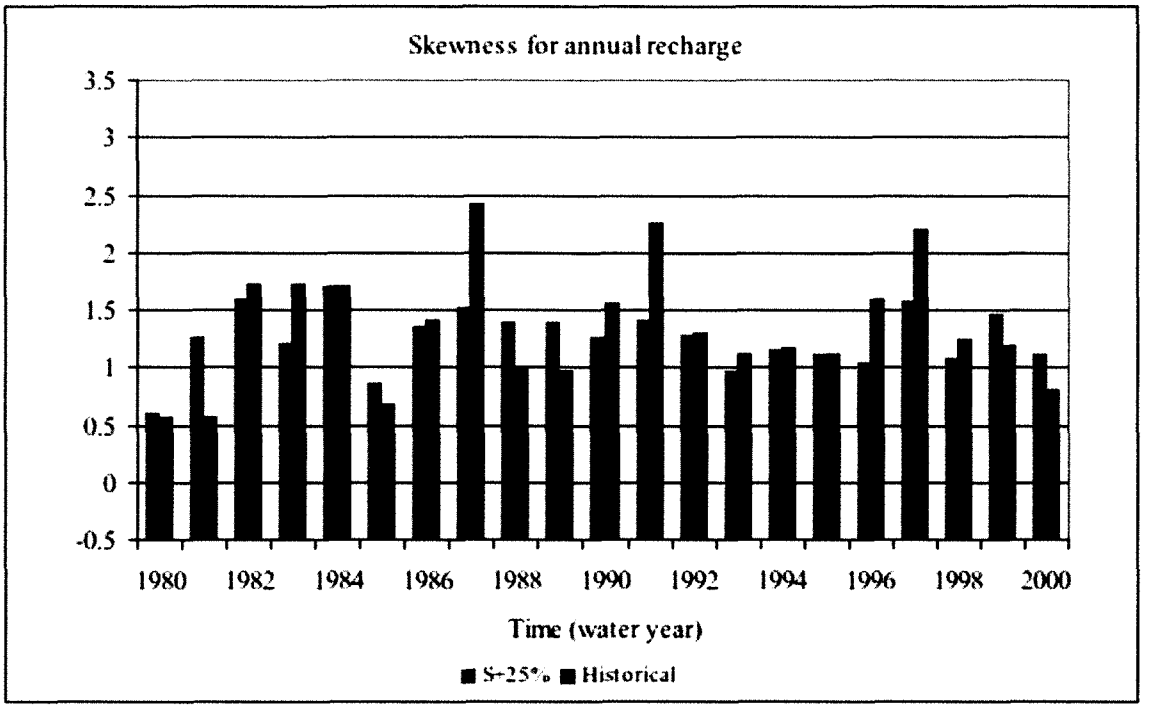

(a)

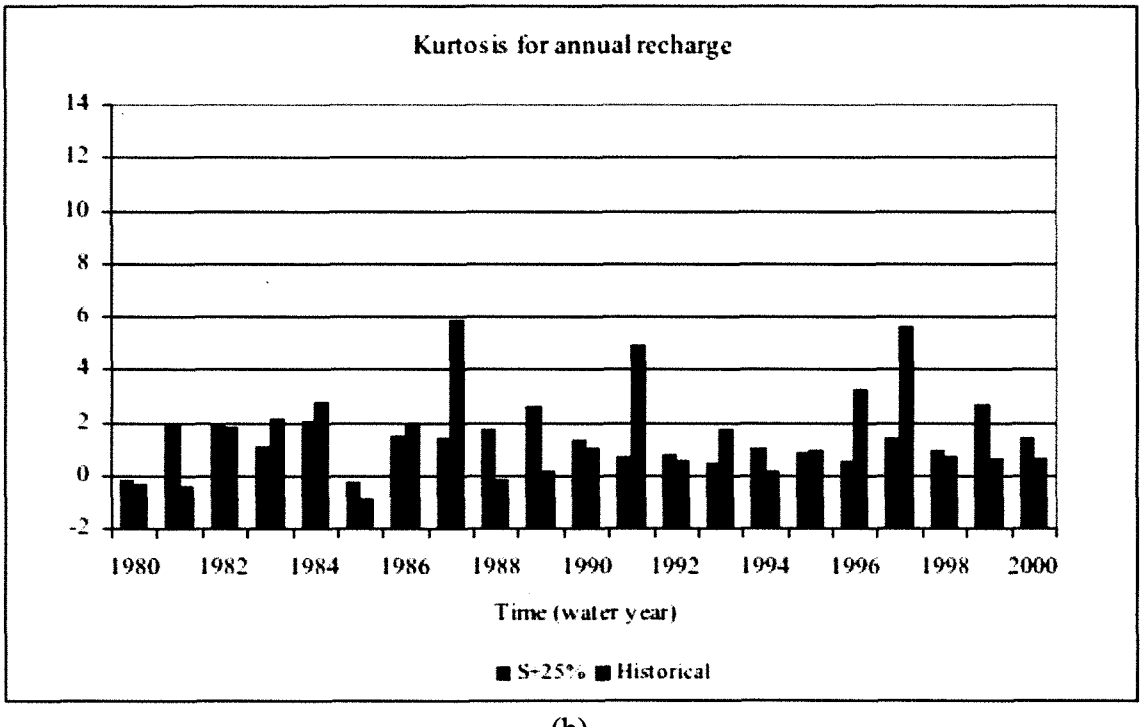

(b)

Figure (5.30): Time series of the (a) Skewness coefficient and (b) kurtosis annual recharge for the third scenario (m^3/day).

5.4.4 Fourth scenario

In this scenario a synthetic data set was generated that maintained the number of wet days per year but removed the seasonality. This simulates a potential climate change without seasonality but with an increase in annual precipitation. The occurrence of wet days was generated by a first order a Markov Chain and an exponential distribution model was used to decreases the rainfall amount of the observed data with an average change ranging between 5 and 45 percent with 10 percent increments. In this section only a decreases of 25 percent is presented as an illustration of the results.

5.4.4.1 Changes to annual recharge flow

The descriptive statistics of the decreased recharge from the different decreases in precipitation for the 25 percent scenario have been analyzed and the mean annual recharge and multi-mean annual recharge were calculated to decreases in precipitation as illustrated in table (5.23). To further illustrate the changes, the data in the table are plotted, as shown in figure (5.31) (a, b). The percentages of the changes are shown in table (5.24). Table shows the yearly average percentages changes to the recharge, which is shown graphically in figure (5.32). The descriptive statistics of the decreased recharge from different decreases in precipitation (the standard deviation, skewness coefficient and kurtosis) were calculated for the annual decreased recharge. The standard deviation for annual recharge and multi-annual standard deviation have been calculated as illustrated in table (5.25). The table were plotted and shown in figure (5.33). Table (5.26) shows the yearly average percentages changes to the standard deviation.

The skewness coefficient and kurtosis are calculated and plotted in figure (5.35) (a, b). These figures showed the standard deviation, skewness coefficients, and kurtosis, for annual decreased precipitation yielded lower and decreasing annual recharge.

Table (5.23): The mean annual recharge (m^3/day) for the fourth scenario.

Time	Historical	S-25%
1980-2000	18926.788	5769.412
1980	17708.163	10856.351
1981	41879.854	10209.553
1982	37911.343	10565.868
1983	28973.994	5076.971
1984	12057.183	3333.298
1985	30296.348	3021.412
1986	9821.543	4399.328
1987	5758.739	3608.148
1988	15813.659	2894.499
1989	11420.047	3549.54
1990	8317.220	5204.603
1991	9557.234	6422.527
1992	26949.585	6089.179
1993	13498.135	4318.966
1994	37135.334	3354.024
1995	36033.397	3502.264
1996	22612.056	4894.374
1997	11818.430	8470.054
1998	12097.975	9206.753
1999	5498.997	6655.289
2000	2327.462	5534.453
Mean	18927.938	5769.879
MAX	41879.854	10856.351
MIN	2327.462	2894.499
SD	12193.138	2616.722

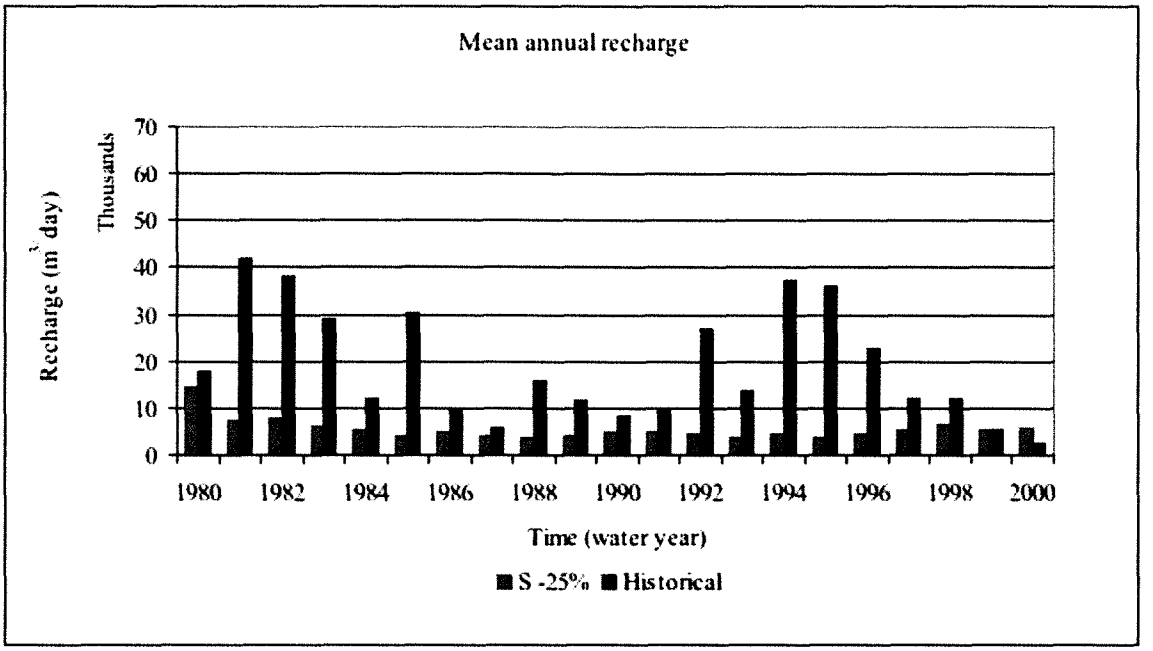

(a)

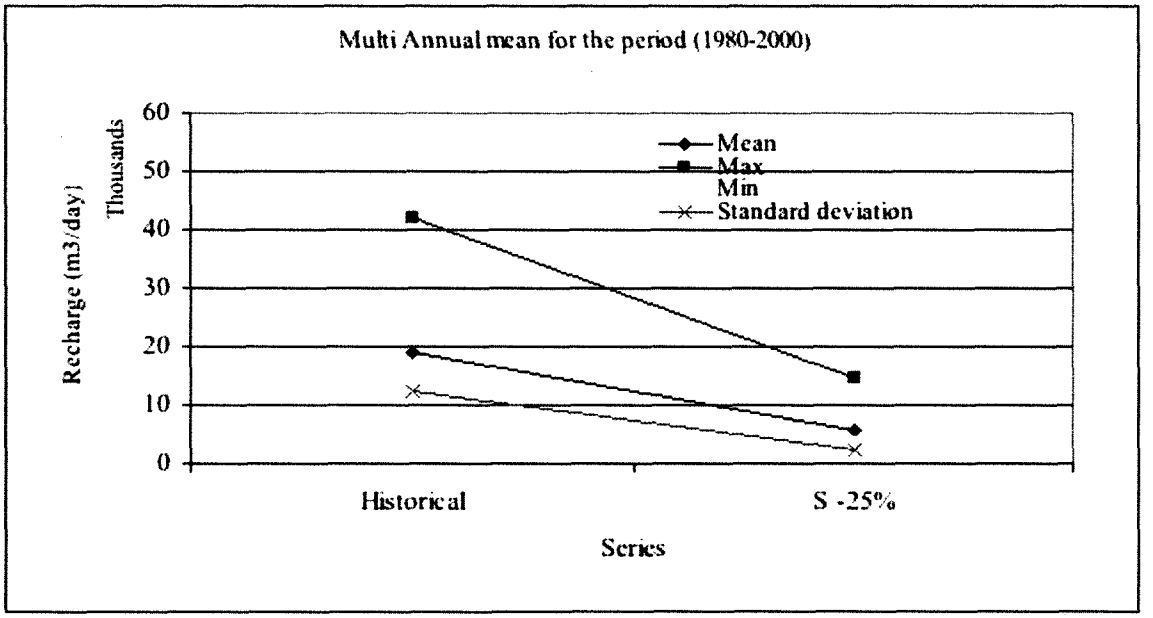

(b)

Figure (5.31): (a) Time series of mean annual recharge and (b) multi-mean annual recharge for the fourth scenario (m^3/day).

Table (5.24): Relative percentage changes of the annual average for the fourth scenario.

Time	S-25%
1980-2000	-70.41
1980	-17.49
1981	-82.03
1982	-78.97
1983	-78.72
1984	-54.00
1985	-86.73
1986	-48.93
1987	-27.46
1988	-75.74
1989	-62.23
1990	-38.27
1991	-48.00
1992	-83.47
1993	-71.86
1994	-87.74
1995	-90.07
1996	-79.51
1997	-54.00
1998	-46.01
1999	-0.02
2000	151.32
Mean	-50.47
MAX	151.32
MIN	-90.07
SD	52.50

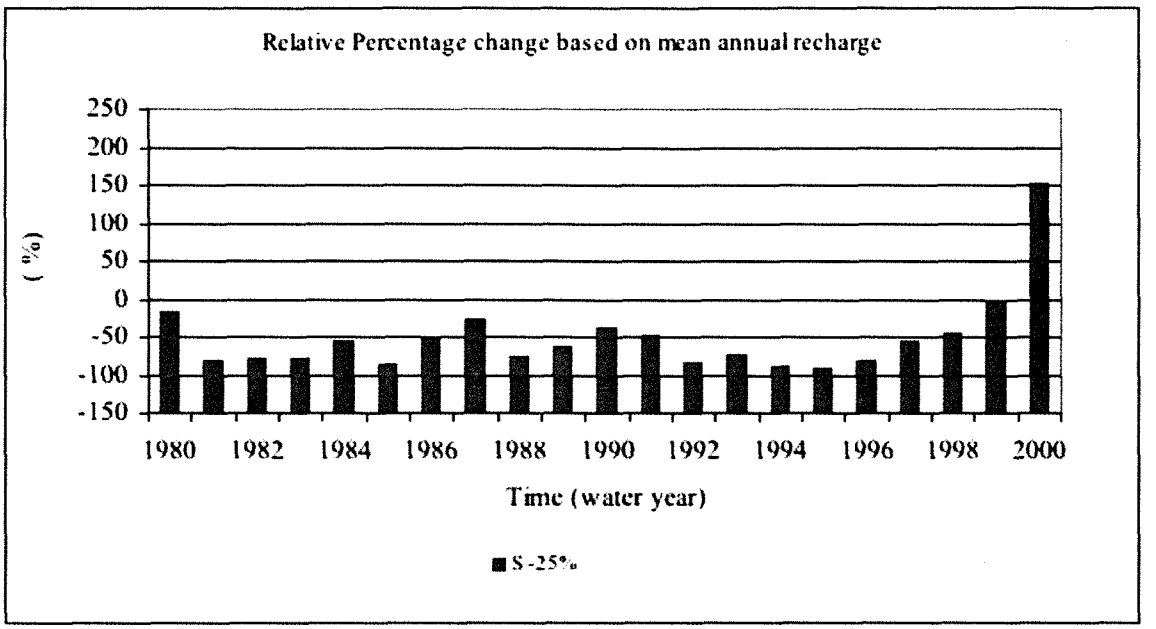

Figure (5.32): Time series of the relative percentage change based on annual recharge for the fourth scenario.

Table (5.25) The standard deviation of annual recharge (m^3/day) for the fourth scenario.

Time	Historical	S-25%
1980-2000	20161.22	4279.53
1980	7731.89	7311.54
1981	23603.27	4656.51
1982	29059.45	5145.36
1983	20038.97	3457.54
1984	7447.23	3697.19
1985	25600.68	2333.84
1986	5641.41	2990.88
1987	4685.37	2629.24
1988	14846.74	2505.72
1989	4473.41	2493.41
1990	4574.19	3144.35
1991	5491.31	2526.76
1992	27090.32	2204.65
1993	5454.27	1409.98
1994	35890.30	2280.91
1995	19295.44	1385.37
1996	12193.18	2124.52
1997	6504.91	2107.28
1998	6107.53	2301.16
1999	2426.48	1544.30
2000	621.51	1940.85
Mean	12798.95	2866.26
MAX	35890.30	7311.54
MIN	621.51	1385.37
SD	10338.30	1399.29

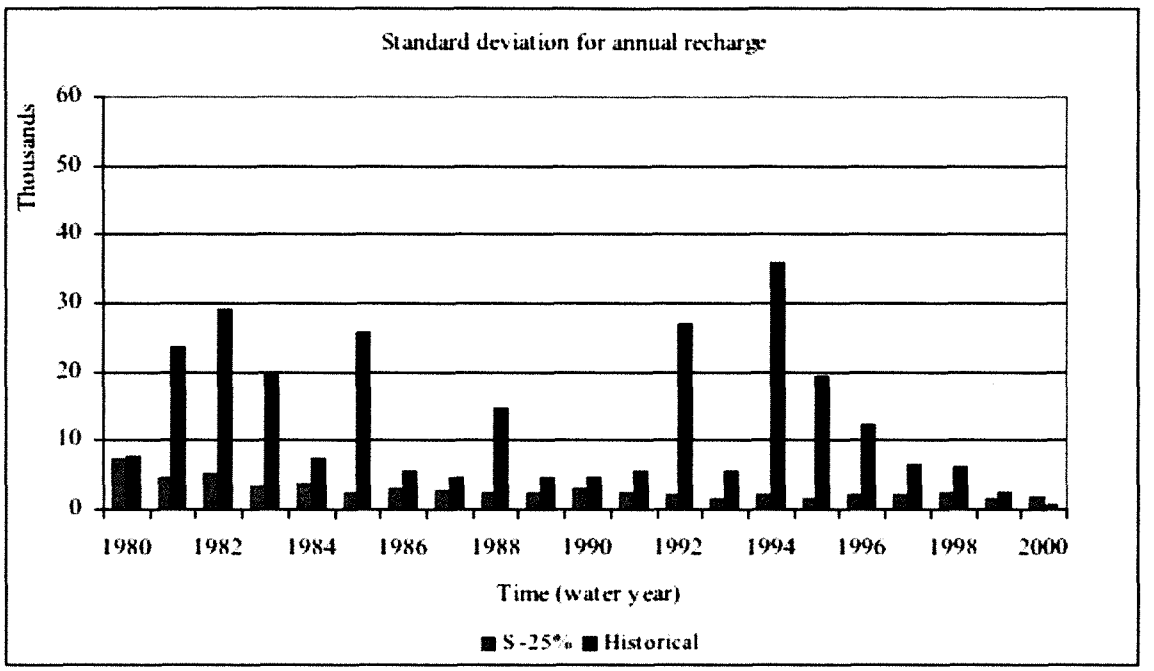

Figure(5.33) : Time series of standard deviation of annual recharge (m^3/day) for the fourth scenario.

Table (5.26): The annual standard deviation for relative percentage change for the fourth scenario.

Time	S-25%
1980-2000	-78.77%
1980	-5.44
1981	-80.27
1982	-82.29
1983	-82.75
1984	-50.35
1985	-90.88
1986	-46.98
1987	-43.88
1988	-83.12
1989	-44.26
1990	-31.26
1991	-53.99
1992	-91.86
1993	-74.15
1994	-93.64
1995	-92.82
1996	-82.58
1997	-67.60
1998	-62.32
1999	-36.36
2000	212.28
Mean	-51.64
MAX	212.28
MIN	-93.64
SD	65.10

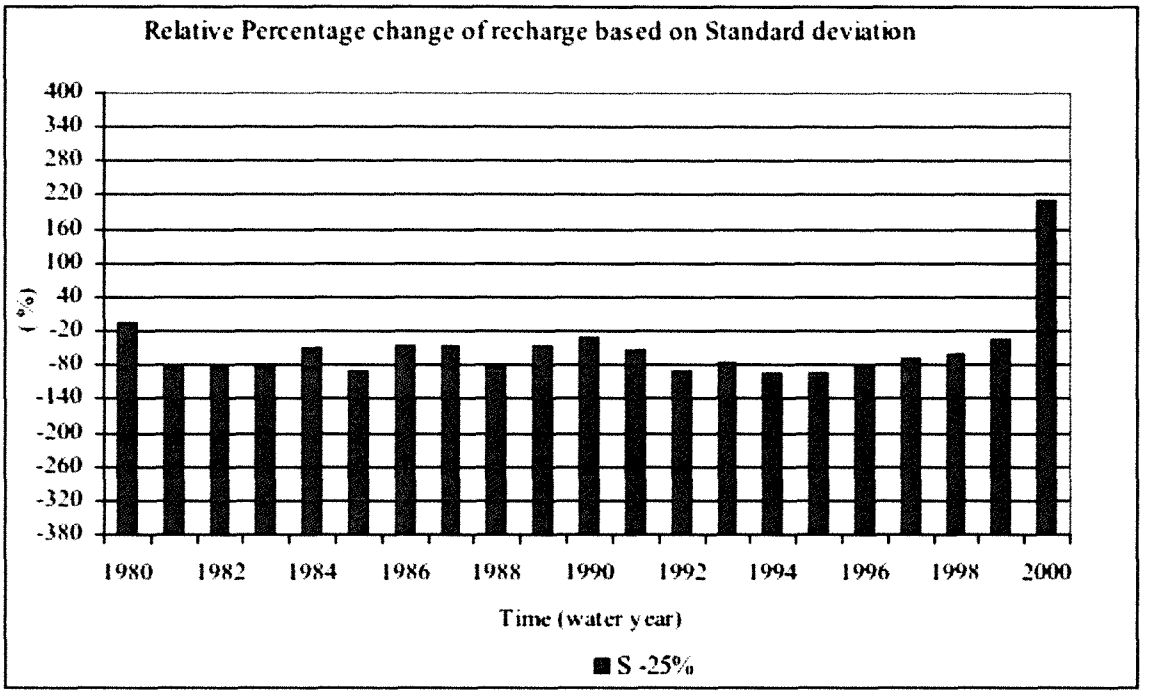

Figure (5.34): Time series of the relative percentage change based on standard deviation for the fourth scenario.

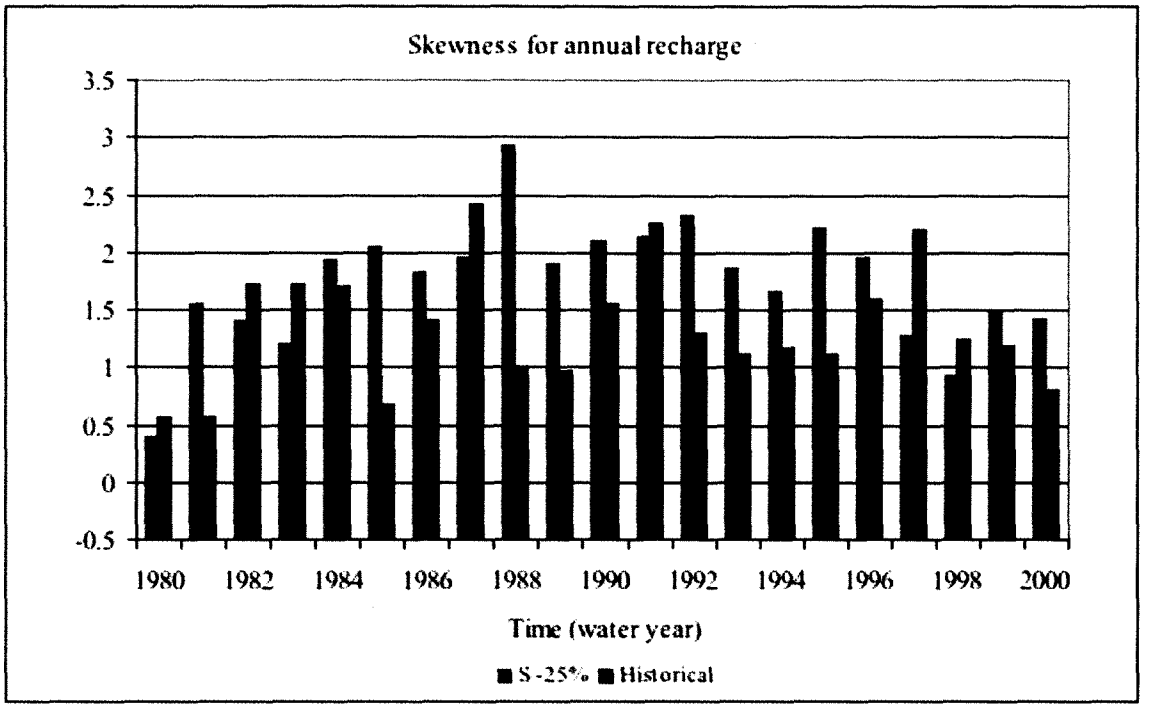

(a)

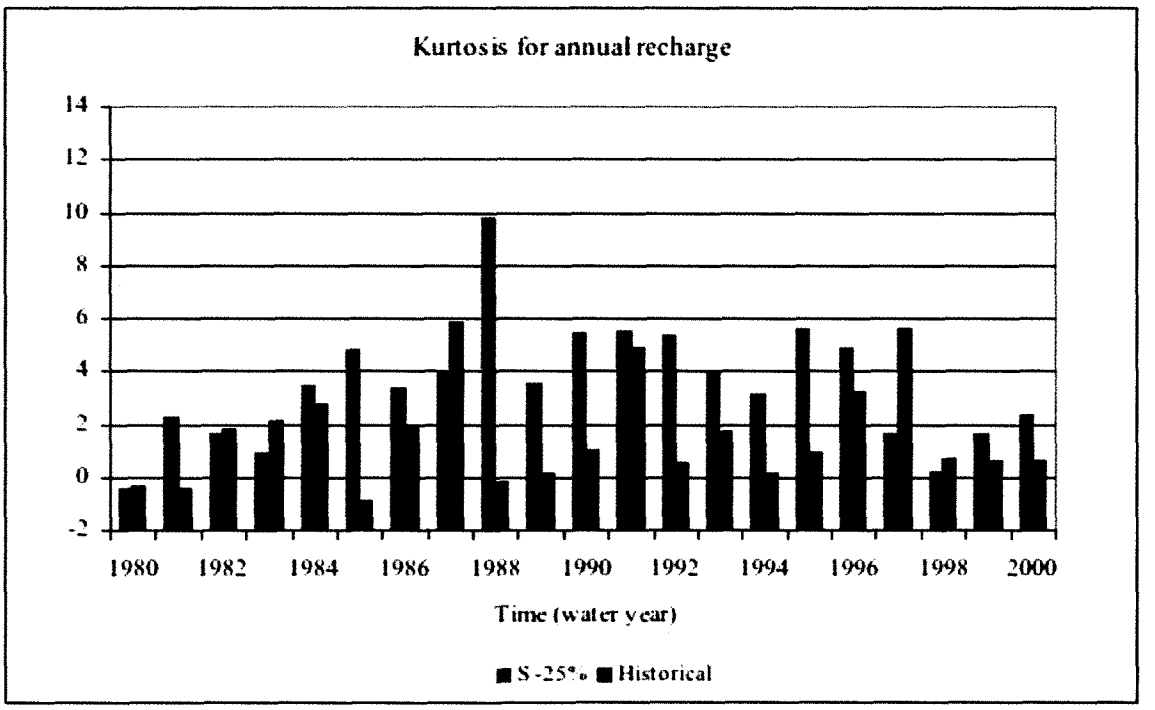

(a)

Figure (5.35): Time series of the (a) skewness coefficient and (b) kurtosis annual recharge (m^3/day) for the fourth scenario.

5.4.5 Fifth scenario

This scenario simulate climate change scenario where the pattern of wet days is preserved but the amount of precipitation on wet day is stochastically generated using an exponential distribution model. The generated the rainfall amounts produce an average increase of 45 percent compared to the historical data. The fifth scenario should be compared with the first scenario to see the impact of different rainfall amount compared to simply increasing historical values.

5.4.5.1 Changes to daily, Monthly and annual recharge flow

The recharge estimated by the GSFLOW model is shown in figures (5.36) (a, b, c and d). The figures show the time series of the recharge flow for the 45 percent increase. All four figures show the change in the recharge, and figure (5.36) (a) shows the time series of the recharge for whole period (1980-2000). The first seven-year period is shown in figure (5.36) (b), the second seven-year period in (c) and the rest of the period in figure (5.36) (d). The figures clearly show that the recharge for this scenario in increasing more than the increase applied to the rainfall.

The descriptive statistics of the increased recharge of the 45 percent increase have been analyzed. The mean annual and multi-mean annual recharge is illustrated in table (5.27) and figures (5.37) (a, b). We note from this table and the figures how the recharge changes according to the change in the stochastically generated precipitation values.

The percentages of the changes are shown in table (5.28). The table shows the daily average of the percentage change compared to the historical recharge. Table (5.29) shows the yearly average percentages changes to the recharge, which are shown in figure (5.38).

To examine the descriptive statistics of the recharge from a different scenario, the standard deviation, skewness coefficient, and kurtosis are calculated for annual recharge.

The standard deviation for annual recharge and multi-annual standard deviation are illustrated in table (5.30). The table information is shown in figures (5.39) . Table (5.31) shows the yearly average percentage changes to the standard deviation of the recharge that is shown in figure (5.40). The skewness coefficient and kurtosis are shown in figure (5.41) (a, b). These figures show how the standard deviation, skewness coefficients, and kurtosis for annual recharge are changed corresponding to the change in the adapted scenario on the precipitation.

The results presented are consistent with the results shown above in terms of changes in precipitation and therefore have increased in daily and annual recharges. The mean monthly recharge for the water years (1980-2000) has been plotted for all months, also plots for specific months in the summers (June, July, and August) and winter (December, January, and February) sessions are provided. Figure (5.42) (a) shows the mean monthly recharge the period (1980-2000). The increase as seen in the table (5.32) of the recharge is greater than increase in the precipitation. The figures (5.44) (a, b, c, d, e) show the flow duration curve based on daily, monthly, and specific monthly (June, July, and August) analysis.

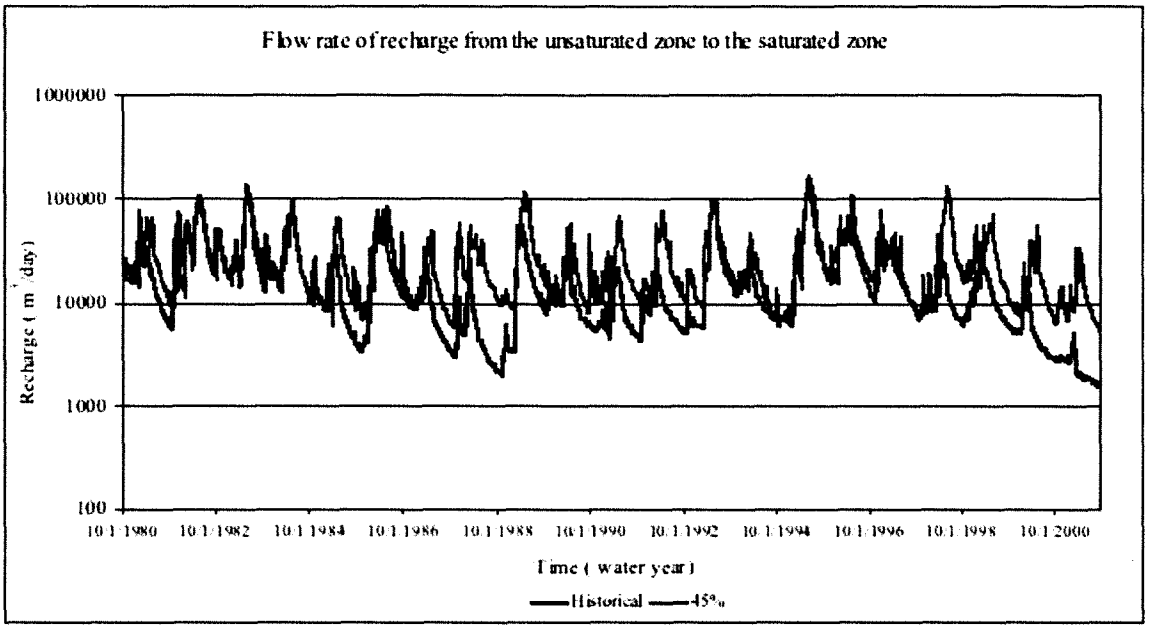

(a)

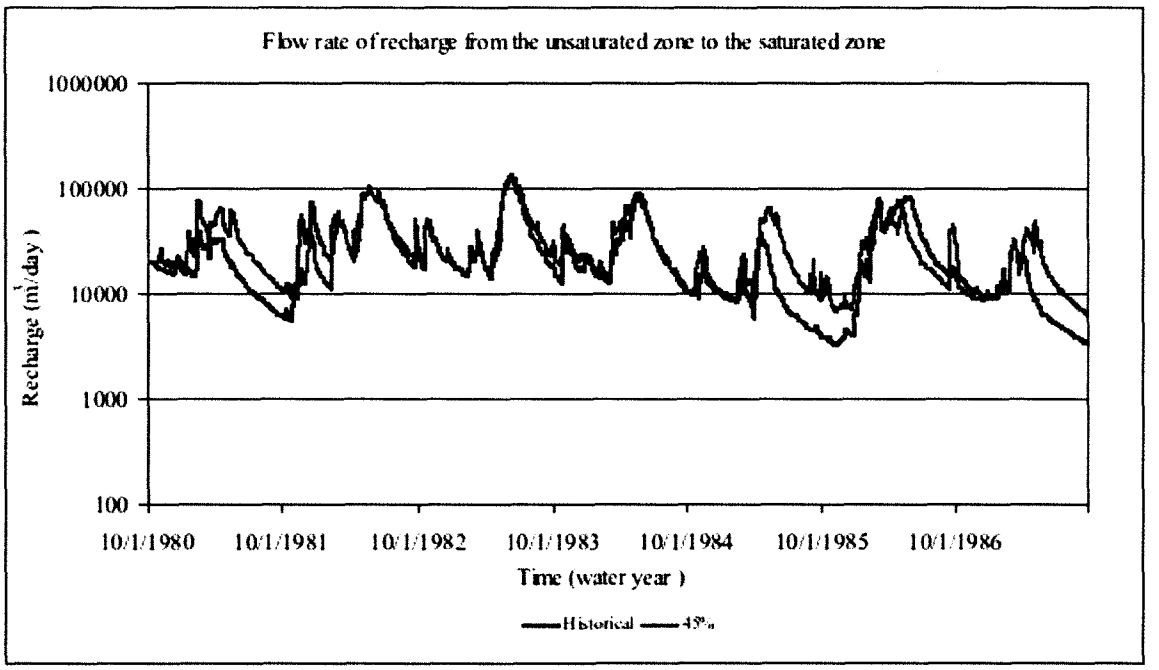

(b)

Figure (5.36): The time series of flow rate of the recharge at whole period (a), first seven years (b), second seven years (c) and rest of the time period (d) for the fifth scenario (m^3/day).

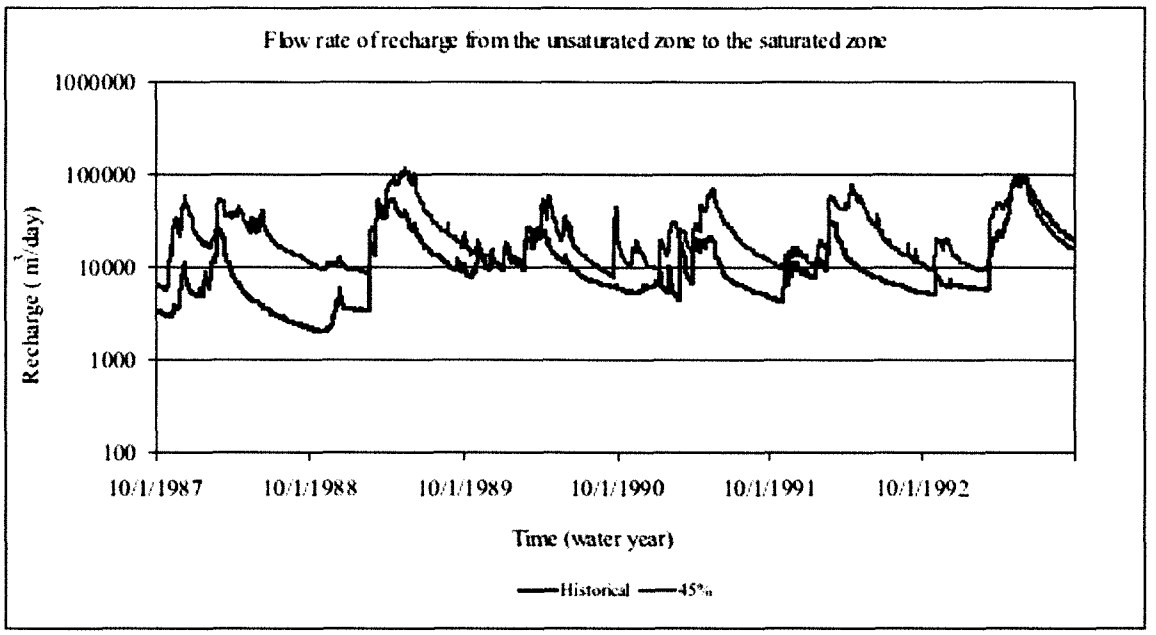

(c)

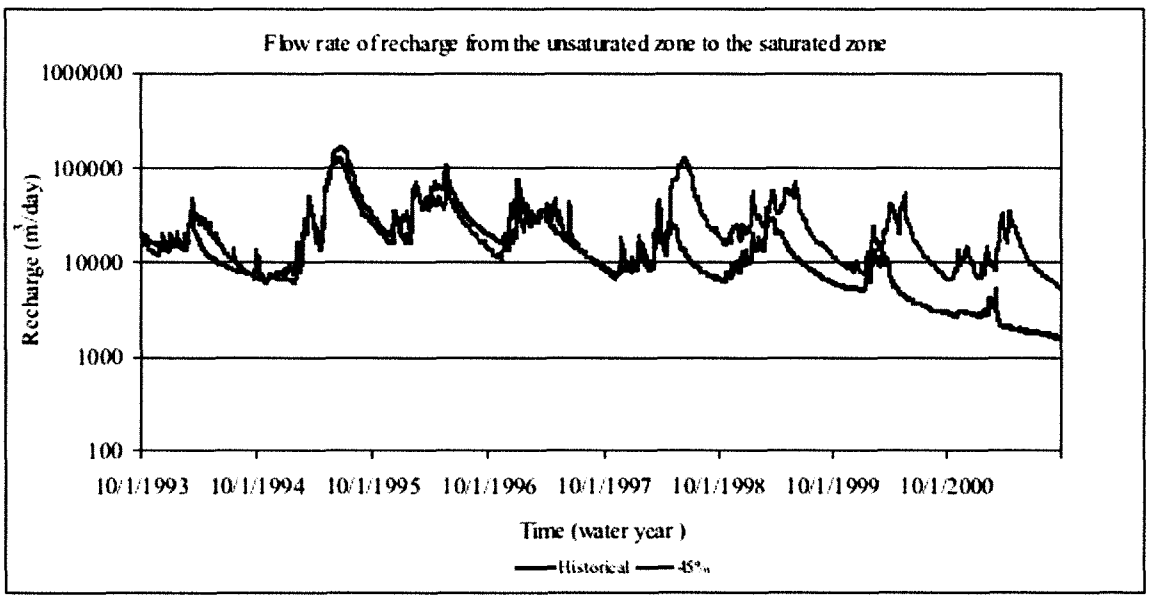

(d)

Figure (5.36): The time series of flow rate of the recharge at whole period (a), first seven years (b), second seven years (c) and rest of the time period (d) for the fifth scenario (m^3/day) (continued).

Table (5.27) The mean annual recharge (m^3/day) for the fifth scenario.

Time	Historical	S+45%
1980-2000	18926.788	26615.8
1980	17708.163	29295.328
1981	41879.854	35155.276
1982	37911.343	42398.561
1983	28973.994	32586.346
1984	12057.183	20326.397
1985	30296.348	26188.809
1986	9821.543	15787.737
1987	5758.739	24178.458
1988	15813.659	34395.363
1989	11420.047	18275.68
1990	8317.220	22377.65
1991	9557.234	24742.128
1992	26949.585	29362.258
1993	13498.135	16259.857
1994	37135.334	44996.388
1995	36033.397	32869.994
1996	22612.056	21121.393
1997	11818.430	32442.172
1998	12097.975	28869.145
1999	5498.997	15662.876
2000	2327.462	11648.308
Mean	18927.938	26616.2
MAX	41879.854	44996.39
MIN	2327.462	11648.31
SD	12193.138	8900.22

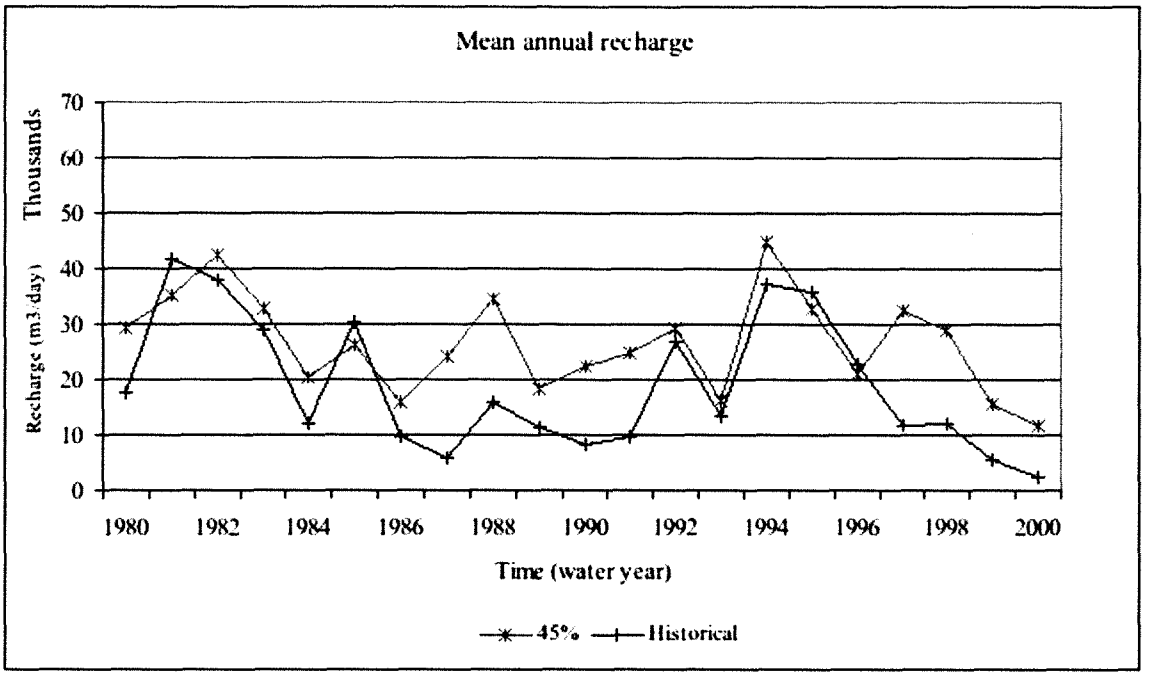

(a)

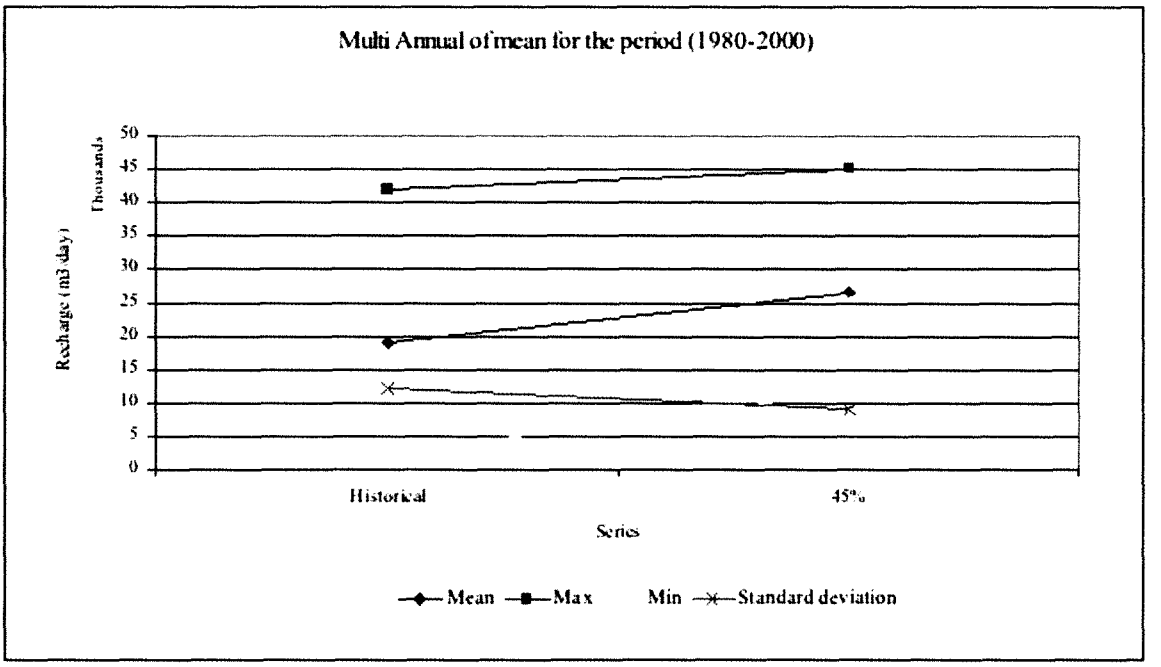

(b)

Figure (5.37): (a) Time series of mean annual and (b) multi-mean annual of recharge for the fifth scenario (m^3/day).

.

Table (5.28): The daily average relative percentage change for the fifth scenario.

Scenario	S+45%
Average	110.94%

Table (5.29): Relative percentage changes of the annual average for the fifth scenario.

Time	S+45%
1980-2000	40.63%
1980	65.43
1981	-16.06
1982	11.84
1983	12.47
1984	68.58
1985	-13.56
1986	60.75
1987	319.86
1988	117.5
1989	60.03
1990	169.05
1991	158.88
1992	8.95
1993	20.46
1994	21.17
1995	-8.78
1996	-6.59
1997	174.5
1998	138.63
1999	184.83
2000	400.47
Mean	92.78
MAX	400.47
MIN	-16.06
SD	112.13

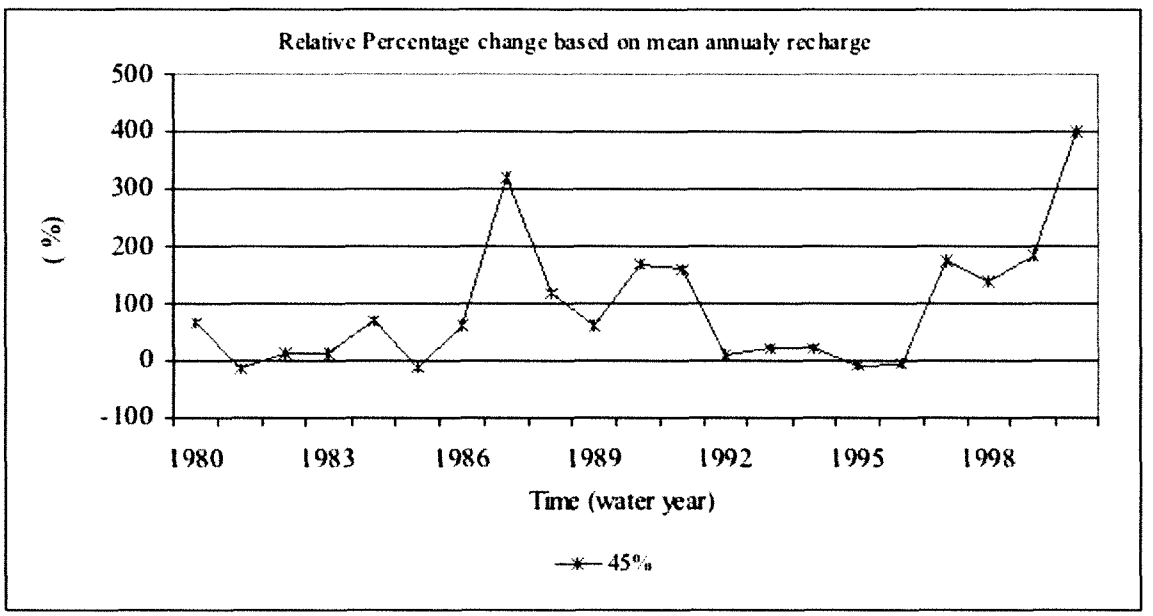

Figure (5.38): Time series of the relative percentage change based on annual recharge for the fifth scenario.

Table (5.30) The standard deviation of annual recharge (m^3/day) for the fifth scenario.

Time	Historical	S+45%
1980-2000	20161.22	22794.32
1980	7731.89	15362.02
1981	23603.27	25451.6
1982	29059.45	32546.75
1983	20038.97	19980.37
1984	7447.23	15766.32
1985	25600.68	17082.45
1986	5641.41	9388.28
1987	4685.37	12372.72
1988	14846.74	30138.31
1989	4473.41	10013.05
1990	4574.19	13208.13
1991	5491.31	17252.45
1992	27090.32	22928.64
1993	5454.27	7884.93
1994	35890.30	49030.24
1995	19295.44	14352.96
1996	12193.18	10641.38
1997	6504.91	33290.69
1998	6107.53	13808.8
1999	2426.48	9751.52
2000	621.51	6693.72
Mean	12798.95	18425.97
MAX	35890.30	49030.24
MIN	621.51	6693.72
SD	10338.30	10546.77

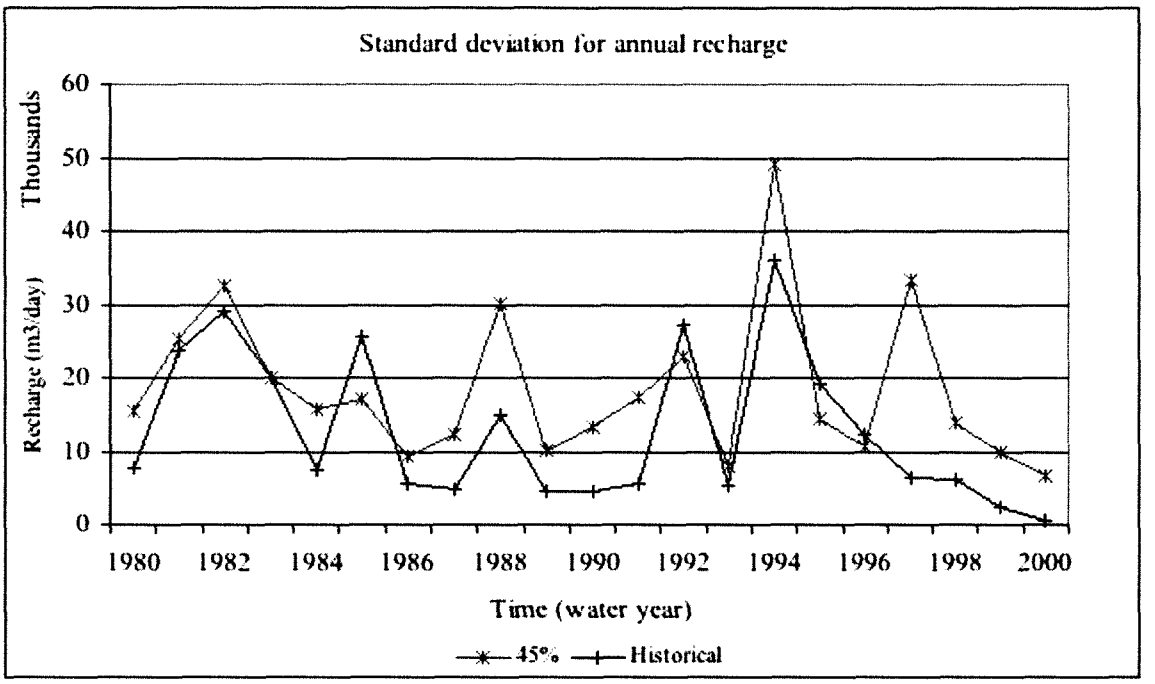

Figure (5.39) : Time series of standard deviation of annual recharge (m^3/day) for the fifth scenario.

Table (5.31): Relative percentages change of the annual standard deviation for the fifth scenario.

Time	S-25%
1980-2000	13.06%
1980	98.684
1981	7.831
1982	12.001
1983	-0.292
1984	111.707
1985	-33.273
1986	66.417
1987	164.071
1988	102.996
1989	123.835
1990	188.753
1991	214.178
1992	-15.362
1993	44.564
1994	36.611
1995	-25.615
1996	-12.727
1997	411.778
1998	126.095
1999	301.879
2000	977.002
Mean	138.149
MAX	977.002
MIN	-33.273
SD	223.273

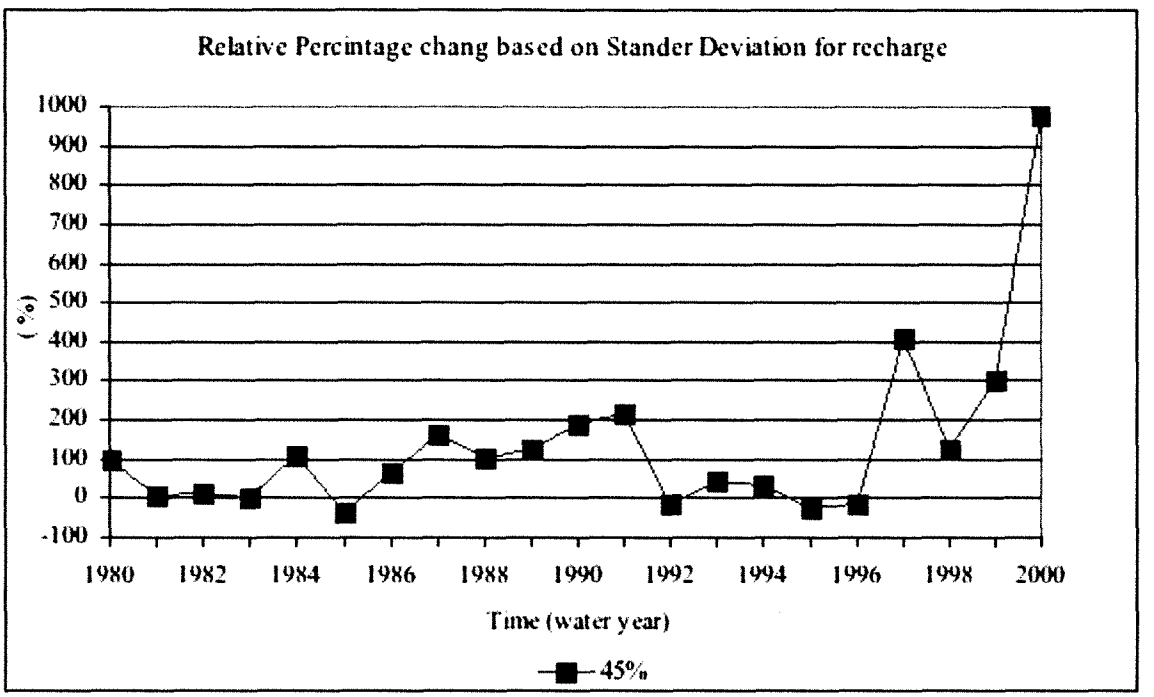

Figure (5.40): Time series of the relative percentage change based on standard deviation for the fourth scenario.

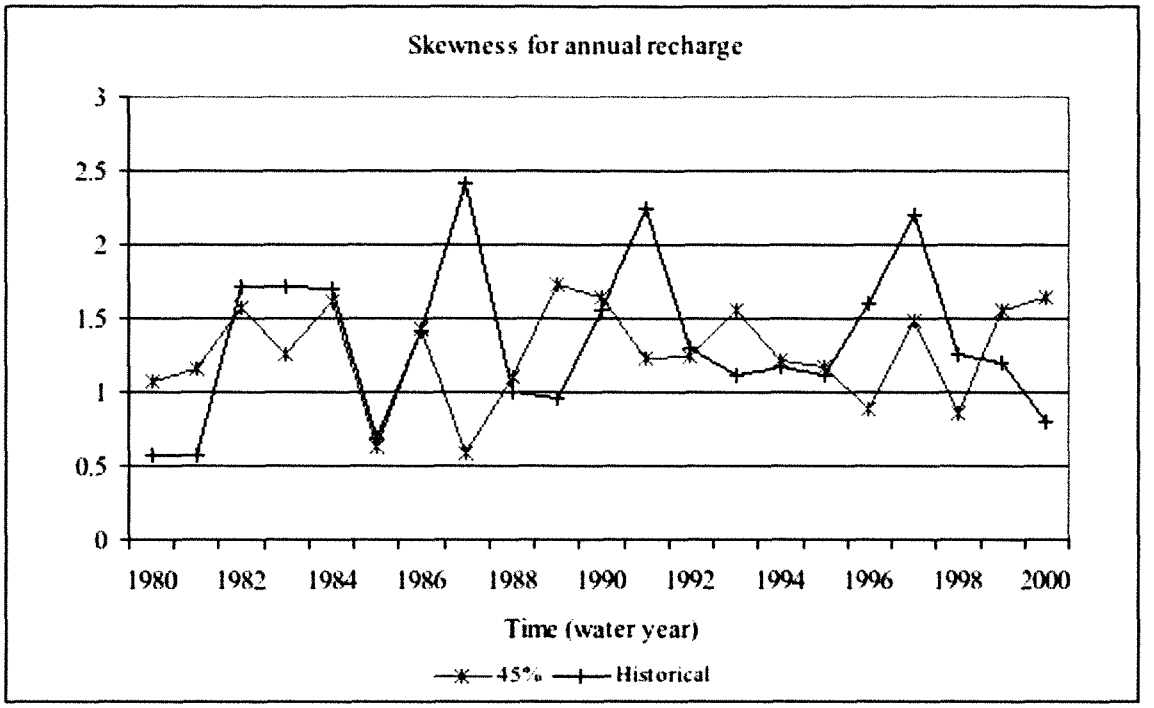

(a)

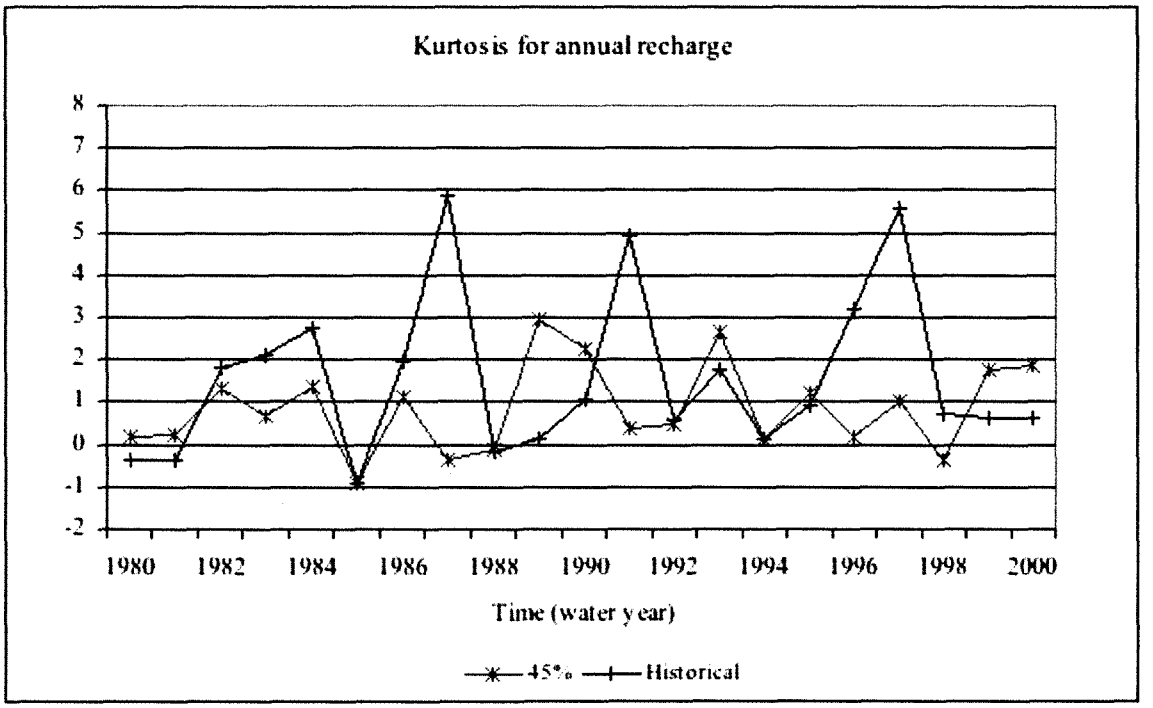

(a)

Figure (5.41): Time series of the (a) skewness coefficient and (b) kurtosis annual recharge (m^3/day) for the fifth scenario.

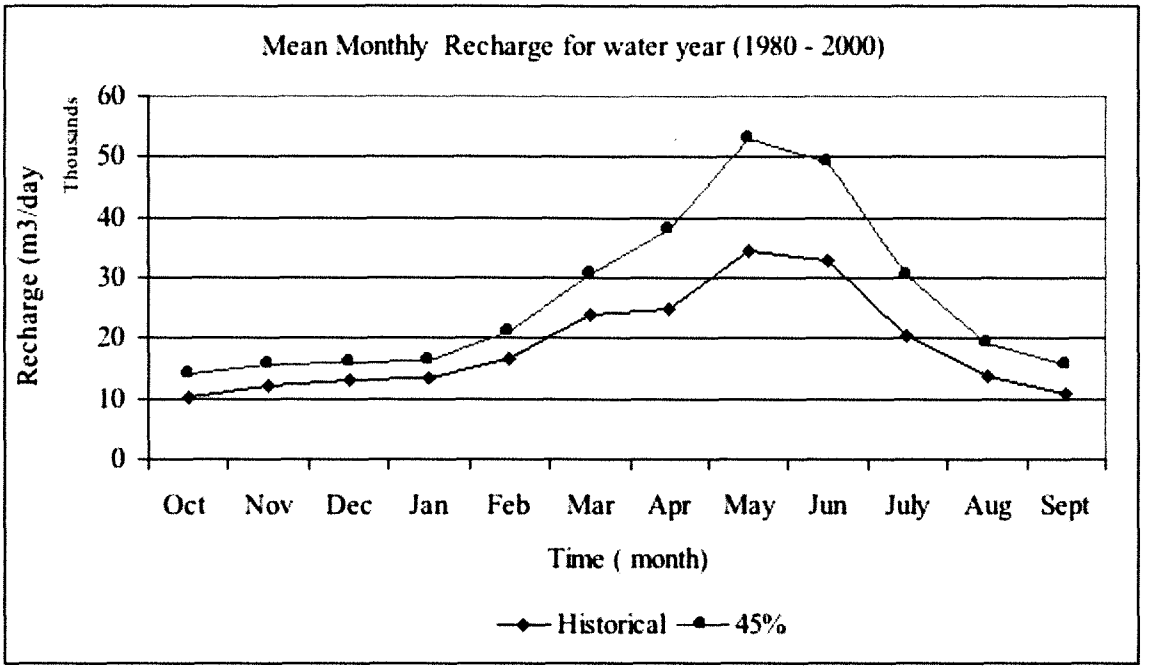

(a)

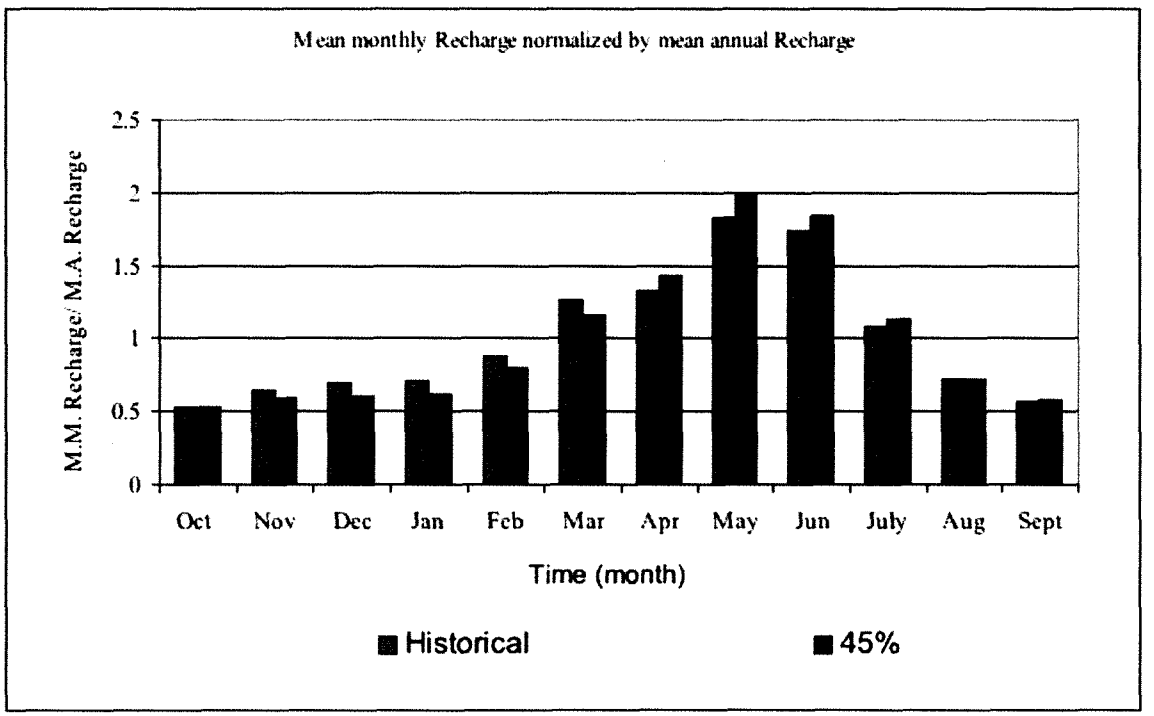

(b)

Figure (5.42): (a) Time series of the mean monthly recharge (b) time series of the mean monthly recharge normalized by mean annual (c) time series of the mean monthly recharge of June, (d) time series of the mean monthly recharge of July, (e) time series of the mean monthly recharge of August (m^3/day) for the fifth scenario.

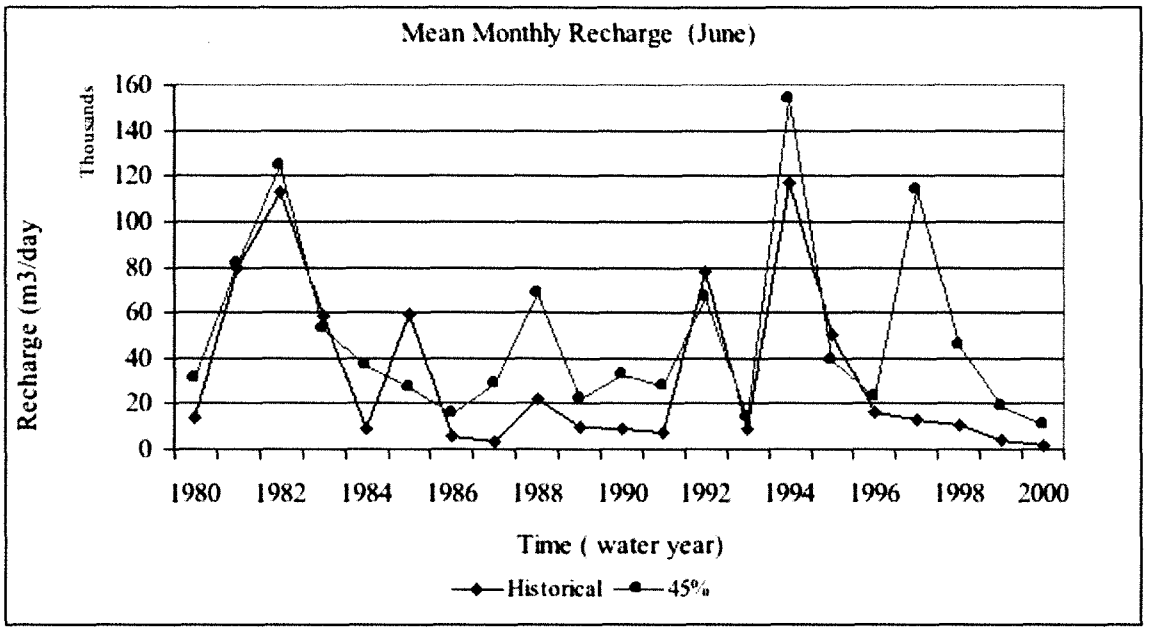

(c)

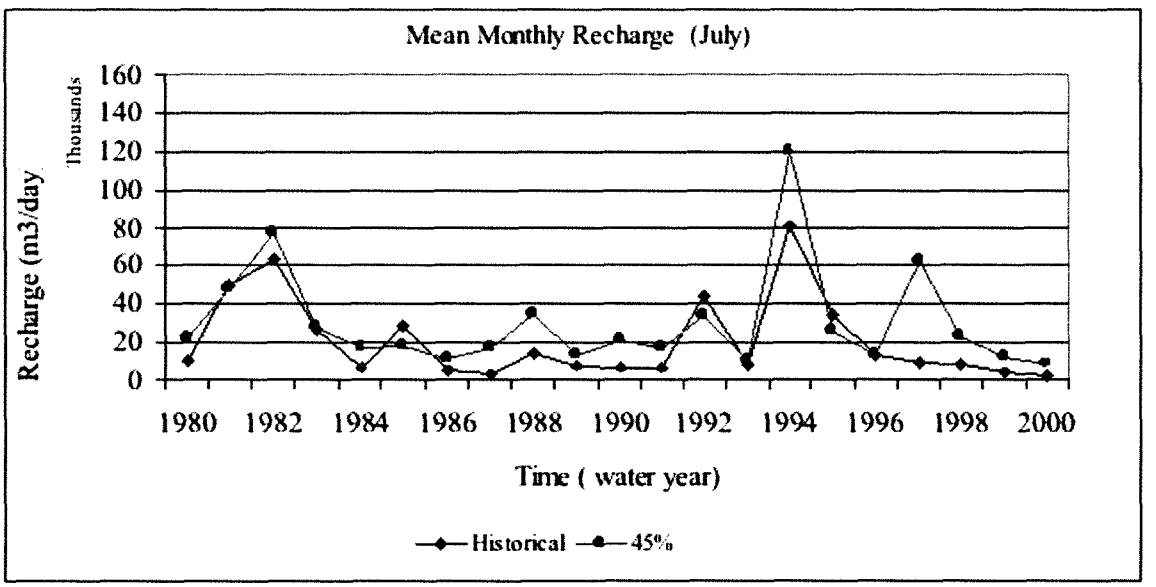

(d)

Figure (5.42): (a) Time series of the mean monthly recharge (b) time series of the mean monthly recharge normalized by mean annual (c) time series of the mean monthly recharge of June, (d) time series of the mean monthly recharge of July, (e) time series of the mean monthly recharge of August (m^3/day) for the fifth scenario (continued).

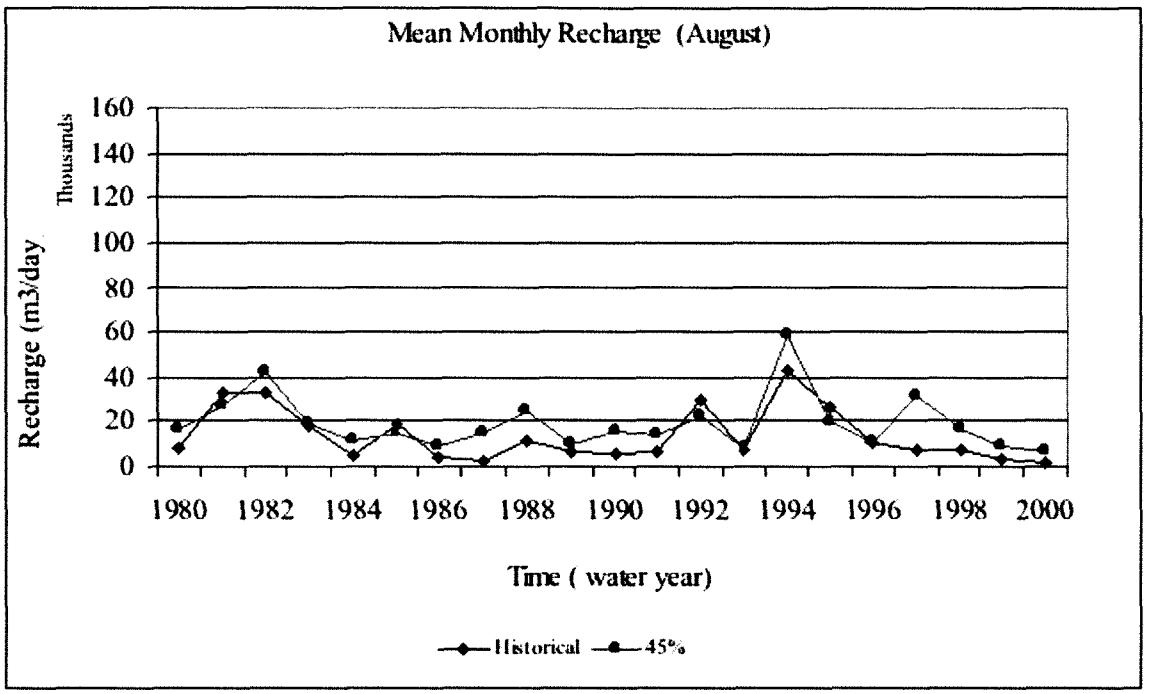

(e)

Figure (5.42): (a) Time series of the mean monthly recharge (b) time series of the mean monthly recharge normalized by mean annual (c) time series of the mean monthly recharge of June, (d) time series of the mean monthly recharge of July, (e) time series of the mean monthly recharge of August (m^3/day) for the fifth scenario (continued).

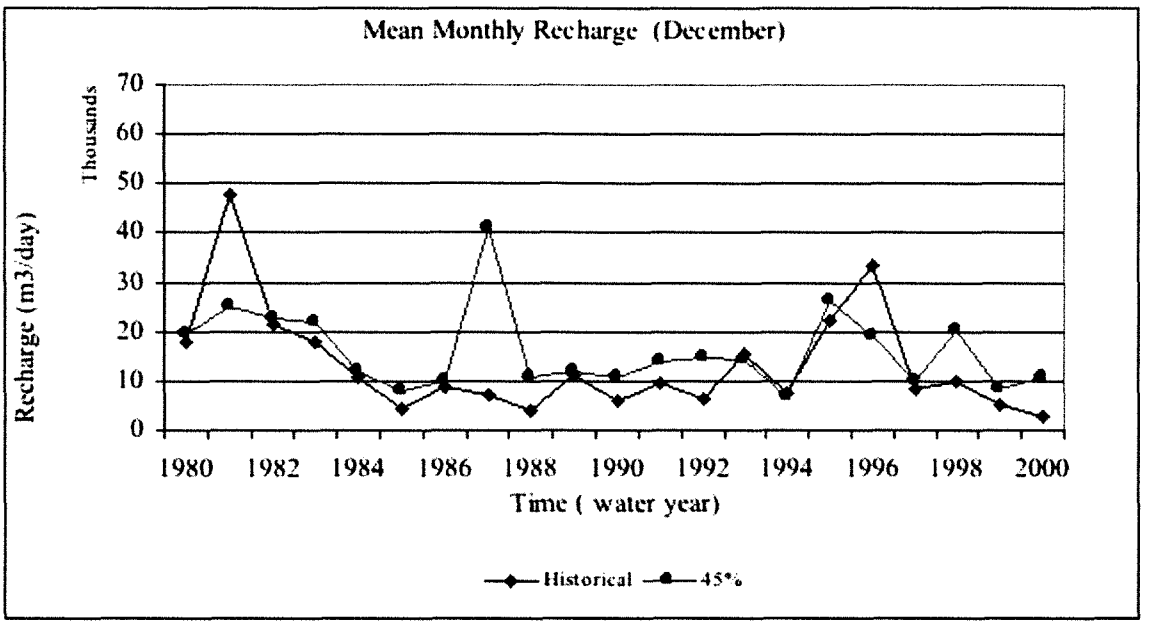

(a)

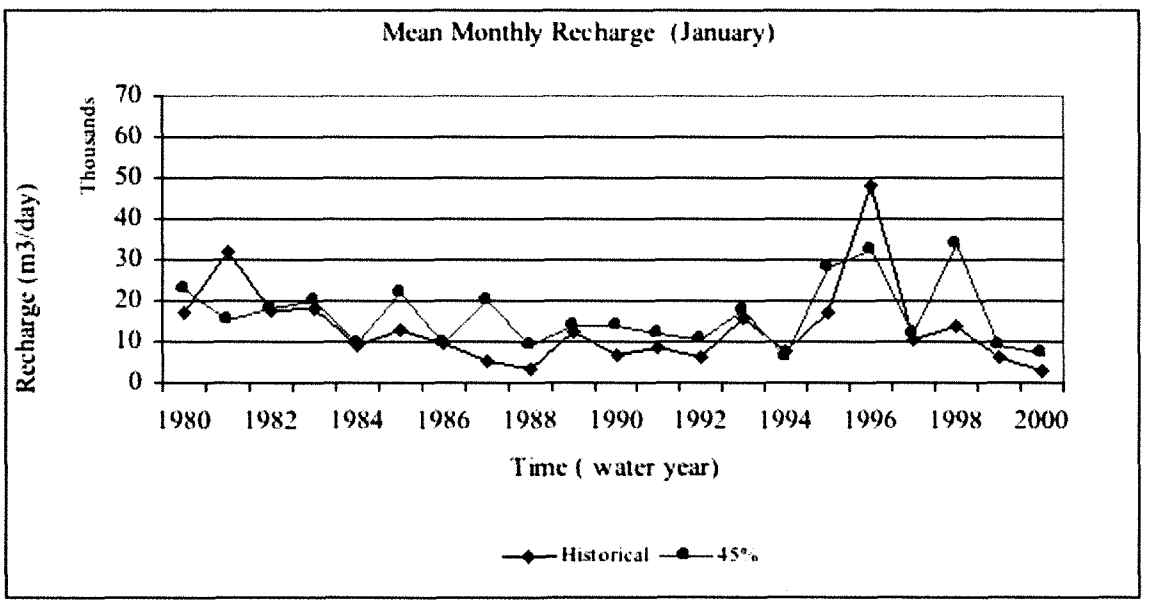

(b)

Figure (5.43): (a) Time series of the mean monthly recharge of December, (b) time series of the mean monthly recharge of January, (c) time series of the mean monthly recharge of February (m^3/day) for the fifth scenario.

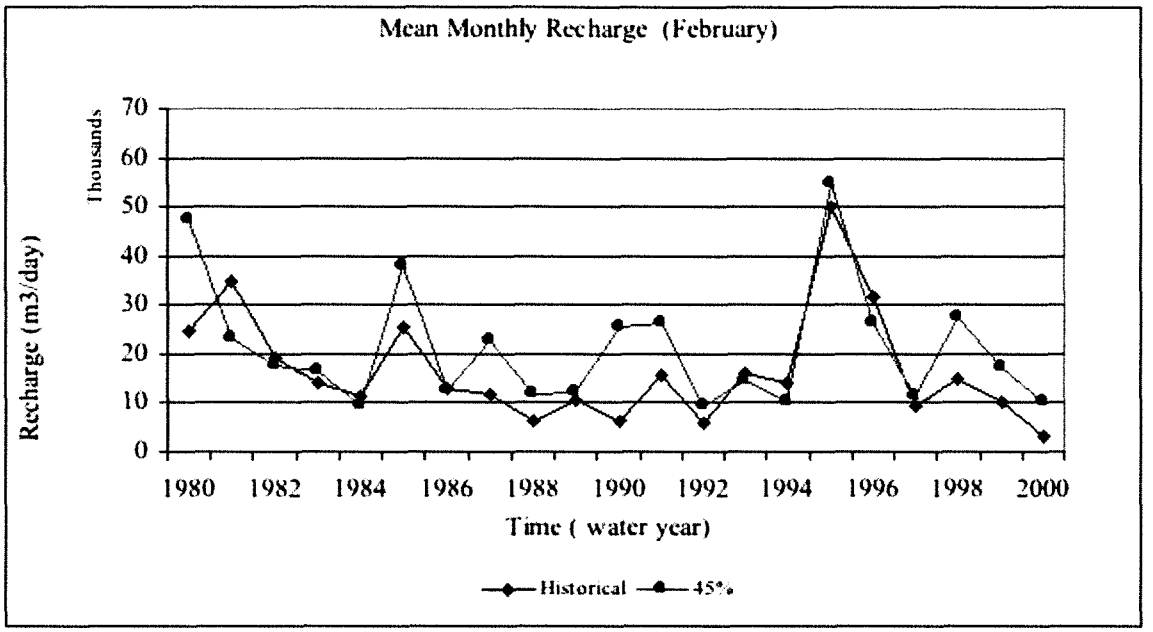

(c)

Figure (5.43): (a) Time series of the mean monthly recharge of December, (b) time series of the mean monthly recharge of January, (c) time series of the mean monthly recharge of February (m^3/day) for the fifth scenario (continued).

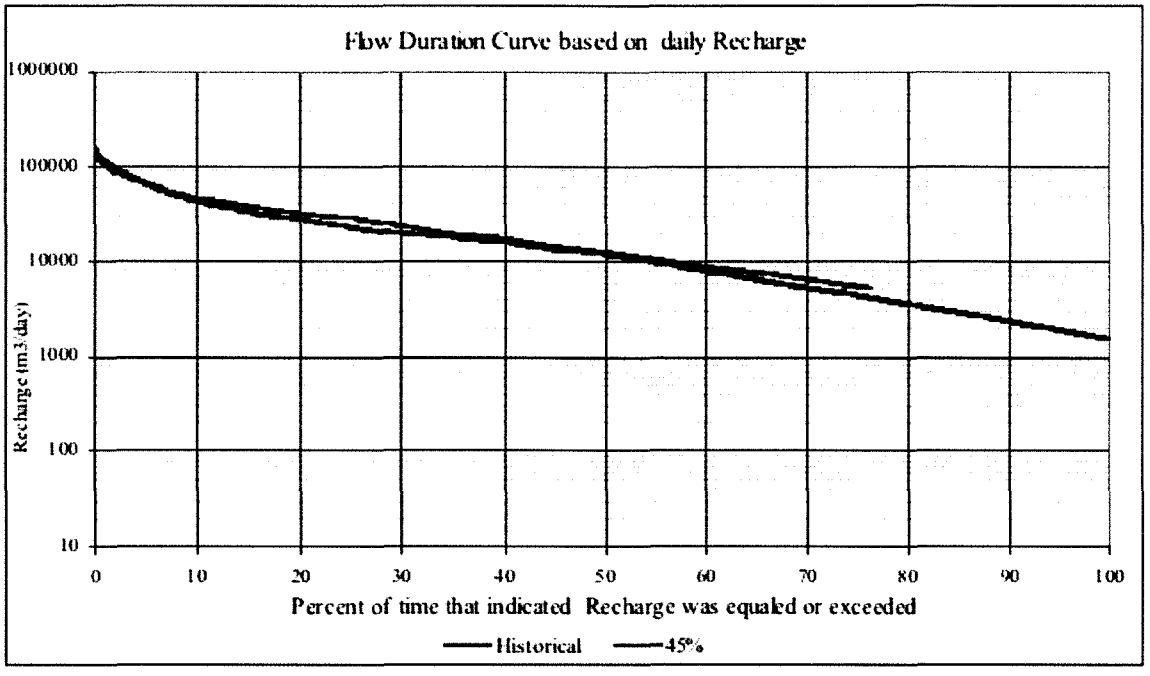

(a)

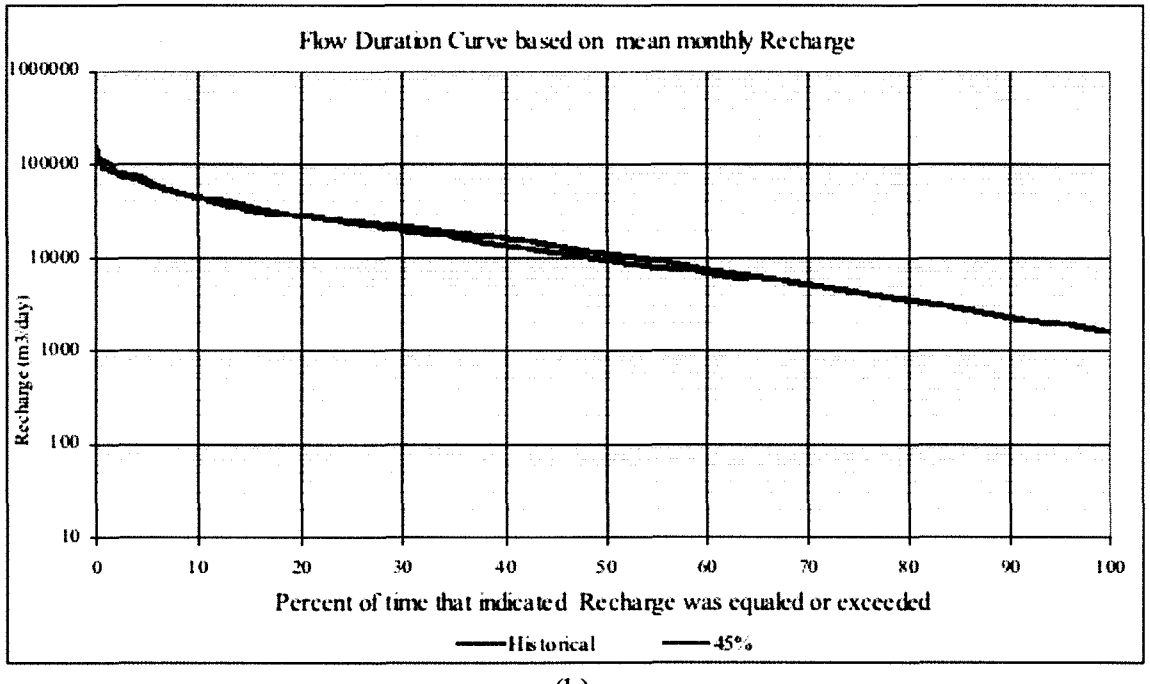

(b)

Figure (5.44): (a) Flow duration curve (daily), (b) Flow duration curve (monthly), (c) Flow duration curve (June), (d) Flow duration curve (July), (e) Flow duration curve (August) (m^3/day) for the fifth scenario.

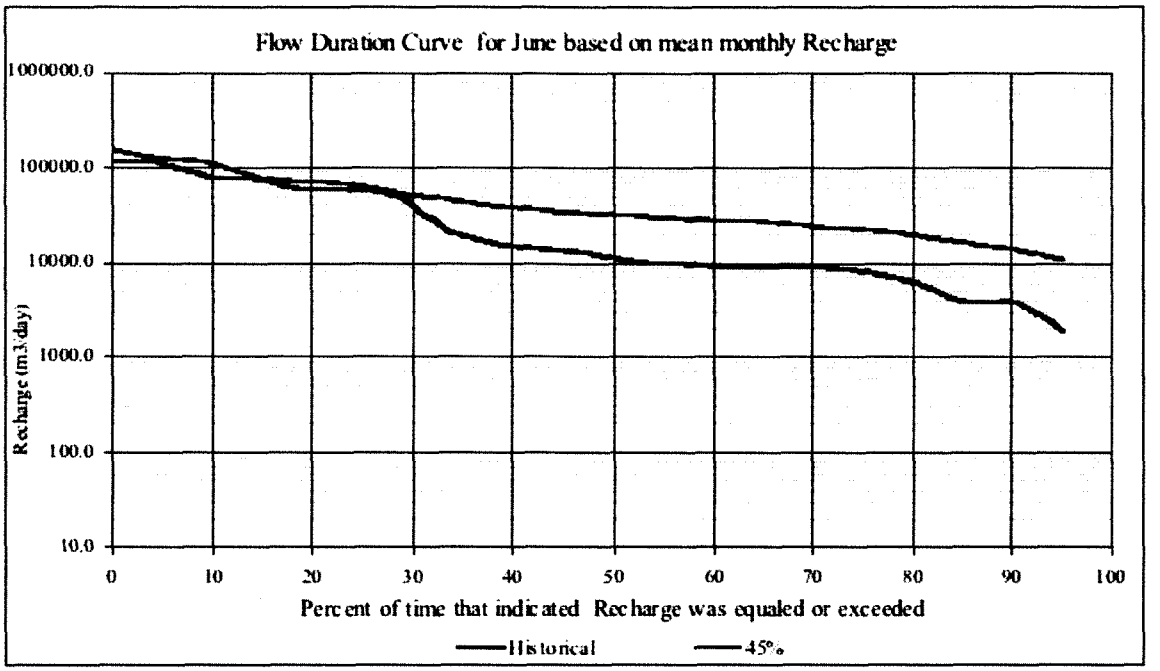

(c)

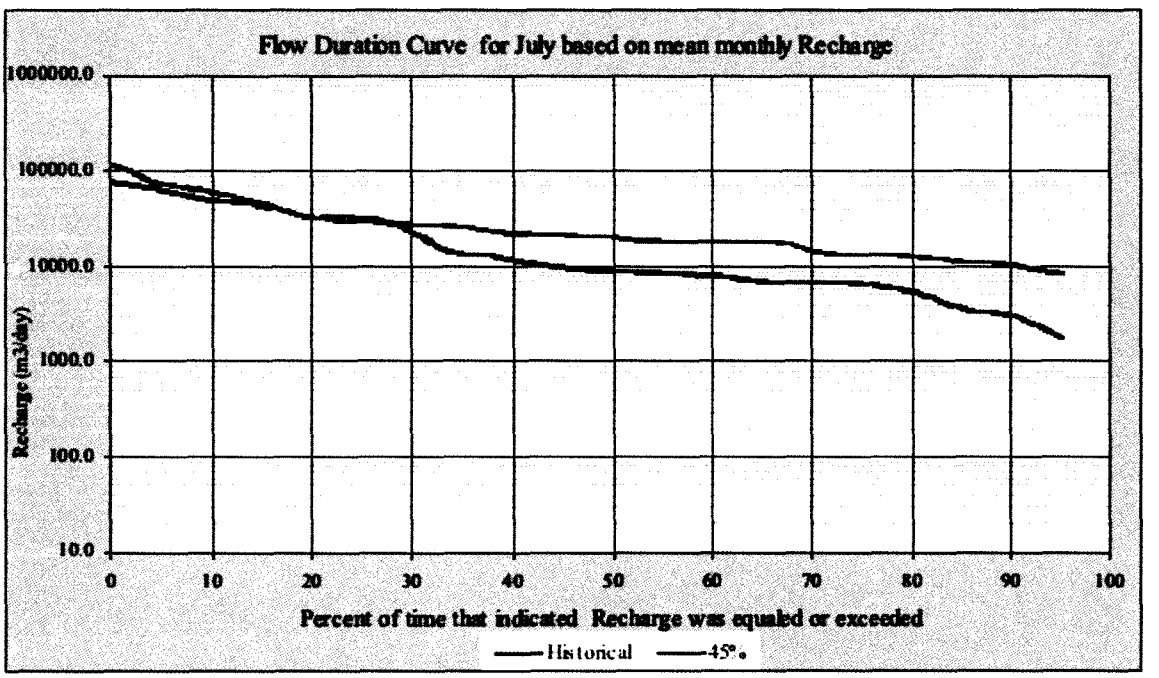

(d)

Figure (5.44): (a) Flow duration curve (daily), (b) Flow duration curve (monthly), (c) Flow duration curve (June), (d) Flow duration curve (July), (e) Flow duration curve (August) (m^3/day) for the fifth scenario (continued).

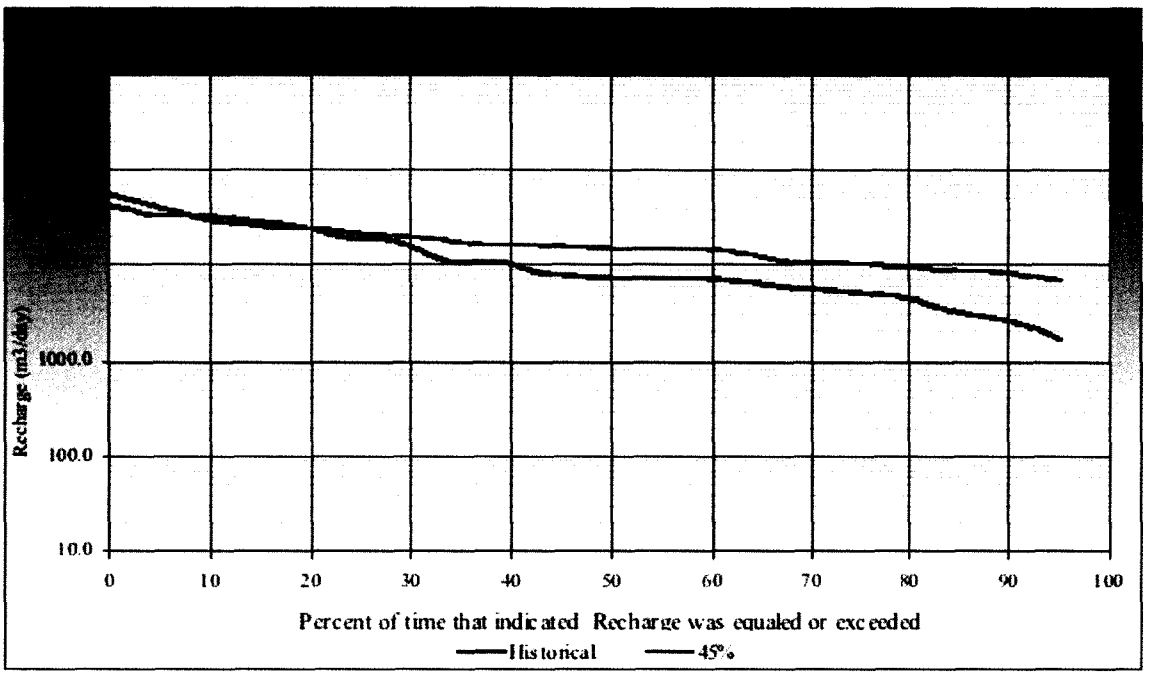

(e)

Figure (5.44): (a) Flow duration curve (daily), (b) Flow duration curve (monthly), (c) Flow duration curve (June), (d) Flow duration curve (July), (e) Flow duration curve (August) (m^3/day) for the fifth scenario (continued).

5.4.6 Sixth scenario

This scenario is similar to the fifth scenario except the generated the rainfall amounts produce an average decrease of 45 percent compared to the historical data.

5.4.6.1 Changes to daily, Monthly and annual recharge flow

Figures (5.45) (a, b, c and d) show the time series of the recharge flow for the 45 percent change. The four figures show the change in the recharge, and figure (5.45) (a)

shows the time series of the recharge for the whole period (1980-2000). The first seven - year periods is shown in figure (5.45) (b), the second-seven year period in (c) and the rest of the period in figure (5.45) (d). The four figures show the recharge decreasing more than decrease applied to the rainfall.

The descriptive statistics of the decreased recharge were analyzed. The mean annual and multi-mean annual recharge have been calculated as illustrated in table (5.32) and figures (5.46) (a, b). We note from this table and the figures how the recharge changes according to the change in the stochastically generated precipitation time series.

The percentages of the changes are shown in table (5.33). The table shows the daily average of the percentage change relative to the historical recharge. Table (5.33) shows the yearly average percentage changes to the recharge, which is shown in figure (5.47). The standard deviation, skewness coefficient, and kurtosis are calculated for the annual recharge. The standard deviation for annual recharge and multi-annual standard deviation are calculated for this scenario as illustrated in table (5.34) and figures (5.48). Table (5.35) shows the yearly average percentage changes to the standard deviation of the recharge that is also shown in figure (5.49).

The skewness coefficient and kurtosis are calculated and plotted in figure (5.50) (a, b). These figures show how the standard deviation, skewness coefficients, and kurtosis for annual recharge are changed corresponding to the change in the adapted scenarios on the precipitations. The results presented are consistent with the results shown above in terms of changes in precipitation and have decreased in the daily and annual recharge. The mean monthly recharge for the water years (1980-2000) has been plotted to all months and also for the specific months of summer (June, July, and August) and winter

(December, January, and February) seasons. Figure (5.51) (a) shows the mean monthly recharge for the stochastically generated precipitation values for the period (1980-2000). The decrease as seen in table (5.36) of the recharge is greater than the decrease in precipitation. The figures (5.53) (a, b, c, d, e) show the flow duration curve based on daily and monthly analyses and for specific months of June, July, and August.

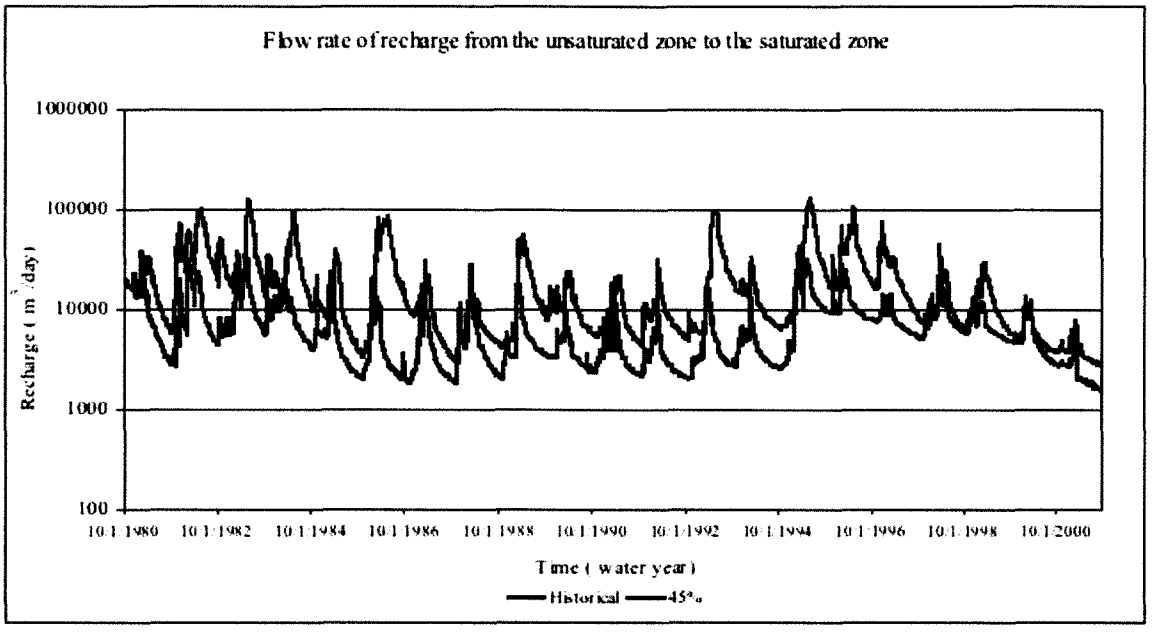

(a)

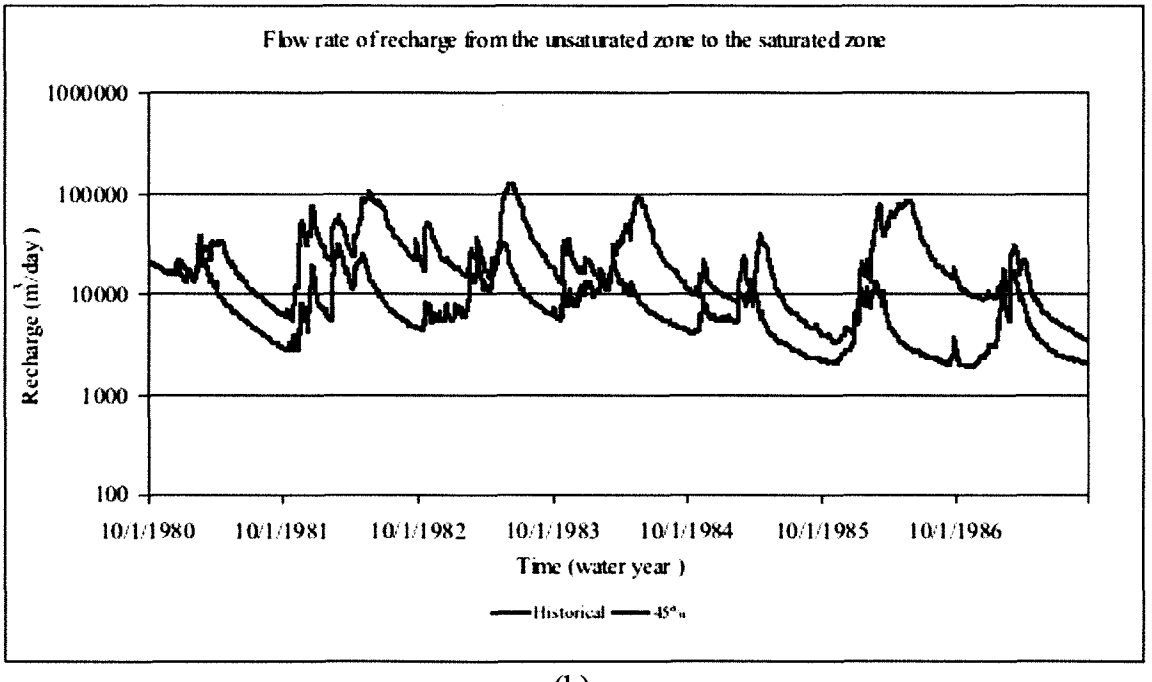

(b)

Figure (5.45): The time series of flow rate of the recharge at whole period (a), first seven years (b), second seven years (c) and rest of the time period (d) for the sixth scenario (m^3/day).

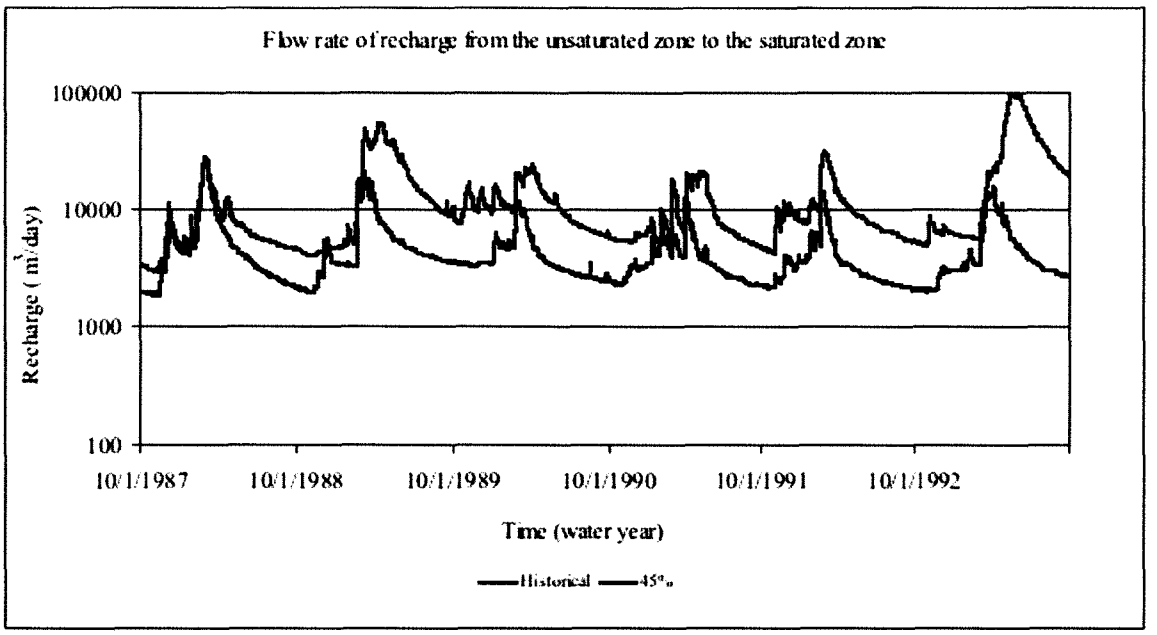

(c)

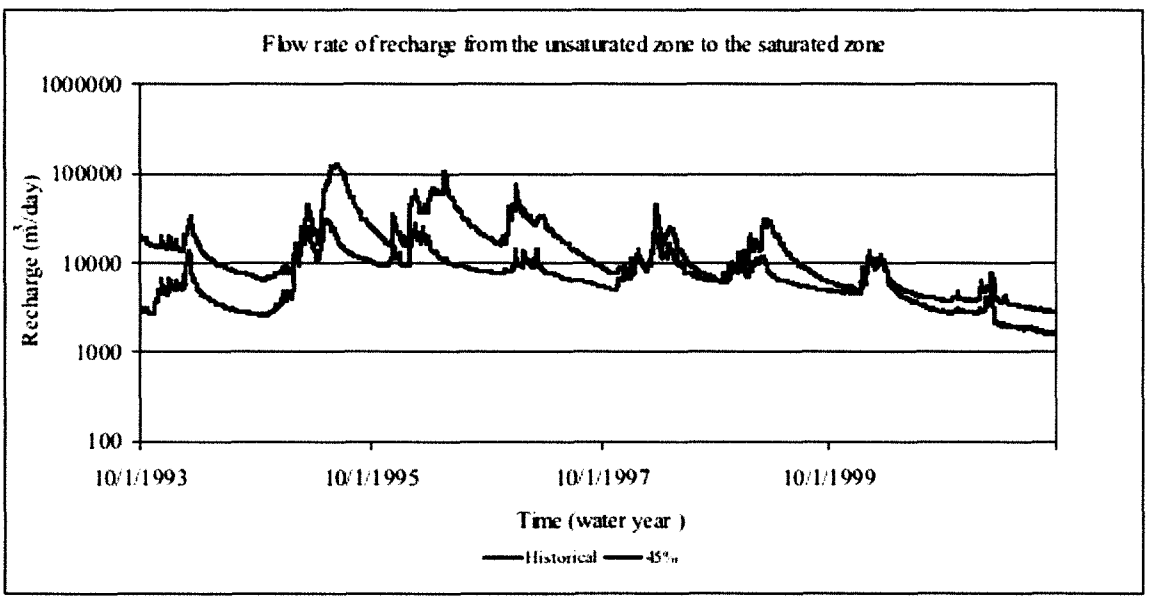

(d)

Figure (5.45): The time series of flow rate of the recharge at whole period (a), first seven years (b), second seven years (c) and rest of the time period (d) for the sixth scenario (m^3/day) (continued).

Table (5.32) The mean annual recharge (m^3/day) for the sixth scenario.

Time	Historical	S-45%
1980-2000	18926.788	6861.9986
1980	17708.163	11239.758
1981	41879.854	10118.011
1982	37911.343	11080.957
1983	28973.994	8948.2825
1984	12057.183	4957.081
1985	30296.348	4156.8411
1986	9821.543	4022.7029
1987	5758.739	6978.574
1988	15813.659	6090.6518
1989	11420.047	4100.4914
1990	8317.220	3865.9145
1991	9557.234	3605.8996
1992	26949.585	4585.4898
1993	13498.135	4278.3707
1994	37135.334	11622.262
1995	36033.397	11642.03
1996	22612.056	7769.0378
1997	11818.430	8826.5994
1998	12097.975	6860.6604
1999	5498.997	5634.7928
2000	2327.462	3710.715
Mean	18927.938	6861.67
MAX	41879.854	11642.03
MIN	2327.462	3605.9
SD	12193.138	2934.5

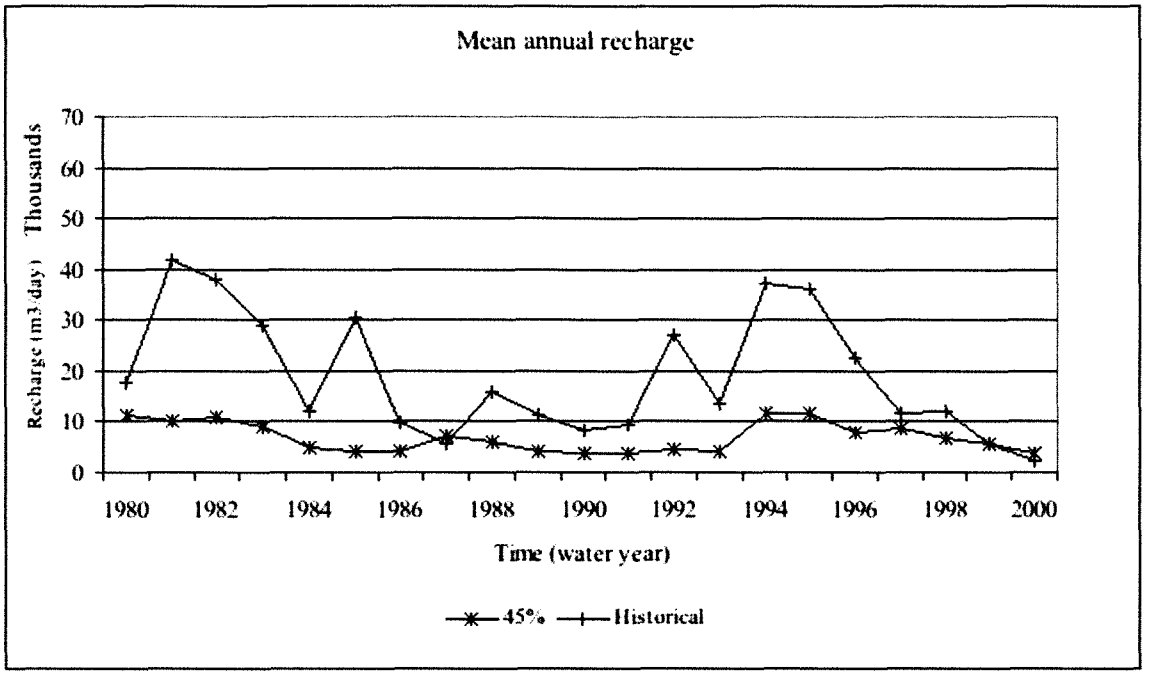

(a)

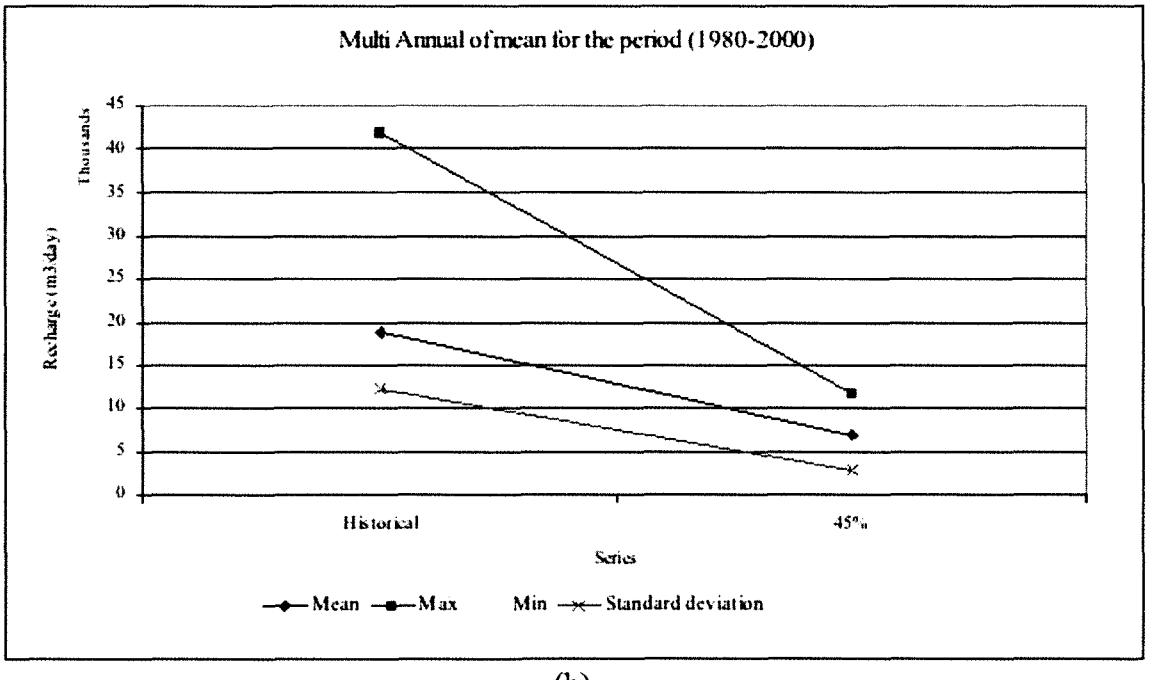

(b)

Figure (5.46): (a) Time series of mean annual and (b) multi-mean annual of recharge for the sixth scenario (m^3/day).

Table (5.33): Relative percentage changes for the daily average recharge for the sixth scenario.

Scenario	S-45%
Average	-41.20%

Table (5.34): Relative percentage changes of the annual average recharge for the sixth scenario.

Time	S -45%
1980-2000	-63.74%
1980	-36.53
1981	-75.84
1982	-70.77
1983	-69.12
1984	-58.89
1985	-86.28
1986	-59.04
1987	21.18
1988	-61.48
1989	-64.09
1990	-53.52
1991	-62.27
1992	-82.98
1993	-68.3
1994	-68.7
1995	-67.69
1996	-65.64
1997	-25.31
1998	-43.29
1999	2.47
2000	59.43
Mean	-49.37
MAX	59.43
MIN	-86.28
SD	36.32

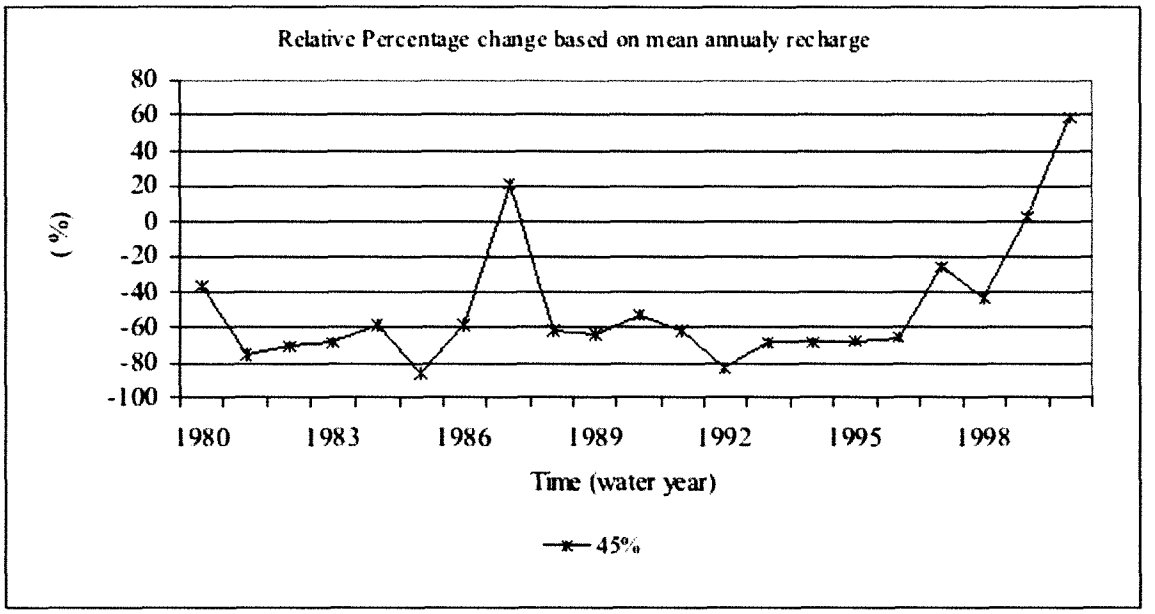

Figure (5.47): Time series of the relative percentage change based on annual recharge for the sixth scenario.

Table (5.35) The standard deviation of annual recharge (m^3/day) for the sixth scenario.

Time	Historical	S - 45%
1980-2000	20161.22	4904.55
1980	7731.89	6251.97
1981	23603.27	6684.4
1982	29059.45	6864.51
1983	20038.97	3523.45
1984	7447.23	2270.17
1985	25600.68	2923.3
1986	5641.41	3122.93
1987	4685.37	5049.46
1988	14846.74	3620.55
1989	4473.41	1977.89
1990	4574.19	1900.81
1991	5491.31	2138.48
1992	27090.32	3187.67
1993	5454.27	2006.1
1994	35890.30	7629.53
1995	19295.44	4338.71
1996	12193.18	1875.51
1997	6504.91	3643.29
1998	6107.53	1779.73
1999	2426.48	2120.93
2000	621.51	821.64
Mean	12798.95	3511
MAX	35890.30	7629.53
MIN	621.51	821.64
SD	10338.30	4904.55

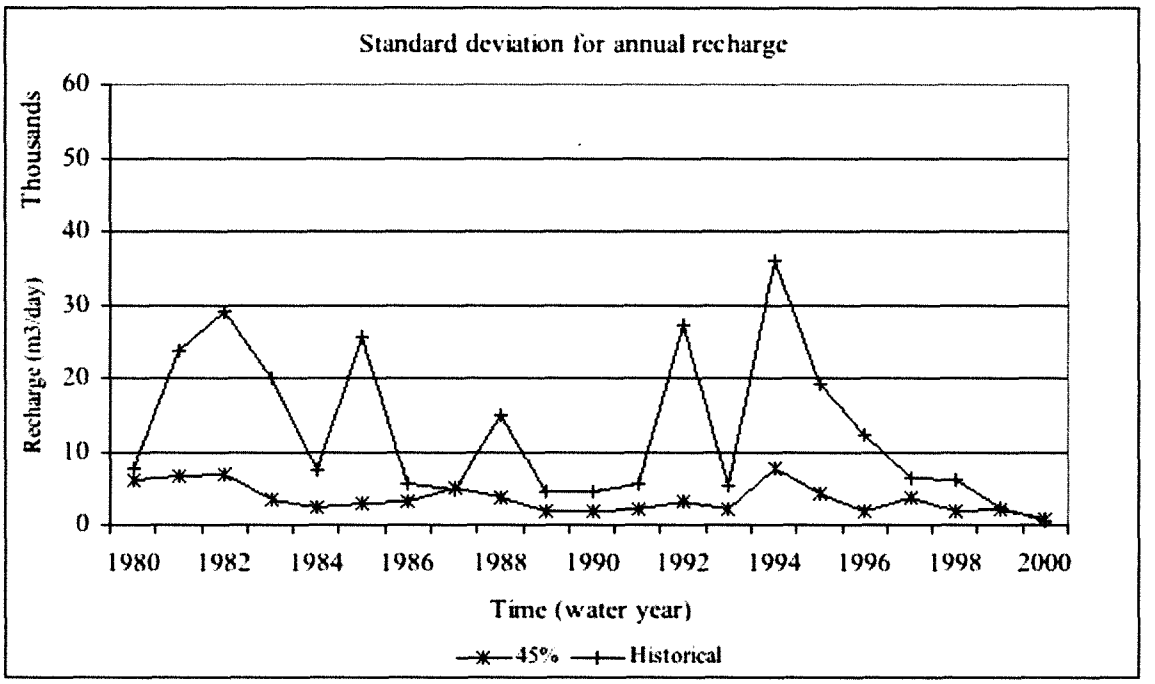

Figure (5.48): Time series of standard deviation of annual recharge (m^3/day) for the sixth scenario.

Table (5.36): Relative percentage change of the annual standard deviation for the sixth scenario.

Time	S-45%
1980-2000	-75.67%
1980	-19.141
1981	-71.68
1982	-76.378
1983	-82.417
1984	-69.517
1985	-88.581
1986	-44.643
1987	7.771
1988	-75.614
1989	-55.786
1990	-58.445
1991	-61.057
1992	-88.233
1993	-63.22
1994	-78.742
1995	-77.514
1996	-84.618
1997	-43.992
1998	-70.86
1999	-12.592
2000	32.199
Mean	-56.336
MAX	32.199
MIN	-88.581
SD	32.78

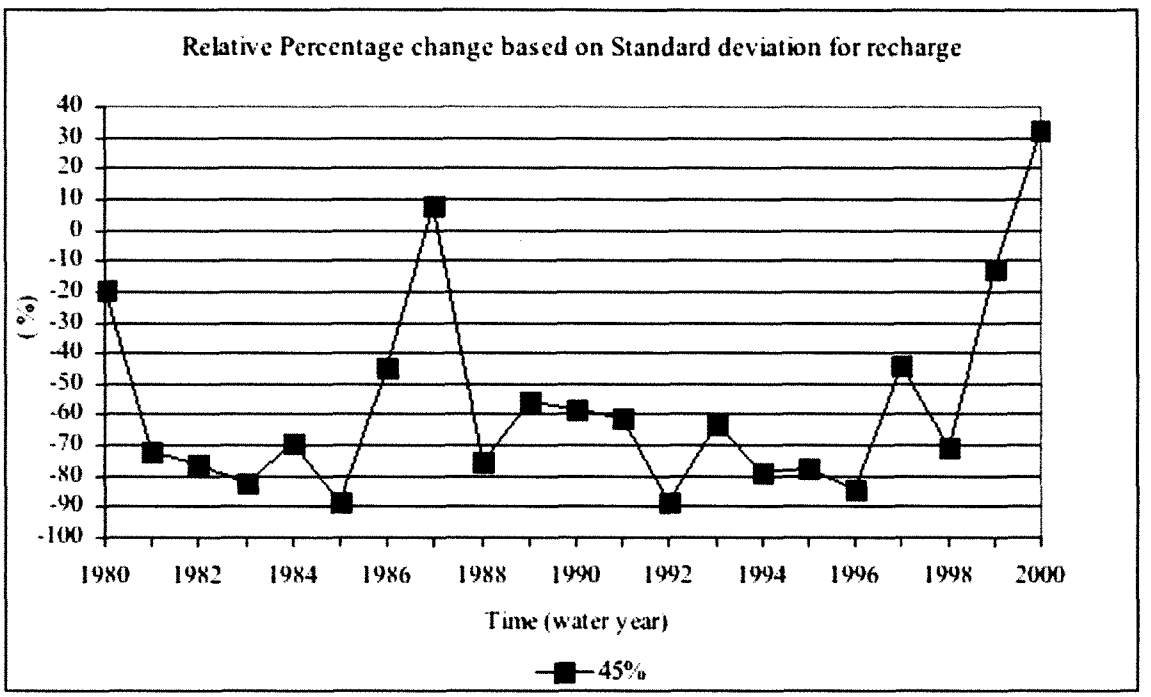

Figure (5.49): Time series of the relative percentage change based on standard deviation for the sixth scenario.

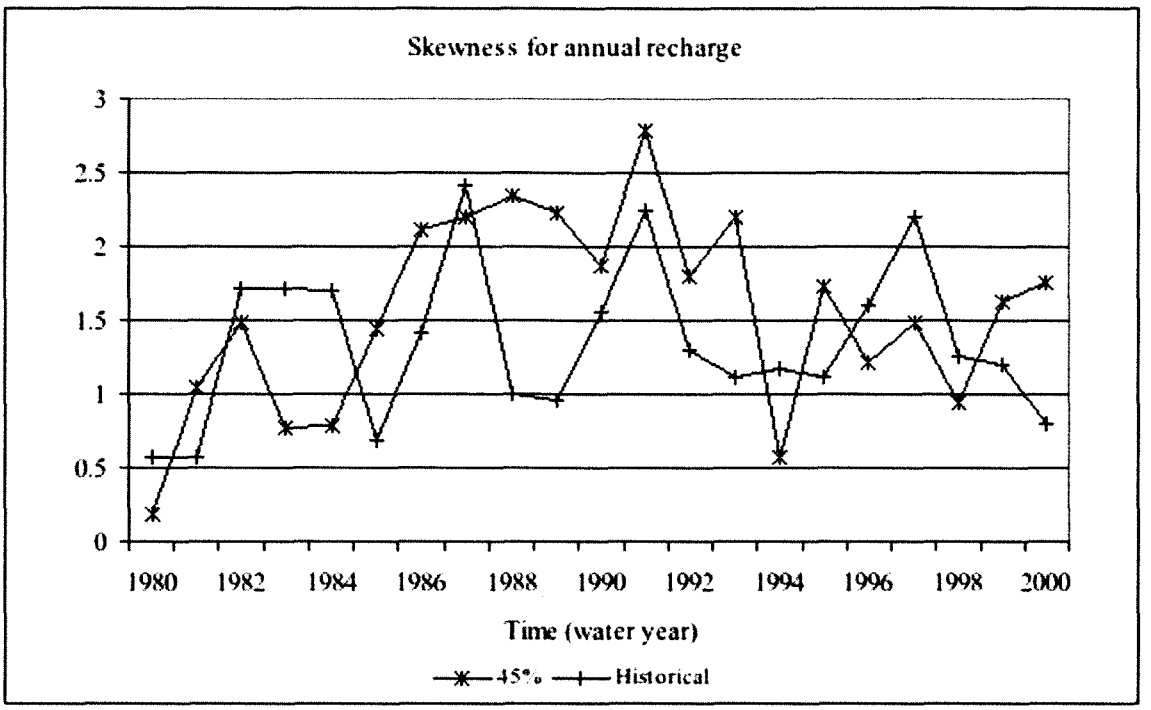

(a)

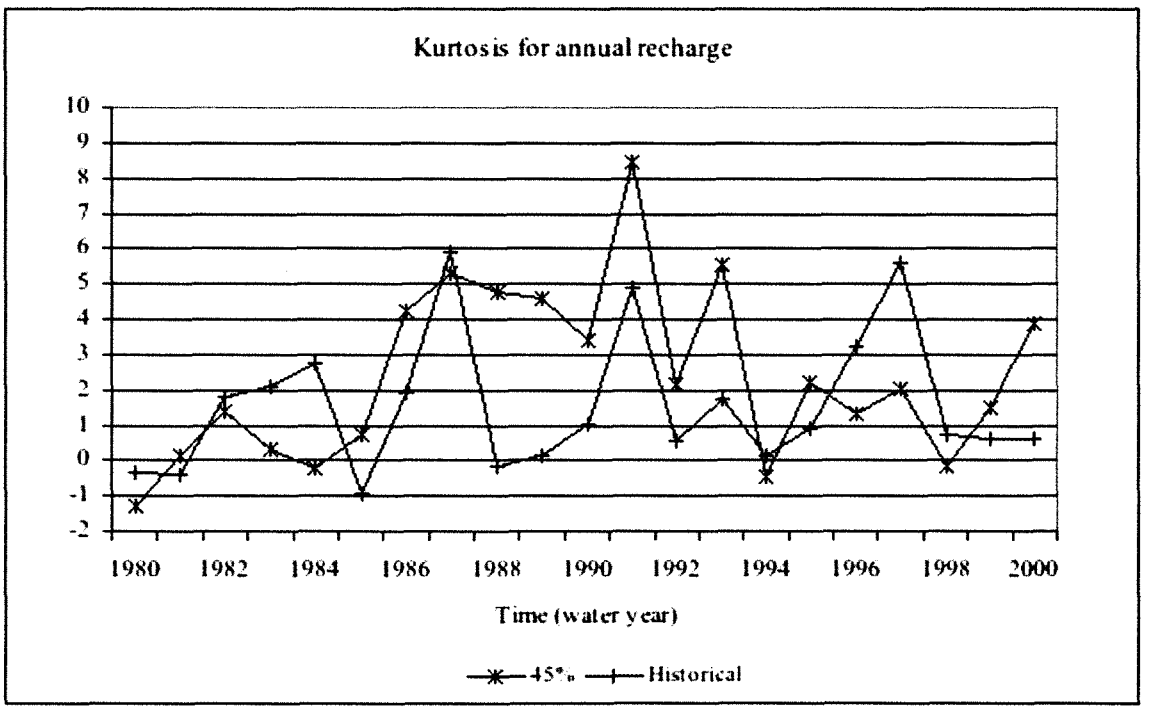

(a)

Figure (5.50): Time series of the (a) skewness coefficient and (b) kurtosis annual recharge (m^3/day) for the sixth scenario.

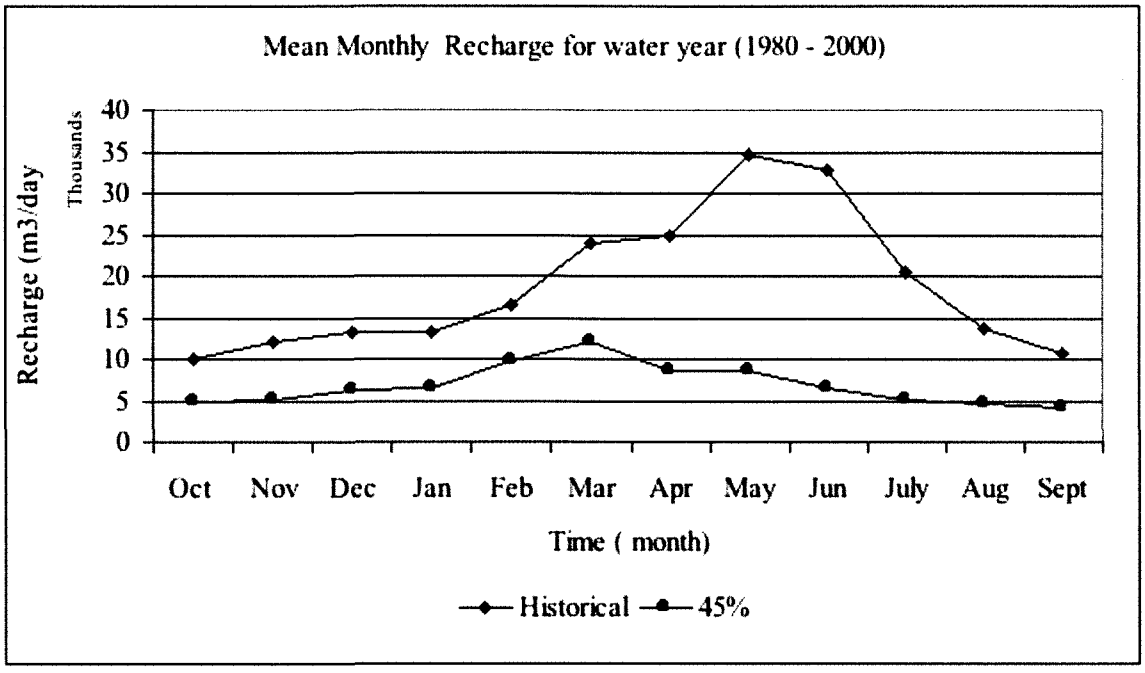

(a)

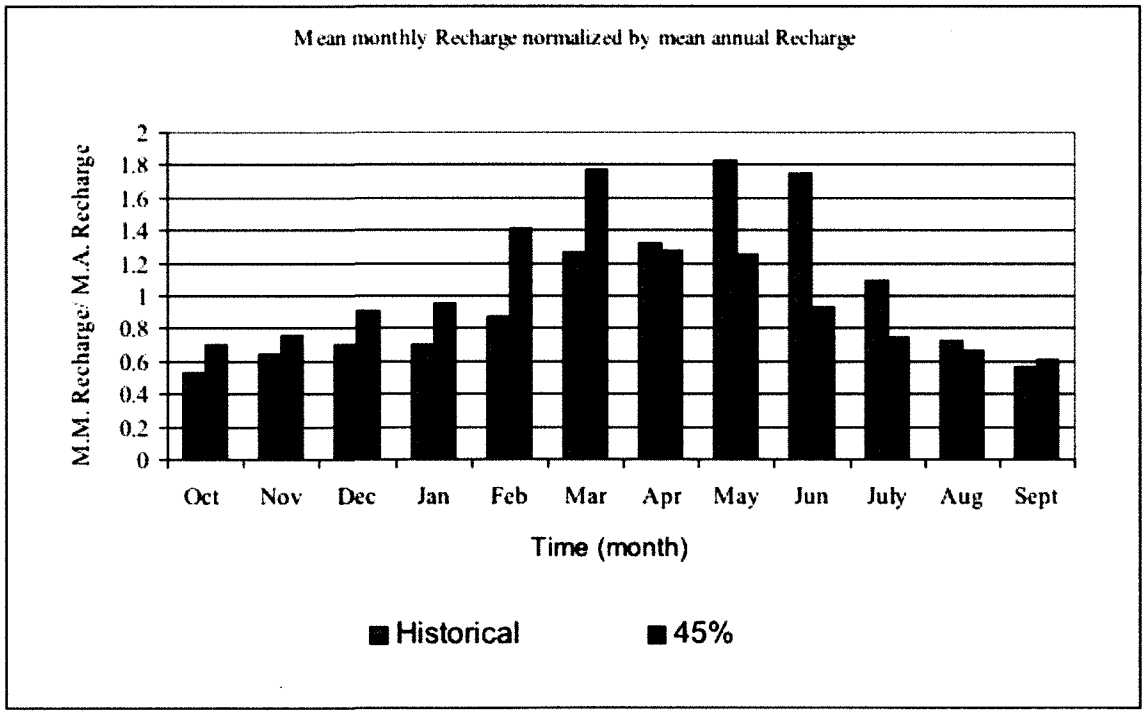

(b)

Figure (5.51): (a) Time series of the mean monthly recharge (b) time series of the mean monthly recharge normalized by mean annual (c) time series of the mean monthly recharge of June, (d) time series of the mean monthly recharge of July, (e) time series of the mean monthly recharge of August (m^3/day) for the sixth scenario.

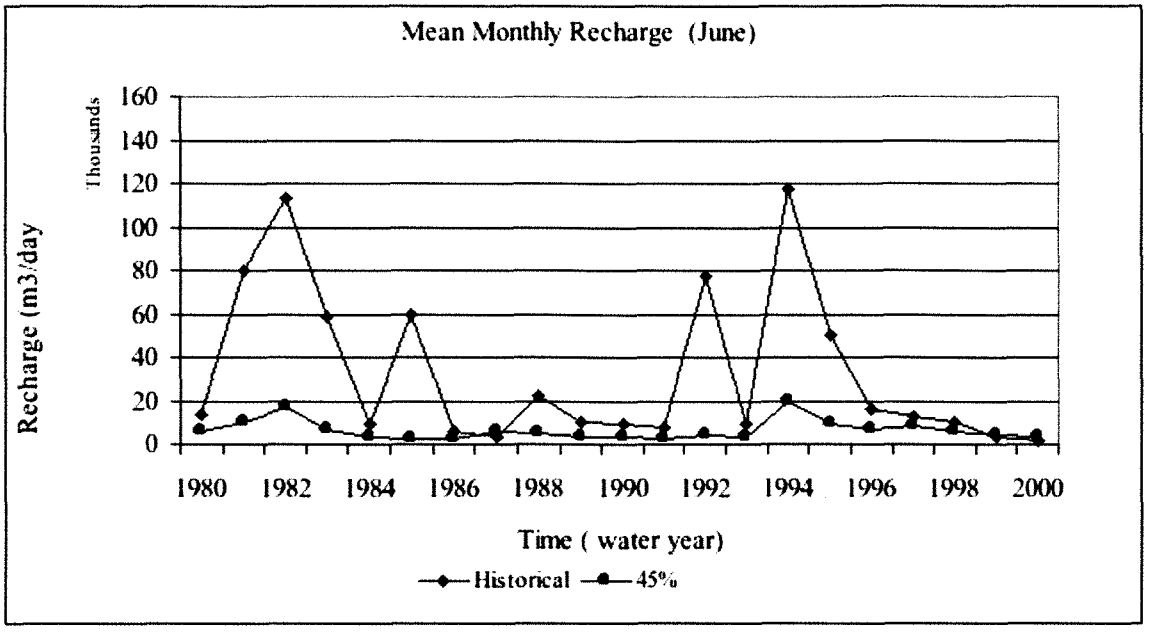

(c)

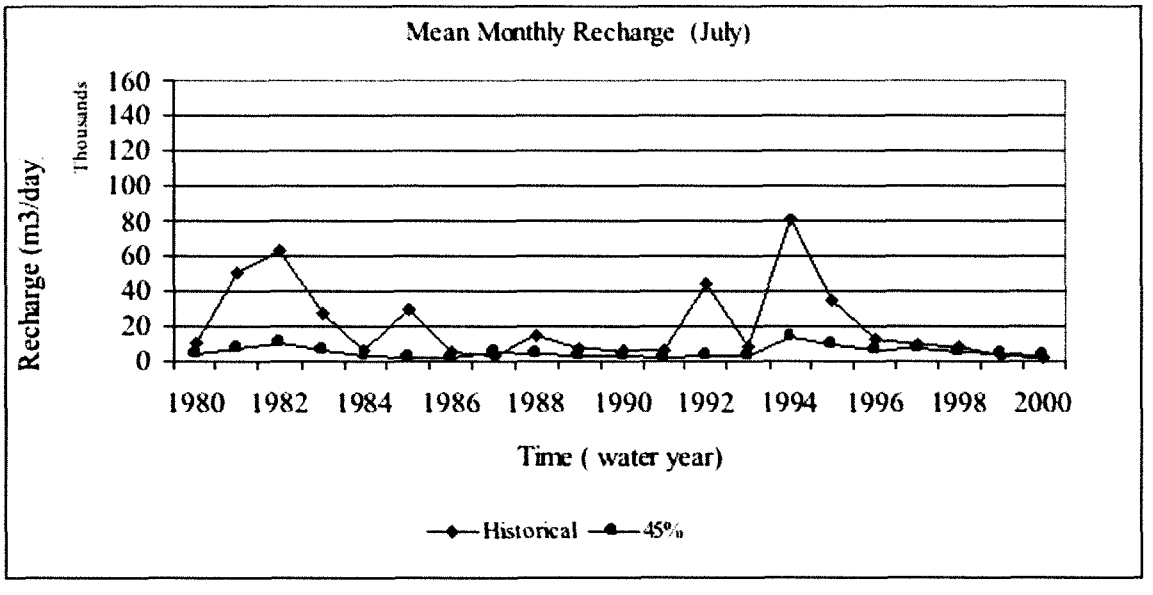

(d)

Figure (5.51): (a) Time series of the mean monthly recharge (b) time series of the mean monthly recharge normalized by mean annual (c) time series of the mean monthly recharge of June, (d) time series of the mean monthly recharge of July, (e) time series of the mean monthly recharge of August (m^3/day) for the sixth scenario (continued).

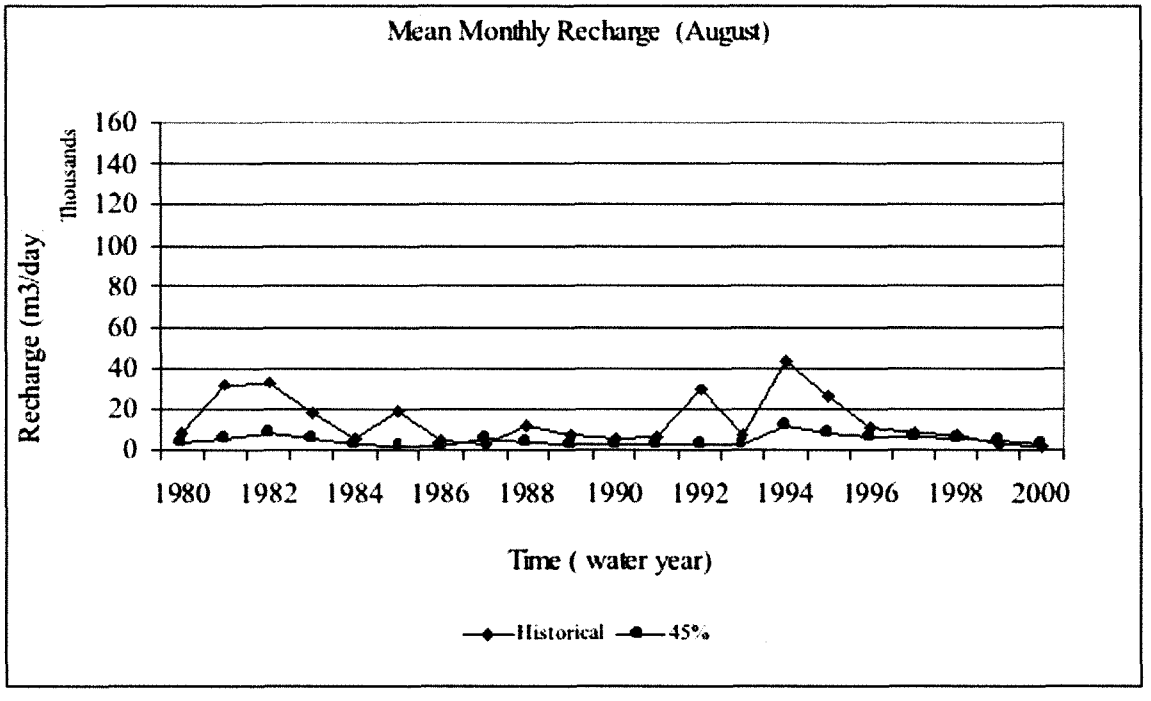

(e)

Figure (5.51): (a) Time series of the mean monthly recharge (b) time series of the mean monthly recharge normalized by mean annual (c) time series of the mean monthly recharge of June, (d) time series of the mean monthly recharge of July, (e) time series of the mean monthly recharge of August (m^3/day) for the sixth scenario (continued).

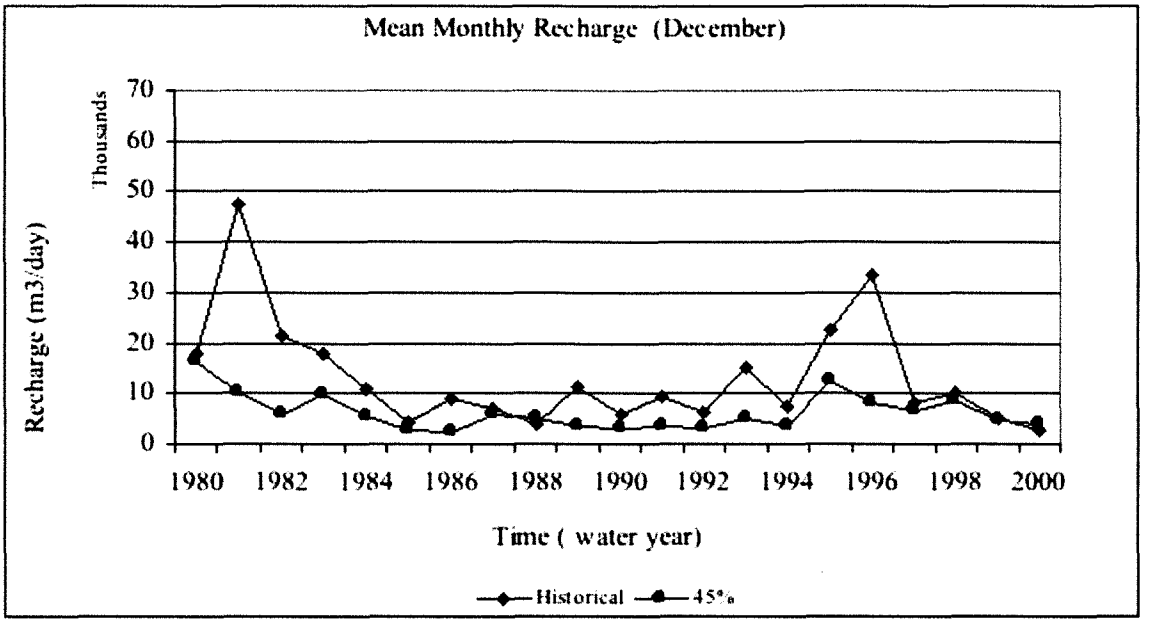

(a)

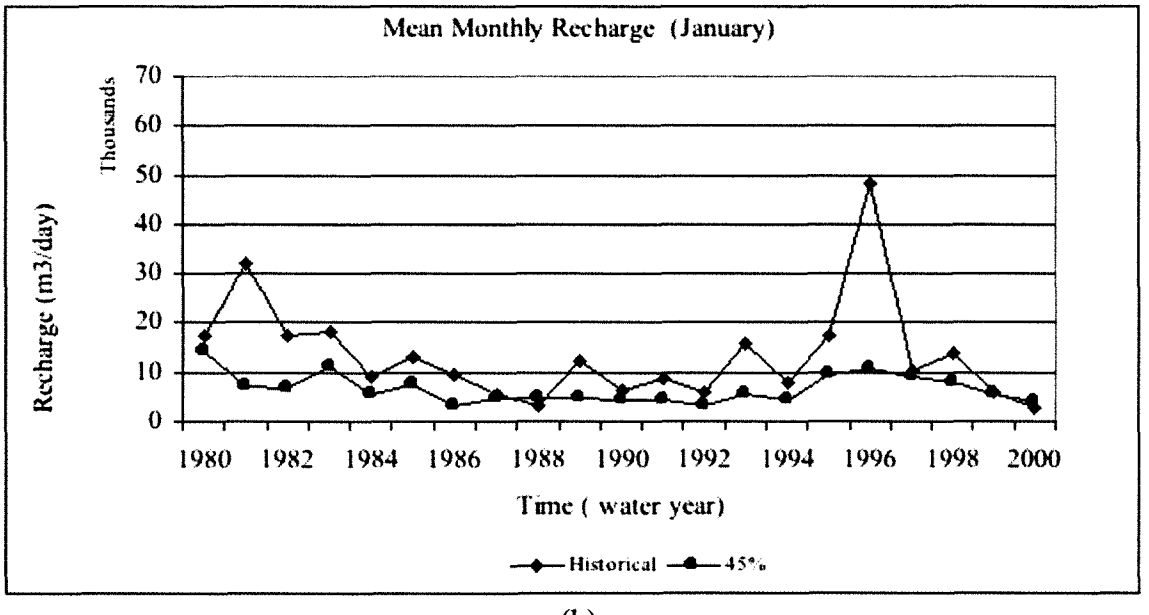

(b)

Figure (5.52): (a) Time series of the mean monthly recharge of December (b) time series of the mean monthly recharge of January, (c) time series of the mean monthly recharge of February (m^3/day) for the sixth scenario.

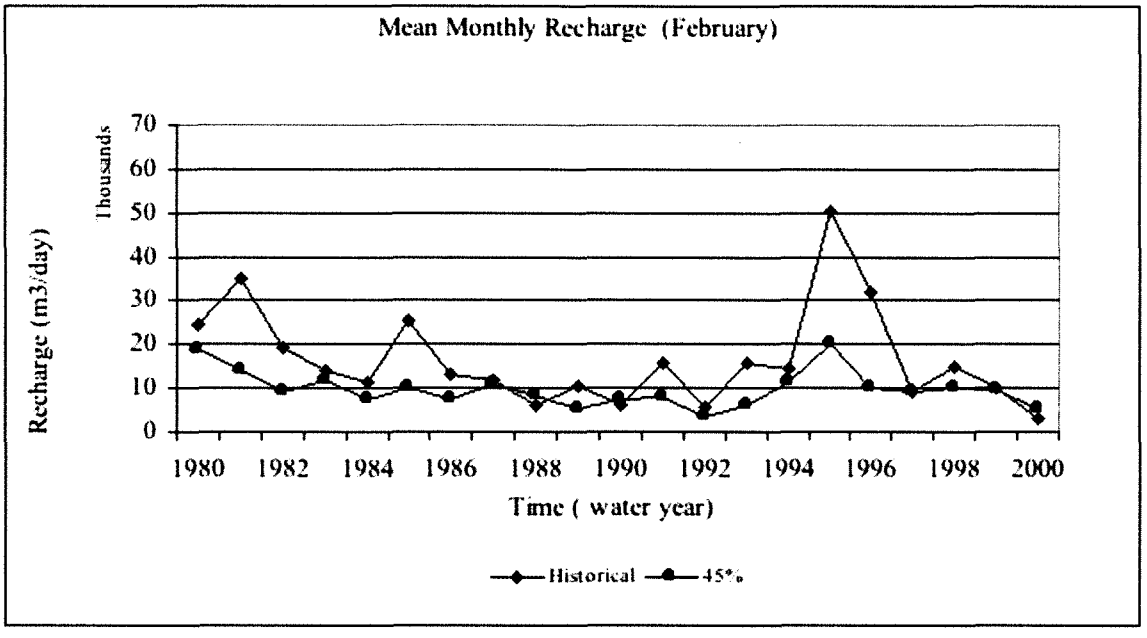

(c)

Figure (5.52): (a) Time series of the mean monthly recharge of December (b) time series of the mean monthly recharge of January, (c) time series of the mean monthly recharge of February (m^3/day) for the sixth scenario (continued).

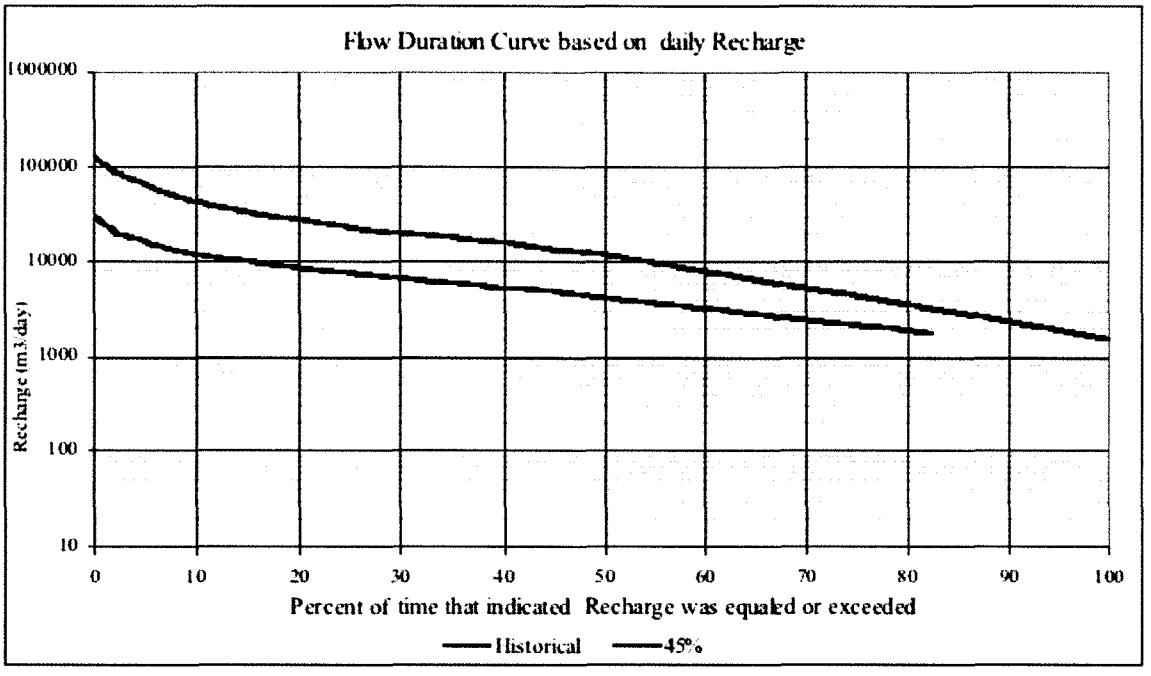

(a)

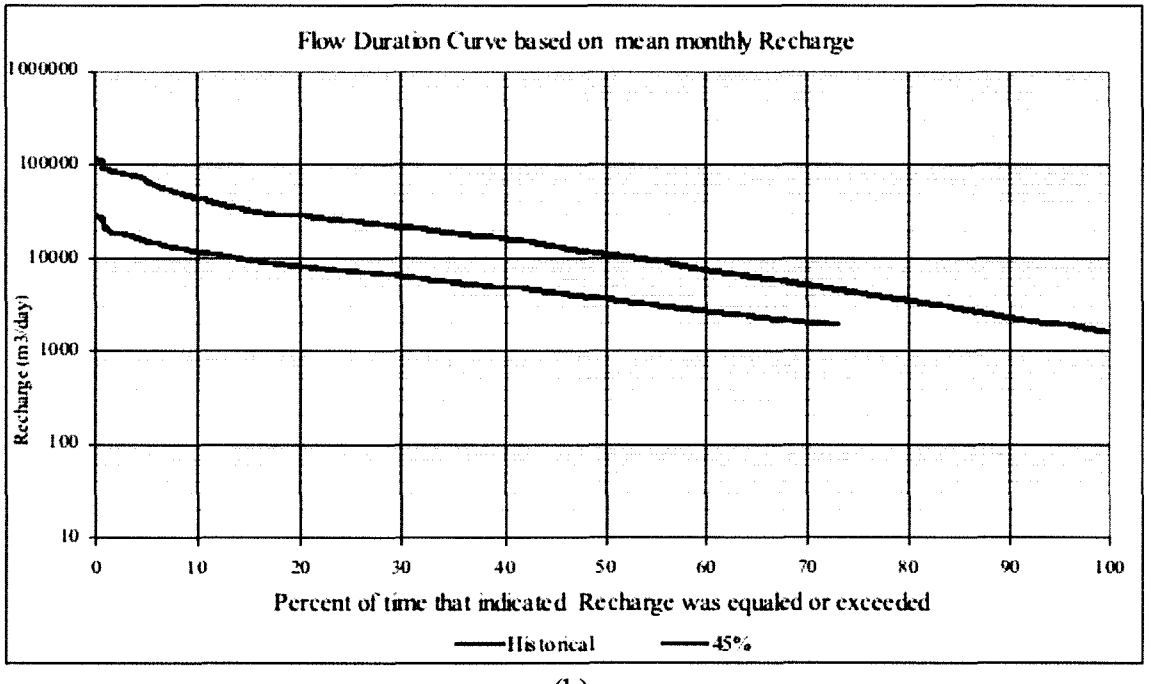

(b)

Figure (5.53): (a) Flow duration curve (daily), (b) Flow duration curve (monthly), (c) Flow duration curve (June), (d) Flow duration curve (July), (e) Flow duration curve (August)(m^3/day) for the sixth scenario.

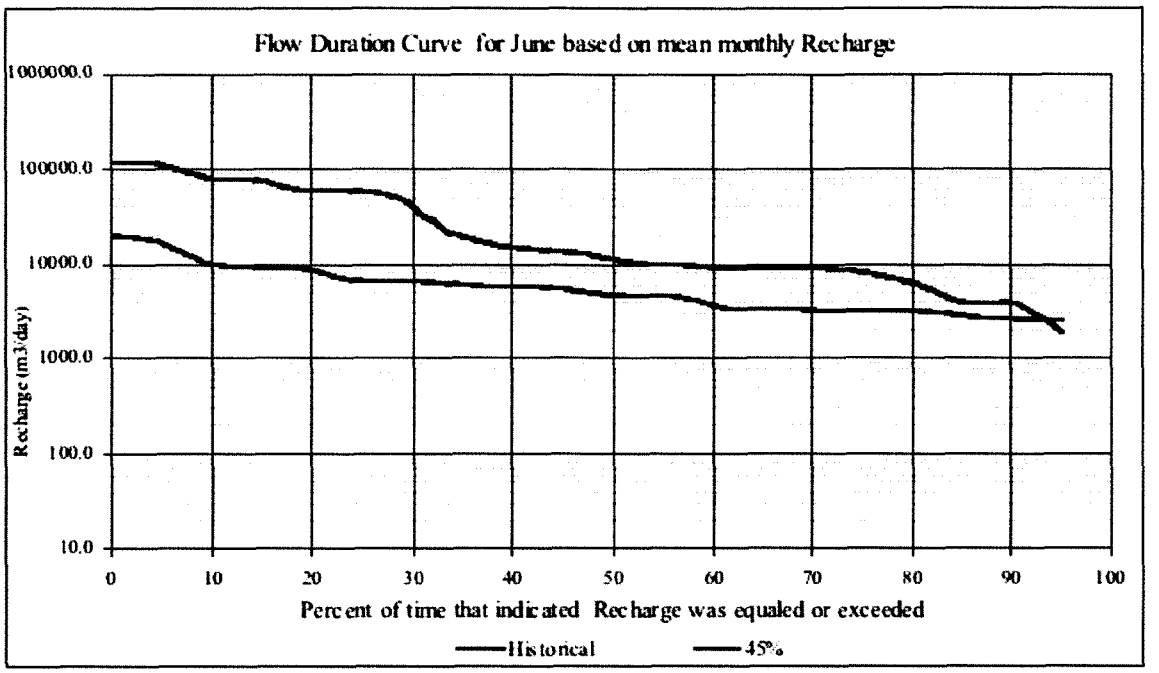

(c)

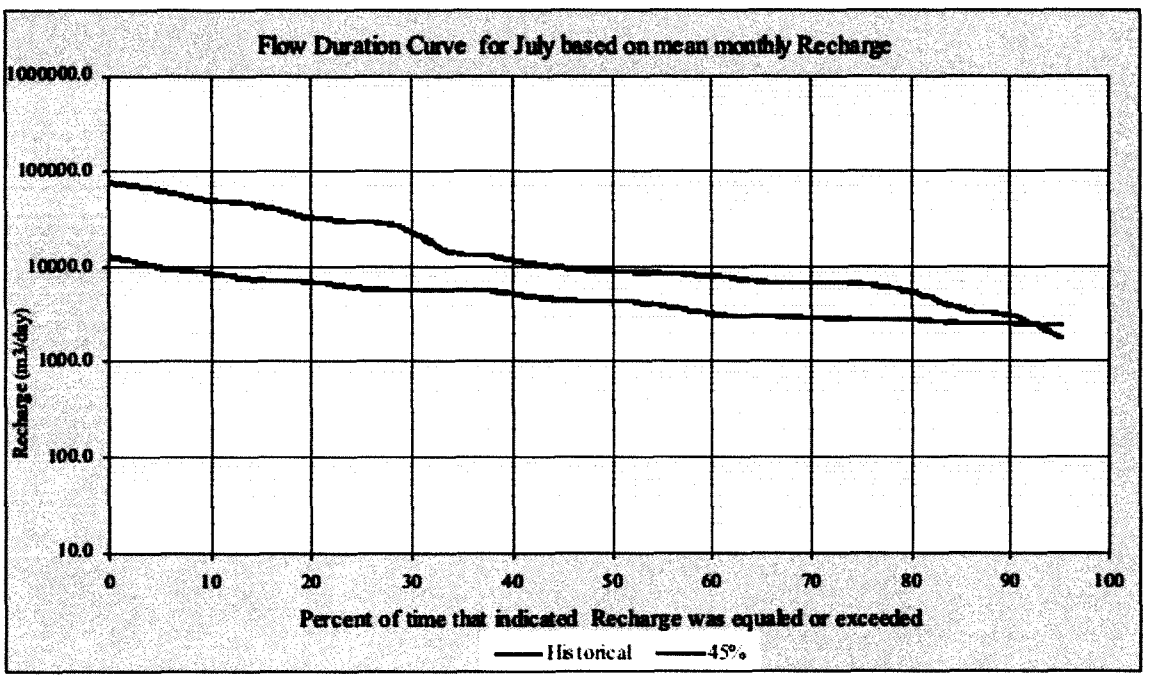

(d)

Figure (5.53): (a) Flow duration curve (daily), (b) Flow duration curve (monthly), (c) Flow duration curve (June), (d) Flow duration curve (July), (e) Flow duration curve (August)(m^3/day) for the sixth scenario (continued).

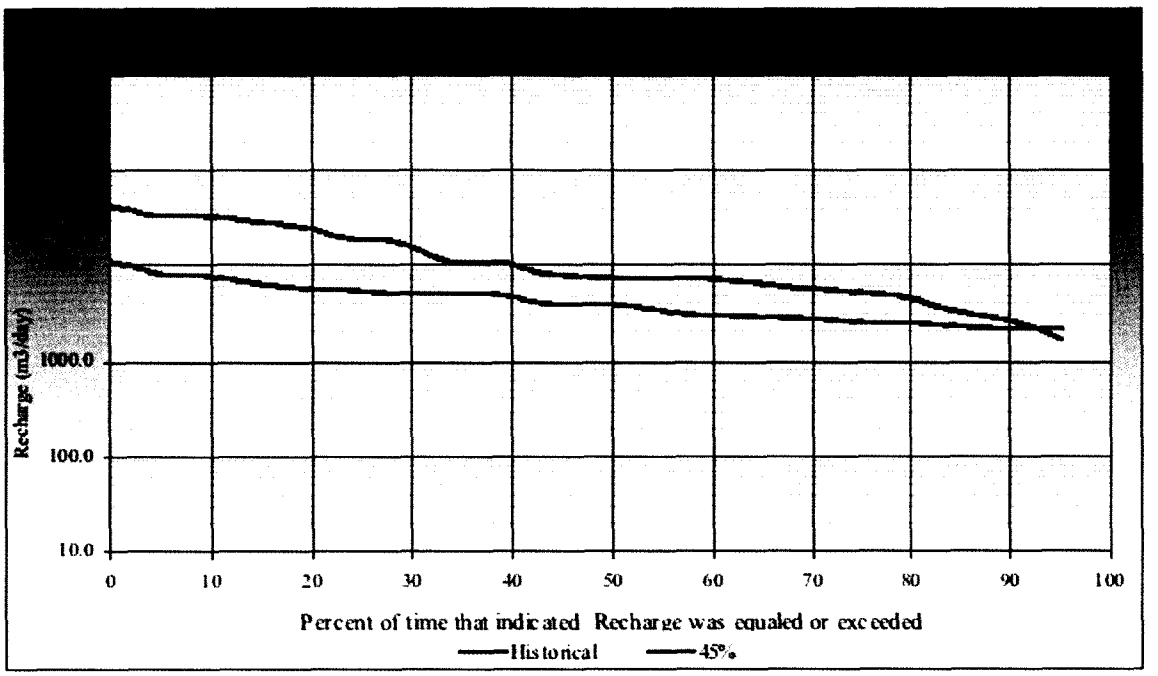

(e)

Figure (5.53): (a) Flow duration curve (daily), (b) Flow duration curve (monthly), (c) Flow duration curve (June), (d) Flow duration curve (July), (e) Flow duration curve (August)(m^3/day) for the sixth scenario (continued).

5.5 Discussion and results comparison from different scenarios

In this study of generation of potential changes in the rainfall and the corresponding impact on groundwater recharge, the recharge responded to the impact of the different rainfall scenarios in different ways. In the first and second scenarios the recharge increased and decreased with approximately the same percentage of increase or decrease in the rainfall. In these scenarios the rainfall patterns is exactly the same and the relative magnitude of rainfall is the same, however, the amount of rainfall on the wet days is uniformly increased or decreased. In the fifth and sixth scenarios the rainfall patterns is exactly the same, however the relative magnitude of rainfall can vary on the wet days. The fifth and sixth scenarios also showed that the recharge increased or decreased at approximately the same percentage as the increase or decrease in the rainfall, although the pattern of these changes was much more variable on daily basis. This would indicate that if the impact of climate change is to maintain the seasonal patterns but change the magnitude of rainfall, the recharge would be strongly related to the change in this precipitation magnitude. The infiltration capacity would be the key to explaining this behavior- if the rainfall rate is lower than the equilibrium of the infiltration capacity, then all rainfall reaching the land surface will infiltrate then percolate and recharge the groundwater (Figure (5.54) (a)). This means the increase or the decrease in the rainfall rate impacted the recharge in the zone below the infiltration capacity curve. Also, the recharge from ground water to streams and rivers in these scenarios (first and second), would not carry a flow of water to the streams or rivers.

Generally, the velocity of subsurface flow is so low that not all of watershed can contribute subsurface flow or saturation overland flow to a stream through a storm except under particular case when the hydraulic conductivity of the soil is very high (Chow et al., 1988). During dry times the water table goes down below the streambed. Baseflow stops. However, after the rainfall has increased the groundwater recharge then the water table rises sufficiently to intersect the streambed and restart base flow discharge and the streams get contributions from ground water throughout their lengths.

In the third and fourth scenarios a reduction in seasonality of precipitation is modeled as one potential impact of climate change. Compared to the scenarios where the rainfall pattern was held constant, the removed of seasonality leads to more uniform rainfall throughout the year. This change can have a dramatic affect on recharge. For example in the third and fourth scenario a 25% increase in precipitation showed an increase in recharge of approximately 60% while a 25% decrease in precipitation showed a 70% decrease in recharge. These dramatic changes from historical conditions coincide with what was reported by David Chandler (2008) in which the MIT research team found that changes in groundwater may actually be much greater than the associated precipitation changes themselves. In a similar study Rosenberg et al. (1999) concluded that the recharge was reduced under all scenarios, ranging up to 77 percent.

The previously mentioned authors did not speculate on the exact causes of this dramatic change in recharge other than to say that the groundwater recharge system is very interconnected complex and non-linear. Groundwater recharge is controlled by many different factors such as: (1) the amount and rate of precipitation, (2) evapotranspiration, (3) the initial soil moisture content or saturation ratio of the soil, (4)

the infiltration capacity of the watershed (5) the elevation of the water table, (6) hydraulic conductivity, and (7) the topography and hydraulic system of the streams. Finally groundwater and surface water are connected resources; they are not separate. When we disturb or use one of these resources, it often affects the other in terms of quantity and quality in a relatively short time frame.

The characterization of the interactions of these factors will likely be the subject of much future research. However it is reasonable to expect that a hydrologic system adapts to a seasonal pattern and if that seasonal pattern is disrupted than the re-adaption of the hydrologic system could be very complex.

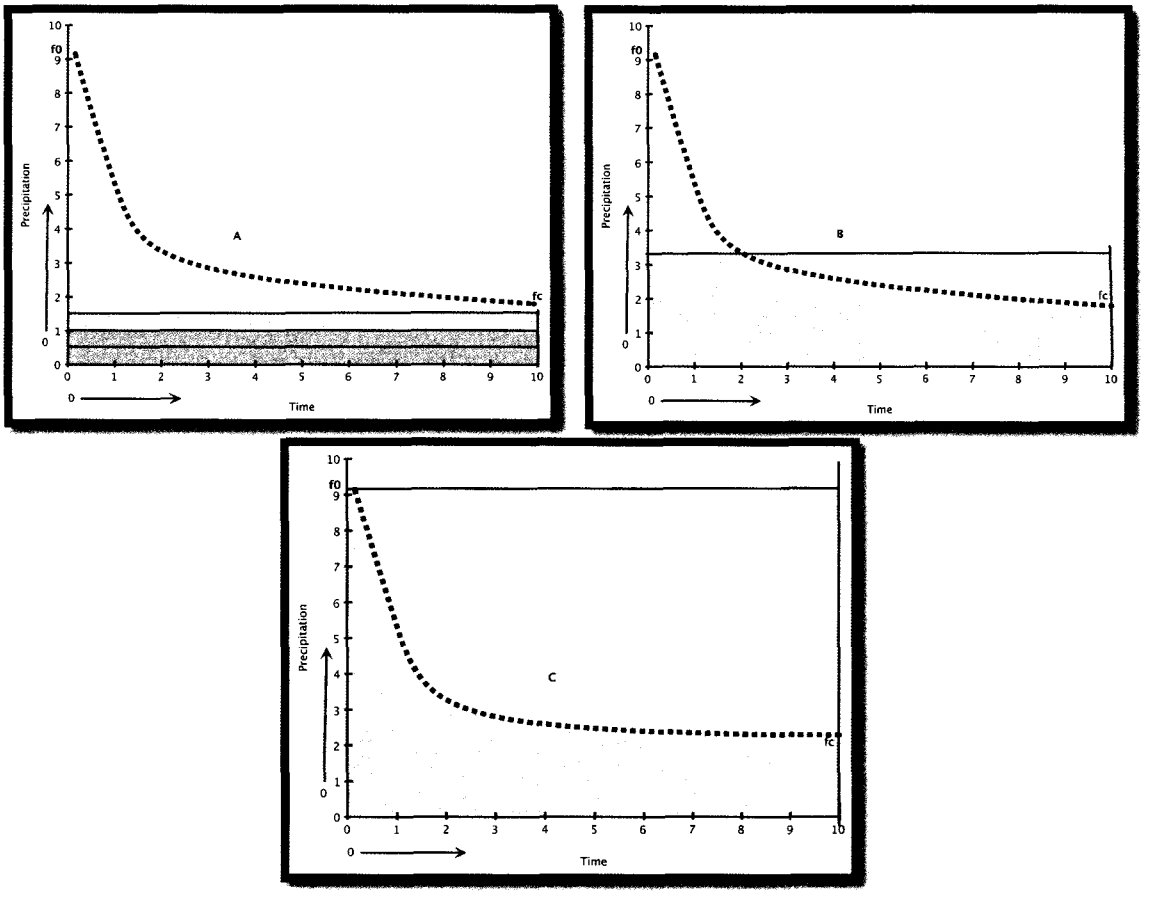

Figure (5.54): The relationship of infiltration capacity and precipitation rate. (a) Precipitation rate less than equilibrium infiltration capacity. (b) Greater than equilibrium infiltration capacity. (c) Greater than infiltration capacity.

5.6 Response of Hydrological Variables (ET, Runoff) Due to Stochastic Generation of Precipitation

Precipitation is the most important parameter in the hydrologic cycle and the main source of fresh water. Evapotranspiration and runoff are elements of the hydrologic cycle that can affect directly the variation of rainfall due to stochastic generation. Since we know evapotranspiration refers to the combined processes of direct evaporation at the

ground surface, direct evaporation on plant surfaces, and transpiration, runoff generated or occurring at the surface by two mechanisms first as infiltration excess and second as saturation excess, all leads to initial accumulation over the soil surface. ET and rainfall are related to the availability of rainfall in any applicable area. This section shows the water balance that was obtained from the GSFLOW and PRMS models for all six scenarios.

Figures (5.55) (a, b, c, d) show the results of scenario 1 at 5%, 15%, 25%, and 35% simulations. The rate per year for ET was in the range of 24-28 inches/year. When the precipitation increased, the ET and runoff increased. Runoff ranged between 14 and 21 inches. The degree of association between precipitation and runoff or correlation coefficient ranged between 0.97 and 0.977 increasing in correlation with increasing precipitation. In this scenario, runoff responded quickly and exceeded the ET for increasing precipitation. The reverse situation is seen in the figures (5.56) (a, b, c, d) for the second scenario. ET was in the range of 23 to 18 inches/year. In addition when the precipitation decreased, the ET and runoff decreased. Runoff ranged between 12 and 7 inches. The correlation coefficient between precipitation and runoff ranged between 0.965 and 0.931 and decreased with decreasing precipitation in these scenarios.

Figures (5.57) (a, b, c, d) show different variability than the previous scenarios. ET was in the range of 32 to 35 inches/year. ET increased about 10 percent while the runoff increased about 50 percent. The same behavior is shown for the fourth scenario, figures (5.68) (a, b, c, d) except it is the reverse of the third scenario. Figure (5.59) shows the results of scenario 5 at a 45 percent increase. The rate per year for ET was 32.26 inches/year. In addition, when the precipitation increased the ET and runoff

increased. Runoff was 20.37 inches. The correlation coefficient between precipitation and runoff was 0.96. The reverse situation is shown in figure (5.60) for the six scenario.

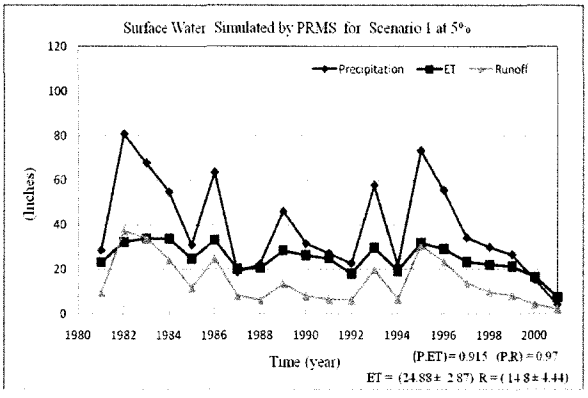

(a)

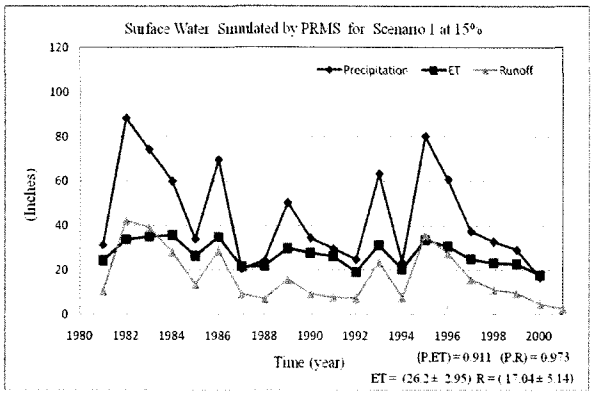

(b)

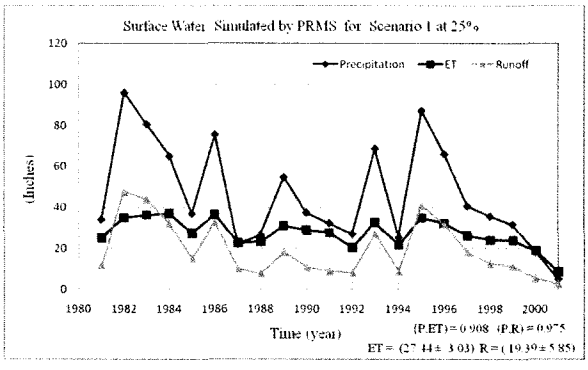

(c)

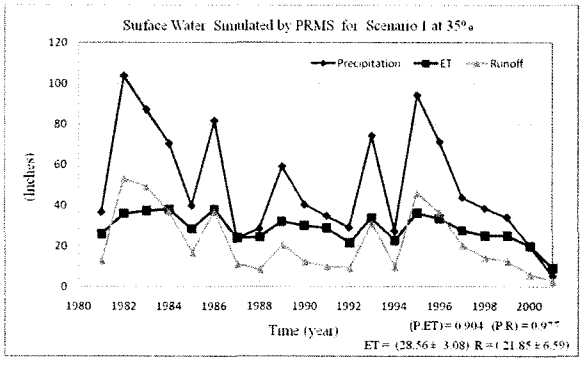

(d)

Figure (5.55): Time series of surface water variables simulated by PRM model for scenario 1.

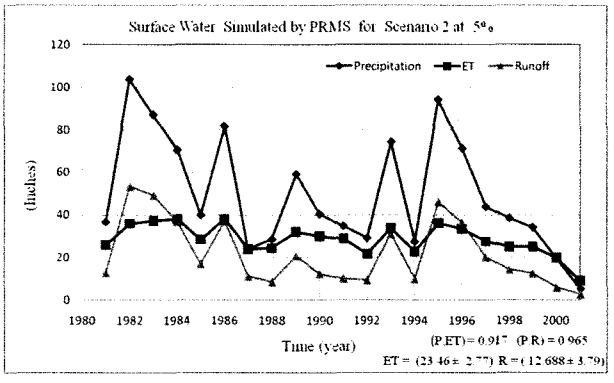

(a)

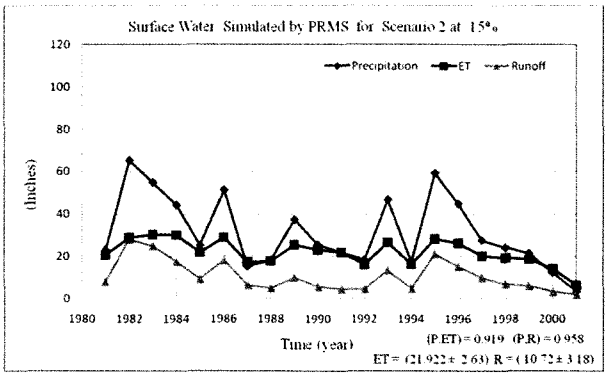

(b)

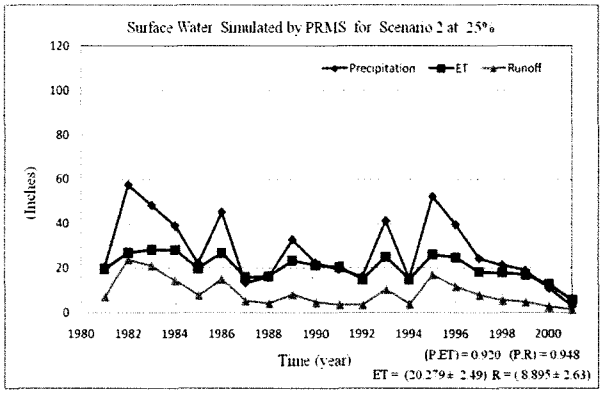

(c)

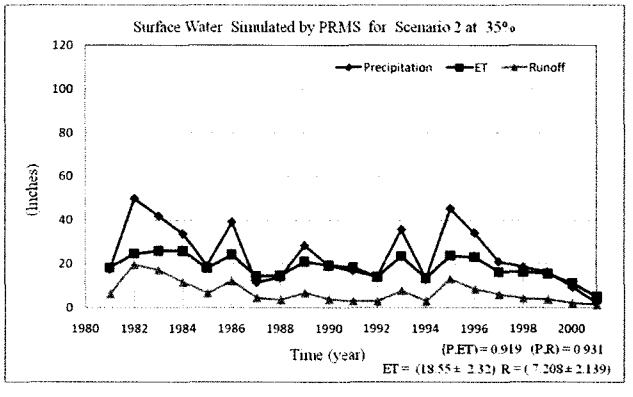

(d)

Figure (5.56): Time series of surface water variables simulated by PRM model for scenario 2.

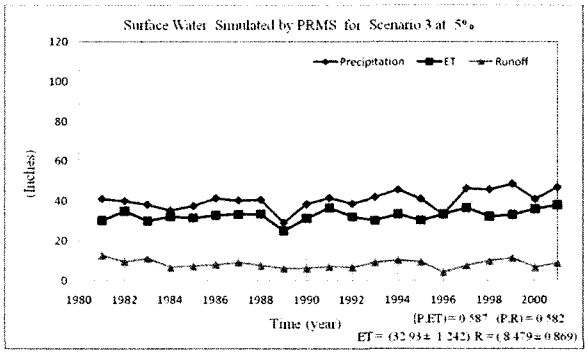

(a)

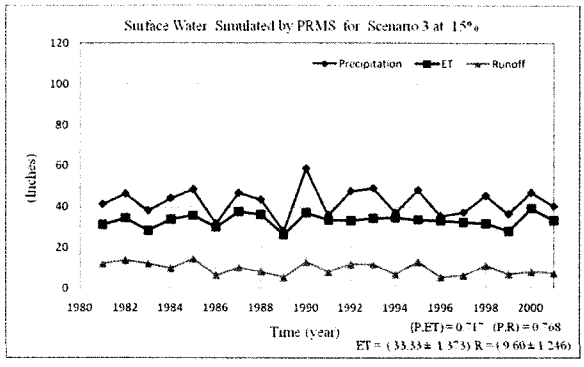

(b)

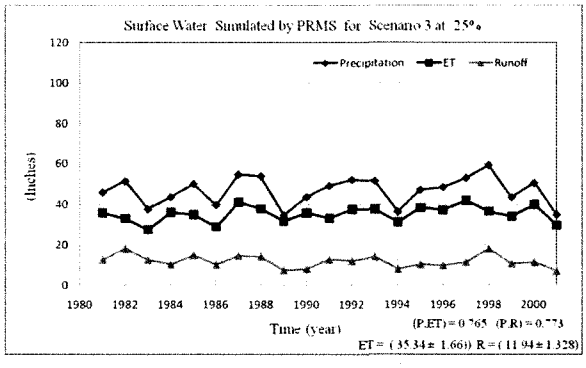

(c)

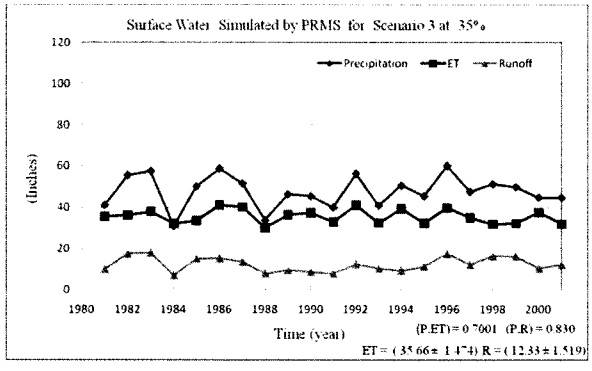

(d)

Figure (5.57): Time series of surface water variables simulated by PRM model for scenario 3.

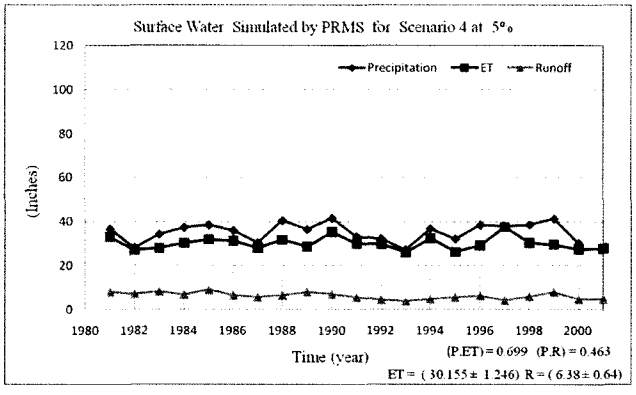

(a)

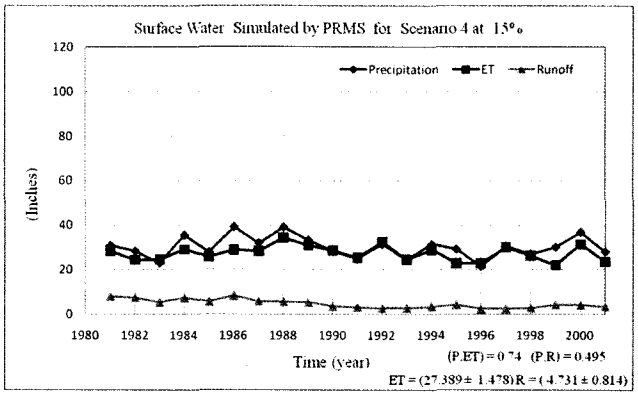

(b)

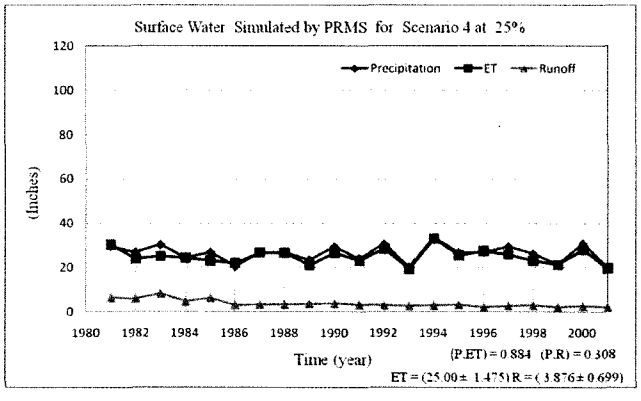

(c)

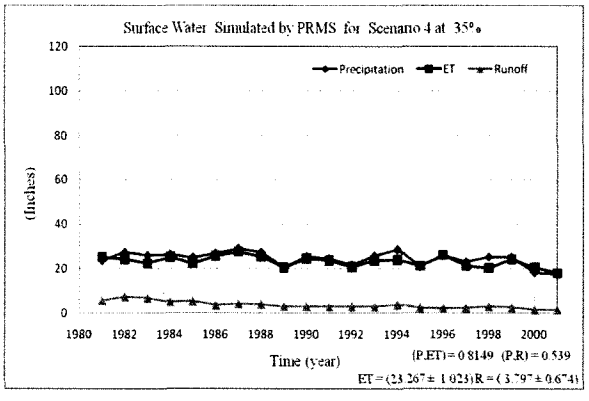

(d)

Figure (5.58): Time series of surface water variables simulated by PRM model for scenario 4.

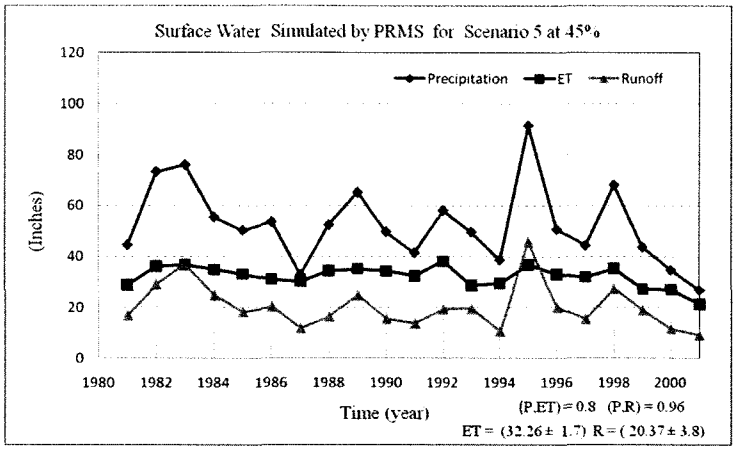

Figure (5.59): Time series of surface water variables simulated by PRM model for scenario 5.

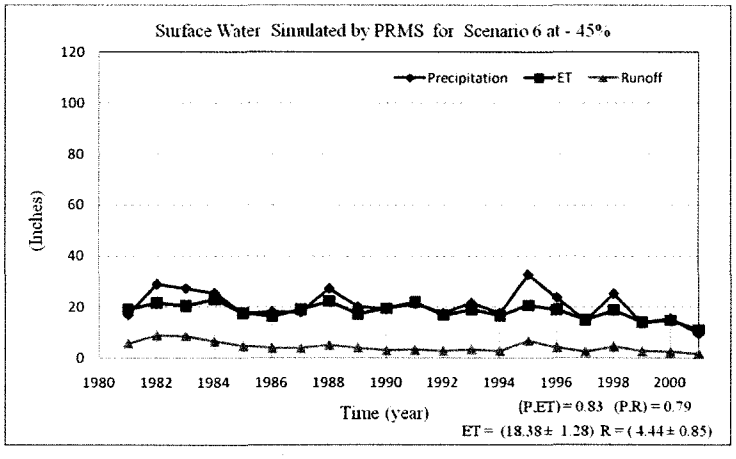

Figure (5.60): Time series of surface water variables simulated by PRM model for scenario 6.

Chapter 6

SUMMARY, CONCLUSIONS, AND RECOMMENDATIONS

6.1 Summary

Changes in groundwater recharge (both increases and decreases) are likely to result from alterations in the annual and seasonal distribution of precipitation. Precipitation is a very important factor in semi-arid and arid regions since groundwater is considered the main water resource. The relationship between the stochastic nature of precipitation, which infiltrates and recharges groundwater, and recharge, is an important research area. The main purpose of this research is to simulate groundwater recharge using a new model released by the U.S under potential precipitation changes resulting from climate change. Geological Survey (USGS). The Ground Water and Surface Water FLOW (GSFLOW) model characterizes the impacts of groundwater recharge resulting from potential precipitation scenarios. A variety of potential stochastic precipitation patterns were used to study the impact on groundwater recharge. This research improves our ability to adequately understand the effects of changing surface water supplies on groundwater resources.

In this study climate change scenarios were constructed, taking into account the uncertainty concerning the stochastic generation patterns of precipitation and changes in groundwater recharge. The fact that groundwater is directly connected to near-surface hydrologic processes was also considered. Groundwater is

intricately connected to the overall hydrologic cycle and could be directly affected by climate change.

A stochastic precipitation generation model was developing using two processes for rainfall. One model, a first-order Markov Chain, is constructed for the occurrence of rainfall. The second model uses an exponential distribution model fitted to the historical time for the amount of rain on rainy days. The US Global Change Research Program reported the following general predictions that the entire US is projected to have increases and decreases in precipitation. In which the average US precipitation has increased by 5-10% over the last century and the decreased exceeding 20%. The largest percentage increases in precipitation are projected to be in the Southwest and Southern California, where in the Sierra Nevada much of the increased precipitation is likely to fall as rain rather than snow.

Following steps summarize the proceedings accomplished in this research.

- **First Scenario:** Precipitation is projected to increase, with an average change ranging between 5 and 45 percent compared to the historical data with the same patterns of occurrences as the historical data.
- **Second Scenario:** Precipitation is projected to decrease, with an average change ranging between 5 and 45 percent compared to the historical data with the same patterns of occurrences as the historical data.
- **Third Scenario:** Generate a synthetic precipitation pattern without regard to seasonality by a stochastic model with an average change with increasing range between 5 and 45 percent, using a 10 percent increment.

- **Fourth Scenario:** Generate a synthetic precipitation pattern without regard to seasonality by a stochastic model with an average change with decreasing range between 5 and 45 percent, using a 10 percent increment.
- **Fifth Scenario:** Generate a synthetic precipitation pattern with regard to seasonality by a stochastic model with an average change increasing only 45 percent.
- **Six Scenario:** Generate a synthetic precipitation pattern with regard to seasonality by a stochastic model with an average change decreasing only 45 percent.
- Each of the time series was input into the GSFLOW model for groundwater recharge modeling.
- The projected groundwater recharge obtained from all the scenarios has been analyzed, and the frequency analysis for different time scales has been plotted.

6.2 Conclusion

The primary objective of this research has to been attempt to characterize the impacts on groundwater recharge by developing potential precipitation patterns, simulating groundwater recharge in a groundwater simulation model, and analyzing the effects of the uncertainty and the variability of precipitation resulting from global warming, which could affect groundwater recharge. The adopted stochastic rainfall and the GSFLOW model approach have proved very useful in reaching the objectives of this research. The results of this research have led to the following conclusions:

- The adopted stochastic precipitation model has been shown to generate a wide variety in the time series of the rainfall estimates and maintaining the seasonality of historical data.

- The generation of the precipitation time series for the next 20 years (with an increasing range between 5 and 45 percent with a 10 percent increment) will generate groundwater recharge with approximately the same percentage as the increase in the precipitation. The relationship between the increasing rainfall and the groundwater recharge is directly correlated in this situation.
- The generation of the precipitation time series for the next 20 years with a decreasing range between 5 and 45 percent (and with a 10 percent increment with constancy of the occurrence) will produce groundwater recharge with the same percentage as the decrease in precipitation.

  As mentioned previously, it appears that the relation between decreasing rainfall and groundwater recharge will be directly correlated.
- The fifth and sixth scenarios also showed that the recharge increased or decreased at approximately the same percentage as the increase or decrease in the rainfall, although the pattern of these changes was much more variable on daily basis. This would indicate that if the impact of climate change is to maintain the seasonal patterns but change the magnitude of rainfall, the recharge would be strongly related to the change in this precipitation magnitude.
- The third and fourth scenarios a reduction in seasonality of precipitation are modeled as one potential impact of climate change. Compared to the scenarios where the rainfall pattern was held constant, the removed of seasonality leads to more uniform rainfall throughout the year. This change can have a dramatic affect on recharge. For example in the third and fourth scenario a 25% increase in precipitation showed an increase in recharge of approximately 60% while a 25%

decrease in precipitation showed a 70% decrease in recharge.

- The intensity and temporal variability of stochastic precipitation patterns affect rainfall models and influence the quantity of groundwater recharge.

6.3 Recommendations

Based on the results and conclusions drawn from this research, the recommendations required to strengthen the techniques and applications for further research are described as follows:

- By using the GSFLOW model, the present study considered the stochastic uncertainty for precipitation in terms of intensity, variability, and temporality. Other studies are needed to investigate the effects of other parameters, such as hydraulic conductivity, variations in soil cover and topographic slope, properties of the soil, and other parameters.
- The degree of sophistication for the stochastic precipitation model may require future work comparing different approaches.
- The GSFLOW model used in this study for the recharge estimation and for other surface groundwater models may require future work for comparison with other models.
- Water resource management (Groundwater) can be improved by considering the effects of the different scenarios for the stochastic precipitation model on groundwater recharge and the GSFLOW model. Therefore, stochastic approaches to precipitation uncertainty and the GSFLOW model would be recommended to manage the water supply, including seasonal storage, long-term storage (drought mitigation), short-term water supply regulation, and emergency supplies.

- Well locations and designs can be improved by learning about the availability of groundwater storage (recharge). Hence, stochastic approaches that implement the GSFLOW model and frequency analysis can also be useful for groundwater recharge.

References

Abbott, M. B., Bathurst, J. C., Cunge, J. A., O'Connell, P. E., & Rasmussen, J. (1986). An introduction to the European Hydrological System—*systeme hydrologique Europeen*, "SHE," 1: History and philosophy of a physically based, distributed modelling system. *Journal of Hydrology, 87,* 45–59.

Abbs, K., & Littleboy, M. (1998). Recharge estimation for the Liverpool Plains. *Australian Journal of Soil Research, 36,* 335–357.

Akaike, H. (1981). Likelihood of a model and information criteria. *Journal of Econometrics, 16,* 3–14.

Akaike, H. (1973). Information theory and an extension of the maximum likelihood principle. In B. N. Petrov & F. Csaki (Eds.), *Second international symposium on information theory* (pp. 267–281). Budapest: AcademiaiKiado.

Akaike, H. (1974). A new look at the statistical model identification. *IEEE Transactions on Automatic Control, 19,* 716–723.

Akaike, H. (1987). Factor analysis and AIC. *Psychometrika, 52,* 317–332.

Allen, D. M., Mackie, D. C., & Wei, M. (2004). Groundwater and climate change: a sensitivity analysis for the Grand Forks aquifer, southern British Columbia, Canada. *Hydrogeology Journal, 12,* 270–290.

Allison, G. B. (1988). A review of some of the physical, chemical, and isotopic techniques available for estimating groundwater recharge. In: Simmers, I. (Ed.) *Estimation of natural groundwater recharge.* NATO ASI Series C, 222 (Proceedings of the NATO advanced research workshop, Antalya, Turkey).

Arnold, J. G., Muttiah, R. S., Srinivasan, R., & Allen, P. M. (2000). Regional estimation of base flow and groundwater recharge in the Upper Mississippi river basin. *Journal of Hydrology, 227,* 21–40.

Arnold, J. G., Srinivasan, R., Muttiah, R. S., & Williams, J. R. (1998). Large area hydrologic modeling and assessment, Part I. Model development. *Journal of the American Water Resources Association, 34,* 73–89.

Arya, L. M., Farrell, D. A., & Blake, G. R. (1975). A field study of soil water depletion patterns in presence of growing soybean roots, I. Determination of hydraulic properties of the soil. *Soil Science Society of America proceeding, 39,* 424–430.

Ball, J. E., & Luk, K. C. (1998). Modeling spatial variability of rainfall over a catchment. *Journal of Hydrologic Engineering, 3,* 122–130.

Batelaan, O., & De Smedt, F. (2001). WetSpass: A flexible, GIS based, distributed recharge methodology for regional groundwater modelling. In: Gehrels, H., N. E. Peters, E. Hoehn, K. Jensen, C. Leibundgut, J. Griffioen, B. Webb, and W. J. Zaadnoordijk (Eds.) *Proceedings of the Conference on Impact of Human Activity on Groundwater Dynamics*. IAHS Publication No. 269, pp. 11–17.

Batelaan, O., De Smedt, F., & Triest, L. (2003). Regional groundwater discharge: Phreatophyte mapping, groundwater modelling and impact analysis of land-use change. *Journal of Hydrology, 275,* 86–108.

Bauer, H. H., & Vaccaro, J. J. (1987). *Documentation of a deep percolation model for estimating groundwater recharge*. Tacoma,WA: U.S. Geological Survey, Open-File Report 86–536.

Bear, J. (1972). *Dynamics of Fluids in Porous Media*. New York: Elsevier.

Beckers, J., & Frind, E. O. (2000). Simulating groundwater flow and runoff for the Oro Moraine aquifer system. Part 1. Model formulation and conceptual analysis. *Journal of Hydrology, 229,* 265–280.

Bekesi, G., & McConchie, J. (1999). Groundwater recharge modelling using the Monte Carlo technique, Manawatu region, New Zealand. *Journal of Hydrology, 224,* 137–148.

Bellot, J., Bonet, A., Sanchez, J. R., & Chirino, E. (2001). Likely effects of land use changes on the runoff and aquifer recharge in a semiarid landscape using a hydrological model. *Landscape and Urban Planning, 55,* 41–53.

Beverly, C. R., Nathan, R. J., Malafant, K. W. J., & Fordham, D. P. (1999). Development of a simplified unsaturated module for providing recharge estimates to saturated groundwater models. *Hydrological Processes, 13,* 653–675.

Black, P. B., & Miller, R. D. (1990). Hydraulic conductivity and unfrozen water content of air-free frozen silt. *Water Resources Research, 26,* 323–329.

Bobba, A. G., Singh, V. P., Jeffries, D. S., & Bengtsson, L. (1997). Application of a watershed runoff model to northeast Pond River, Newfoundland: To study water balance and hydrological characteristics owing to atmospheric change. *Hydrological Processes, 11,* 1573–1593.

Bonomi, T., & Cavallin, A. 1999. Three-dimensional hydrogeological modelling application to the Alvera mudslide (Cortina d'Ampezzo, Italy). *Geomorphology, 30,* 189–199.

Boughton, W. C. (1966). A mathematical model for relating runoff to rainfall with daily data. *Civil Engr. Trans. Inst. Engrs. (Aust.). C.E., 8,* 83–87.

Bouraoui, F., & Dillaha, T. A. (1996). ANSWERS-2000: Runoff and sediment transport model. *Journal of Environmental Engineering, ASCE, 122,* 493–502.

Bouraoui, F., Vachaud, G., Li, L. Z. X., Le Treut, H., & Chen, T. (1999). Evaluation of the impact of climate changes on water storage and groundwater recharge at the watershed scale. *Climate Dynamics, 15,* 153–161.

Broadbridge, P., & White, I. (1988). Constant rate rainfall infiltration: A versatile nonlinear model, 1. Analytical solution. *Water Resources Research, 24*(1), 145–154.

Brodie, R. S. (1999). Integrating GIS and RDBMS technologies during construction of a regional groundwater model. *Environmental Modelling & Software, 14,* 119–128.

Brouyere, S., Carabin, G., & Dassargues, A. (2004). Climate change impacts on groundwater resources: Modelled deficits in a chalky aquifer, Geer Basin, Belgium. *Hydrogeology Journal, 12,* 123–134.

Burges, S. J., Wigmosta, M. S., & Meena, J. M. (1998). Hydrological effects of land-use change in a zero-order catchment. *Journal of Hydrologic Engineering, 3,* 86–97.

Burgess, S. S. O., Adams, M. A., Turner, N. C., & Ong, C. K. (1998). The redistribution of soil water by tree root systems. *Oecologica, 115,* 306–311.

Burgess, S. S. O., Adams, M. A., Turner, N. C., White, D. A., & Ong, C. K. (2001). Tree roots: conduits for deep recharge of soil water. *Oecologia, 126,* 158–165.

Burnett, J. L., & Jennings, C. W. (1965). Chico Quadrangle, Scale 1:250,000: State of California, Division of Mines and Geology.

Canadell, J., Jackson, R. B., Ehleringer, J. R.,Mooney, H. A., Sala, O. E., & Schulze, E. D. (1996). Maximum rooting depth of vegetation types at the global scale, *Oecologia, 108,* 583–595.

Coe, R., & Stern, R. D. (1982). Fitting models to daily rainfall data. *J. Appl. Meteor., 21,* 1024–1031.

Corradini, C., Melone, F., & Smith, R. (1994). Modeling infiltration during complex rainfall sequence. *Water Resources Research, 30*(10), 2777–2784.

Croley II, T. E., & Luukkonen, C. L. (2003). Potential effects of climate change on ground water in Lansing, Michigan. *Journal of the American Water Resources*

Association, 39, 149–163.

David ,Chandler,(2008): water supplies could be strongly affected by climate change.changes in rainfall can be amplified, up or down, in changes to aquifers., Massachusetts Institute of Technology News, December 18, 2008. See: http://web.mit.edu/newsoffice/2008/agu-groundwater-1218.html

Delleur, J. W. (1999). *The handbook of groundwater engineering.* New York: CRC Press. Dunin, F. X. (1976). Infiltration: Its simulation for field conditions, Chapter 8. In J. C. Rodda (Ed.), *Facets of hydrology* (pp. 199–227). New York: John Wiley & Sons.

Dunne, T., Zhang, W., & Aubry, B. F. (1991). Effects of rainfall, vegetation, and microtopography on infiltration and runoff. *Water Resources Research, 27*(9), 2271–2285.

Eckhardt, K., & Ulbrich, U. (2003). Potential impacts of climate change on groundwater recharge and streamflow in a central European low mountain range. *Journal of Hydrology, 284*, 244–252.

El-Hames, A. S., & Richards, K. S. (1995). Testing the numerical difficulty applying Richards' equation to sandy and clayey soils. *J. Hydrol.,167*(1–4), 381–391.

El-Kadi, A. I. (1989). Watershed models and their applicability to conjunctive use management. *Water Resources Bulletin, 25,* 125–137.

Fisher, R.A. (1941), "The Negative Binomial Distribution", Annals of Eugenics,London, 111 182-187

Freeze, R. A. (1971). Three-dimensional, transient, saturated/unsaturated flow in a groundwater basin. *Water Resources Research, 7*(2), 347–366.

Gabriel, K. R., & Neumann, J. (1962). A Markov chain model for daily rainfall occurrence at Tel Aviv. *Quart. J. Roy. Meteor. Soc., 88,* 90–95.

Glover, P. E., Glover, J., & Gwynne, M. D. (1962). Light rainfall and plant survival in E. Africa, II, Dry grassland vegetation. *J. Ecol., 50,* 199–206.

Green, W. H., & Ampt, C. A. (1911). Studies on soil physics I: The flow of air and water through soils. *Journal of Agricultural Science, IV* (Part I 1911), 1–24.

Hann, C. T. (2002). *Statistical methods in hydrology.* Ames, IA: Iowa State University Press. (Original work published 1997).

Hann, C. T., Allen, D. M., & Street, J. O. (1976). A Markov chain model of daily rainfall. *Water Resources Research, 12,* 443–449.

Harbaugh, A.W., 2005, MODFLOW-2005, The U.S. Geological Survey modular ground-water model—the Ground-Water Flow Process: U.S. Geological Survey Techniques and Methods 6-A16,2-3 p.

Harrold, S., & Sheather, J. (2003). A nonparametric model for stochastic generation of daily rainfall amounts. *Water Resources Research, 39*(12), 1343.

Heermann, D. F., Finkner, M. D., & Hiler, E. A. (1968). Probability of sequences of wet and dry days for eleven Western states and Texas. *Colorado A.E.S. Tech. Bull, No. 117.*

Herman, B. (1986). Intake rate: Cylindrical infiltrometer. In Klute & Arnold (Eds.), *Methods of soil analysis* (2nd ed.).

Hershfield, D. M. (1984). Extreme rainfall intensities. Arch. Met. *Geoph. Biocl., Ser. B, 35,* 67–80.

Hillel, D. (1980). *Applications of soil physics.* New York: Academic Press.

Hillel, D. (1982). *Introduction to soil physics.* New York: Academic Press.

Holtan, H. N. (1961). A concept for infiltration estimates in watershed engineering. *USDA-ARS,* 41–51.

Horton, R. E. (1940). An approach towards a physical interpretation of infiltration capacity. *Soil Science Society of America Proceedings, 5,* 399–417.

IPCC, 1990: Climate Change, The IPPC Scientific Assessment. J.T. Houghton, G.J. Jenkins and J.J. Ephraums (eds.), Cambridge University Press, Cambridge, UK, 365 pp.

IPCC, 1992: Climate Change 1992: The Suppliementary Report to the IPCC Scientific Assessment. J.T. Houghton, B.A. Callander and S.K. Varney (eds.), Cambridge University Press, Cambridge, UK, 198 pp.

IPCC, 1996: Climate Change 1995: The Science of Climate Change. Contribution of Working Group I to the Second Assessment Report of the Intergovernmental Panel on Climate Change [Houghton, J.T., L.G. Meira Filho, B.A. Callander, N. Harris, A. Kattenberg, and K. Maskell (eds.)]. Cambridge University Press, Cambridge, United Kingdom and New York, NY, USA, 572 pp.

IPCC, 1999: IPCC Special Report Aviation and the Global Atmosphere. Cambridge University Press, Cambridge, UK, 373 pp.

Jones, W., Rex, R. C., & Threadgill, D. E. (1972). A simulated environmental model of

temperature, evaporation, rainfall, and soil moisture, *Transactions of American Society of Agricultural Engineers, 15*, 366–392.

Khalil, M., Sakai, M., Mizoguchi, M., & Miyazaki, T. (2003). Current and prospective applications of Zero Flux Plane (ZFP) Method. *J. Jpn. Soc. Soil Phys., 95*, 75–90.

Kirshen, P. H. (2002). Potential impacts of global warming on groundwater in Eastern Massachusetts. *Journal of Water Resources Planning and Management, 128*, 216–226.

Kostiakov, A. N. (1932). On the dynamics of the coefficient of water percolation in soils and on the necessity of studying it from a dynamic point of view for the purposes of amelioration. *Trans. Com. Int. Soc. Soil Sci. 6th Moscow A,* 17–21.

Kramer, P. J., & Boyer, J. S. (1995). *Water relations of plants and soils.* San Diego, CA: Academic Press.

Leavesley, G.H., Lichty, R.W., Troutman, B.M., and Saindon, L.G.(1983)."Precipitation runoff modeling system—User's manual," U.S. Geological Survey Water-Resources Investigations Report 83-4238, 207 p.

Leavesley G.H., Restrepo, P.J., Markstrom, S.L., Dixon, M., and Stannard, L.G. (1996). "The modular modeling system - MMS: User's manual," U.S. Geological Survey Open File Report 96-151, 142 p.

Loaiciga, H. A. (2003). Climate change and ground water. *Annals of the Association of American Geographers, 93,* 30–41.

Lung, I. A., & Grantham, D. D. (1977). Persistence, runs, and recurrence of rainfall. *J. Appl. Meteor., 16,* 346–358.

Matthew ELY, D. and KAHLE, Sue C (2009) Groundwater and surface water flow modeling of Chamokalne Creek basin, Stevens County, Washington. Portland GSA Annual Meeting (18-21 October 2009)

Markstrom, S.L., Niswonger, R.G., Regan, R.S., Prudic, D.E., and Barlow, P.M., 2008, GSFLOW—Coupled ground- water and surface-water flow model based on the integration of the Precipitation-Runoff Modeling System (PRMS) and the Modular Ground-Water Flow Model (MODFLOW-2005): U.S. Geological Survey Techniques and Methods 6-D1, 240 p.

McClaran, M. P., & Van Devender, T. R. (Eds.). (1995). *The desert grassland.* Tucson: University of Arizona Press.

McDonald, M.G., and Harbaugh, A.W. (1988). "A modular three-dimensional finite-difference ground-water flow model," U.S. Geological Survey Techniques of Water resources Investigations, book 6, chap. A1, 586 p.

McKenzie, N., Coughlan, K., & Cresswell, H. (2002). *Soil physical measurement and interpretation for land evaluation.* Melbourne: CSIRO Publishing.

Mimikdu, M. (1983). Daily rainfall occurrences modeling with Markov chain of seasonal order. *Hydrological Sciences, 28,* 2–6.

Nicks, A. D., & J. F. Harp. (1980). Stochastic generation of temperature and solar radiation data. *Journal of Hydrology, 48,* 1–7.

National Assessment Synthesis Team. 2000.Climate Change Impacts on the United States The Potential Consequences of Climate Variability and Change. US Global Change Research Program.

Niswonger, R.G., Prudic, D.E., and Regan, R.S. (in press). "Documentation of the Unsaturated Flow (UZF1) Package for modeling percolation between the land surface and the water table with MODFLOW-2000," U.S. Geological Survey Techniques and Methods Book 6, Chapter A1X.

Niswonger, R.G., and Prudic, D.E., (2005). "Documentation of the Streamflow-Routing (SFR2) Package to include unsaturated flow beneath streams—a modification to SFR1," U.S. Geological Survey Techniques and Methods Book 6, Chapter A13.

Niswonger, R. G., Prudic, D. E., Markstrom, S. L., Regan, R. S., & Viger, R. J. (2006). GSFLOW: A basin-scale model for coupled simulation of groundwater and surface water flow, Part B. Concepts for modeling ground-water flow with the U.S. Geological Survey MODFLOW model.

Ochola O. W, and P. Kerkides.(2003). A Markov chain simulation model for predicting critical wet and dry spells in Kenya: analysing rainfal events in the Kano Plains. Irrig. and Drain. 52: 327-342, 2003.

Parlange, J. Y. (1971). Theory of water movement in soils: One dimensional absorption. *Soil Sci., 111*(2), 134–137.

Parzen, E. (1962). On estimation of a probability density function and mode. *Annals of Mathematical Statistics, 33,* 1065–1076.

Peters, O. C., Hertlien, K., & Christensen, . (2002). *Phys. Rev. Lett., 88,* 1.

Philip, J. R. (1957). Theory of infiltration: The infiltration equation and its solution. *Soil Sci., 83,* 345–357.

Philip, J. R. (1969). Theory of infiltration. *Soil Sci., 5,* 215–296.

Philip, J. R., & Knight, J. H. (1974). On solving the unsaturated flow equation: New quasi-analytical technique. *Soil Sci., 117*(1), 1-13.

Phillips, W. S. (1963). Depth of roots in soil. *Ecology, 44*(2), 42.

Rademacher, L. K., Clark, J. F., Clow, D. W., & Hudson, G. B. (2005). Old groundwater influence on stream hydrochemistry and catchment response times in a small Sierra Nevada catchment: Sagehen Creek, CA: Water Resources Research, v. 41, no. W02004, doi:10.1029/2003WR002805, 10.

Rainhart Co. (2008). Retrieved from http://www.rainhart.com/contact.html

Rajagopalan, B., Lall, U., & Tarboton, D. G. (1996). A nonhomogeneous Markov model for daily precipitation simulation. *J. Hydrol. Eng. ASCE, 1,* 33–40.

Rajagopalan, B., Lall, U., Tarboton, D. G., & Bowles, D. S. (1997). Multivariate non-parametric resampling scheme for generation of daily weather variables. *Stoch. Hydrol. Hydraul., 11,* 65–93.

Ramesh, N. I. (1998). Temporal modeling of short-term rainfall using Cox processes. *Environmetrics, 9,* 629–643

Rao, N. J. M., & Biazi, E. (1983). Probability distribution models for daily rainfall data for an interior station of Brazil. *Arch. Met. Geoph. Biocl., Set. B, 33,* 261–265.

Reynolds, J. F., Fernández, R. J., & Kemp, P. R. (1999). Drylands and global change: The effect of rainfall variability on sustainable rangeland production. In K. N. Watanabe, & A. Komanine (Eds.), Proceedings of the Twelfth Toyota Conference: Challenge of plant and agricultural sciences to the crisis of biosphere on the earth in the 21st century. November 25–28, Mikkabi, Shizuoka, Japan. Landes Biosciences, Austin, TX.

Richard G. Niswonger1, David Rassam, and David E. Prudic, (in press). Assessing Water Resources Using a New Hydrologic Model,U.S.Geological Survey, Carson City, Nevada, USA CSIRO, Indooroopilly, Queensland, AUS

Richardson, C. W. (1981). Stochastic simulation of daily precipitation, temperature, and solar radiation. *Water Resources Research, 17*(1), 182–190.

Richardson, C. W. (1985). Weather simulation for crop management models. *Trans. ASAE, 8,* 1602–1606.

Richardson, C. W., & Wright, D. A. (1984). WGEN: A model for generating daily weather variables. SDA-ARS, ARS-8.

Richardson, C. W., & D. A. Wright. (1984). WGEN: A model for generating daily weather variables. ARS-8, Agricultural Research Service, U.S. Dept. of Agriculture, Washington, DC.

Rosbjerg, D., Madsen, H., & Rasmussen, P. (1992). Prediction in partial duration series with generalized pareto-distributed exceedances. *Water Resources Research, 28,* 3001–3010.

Rosenberg, N. J., Epstein, D. J., Wang, D., Vail, L., Srinivasan, R., & Arnold, J. G. (1999). Possible impacts of global warming on the hydrology of the Ogallala Aquifer Region. *Climatic Change, 42,* 677–692.

Salas, J. D., Smith, R. A., Tabios, J. Q., & Heo, J. H. (2002). Statistical computer techniques in water resources and environmental engineering. *Chapters 1–15, unpublished manuscript, Department of Civil Engineering, Colorado State University.* Fort Collins, CO.

Sampford, M.R. (1955), "The truncated Negative Binomial Distribution", Biometrika, 42, 58-69

Schlesinger, W. H., Reynolds, J. F., Cunningham, G. L., Huenneke, L. F., Jarrell, W. M., Virginia, R. A., et al. (1990). Biological feedbacks in global desertification. *Science, 247,* 1043–1048.

Serrano, S. E. (1998). Analytical decomposition of the nonlinear unsaturated flow equation. *Water Resources Research, 34*(3), 397–407.

Singh, V. P., & Deng, Z. Q. (2003). Entropy-based parameter estimation for kappa distribution. *J. of Hydrologic En. (ASCE), 2,* 81–92.

Smith, W. O. (1967). Infiltration in sands and its relation to groundwater recharge. *Water Resources Research, 3*(2), 539–555.

Snedecor, G. W., & Cochran, W. G. (1989). *Statistical methods, eighth edition.* Ames, IA: Iowa State University Press.

Stammers, W. N., Igwe, O. C., & Whiteley, H. R. (1973). Calculation of evaporation from measurements of soil water and the soil water characteristics. *Canadian*

Agricultural Engineering, 15, 2–5.

Sutton, R. F., & Tinus, R. W. (1983). Root and root system terminology. *Forest Science Monograph, 24,* 137.

Todorovic, P., & Zelenhasic, E. (1970). A stochastic model for flood analysis. *Water Resources Research, 6,* 1641–1648.

Tsakeris, G. (1988). Stochastic modeling of rainfall occurrences in continuous time. *Hydrological Sciences, 33,* 5.

Turkey. (March 1987). Dordrecht, Netherlands: D. Reidel Publication Company.

USDA Soil Conservation Service. (1957). Hydrology. *National Engineering Handbook, Sect. 4, Supplement A.*

Wilks, D. S. (1999). Interannual variability and extreme-value characteristics of several stochastic daily precipitation modela. *Agricultural and Forest Meteorology, 93,* 153–169.

Wu, L., Jury, W. A., Chang, A. C., & Allmaras, R. R. (1997). Time series analysis of field-measured water content of a sandy soil. *Soil Sci. Soc. Am. J., 61,* 736–742.

Yong Wu and Yongxin Xu, 2005:Snow Impact on Groundwater Recharge in Table Mountain Group Aquifer Systems with a Case Study of the Kommissiekraarivier Catchment South Africa. Water SA Vol. 31 No.3 p275-282.